CANADIAN THESES ON MICROFICHE

THÈSES CANADIENNES SUR MICROFICHE

National Library of Canada
Collections Development Branch

Canadian Theses on
Microfiche Service

Ottawa, Canada
K1A 0N4

Bibliothèque nationale du Canada
Direction du développement des collections

Service des thèses canadiennes
sur microfiche

NOTICE

The quality of this microfiche is heavily dependent upon the quality of the original thesis submitted for microfilming. Every effort has been made to ensure the highest quality of reproduction possible.

If pages are missing, contact the university which granted the degree.

Some pages may have indistinct print especially if the original pages were typed with a poor typewriter ribbon or if the university sent us an inferior photocopy.

Previously copyrighted materials (journal articles, published tests, etc.) are not filmed.

Reproduction in full or in part of this film is governed by the Canadian Copyright Act, R.S.C. 1970, c. C-30. Please read the authorization forms which accompany this thesis.

AVIS

La qualité de cette microfiche dépend grandement de la qualité de la thèse soumise au microfilmage. Nous avons tout fait pour assurer une qualité supérieure de reproduction.

S'il manque des pages, veuillez communiquer avec l'université qui a conféré le grade.

La qualité d'impression de certaines pages peut laisser à désirer, surtout si les pages originales ont été dactylographiées à l'aide d'un ruban usé ou si l'université nous a fait parvenir une photocopie de qualité inférieure.

Les documents qui font déjà l'objet d'un droit d'auteur (articles de revue, examens publiés, etc.) ne sont pas microfilmés.

La reproduction, même partielle, de ce microfilm est soumise à la Loi canadienne sur le droit d'auteur, SRC 1970, c. C-30. Veuillez prendre connaissance des formules d'autorisation qui accompagnent cette thèse.

THIS DISSERTATION
HAS BEEN MICROFILMED
EXACTLY AS RECEIVED

LA THÈSE A ÉTÉ
MICROFILMÉE TELLE QUE
NOUS L'AVONS REÇUE

Canada

NL 339 (r. 86/09)

Application of vortex behaviour to oil-water separation and slurry decantation

by

Chi-Fun Wong

A thesis
presented to the University of Ottawa
in partial fulfillment of the
requirements for the degree of
Master of Applied Science
in
Department of Chemical Enginerring

UNIVERSITÉ D'OTTAWA
UNIVERSITY OF OTTAWA

ABSTRACT

Separation of surface oil from water is an important operation for the control of oil pollution and for wastewater treatment. The aim of this study is to develop a method to effectively remove surface oil from water.

A vortex separation method was examined in this research. A steady-state vortex was generated by combining three major actions, namely, (1) the liquid was rotated in the cylindrical vortex tank by means of an inverted 'horse-shoe' stirrer (2) the liquid was withdrawn through the inner outlet pipe from the vortex tank (3) the liquid was recirculated through the annular opening surrounding the inner pipe back into the vortex tank. Under specified operating conditions of stirrer speed and outlet flow rates, vortices of up to 30-cm depth or more could be obtained. When a layer of oil was present on the liquid surface and the vortex depth was equivalent to the liquid depth in the vortex tank, the oil in the vortex-core could be withdrawn together with some of the liquid from the vortex tank. Therefore, the possible application of vortices for removing surface oil from water became apparent.

The present study can be divided into three phases because three different categories of experiments were performed during the course of project. The major variables involved in this study were rotation speed of the stirrer (Ω), depth of the liquid in the vortex tank (H), inner outlet velocity (Vi) and annular outlet velocity (Va).

The first phase of this research, the characteristics of air-water vortices were studied. It was found that the flow pattern of the vortex in this study was similar to Rankine's combined vortex, and the vortex depth was directly related to the above four variables (Ω,H,Vi,Va). The air-water vortex formation was affected when a layer of froth was present on the surface of the water. The effect of the froth on the vortex depth depended on the stirrer rotational speed and the thickness of the froth.

In the second phase of this research, the effectiveness of oil removal under various operating conditions was studied. The oil removal effectiveness was represented by oil removal rate and oil content of the withdrawn two-phase mixture. It was found that the oil removal rate was directly related to the stirrer speed, the inner outlet velocity and the annular outlet velocity, but it decreased as the liquid depth increased. The oil content increased with increasing stirrer rotational speed and annular outlet velocity, but it decreased with increasing liquid depth. Two oil types hav-

ing very different viscosities were utilized in this study, namely Esso#2 furnace oil and paraffin oil. It was found that the oil removal rate was influenced by the viscosity of the oil. The oil removal rate of paraffin oil of high viscosity was much higher than the rate for furnace oil of low viscosity under the same operating condition. The oil removal rate (or the oil content) of the furnace oil increased significantly when a layer of froth was present on the surface of the oil. Under the operating conditions of this study, the maximum oil content was 59.2 % for the paraffin oil, and 48.7 % for the furnace oil. However, the maximum oil content increased up to 94.1 % if a layer of froth was present on the surface of the furnace oil. It might be concluded that the vortex apparatus used in this research could remove surface oil from water effectively. However, some degree of emulsification of the oil and water occurred due to the high shear from the vortex motion. This was a disadvantage for this separation device.

The last phase of this research was a feasibility study of the application of the vortex apparatus for slurry decantation. The results of this phase indicated that the modified vortex apparatus as developed in this study was not successful in separating solid particles from dilute slurry.

ACKNOWLEDGEMENTS

The writer wishes to express his sincere appreciation to Dr. W. Hayduk for his suggestions, valuable comments and friendship throughout the course of this project.

The help received from the technical presonnel of the Chemical Engineering Department made the experimental work possible and is gratefully acknowledged.

Finally, the writer is most indebted to his parents and sisters for their encouragement and support.

NOMENCLATURE

Ai	inside cross-sectional area of the inner outlet pipe.
Aa	area of the annular opening.
d	exit pipe diameter.
da	inside diameter of the outer outlet pipe.
di	inside diameter of the inner outlet pipe.
dp	diameter of particle.
D1	diameter of the vortex tank.
D2	inside diameter of the 'horse-shoe' stirrer.
g	gravitational acceleration.
H	depth of liquid in a tank.
Hc	critical height of liquid in a tank at which air-entraining vortex occurs or top liquid begins to withdraw.
Ho	thickness of surface oil.
Hv	vortex depth (height).
p	pressure within liquid.
p_o	pressure at the surface of liquid.
P	resultant pressure force due to the pressure of the surrounding fluid particles.
P(r)	pressure function, $\int \omega^2 r dr$.
Q	liquid volumetric flow rate in outlet pipe.

Qa liquid volumetric flow rate in the annular outlet pipe.

Qi liquid volumetric flow rate in the inner outlet pipe.

Qoil oil removal rate.

r radial distance of a point from a vertical axis.

s transition radius from forced vortex to free vortex.

ssq local sum of squares of the difference between Vc(s) and its mean, $\sum_{j=1}^{m} (Vcij-\overline{Vc}i)^2$.

S overall sum of squares, $\sum_{i=1}^{n} ssq_i$.

$\overline{V}$ average outlet velocity, (Va+Vi)/2.

Va velocity of a flow in the annular outlet pipe.

Vc combined velocity.

$\overline{Vc}$ mean of combined velocity.

Vi veloctiy of a flow in the inner outlet pipe.

Vs terminal settling velocity of particle.

V_t tangential velocity at a vortex surface.

W weight of the particle of fluid.

z vertical distance of a point from the bottom of of a vortex-core.

Ω rotational speed of the stirrer (rpm)

ρ density of liquid.

ρ_1 density of bottom liquid.

ρ_2 density of top liquid.

ρ_s density of solid particle.

μ viscosity of liquid.

μ_{oil} viscosity of surface oil.

υ kinematic viscosity of liquid (μ/ρ).

ω angular velocity about a vertical axis (radius per unit time).

Γ_f circulation in the region of free vortx = $V_t \cdot r$.

CONTENTS

LIST OF TABLES

LIST OF FIGURES

Chapter I

INTRODUCTION

1.1 GENERAL

Oil spills have disastrous effects on marine life. A major source of accidental oil spills is off-shore drilling. Several chemical and physical treatment methods are available. Nevertheless chemical treatment methods usually involve chemicals which are highly toxic to aquatic life and can do more harm than would have been done by oil. The best way to control accidental oil spills is to confine the oil on the water surface and to remove the oil physically. Therefore, mechanical separation devices are useful for the separation of surface oil from water.

Removal of oily waste from water is an important treatment in wastewater treatment processes. Three major industrial sources of oily waste are the industries for petroleum refining, for manufacturing and machining of metals, and for food processing. In the treatment of oily waste, the primary treatment involves separating the surface oils from water and emulsified oily material. Gravity-type separators are the most commonly used devices in this treatment. A secondary treatment is then required to break the oil-water emulsion and to separate the remaining oil and water. Emulsion can be broken by chemical, electrical or physical methods.

Separation of surface (floatable) oil from water is an important operation for the control of oil pollution and for wastewater treatment. Several different types of oil recovery devices are available for removing surface oil from water, including for example, gravity-type separators and centrifuges. However, some of these devices have a limited capacity and are applicable only in calm waters. As a result, further studies to develop more effective oil recovery devices are necessary.

A vortex can be formed when a liquid is slowly stirred using an inverted 'horse-shoe' stirrer and is simultaneously withdrawn through a central orifice at the bottom of a cylindrical tank. Air-liquid vortex formations in stirred draining tanks have been studied previously at the University of Ottawa, Canada (15,16). Under specified conditions of outlet flow and rotation speed of the stirrer, vortices of up to thirty cm in depth or more can be observed. When a layer of oil is present on the surface of the liquid, and the vortex depth is equivalent to the depth of liquid in the vortex tank, the oil in the vortex-core can be withdrawn together with some of the liquid from the vortex tank. The possible application of vortices for removing surface oil from water becomes apparent. Under controlled conditions, it is possible to produce a vortex which withdraws oil and water (oil-entraining vortex), but not air and oil and water (air-entraining vortex) through the central outlet orifice.

An apparatus was designed utilizing the oil-entraining vortex for removing surface oil from water, and some preliminary studies were carried out in this University (17). Based on the results from the preliminary studies, it was found that modifications were required for the equipment because of the low oil content obtained in mixture withdrawn. A major innovation to the equipment involved the installation of a concentric tube inside the outlet tube of the vortex tank. This inner tube allowed the withdrawal of liquids mainly from the central vortex-core; as a result, the oil content of the withdrawn two-phase mixture was much higher than previously. Whereas water was recirculated through the annular region surrounding the inner tube back to the vortex tank.

The aim of this study was to develop a method to effectively remove surface oil from water. Based on the preliminary information, an improved equipment has been constructed for studying the effectiveness of oil removal under various operating conditions. The major variables involved in the present study were the rotation speed of the stirrer, depth of water in the vortex tank, flow rate in the inner outlet tube, and flow rate in the annular outlet tube. The oil removal rate and the oil content in the withdrawn two-phase mixture were measured for various combinations of these four variables. Two oil types having very different viscosities were utilized in this study, namely Esso #2 furnace oil (low viscosity) and paraffin oil (high viscosity).

The vortex apparatus for oil-water separation can produce steady vortices for a wide range of conditions. Since the vortex motion in the vortex tank generates centrifugal acceleration acting radially outward which is much higher than the gravitational acceleration, it is effective for oil removal and the possible application of vortices for separating solid particles from liquid becomes apparent. A feasibility study for the latter application utilizing a modified vortex apparatus for slurry decantation is included in this study.

1.2 STUDY GOAL

The present study can be divided into three phases because three different categories of experiments were carried out during the course of the project. However, all the experiments were performed at steady-state conditions in which the liquid level and the depth of the oil layer in the vortex tank remained constant; these were accomplished by recirculating the liquid withdrawn and by adding oil to the vortex tank at the same rate it was removed.

The first phase of this research, the characteristics of air-water vortices were studied. Because the outlet of the improved vortex tank consisted of inner and annular outlet tubes, two outlet flows instead of one were considered. In addition, the flow pattern surrounding the vortex was different than that in previous studies. Experiments were per-

formed to study the combined effect of variations in these two outlet flows on vortex formation. The purpose of the first phase can be summarized as follows:

1. To study the effects of the rotational speed of the stirrer, the depth of liquid in the vortex tank, the inner outlet flow rate, and the annular outlet flow rate on the vortex depth.
2. To discover how the inner outlet velocity and the annular outlet velocity may be combined to yield an equivalent vortex-forming condition.
3. To study the effect of surface froth on vortex formation.

In the second phase of this research, the effectiveness of oil removal under various operating conditions was studied. The objectives for the second phase are:

1. To study the effectiveness of oil removal under various operating conditions of the four previously mentioned variables (Ω,H,Vi,Va).
2. To study the effect of oil viscosity on the oil removal rate.
3. To study the effect of the surface froth on the oil removal rate.

The last phase of this research was a feasibility study of the application of the vortex apparatus for separating solid particles from liquid.

Chapter II

REVIEW OF THE LITERATURE

2.1 GENERAL REMARKS

Vortex phenomena have been interesting subjects for physicists and engineers for the past three decades. A considerable amount of experimental research about free vortices and forced vortices have been reported.

When an initially stationary liquid is drained from a vessel through an outlet orifice at the bottom, a vortex is generated on the surface of the liquid just above the drain hole. This is called a 'bath-tub' vortex or a free vortex. The origin of a free vortex has been considered to be the result of the Coriolis forces due to the earth's rotation. However, the Coriolis forces are small compared with other effects such as initial residual motion from the filling of the vessel and boundary layer shearing at the bottom of the vessel. Shapiro (3) performed carefully controlled experiments involving the 'bath-tub' vortex; the results indicated that the free vortex could be developed from the Coriolis forces due to the earth's rotation. Binnie (4) repeated Shapiro's experiments but with an exit pipe protruding a considerable distance upward from the bottom of the tank.

In this way shearing action of the tank bottom on discharging water was reduced. He obtained a counterclockwise rotation (the sense to be expected if the earth's rotation was the cause) in 15 consecutive tests. Sibulkin (5) found that the direction of rotation for the free vortex reversed as the liquid surface approached the bottom of the vessel. He suggested that the boundary-layer vorticity was carried down through the orifice according to Helmholtz's theorem. Kelly, Martin and Taylor, (6) repeated Sibulkin's experiments. They observed that reversal of the initial direction of rotation for the free vortex also occurred if a shock was applied to the system during draining of the vessel, and they proposed an explanation, based on a consideration of the surface waves generated by a shock. Marris (7) and Harada (8) reported detailed theoretical analyses of the free vortex which included the effect of initial liquid rotation.

When a liquid is rotated in a cylindrical tank, a vortex is generated. This is called a forced vortex. Le Lan and Angelino (9) measured vortex shapes and depths of the forced vortices, and observed the effect of stirrer position. Nagata, Yoshioka and Yokoyama (10) studied the angular velocity distribution of the liquid in a cylindrical vessel agitated by a concentric agitator. They reported that the flow pattern in the vessel was similar to Rankine's combined vortex. This latter combined vortex consisted of a forced vortex at center of the vortex and a free vortex in outer region of the vortex.

2.2 PREVIOUS RESEARCH

A vortex can result from many different liquid flow situations. There have been a number of research papers dealing with different aspects of vortex formation.

Lubin and Springer (11) studied the formation of vortices on the surface of an initially stationary liquid draining through a concentric circular orifice at the bottom of a cylindrical tank. Experiments were performed not only with water in contact with air but also with a second immiscible liquid placed on top of the water. They reported that a vortex formed above the outlet orifice on the surface of the bottom liquid at a critical height (Hc), and that, once formed, it grew rapidly and extended into the outlet tube. They also found that the critical height was independent of initial height of the liquid in the tank, and that the outlet volumetric flow rate was nearly constant up to the instance of vortex formation. A simple analytical expression was derived by Lubin and Springer to predict the critical height (Hc) of the liquid at which air-entraining vortex formed or top liquid began to withdraw, The expression was:

$$\frac{Hc}{d} = 0.69 \left[\frac{Q^2}{\left(1 - \frac{\rho_2}{\rho_1}\right) g d^5} \right]^{0.2} \qquad (2.1)$$

This expression is limited to shallow water depths and to situations when there is no induced circulation in the tank.

McDuffie (12) studied the conditions for preventing vortex formation in a downflow system. He presented the critical relation between depth of liquid in the system and liquid volumetric outflow rate for the transition from full liquid outflow to two-phase outflow first for the air-water system (equation 2.2), and next for the liquid-liquid system (equation 2.3):

$$Q \leq 1.26 \left[\frac{g(\rho_{H_2O} - \rho_{AIR})d}{\rho_{H_2O}} \right]^{0.5} H^2 \qquad (2.2)$$

$$Q \leq 1.61 \left[\frac{g(\rho_1 - \rho_2)}{\rho_1} \right]^{0.5} H^{2.5} \qquad (2.3)$$

These equations are also restricted for shallow water depths ($H/d<3$) and outlet pipes of small diameter.

Toyokura and Akaike (13) studied the flow mechanism of the steady 'bath-tub' vortex in a water tank and the formation of air-entraining vortex in the presence of a slight internal tank rotation which was produced by means of guide vanes. They reported the relationship between the critical depth (Hc) at which the air-entraining vortex occurred and the magnitude of circulation (Γ_f) when water was drained from a tank as:

$$\frac{Hc}{d} = 10\left[6.67\left(\frac{\Gamma_f^2}{d^2 g Hc}\right)^{0.25} - 1.34\right] \qquad (2.4)$$

The circulation in this case was written in terms of the tangential velocity.

$$\Gamma_f = V_t . r \qquad (2.5)$$

The above expression is valid for the air-entraining vortex which is generated by draining the water from a cylindrical tank and by simultaneously rotating the water slightly. However, the liquid rotational rates used by Toyokura and Akaike were much lower than those used in the present study. Therefore, this expression cannot be utilized for comparison with results from the present study.

Vortex formation in a stirred draining tank is a complicated phenomenon, because it combines both the forced vortex and the free vortex phenomena.

Lewellen (14) performed a complex analysis of vortex formation in a stirred draining tank. However, the solution of his analysis was limited only to specific cases.

Neale and Hayduk (15,16) studied the factors influencing the vortex depth when liquid was withdrawn from a vessel through a central orifice at the bottom, and was simultaneously stirred by means of an inverted 'horse-shoe' stirrer.

They examined a steady-state situation in which the withdrawn liquid was recirculated back into the vessel via a sparge pipe. They found that the vortex depth was highly dependent upon the stirrer rotational speed, exit flow rate, and exit pipe diameter, and the vortex depth decreased significantly as the liquid viscosity increased.

The flow characteristics near the vortex were studied by injecting blue dye into the water in the above study. It was found that liquid moved rapidly downward at the vortex-core, and moved slowly upward at a little further away from the vortex surface. A postulated flow pattern of vortex is shown in Figure 2.1 .

A relationship between the vortex depth and the pertinent variables was developed using dimensional analysis. For water, the correlation was expressed as:

$$\frac{Hv}{d} = 7.35\times10^{-5}\left(\frac{\Omega d^3}{Q}\right)^{-0.76}\left(\frac{Q}{\upsilon d}\right)^{1.22}\left(\frac{D2\Omega^2}{g}\right)^{0.83}\left(\frac{D2}{d}\right)^{1.62}\left(\frac{H}{d}\right)^{-0.17} \qquad (2.6)$$

For a slightly viscous liquid (viscosity less than 3 mPa.s), the correlation was:

$$\frac{Hv}{d} = 0.035\left(\frac{\Omega d^3}{Q}\right)^{-1.11}\left(\frac{Q}{\upsilon d}\right)^{0.67}\left(\frac{D2\Omega^2}{g}\right)^{0.89}\left(\frac{D2}{d}\right)^{0.95}\left(\frac{H}{d}\right)^{-0.40} \qquad (2.7)$$

The correlations developed by Neale and Hayduk are suitable for relatively high water depths and high stirrer rotation rates. However, these correlations must be used with caution, especially when applied to experiments outside the range used in the original study.

Francois Leclerc studied oil-water separation using a vortex in his senior project; the results of which were reported in his undergraduate thesis (17). He used an apparatus similar to that of Neale and Hayduk (15). Under specified conditions of stirrer speed and outlet flow, a vortex whose depth was equivalent to the liquid height in the vortex tank, was formed. When a layer of oil was present on the top of water, the oil in the vortex-core was withdrawn together with some water through the outlet orifice. Leclerc performed experiments to study the effects of effluent flow rate and orifice diameter on oil removal rate. He concluded that the oil removal rate increased as the effluent flow increased, and the 2.54 cm orifice diameter was the best among the three testing orifice diameters. Leclerc also mentioned that water depth in the vortex tank and rotational speed of the stirrer also affected the oil removal rate.

The maximum oil content of the two-phase liquid mixture in Leclerc's experiments was 33%, with an average of approximately 20%. Based on Leclerc's study, several changes were

made to the experimental apparatus, which later became the improved vortex apparatus used in this study.

2.3 PROCESS DEVICES FOR OIL-WATER SEPARATION

Gravity-type separators are the most common devices employed for the removal of surface (floatable) oil from water. The operation of such separators is usually accompanied by the use of gas flotation, heat, or chemicals addition. The effectiveness of a gravity separator is dependent upon a suitable hydraulic design and an appropriate retention time.

The separation of immiscible liquids by hydrocyclones is attractive from the standpoint of low capital investment and simplicity of operation. A hydrocyclone is a device which utilizes the centrifugal forces for phase separation. By comparison, vortex motion leads to high centrifugal forces, which aid phase separation. Vortex motion can be produced by using a tangential inlet to the cyclone or by providing suitable directing vanes within the equipment. However, liquid-liquid hydrocyclones are much less effective than those employed in solid-liquid separations, because liquid particles tend to disintegrate under the intense shear encountered in the cyclone. Frequently, this size reduction in the liquid droplets leads to emulsification. Therefore, hydrocyclones are not widely used for oil-water separation.

Centrifuges also utilize centrifugal forces for phase separation. There are two popular designs of centrifuge, namely the tubular type and the disk type. The most commonly used design today is the disk type centrifuge which is often operated to generate forces up to 9000 times that of gravity. Centrifuges can be effectively used to separate immiscible liquids of different densities. However, they require a good deal of power and are of relatively low capacity.

2.4 PROCESS DEVICES FOR SLURRY DECANTATION

Sedimentation is an operation used to clarify liquid wastes or to concentrate solid suspensions. Many of the needs in these area are currently handled by gravity clarifiers. However, while effective, gravity clarifiers occupy a considerable amount of space, and the performance is limited by factors such as zeta potential and Brownian movement. Therefore, several solid-liquid separators which occupy less space and perform more successfully have been invented; these are hydrocyclones and centrifuges as discussed in the section concerning oil-water separation.

Whereas hydrocyclones are capable of removing some of the suspended solids in wastewater, they are unable to achieve an effluent quality as high as that achieved by gravity clarifiers. It is found that hydrocyclones tend to disperse

fine floc which may be removed by settling. The use of 'solid-body rotation' such as that obtained in centrifuges is considered to be a better method of separation.

All centrifuges have the same basic operating principles. Solids are removed from the fluid which flows through the machine under the influence of the centrifugal forces. Centrifuges can provide good separation only at low flow rates. Eddy currents, created in the separating zone in the centrifuge at high flow rates, cause the redispersion of settled solids.

Recently, the Bird Machine Company introduced a Vortex Clarifier which was originally developed at Queen's University, Kingston, Ontario. The Vortex Clarifier, a novel form of centrifuge, provides a fairly high fluid-handling capacity. Operation of the Vortex Clarifier is based on a forced-vortex principle. Liquid introduced into the Vortex Clarifier rotates as a solid body with little or no fluid shear which may create turbulence and redispersion of settled solids. The settled solids are collected on the wall of the rotating bowl and subsequently discharged using a predetermined automatic sequence. The Vortex Clarifier is suitable for removing fine particles from fluids at relatively high flow rates; its chief disadvantages are its high cost, and high energy consumption.

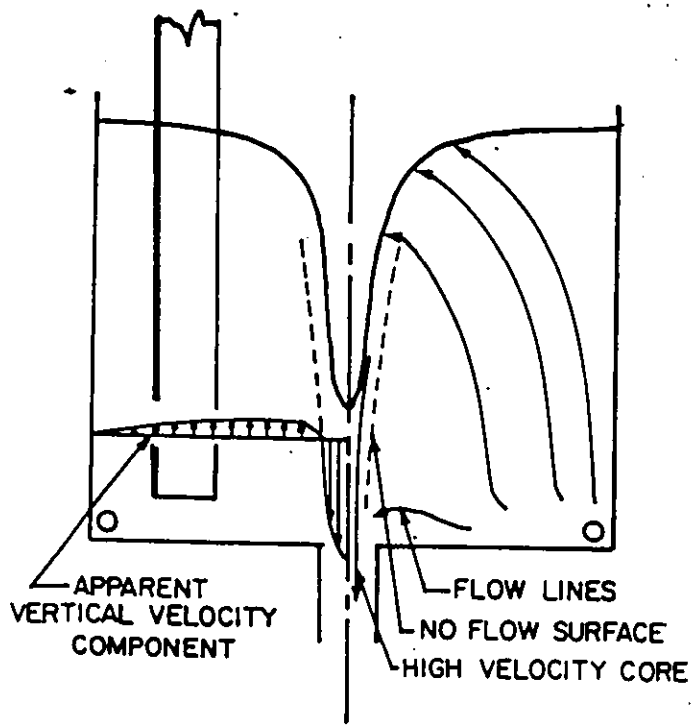

Figure 2.1: POSTULATED FLOW PATTERN (VERTICAL COMPONENT)(15)

Chapter III

THEORETICAL SHAPE OF FORCED VORTEX, FREE VORTEX AND RANKINE'S COMBINED VORTEX

3.1 GENERAL REMARKS

Vortices are frequently encountered in day-to-day life. There are many different liquid flow situations which may result in the formation of a vortex. A free vortex is formed when an initially stationary liquid is drained by gravity from a vessel through an orifice at the bottom. A forced vortex is formed when a liquid is rotated in a cylindrical tank. A compound vortex motion has been well known for a long time, and is called Rankine's combined vortex. It consists of an inner cylindrical core rotating as a solid body (forced vortex), surrounded by a free vortex. Equations of the surfaces of constant pressure for the above three vortex types will be discussed in detail in the following section.

3.2 THEORETICAL SHAPE OF FORCED VORTEX, FREE VORTEX, AND RANKINE'S COMBINED VORTEX

3.2.1 General Consideration

A fluid of constant density and viscosity, rotated about a vertical axis, is shown in Figure 3.1 . The motion is

steady, and the angular velocity (ω) about the vertical axis is assumed to be a function only of r, where r is the radial distance of the point from the axis. Hence a particle of fluid having a weight of W describes a circular path in a horizontal plane with a constant speed of ωr; its acceleration is radial and inward and has a magnitude of $\omega^2 r$. An inertia force $(W/g)\omega^2 r$ acts in a radial direction away from the axis of rotation. This is called the centrifugal force. The pressure is dependent upon r because of the centrifugal force and upon z because of the gravitational force. Thus the pressure gradients can be expressed as follows:

$$\frac{\partial p}{\partial r} = \rho \omega^2 r \tag{3.1}$$

$$\frac{\partial p}{\partial z} = -g\rho \tag{3.2}$$

A pressure function may be defined as follows:

$$P(r) = \int \omega^2 r dr \tag{3.3}$$

It can be determined when ω is a given function of r. Since p is an analytic function of position, p=p(r,z), dp can be written as:

$$dp = \frac{\partial p}{\partial r} dr + \frac{\partial p}{\partial z} dz \tag{3.4}$$

Substituting equations (3.1) and (3.2) into equation (3.4) and integrating yields:

$$p = \rho P(r) - g\rho z + K \tag{3.5}$$

In the above expression, K is a constant of integration.

3.2.2 Forced Vortex

For a forced vortex, the fluid rotates about the vertical axis like a rigid body; in this case the rotation speed ω is independent of r. Equation (3.3) can now be written as:

$$P(r) = \frac{1}{2}\omega^2 r^2 \tag{3.6}$$

By applying the condition that $p=p_o$ at $r=0$ and $z=0$, equation (3.5) becomes:

$$p = \frac{1}{2}\rho\omega^2 r^2 - g\rho z + p_o \tag{3.7}$$

In the above expression, p_o is the pressure on the liquid surface. The surfaces of constant pressure are therefore the paraboloids of revolution:

$$z = \frac{\omega^2 r^2}{2g} + \frac{p_o - p}{g\rho} \tag{3.8}$$

In particular, the free surface of the liquid ($p=p_o$) for the forced vortex is parabola in shape (Figure 3.2).

An analysis of a forced vortex can be performed using another approach. The free surface of the liquid for the force vortex is curved as indicated in Figure 3.3 . There are a total of three forces acting on the fluid element at point A. They are the weight of the element W, the resultant force due to the pressure of the surrounding fluid particles P which is normal to the curved surface, and the centrifugal force $(W/g)\omega^2 r$ acting radically outward. Since these three forces are in equilibrium, we have:

$$P \sin\theta = \frac{W}{g}\omega^2 r \qquad (3.9)$$

$$P \cos\theta = W \qquad (3.10)$$

It is apparent that:

$$\tan\theta = \frac{\omega^2 r}{g} = \frac{dz}{dr} \qquad (3.11)$$

The tangential velocity V_t is equal to ωr; then from equation (3.11), V_t can be obtained as:

$$V_t = \sqrt{g.r.\tan\theta} \qquad (3.12)$$

Integration of equation (3.11) gives the equation of the curved free surface which is the equation of a parabola:

$$z = \frac{1}{2}\frac{\omega^2 r^2}{g} \qquad (3.13)$$

Equation (3.13) is actually equivalent to equation (3.8) for $p=p_o$ at the free surface.

3.2.3 Free Vortex

For a free vortex, the motion of the fluid is irrotational, which means that although each small element of fluid describes a fixed circular path, it has a zero rate of spin about its own axis.

Consider an infinitesimal element of fluid between two concentric streamlines as shown in Figure 3.4 . The radius of curvature of the path is r, and the tangential velocity is V_t . The infinitesimal element has a height dr, and an average area dA along the curved surface. There is a centrifugal force $\rho dAdr(V_t^2/r)$ acting on the element radially outward, and a resultant pressure force dpdA acting on the element radially inward. Due to the balance of forces in the radial direction, the following equation can be obtained.

$$dpdA = \rho\frac{V_t^2}{r}dAdr$$

$$dp = \rho \frac{V_t^2}{r} dr \qquad (3.14)$$

For a free vortex, the streamlines are concentric circles. If the fluid is incompressible and frictionless, and the elevation changes are negligible, the Bernoulli's equation for one streamline can be represented as:

$$p + \frac{1}{2} \rho V_t^2 = \text{constant} \qquad (3.15)$$

Equation (3.14) can be rewritten as:

$$\frac{dp}{dr} = \rho \frac{V_t^2}{r} \qquad (3.16)$$

and the derivative of equation (3.15) with respect to r is:

$$\frac{dp}{dr} = - \rho V_t \frac{dV_t}{dr} \qquad (3.17)$$

Combining equations (3.16) and (3.17) gives a differential equation which can be separated and integrated to yield:

$$\frac{dV_t}{V_t} + \frac{dr}{r} = 0$$

$$V_t . r = c = \text{constant}$$

or

$$V_t = \frac{c}{r} \tag{3.18}$$

For this situation, the velocity varies inversely as the radial distance from the axis, and the angular velocity varies inversely with square of the radial distance:

$$\omega = \frac{c}{r^2} \tag{3.19}$$

According to equation (3.3), we therefore have:

$$P(r) = \frac{-c^2}{2r^2} \tag{3.20}$$

Equation (3.5) becomes:

$$p = K - \frac{\rho c^2}{2r^2} - g\rho z \tag{3.21}$$

The surfaces of constant pressure are given by:

$$z = \frac{(K-p)}{g\rho} - \frac{c^2}{2gr^2} \tag{3.22}$$

Therefore, the free surface of the liquid for the free vortex is hyperboloidal in shape (Figure 3.5).

Equation (3.18) indicates that the tangential velocity becomes infinitely large when r approaches zero. An infinite velocity is not realistic for real fluid. In actual flows, viscous shear effects cause a portion of the fluid in the region near r = 0 to rotate like a solid body. Outside this central core is a transition region; outside the transition region is a free vortex. The velocity distribution for this combination of vortex types is shown in Figure 3.6 . This flow pattern is known as Rankine's combined vortex.

3.2.4 Rankine's Combined Vortex ,

Rankine's combined vortex consists of an inner cylindrical core of radius s rotating as a solid body with an angular velocity ω , surrounded by a free vortex. The velocity is continuous at the radius s of the combined vortex. By equation (3.19):

$$c = \omega s^2 \qquad (3.23)$$

The pressure in the core ($s \geq r \geq 0$) is given by the equation as obtained for a forced vortex (equation 3.7), and the surfaces of constant pressure in the core are described by equation (3.8). The pressure at s is:

$$p(s) = \frac{1}{2} \rho \omega^2 s^2 - g\rho z + p_o \qquad (3.24)$$

However the pressure is continuous at s and can be described by equation (3.21):

$$p(s) = K - \frac{\rho_c^2}{2s^2} - g\rho z$$

or

$$K = p(s) + \frac{\rho_c^2}{2s^2} + g\rho z \qquad (3.25)$$

Substituting equations (3.23) and (3.24) into equation (3.25) yields:

$$K = \rho\omega^2 s^2 + p_o \qquad (3.26)$$

Hence, by using equations (3.21) and (3.23), the pressure when $r > s$, is given by:

$$p = p_o + \rho\omega^2 s^2 \left(1 - \frac{s^2}{2r^2}\right) - g\rho z \qquad (3.27)$$

The surfaces of constant pressure are therefore given by:

$$z = \frac{\omega^2 s^2}{g}\left(1 - \frac{s^2}{2r^2}\right) + \frac{p_o - p}{\rho g} \qquad (3.28)$$

Thus, as indicated by equations (3.8) and (3.28), the free surface of the liquid for Rankine's combined vortex has a dimple form as shown in Figure 3.7 .

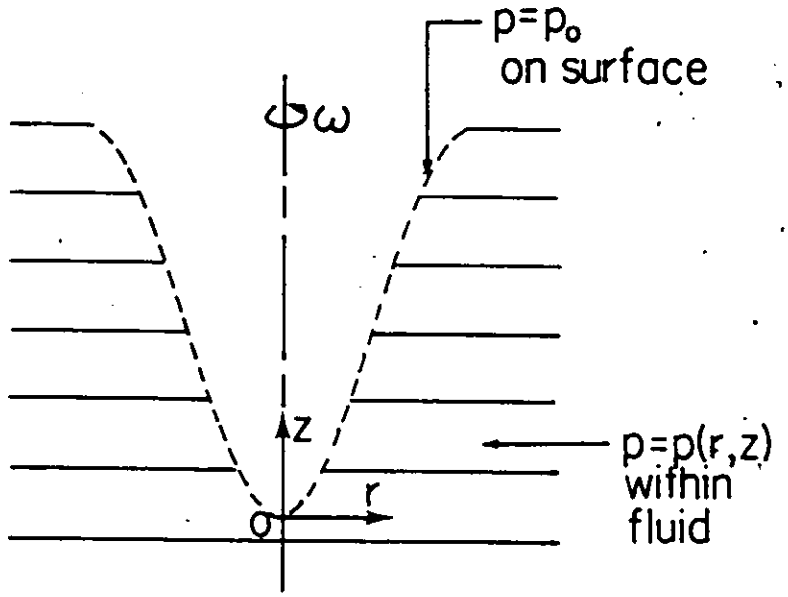

Figure 3.1: STEADY ROTATION OF A FLUID ABOUT A VERTICAL AXIS

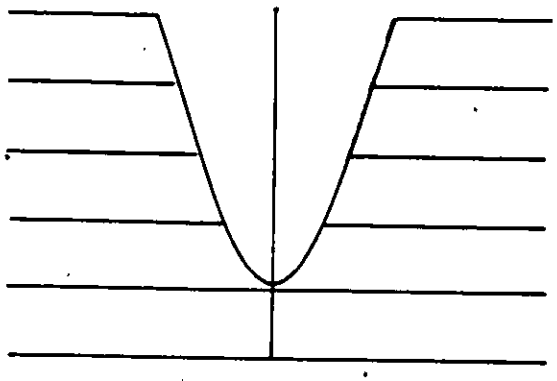

Figure 3.2: SHAPE OF A FORCED VORTEX

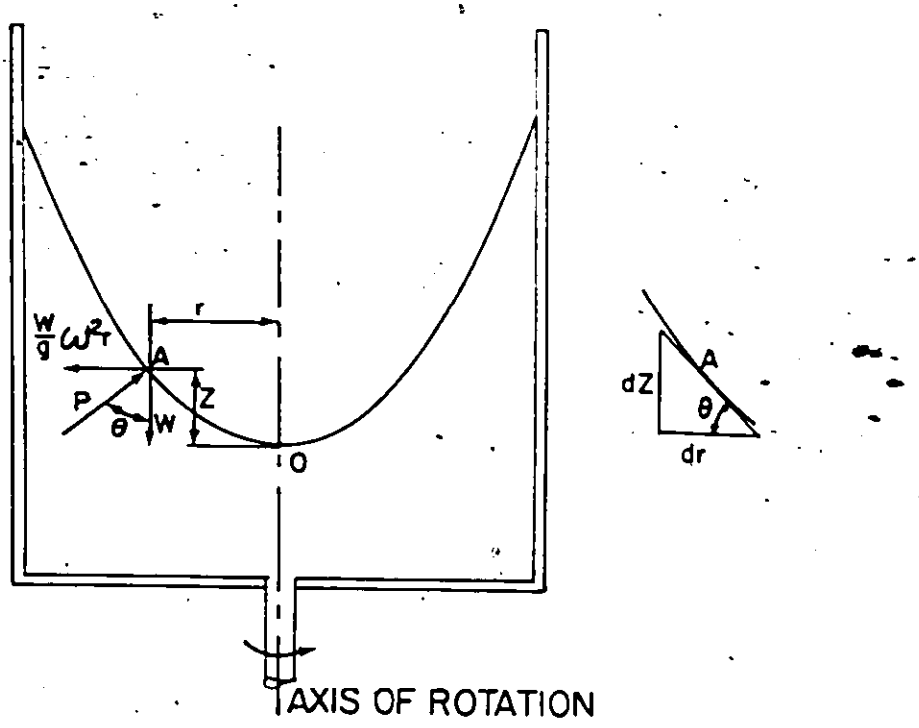

Figure 3.3: ROTATING BODY OF LIQUID

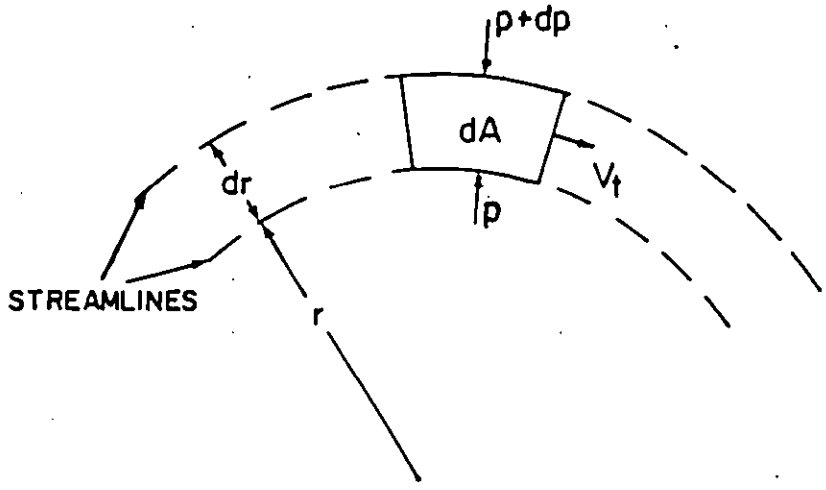

Figure 3.4: AN ELEMENT OF FLUID IN A CURVED PATH

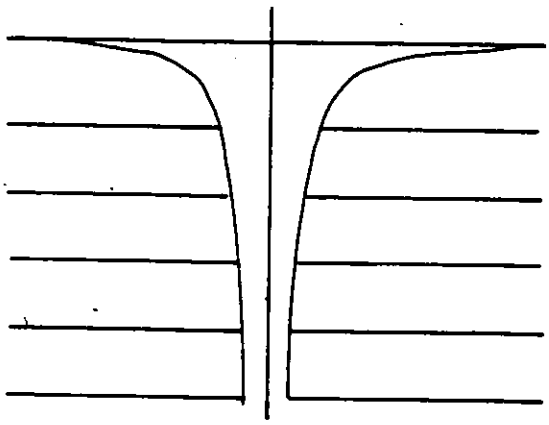

Figure 3.5: SHAPE OF A FREE VORTEX

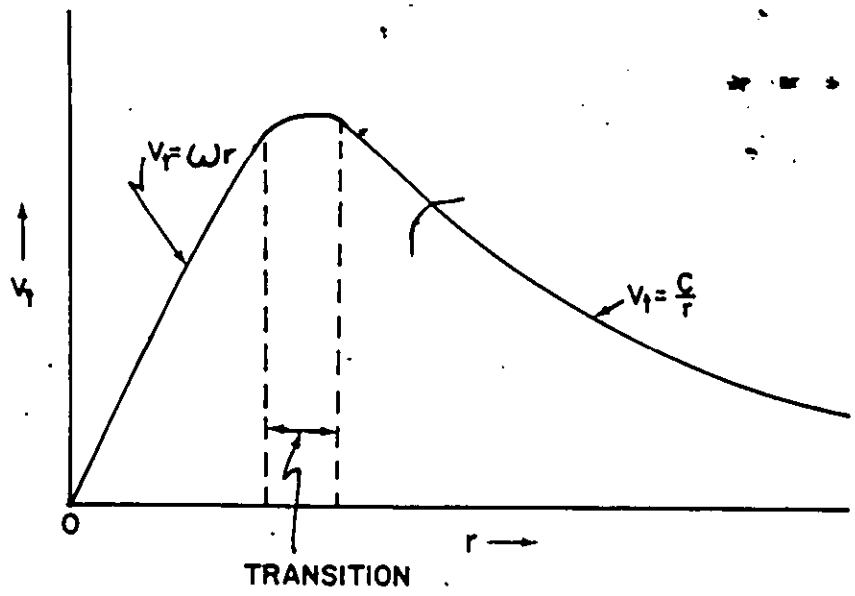

Figure 3.6: VELOCITY DISTRIBUTION OF A COMBINED VORTEX

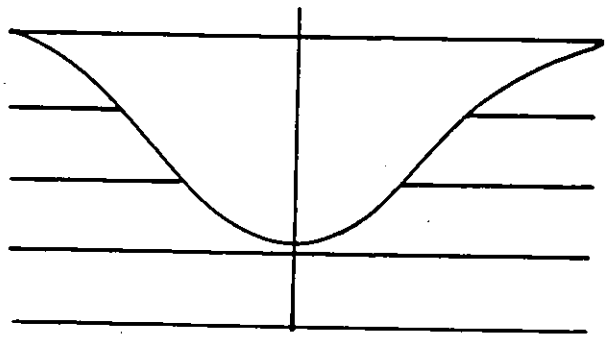

Figure 3.7: SHAPE OF A COMBINED VORTEX

Chapter IV

EXPERIMENTAL WORK AND INSTRUMENTATION

4.1 GENERAL CONSIDERATION OF EXPERIMENTAL APPARATUS

Based on the information from the preliminary study (17), an improved experimental apparatus has been constructed. A schematic sketch of the experimental set up is shown in Figure 4.1, and detailed descriptions of the equipment are listed in Table 4.1 .

The equipment consisted mainly of a 60-cm diameter cylindrical plexiglas vortex tank (T1) equipped with a 'horse-shoe' stirrer, a plexiglas vacuum tank (T2) and an oil supply tank (T3). All these tanks were interconnected with circulation pumps and rotameters for circulation and flow measurement.

The 'horse-shoe' stirrer, of 37.5 cm inside diameter, was mounted concentrically within the vortex tank, with its rotation speed being controlled by a variable speed drive of speed ranging from 0 to 50 rpm. The stirrer blades were 5 cm wide, and were mounted 3 cm above the bottom of the vortex tank (T1) and 5 cm from the tank wall. The dimensions of the 'horse-shoe' stirrer are shown in Figure 4.2 .

An outlet pipe of 2.54 cm inside diameter was centrally located at the bottom of the vortex tank, and an inner outlet pipe of 1.6 cm outside diameter and 1.27 cm inside diameter with a bevelled sharp-edge was located concentrically inside the 2.54 cm i.d. outlet pipe. The arrangement of the outlet pipes at the bottom of the vortex tank is shown in Figure 4.3 .

Liquid was withdrawn from the vortex tank through the annular opening, and was recirculated back into the vortex tank by means of a centrifugal pump (P1). The recirculated stream was distributed through a sparge tube. This sparge tube located at the bottom perimeter of the vortex tank and with holes facing the tank wall, precluded any disturbance to a steady vortex formation. The annular flow was measured by a rotameter (R1) and was controlled by a valve (V1). As a result of the pump work, the liquid temperature tended to rise slowly during the experiments; a shell-and-tube heat exchanger (H1) was installed on line to keep the liquid at a constant temperature.

A portion of the liquid in the vortex tank could be withdrawn through the inner outlet pipe into the vacuum tank utilizing the pressure difference between the vortex tank and the vacuum tank. This inner flow was controlled by a valve (V3) as well as the degree of vacuum in the vacuum tank.

The liquid in the vacuum tank could be transferred back into the vortex tank by means of a centrifugal pump (P2) through the sparge tube. This flow was again, measured and controlled by a rotameter (R2) and a valve (V2). A heat exchanger (H2) was installed to control the liquid temperature.

Whereas the first phase of the experiments involved air-water vortices, the second phase involved oil-water vortices. For the oil-water separation experiments, oil-water mixtures were withdrawn from the vortex tank through the inner outlet pipe into the vacuum tank. The oil was accumulated in the vacuum tank while the water was continuously pumped back to the vortex tank by means of the pump (P2) to maintain a steady water level in the vortex tank. The purpose for utilizing the vacuum tank instead of a pump was to prevent emulsification of oil and water and to prevent air-entrainment in the pump.

The steady state oil removal rate was determined by measuring the rate of oil accumulation in the vacuum tank. The thickness of the oil layer in the vortex tank was kept steady by adding oil to the vortex tank from the oil supply tank (T3) at the same rate as it was removed.

For certain experiments, the vortex motion generated complicated internal flow patterns and high shear rates which caused emulsification of oil and water. Therefore, an emul-

sion breaker was installed at the inlet to the vacuum tank; it consisted of a 7.6 cm inside diameter Plexiglas tube packed with small (0.6 cm) Berl saddles to a depth of 28.0 cm. Compared to other packing materials of similar size, the ceramic Berl saddle packing was found to be the most effective.

The third phase of this research involved utilizing a vortex for the separation of solid particles from a slurry. Procedures, for the experiments and modifications of the equipment for each of the three phases will now be decribed in detail in the following sections.

4.2 EXPERIMENTAL WORK FOR PHASE I, INVOLVING AIR-WATER VORTICES

4.2.1 Air-Water Vortex Experiments

Phase I was aimed to study the effects of rotation speed of the stirrer (Ω), water depth in the vortex tank (H), inner outlet flow rate (Vi) and annular circulation flow rate (Va) on the vortex depth (Hv).

The equipment was set up as shown in Figure 4.1, but with the emulsion breaker removed. Rotameters except the one for oil supply (R4) were calibrated using distilled water as a fluid at 25.0°C. Calibration curves for the annular circulation rotameter (R1), the water return rotameter (R2), and the inner outlet flow rotameter (R3) are included in Appendix A.

The inner outlet velocity (Vi) and the annular outlet velocity (Va) were systematically measured for vortex depths (Hv) equivalent to half of the water depth (H) and also equivalent to the full water depth, at each of nine combinations of the stirrer rotational speeds (Ω=3,5,10 rpm) and the water depths in the vortex tank (H=10.0,20.0,30.0 cm). The procedure for the experiments is summarized as follows: the vortex tank (T1) was filled with distilled water to a predetermined height. The annular circulation valve (V1), the water return valve (V2), the inner flow valve (V3) and the oil supply valve (V4) were initially kept closed. With the vacuum pump (P3) turned on, the vacuum indicator (PI) was set to about -15 in. Hg by adjusting the vacuum control valve (V5). The inner flow valve (V3) was then opened, and the water was withdrawn through the inner outlet pipe into the vacuum tank until the water depth in the vortex tank had reached a pre-specified depth. The inner flow rate (Vi) was now adjusted to a specified experimental value by means of the valve (V3) and the rotameter (R3), while the water in the vacuum tank was pumped back, at the same rate as that of the inner flow, using the pump (P2). Therefore, the water level in the vortex tank was kept constant by adjusting the flow rate of the returned water. Once a steady water level was achieved in the vortex tank, the stirrer was switched on and set to a specified experimental speed. The rotation speed of the stirrer was measured using a stopwatch. Under

the above liquid flow condition, a stable vortex was formed. The annular circulation pump (P1) was then turned on, and the annular flow rate was increased slowly by means of the annular circulation valve (V1) until a vortex depth (Hv) equivalent to half of the water depth (H) was observed. The vortex depth was measured by using two metric scales which were located at opposite sides of the vortex tank. The temperature of water in the system was maintained at 25±0.5°C by means of the coolers (H1 and H2). The steady-state vortex depth was kept under close observation for at least 5 minutes; then the inner and annular flow rates were recorded. The same procedure was repeated for a vortex depth (Hv) equivalent to the full depth of water (H).

The range of the four principal variables for which measurements were made were: (1) rotation speed of the stirrer of 3 rpm to 10 rpm, (2) water depth in the vortex tank of 10.0 cm to 30.0 cm, (3) inner outlet velocity of 0.00 cm/s to 92.71 cm/s, and (4) annular outlet velocity of 0.00 cm/s to 149.50 cm/s. It was found that any serious vibration or jolting of the vortex tank reduced the vortex depth. It was also found that if the vortex tank was not set up vertically, the vortex depth was affected. Therefore four levelling screws were mounted at the base of the equipment to ensure that the vortex tank was level. Some experiments were reproduced as replicates. In general, the experimental results obtained in this phase were highly reproducible.

4.2.2 Air-Water Vortex Experiments "With Surface Froth"

Experiments were carried out to study the effect of surface froth on vortex formation. 'Steinberg' dish detergent was used to produce froth simply because this detergent proved to be a very good foaming agent.

A thick layer of froth was created on the surface of water by stirring approximately 1 part of detergent to 3,000 parts of water in the vortex tank. The mean thickness of the froth was about 1.5 cm, and the distribution of the froth in the tank was not uniform (Figure 4.4a). The procedure for these experiments was identical to that for the air-water vortex experiments (section 4.2.1). Some sixteen selected tests were performed using the same operating conditions as for some of the air-water vortex experiments, so that the effect of the surface froth on vortex formation could be observed.

A second set of experiments using a thin layer of froth, produced on the surface of the water by stirring approximately 1 part of detergent to 30,000 parts of water were performed. The mean thickness of the froth was about 0.5 cm, and the distribution of the froth was quite uniform (Figure 4.4b). Eleven tests were carried out for the same operating conditions of the above 'with froth' experiments. Hence, the effect of the froth thickness could be observed. Some replicate experiments were performed to determine the reproducibility.

4.3 EXPERIMENTAL WORK FOR PHASE II, INVOLVING OIL-WATER VORTICES

4.3.1 General Considerations

The experiments carried out in this phase can be divided into three series based on their scope. The first series of the experiments was utilized to determine the operating conditions of the principal variables (Ω,H,Va,Vi) for incipient oil entrainment and incipient air-oil entrainment. The second series of experiments were performed to study the effects of the four major variables (Ω,H,Va,Vi) and the viscosity of the oil on the oil removal rate. The last series was used to study the effect of surface froth on the oil removal rate.

The equipment for oil-water separation experiments was set up exactly as shown in Figure 4.1 . All experiments in this phase were carried out at steady state. The water and oil depths in the vortex tank were kept constant by returning water from the vacuum tank and by adding oil to the vortex tank respectively. All the measurements were carried out at 25.0±0.5°C, and the temperature of the liquid was controlled by means of the two heat exchangers.

Distilled water was used in all oil-water separation experiments, because preliminary trials with tap water indicated that a high degree of emulsification of oil and tap water occurred. Even with distilled water , some emulsifi-

cation of the oil and water did occur and as a result, the water became somewhat opaque.

4.3.2 Measurements of Density, Viscosity and Surface Tension of the Oils Used

Two types of oil having very different viscosities were used in this study, so that the effect of viscosity on oil-vortex formation and on oil removal rate could be examined. The paraffin oil (high viscosity) was purchased from Fisher Scientific Company (white, heavy paraffin oil, Saybolt viscosity 335/365), whilst the Esso#2 furnace oil (low viscosity) was the household delivery grade obtained from the Esso distribution centre. The densities of the oils were measured by means of calibrated pycnometer bottles. The viscosities of the oils were measured by calibrated Cannon-Fenske routine viscometers utilizing a 'Temp-Trol' viscosity bath. The surface tensions of the oils were measured by means of a Fisher, Model 215 Autotensiomat Surface Tension Analyzer which was based on the principles of du Nouy ring and Wilhelmy plate method. The properties of the two oils at three different temperatures are shown in Table 4.2 , and the experimental data for the above measuremants are shown in Appendix B.

4.3.3 Calibration of the Rotameters

Since the densities and the viscosities of the oils were relatively different from those of water, different rotameter calibrations were required for each liquid used. The calibration curves for the inner outlet flow rotameter (R3) and the oil supply rotameter (R4) for the two oils are given in Appendix C. However, the calibration of the inner outlet flow rotameter (R3) was difficult because two-phase mixtures having both a high oil content and a low oil content flowed through this rotameter during different operating conditions. It was impractical to calibrate the rotameter for each operating condition. Hence, an approximate method was used to calibrate this rotameter by taking the average value of the volumetric flow rate of the high oil content and the low oil content mixtures at the same reading of the rotameter for the calibration. The high oil content and low oil content withdrawn mixtures could be achieved by varying the annular circulation flow. Because the densities of liquids flowing through the annular circulation rotameter (R1) and water return rotameter (R2) were close to the density of water, the rotameter calibration curves for distilled water could be used (Figures A1 and A2).

4.3.4 Procedure for the First Series of Experiments in Phase II

The purpose of the first series of experiments was to define the conditions of the two outlet flows for incipient oil entrainment and incipient air-oil entrainment at various conditions of the water depth (H) and the rotation speed of the stirrer (Ω). Thus the operating range of the inner and annular flow rates for oil entraining vortex could be determined.

The incipient oil entrainment is defined as the oil-vortex depth equivalent to the water depth (H) in the vortex tank (Figure 4.5), but with no oil being actually withdrawn out of the tank. The incipient air-oil entrainment is defined as the depth of the air-core of the oil-vortex equivalent to the water depth (H) in the vortex tank (Figure 4.6); however, in this case, some oil (but no air) were being withdrawn from the tank.

The experimental procedure for the two types of oil were identical. The vortex tank (T1) was filled with distilled water to a predetermined height. All the control valves were initially closed. After the vacuum pump (P3) was turned on, the inner flow valve (V3) was opened; the water was withdrawn from the vortex tank into the vacuum tank until the water level in the vortex tank had reached a desired experimental height (H). The oil supply valve (V4) was then

opened, and the oil was pumped into the vortex tank from the oil supply tank (T3) by the pump (P4) until 1.0 cm of oil was accumulated on the surface of the water. The annular circulation pump (P1) was turned on, and the annular flow rate (Va) was set to a pre-specified rate using the annular circulation valve (V1). The stirrer was switched on, and was set to the desired speed. The stirrer rotational speed was measured by a stopwatch. The vacuum pump was turned on again, and the vacuum indicator was set to about -15 in. Hg. The inner flow rate was increased slowly using the inner flow valve (V3) until incipient oil entrainment existed. At the same time, water in the vacuum tank was returned at the same rate as the inner flow rate to the vortex tank to maintain a steady water level in the vortex tank. Once the inner flow rate for incipient oil entrainment was recorded, the inner flow rate was continuously increased until the incipient air-oil entrainment occurred, and this inner flow rate was then also recorded. For incipient air-oil entrainment, oil and water were withdrawn together out of the vortex tank. Therefore, it was necessary that the oil thickness in the vortex tank remained steady; this was accomplished by adding oil from the oil supply tank (T3). The above procedure was repeated for different combinations of the inner flow rate and the annular flow rate for incipient oil and incipient air-oil entrainments at various water depths and rotation speeds.

Some emulsification of the oil and water did occur during the experiments because the vortex motion and flow through the equipment generated high shear. The water thus became somewhat opaque, and the observations for the depth of the oil-vortices were difficult. Therefore, the distilled water was replaced frequently in this series of experiments for better observations and more accurate results. Nine groups of experiments were carried out at different combinations of the stirrer rotational speeds (3,5,10 rpm) and the water depths (10.0,20.0,30.0 cm). The ranges of the four principal variables in this series of experiments were: (1) the rotation speed from 3 rpm to 10 rpm, (2) the water depth of 10.0 cm to 30.0 cm, (3) the annular outlet velocity from 0.00 cm/s to 47.36 cm/s and (4) the inner outlet velocity from 0.55 cm/s to 98.55 cm/s.

4.3.5 Procedure for the Second Series of Experiments in Phase II

The purpose of the second series of experiments was to study the effects of the four principal variables (Ω,H,Va,Vi) and the viscosity of the oil on the oil removal rate. Based on the results of the first series of experiments, the operating conditions of the four principal variables for oil-water entraining vortex were determined for the oils. The oil removal rates were measured for at least three different levels of each of the four variables. The

ranges of the variables for which measurements were made included: (1) the rotation speed of the stirrer of 3 rpm to 10 rpm, (2) the water depth of 10.0 cm to 30.0 cm, (3) the annular outlet velocity from 0.00 cm/s to 70.58 cm/s and (4) the inner outlet veloctiy from 28.61 cm/s to 106.47 cm/s.

The procedure in this series of experiments was similar to that for the first series of experiments. The water level and oil depth in the vortex tank were first set to desired experimental values such as in the first series. The stirrer was then turned on at a pre-set speed. The annular flow rate was adjusted to a predetermined rate. The vacuum pump (P3) was turned on, and the pressure ajusted to -15 in. Hg using the valve (V5). The inner flow rate (Vi) was then set to a pre-specified rate while the water in the vacuum tank was returned into the vortex tank to maintain a constant water level in the vortex tank. Under the above condition, a stable oil-vortex formed. The oil layer in the vortex tank was kept steady by adding oil into the tank. Usually the system became steady after about 5 minutes, and the thickness of the oil accumulated in the vacuum tank at that time was recorded. The system was operated at steady state for another 5 minutes, and then shut down. The thickness of oil accumulated in the vacuum tank was recorded after an elapsed time of about 30 minutes for the coalesence of the oil. The oil removal rate and the oil content in the inner flow were determined from the difference in quantity of the oil accumulated in the vacuum tank.

4.3.6 Procedure for the Third Series of Experiments in Phase II

The last series of experiments were performed to study the effect of the surface froth on the oil removal rate. The froth was produced by introducing the feed oil from a tube located some distance above the surface of the oil in the vortex tank. The feed oil carried a small amounts of air into the oil layer, which continuously generated a thin layer of froth on the surface of the oil. However, this froth producing method was successful only with furnace oil but not with the more viscous paraffin oil, because most of the air bubbles were trapped inside the high viscous paraffin oil layer. The procedure of the experiments was exactly the same as for the second series of experiments in this phase.

The surface froth for the separation of paraffin oil from water was generated by means of a detergent. The foam from the detergent was first generated in a small tank, and then transferred to the surface of the oil. However, these tests did not appear to work well because there were some reactions between the oil and the detergent foam.

4.4 EXPERIMENTAL WORK FOR PHASE III

Finally some experiments were performed as a feasibility study utilizing the vortex apparatus for the purpose of slurry decantation. It was considered that there were two significant forces acting on the particles of the slurry during the experiments, namely a gravity force acting vertically downward and a centrifugal force from the vortex motion acting radially outward. Therefore, this separation process was assumed to combine sedimentation and centrifugal separation simultaneously.

The slurries in these experiments were perpared using distilled water and a small amounts of fine USP calcium carbonate precipitated powder which was purchased from the J. T. Baker Chemical Company. The distribution of the particle sizes was estimated by a settling method. The distribution curve and the experimental data are presented in Appendix D. The average particle size of 10.2 μm was estimated by means of a settling experiment utilizing a 3 wt. % calcium carbonate slurry. The procedure for the above estimation is reported in Appendix D.

The concentration of the slurry was measured by a Fisher, model DRT 100, light scattering photometer. The photometer was calibrated using known concentrations of calcium carbonate slurries. The calibration curve is shown in Appendix E. The concentrations of the slurries used in these experiments ranged from 0.0219 wt.% to 0.0969 wt.% calcium carbonate.

Some equipment modifications were necessary in this phase of the research. An agitator was installed in the oil supply tank (T3), that became a slurry preparation tank. Two sampling points were installed, one was at 12.0 cm above the bottom of the vacuum tank, and the other was at the water return line. A 65.0-cm pipe instead of the emulsion breaker was installed at the inlet of the vacuum tank for better mixing in the vacuum tank.

Since very dilute calcium carbonate solutions were used in these experiments, and the solubility of calcium carbonate was low, the densities and the viscosities of the solutions were expected to be very close to those of the distilled water. The rotameter calibration curves for distilled water were used to represent the calibration curves for the dilute slurry.

For these experiments, the vortex depth was required to be equivalent to the liquid depth in the vortex tank. The operating conditions for the four variables (Ω,H,Va,Vi), for a vortex whose depth was equal to the liquid depth in the vortex tank, were previously determined as described in the initial experiments of phase I.

The procedure for the experiments in this phase is summarized as follows: a dilute calcium carbonate slurry was prepared in the slurry preparation tank (T3) and was agitated by the agitator. The slurry was allowed to stay in the

tank for 5 minutes so as to settle out the larger-sized particles. This dilute slurry was then transferred into the vortex tank by means of the pump (P4). The above procedure was repeated until a predetermined liquid height in the vortex tank was reached. The pre-set stirrer and annular circulation pump (P1) were turned on to stir and to circulate the solution in the vortex tank to reduce the rate of sedimentation. The solution was then withdrawn from the vortex tank into the vacuum tank until the desired experimental liquid height in the vortex tank was reached. After the annular flow rate was set to the desired rate, the vacuum pump (P3) was turned on again, and the vacuum indicator (PI) was adjusted to -15 in. Hg. The inner flow rate could be set to the pre-specified rate by the inner flow valve (V3), while the slurry depth in the vortex tank was kept steady by returning liquid from the vacuum tank. The temperature of the solution was maintained at 25.0±0.5°C by means of the two heat exchangers (H1 & H2). Under the above conditions, a stable vortex could be formed. Two samples were taken by means of a 50-ml pipet, from the top and the bottom liquid levels in the vortex tank; the average concentration of these two samples represented the initial concentration of the solution in the vortex tank. The system was kept steady, and allowed to run for at least another 30 minutes (at least 3 retention times of liquid in the vacuum tank). The system then shut down, and 50.0 ml samples were with-

drawn from the two sampling points (S1 & S2). The average concentration of these samples represented the concentration of 'clarified' liquid. Again, two samples were withdrawn from the top and the bottom liquid levels in the vortex tank; the average concentration of these samples represented the final concentration of solution in the vortex tank.

However, after several data were collected, it was found that the results were somewhat inconsistent. For instance, the concentrations of the liquid in the vacuum tank in some cases were higher than the initial average concentrations of the solution in the vortex tank. The probable reason for this inconsistency is as follows: the solution at the lower level of the vortex tank was continuously withdrawn into the vacuum tank, and the solution at that level was slightly more concentrated than that at the top of the liquid due to sedimentation. Therefore, it was considered that the outlet tubes were required to extend upward for the purpose of preventing the concentrated of the slurry at the lower level of the tank to be withdrawn. Two 5-cm long tubes with suitable diameters were fitted onto the inner outlet tube and the annular circulation tube, and these were designed so that they could be installed or removed easily. As a result, three different outlet layouts were possible: (1) only annular tube to be extended (layout A); (2) both inner and annular tubes to be extended (layout B) and (3) only inner tube to be extended (layout C). These three layouts are shown in Figures 4.7 .

Six experiments for each layout were carried out at a water depth of 10.0 cm and at various conditions of the stirrer rotational speed, the inner and annular outlet velocities. The results of the experiments showed that the layout C (only inner tube extended) was the best among those three layouts. Therefore, layout C was adopted for the rest of the experiments, and the procedure for the experiments was the same as that previously described. The ranges of the four major variables in these experiments were: (1) the rotation speed of the stirrer from 3 rpm to 10 rpm, (2) the water depth of 10.0 cm to 20.0 cm (3) the annular outlet velocity from 0.00 cm/s to 149.50 cm/s and (4) the inner outlet velocity from 21.19 cm/s to 65.46 cm/s.

TABLE 4.1

LIST OF EQUIPMENTS

SYMBOL	DESCRIPTIONS
EB	Emulsion breaker length= 30.0cm; inside diameter= 7.6cm.

H1	Heat exchanger (or water cooler) for annular flow
	type: shell-and-tube
	shell side data: length= 134.5cm;
	o.d= 9.0cm.
	tube side data: no. of tubes= 10;
	length= 122.0cm;
	o.d.= 1.27cm;
	i.d.= 1.00cm.

H2	Heat exchanger for 'water return' flow
	type: shell-and-tube
	shell side data: length= 56.6cm;
	o.d.= 7.6cm.
	tube side data: no. of tubes= 5;
	length = 45.0cm;
	o.d.= 1.27cm;
	i.d.= 1.00cm.

M	Variable speed motor speed range: 0 to 50 rpm.
P1	Circulation pump for annular flow type: centrifugal pump.
P2	Water recycle pump type: centrifugal pump.
P3	DUG 'seal' vacuum pump.
P4	Oil supply and recycle pump type: centrifugal pump.
PI	Vacuum indicator.
R1	Rotameter for annular flow range: 1 to 8 USGPM.
R2	Rotameter for water return flow range: 1 to 5 USGPM.
R3	Rotameter for inner outlet flow range: 1 to 5 USGPM.

(Table 4.1 cont.)

SYMBOL	DESCRIPTIONS
R4	Oil supply rotameter range: 1 to 5 USGPM.
S1	Sampling point at the vacuum tank.
S2	Sampling point at water return line.
T1	Vortex tank diameter= 60.0cm; height= 60.0cm.
T2	Vacuum tank diameter= 29.25cm; height= 88.00cm.
T3	Oil supply tank diameter= 29.20cm; height= 60.00cm.
T4	Storge tank for clean up purpose dimension: 40cm x 27cm x 80cm.
V1	Annular circulation valve.
V2	Water return valve.
V3	Inner flow valve.
V4	Oil supply valve.
V5	Vacuum control valve.

TABLE 4.2

PROPERTIES OF FURNACE OIL AND PARAFFIN OIL

PROPERTY	TEMPERATURE (°C) 21.0	25.0	30.0
ESSO#2 FURNACE OIL			
DENSITY (g/cm^3)	0.8530	0.8491	0.8448
VISCOSITY (g/cm.s)	0.0328	0.0298	0.0264
(cp)	3.28	2.98	2.64
SURFACE TENSION (dynes/cm)	31.75	30.40	28.70
PARAFFIN OIL			
DENSITY (g/cm^3)	0.8763	0.8726	0.8678
VISCOSITY (g/cm.s)	1.748	1.366	1.100
(cp)	174.8	136.6	110.0
SURFACE TENSION (dynes/cm)	33.73	33.10	32.30

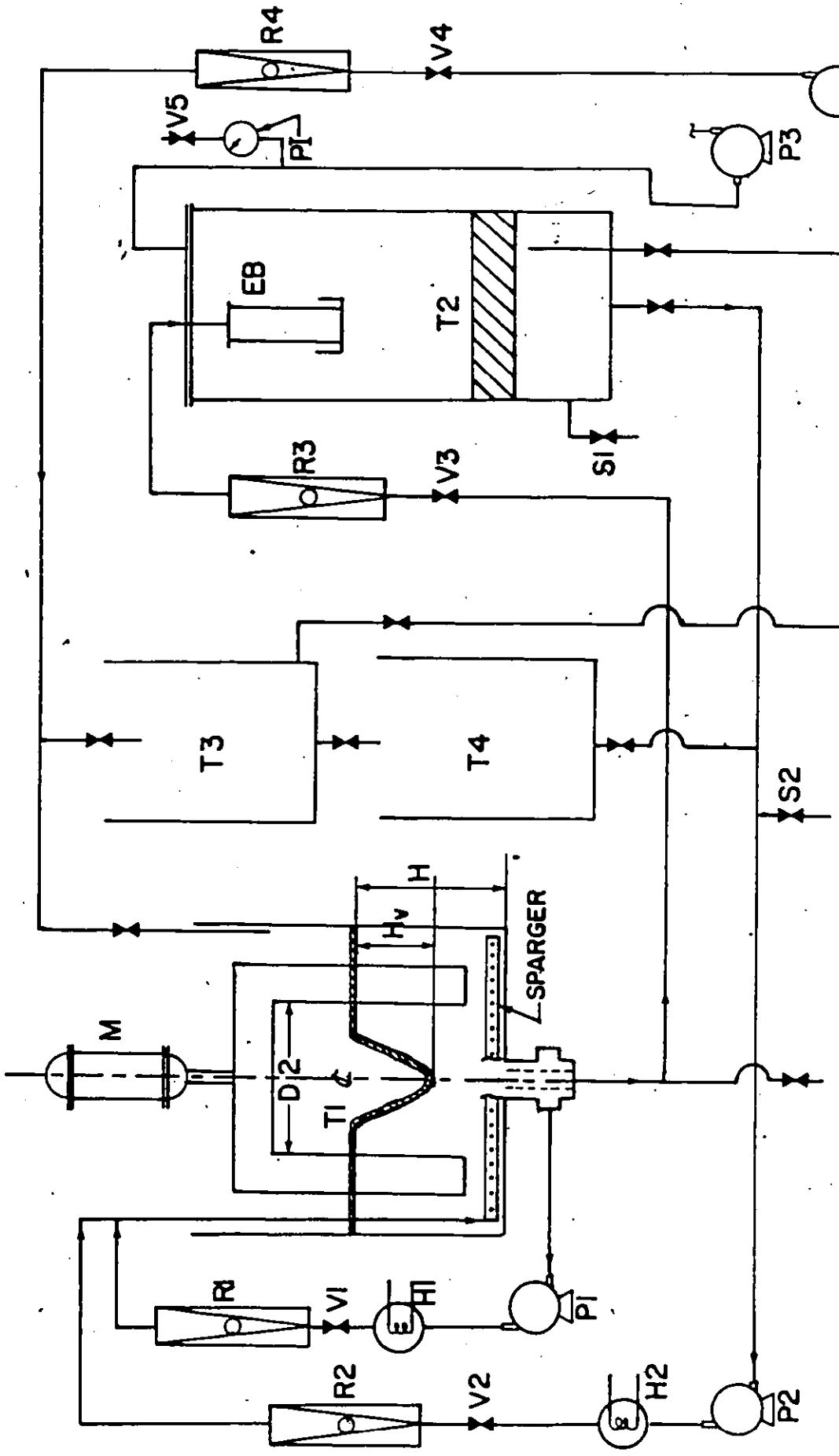

Figure 4.1: SCHEMATIC SKETCH OF THE EXPERIMENTAL SET UP

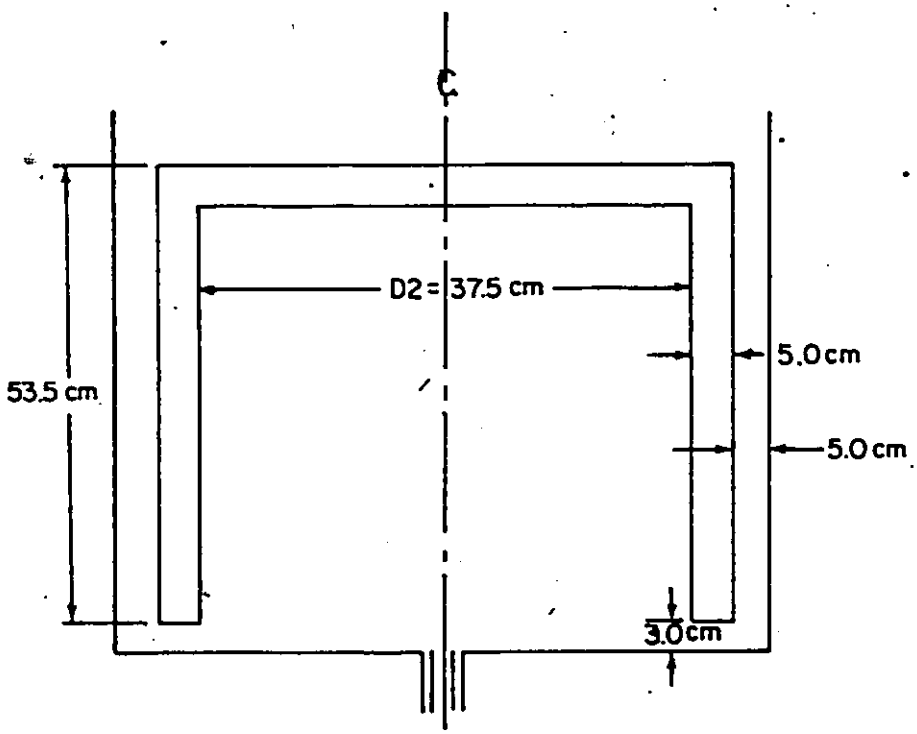

Figure 4.2: DIMENSIONS OF THE STIRRER

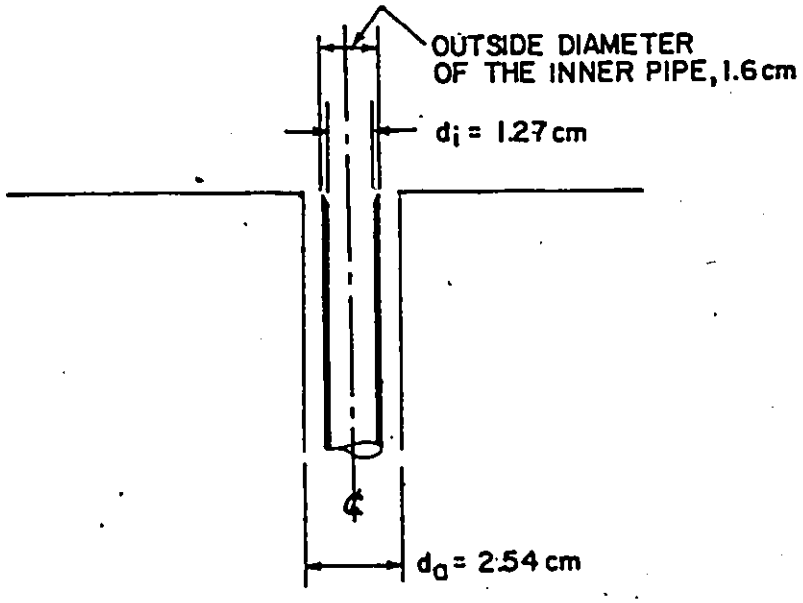

Figure 4.3: ARRANGEMENT OF THE OUTLET PIPES

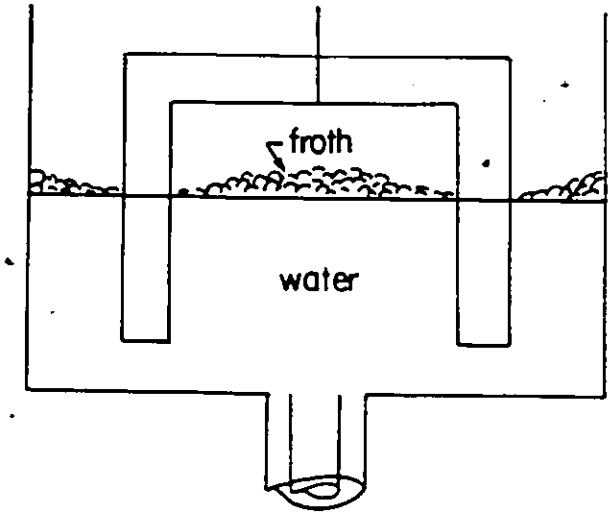

(a) AVERAGE FROTH THICKNESS = 1.5 cm

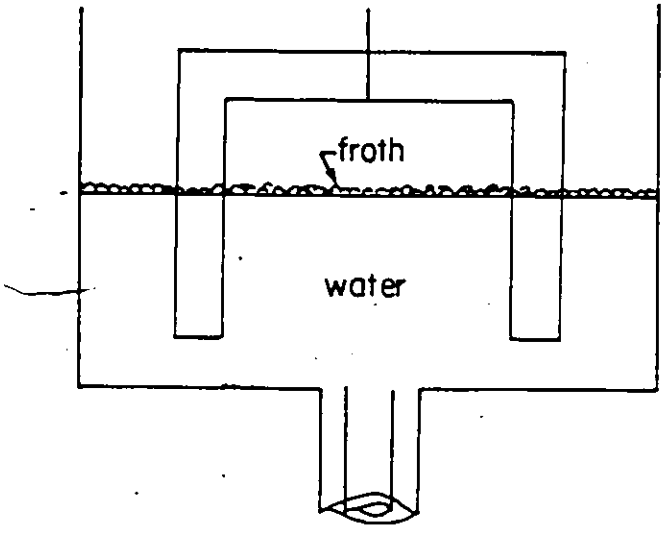

(b) AVERAGE FROTH THICKNESS = 0.5 cm

Figure 4.4: DISTURBUTION OF THE FROTH IN THE VORTEX TANK FOR DIFFERENT FROTH THICKNESS

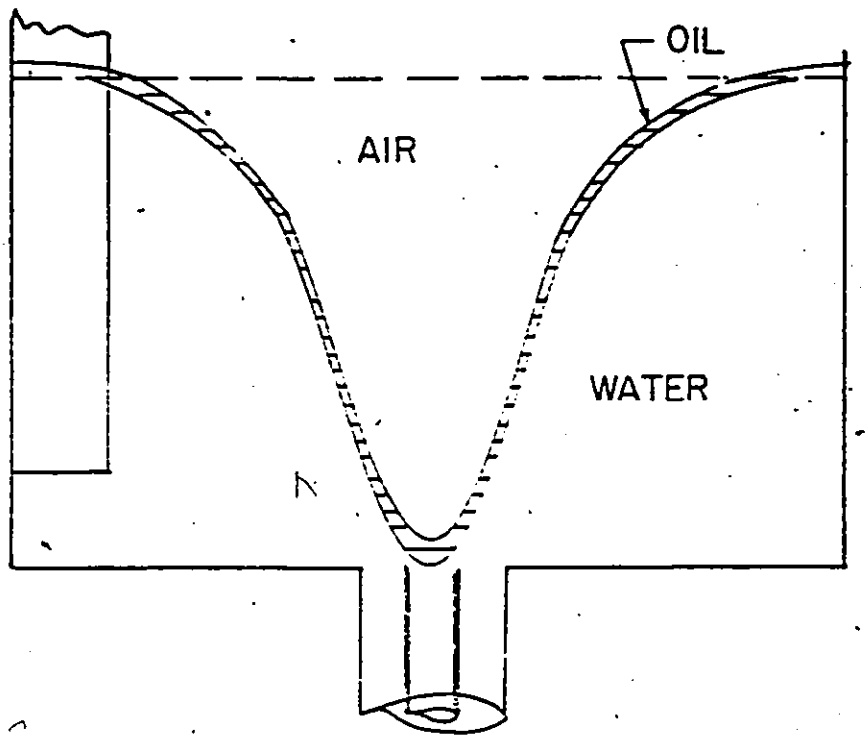

Figure 4.5: INCIPIENT OIL ENTRAINMENT

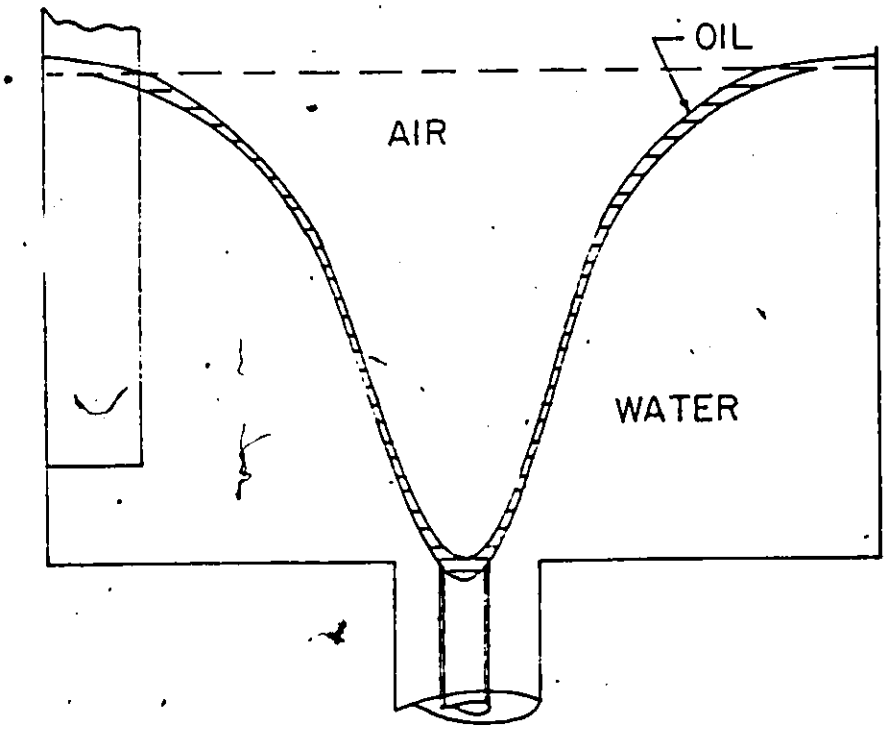

Figure 4.6: INCIPIENT AIR-OIL ENTRAINMENT

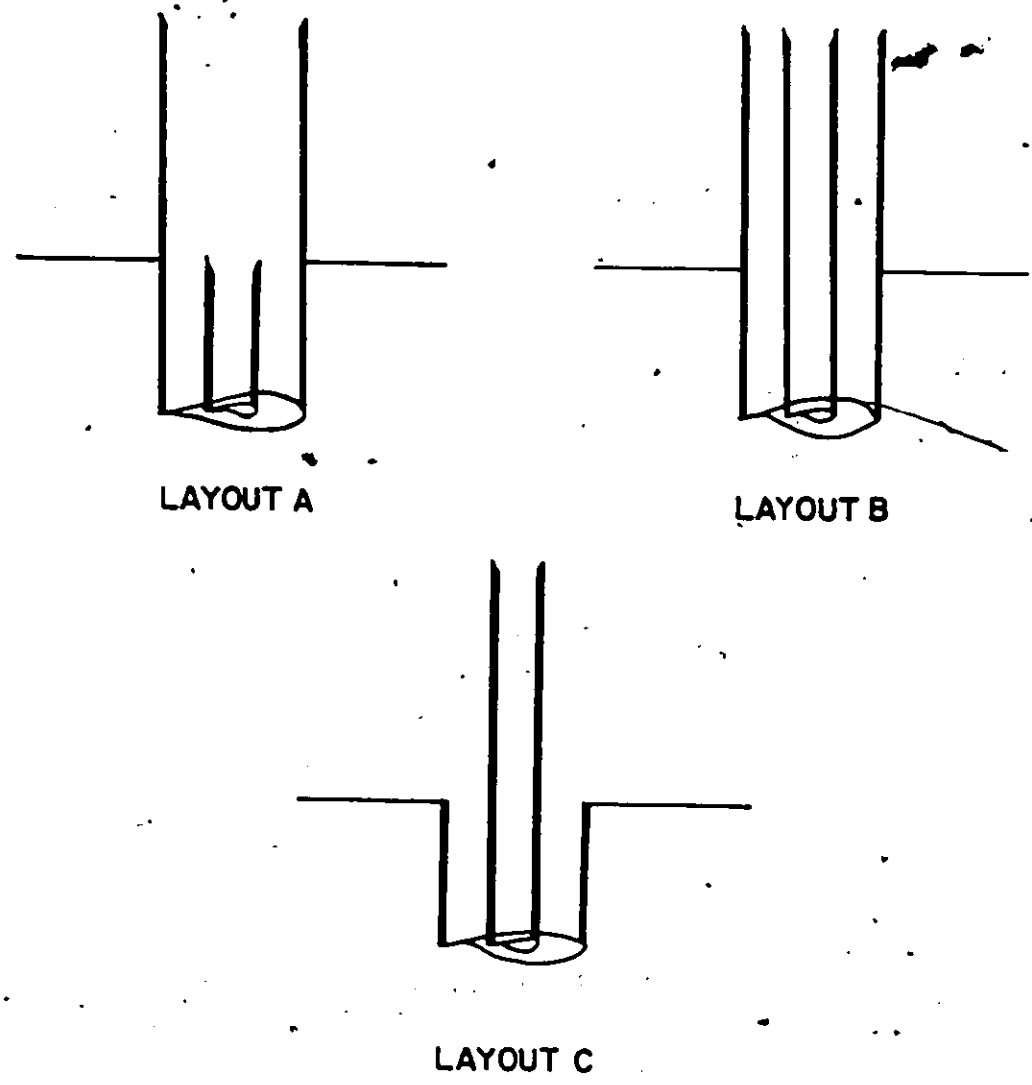

Figure 4.7: THREE DIFFERENT LAYOUTS OF OUTLET PIPES

Chapter V

PRESENTATION AND DISCUSSION OF RESULTS

5.1 RESULTS AND DISCUSSIONS OF PHASE I, AIR-WATER VORTEX EXPERIMENTS

5.1.1 General Remarks

A vortex can be generated in many different liquid flow situations. A complicated steady-state vortex phenomenon was examined in this study. The vortex was formed by combining three major actions, namely, (1) the liquid was stirred in the cylindrical vortex tank by means of the 'horse-shoe' stirrer (2) the liquid was withdrawn through the inner outlet pipe from the vortex tank and (3) the liquid was recirculated through the annular opening back into the vortex tank. Based on the physical considerations, the vortex formation was dependent upon the following parameters:

1. rotation speed of the stirrer,
2. water depth in the vortex tank,
3. inner outlet velocity (or flow rate),
4. annular outlet velocity (or flow rate),
5. density of the liquid,
6. viscosity of the liquid,
7. surface tension of the liquid,

8. inside diameter of the 'horse-shoe' stirrer (D2),
9. diameter of the inner outlet pipe,
10. area of the annular opening,
11. gravity acceleration, and
12. diameter of the vortex tank.

Based on the design of the experiments, only the effects of the first four parameters on vortex formation were emphasized. Therefore, these four parameters were considered as four principal variables in this phase.

Totally 112 data were collected to study the effects of rotation speed of the stirrer (Ω), water depth in the vortex tank (H), inner outlet velocity (Vi) and annular outlet velocity (Va) on the vortex depth (Hv). Among these data, 68 of them involved combining the inner outlet flow and the annular outlet flow together for vortex formation at varied Ω and H, 18 of them involved using only the annular outlet flow for vortex formation, and 26 of them involved using only the inner outlet flow for vortex formation at varied Ω and H. The data are presented in Appendix F. The accuracy of the vortex depth data was estimated to be within ±1.0 cm.

The shape of vortex varied with different operating conditions of the four principal variables. The following phenomena were observed during the experiments:

1. For a vortex which was generated using only the annular circulation flow at the outlet at various Ω and

H values, the shape of the bottom of the vortex was relatively flat, especially at a low water depth (Figure 5.1). Because there was no fluid passing through the inner outlet pipe, a 'no-flow' region existed above the inner pipe. The annular circulation flow created a ring shape force field acting downward above the annular opening. These two effects combined together to make the bottom of the vortex relatively flat.

2. The vortex diameter (looking down from the top of the vortex tank) increased as the rotation speed of the stirrer increased. It was obvious that the stirrer rotational speed had an effect on the vortex shape.
3. The surface of the vortex was relatively smooth at low Ω, Vi, and Va (the flow appeared to be laminar), but the surface of the vortex became rough, which looked like a screw at high Ω, Vi, and Va (the flow appeared to be turbulent).
4. For high stirrer rotational speed (Ω=10 rpm), the vortex was unstable. The vortex depth usually fluctuated to the extent of several centimeters, and the vortex air-core always rotated around its axis in a small circular path in the same direction as the stirrer. For some cases, the vortex air-core appeared and then disappeared. The reason for these phenomena may be the high turbulence of the flow and the high

shear between the liquid and the tank wall at high stirrer rotational speeds.

Most of the inner and the annular outlet flows used in this phase were considered to be in the turbulent flow region. The stirrer rotational speed of 3 rpm was in laminar-turbulent transition region, and those of 5 rpm and 10 rpm were turbulent. Calculations of the Reynolds numbers for the stirrer rotational speeds and for the two outlet velocities to define the laminar-turbulent transition region are given in Appendix G.

5.1.2 Comparison of the Observed Vortex Shape with the Shape Predicted by the Combined Vortex Equations

The flow pattern for the vortex formation in a stirred draining tank is complex. It became obvious that the vortex phenomenon in this study could be described by neither the forced vortex equation nor the free vortex equation as described in Chapter 3. However, based on the observation of the shape of the vortex, it was considered that it was similar to that of Rankine's combined vortex.

The shapes of three experimental vortices were compared with the predicted shapes based on the equations for the combined vortices (equation 3.8 and 3.28). The detailed procedure for the comparison is given in Appendix H, and the comparisons of the observed vortex shapes with those pre-

dicted by the combined vortex equations for three experimental vortices are shown in Figures 5.2, 5.3 and 5.4 .

For all three comparisons, the vortex shapes predicted by the combined vortex equations showed a fair agreement with the observed vortex shapes, except that there were some deviations at the outer section of the vortex. As a result, it might be concluded that the flow pattern of the vortex in this study was similar to Rankine's combined vortex, which involved a forced vortex in the central portion of the vortex and a free vortex in the outer region of the vortex.

5.1.3 Comparison of Experimental Hv/d with Predicted Values Using the "Neale and Hayduk" Correlation Equation

The flow pattern of the vortex in the present study was similar to the flow pattern in Neale and Hayduk study (15,16), if the vortex in this study was considered to be formed by combining the actions of the stirrer and the inner outlet flow together but excluding the annular flow. Thus the correlation equation obtained by Neale and Hayduk might be suitable to predict the vortex depth for a specified case (Va= 0.00 cm/s) in this study.

Twenty vortex depth data, which the vortices were formed under different conditions of the inner outlet velocity (Vi), the stirrer rotational speed (Ω), and the water depth (H), were compared with values predicted by the Neale and

Hayduk correlation (equation 2.6). The experimental and predicted values of Hv/d are compared in Table 5.1 . The results indicate that the predicted values are at least three times greater than the experimental values. Therefore, the Neale and Hayduk correlation equation cannot be used for predicting the vortex depth in this study.

The reason for the large deviation between the experimental and predicted values of Hv/d can be explained as follows: the Neale and Hayduk correlation is only valid inside their experimental range of the parameters. However, some parameters in the present study were outside the range of the parameters used in Neale and Hayduk study. Thus, the correlation equation obtained by Neale and Hayduk is no longer valid for this study. The ranges for the important parameters in the two studies are compared in Table 5.2 .

It was not surprising that the predicted values of the vortex depth by the Neale and Hayduk correlation were much higher than the experimental values in the present study. This result could be explained by means of a mathematical method. The Neale and Hayduk correlation can be rewritten as the following form:

$$\frac{Hv}{d} = 7.35\times10^{-5}\, g^{-0.83}\, \upsilon^{-1.22}\, D2^{2.45}\, \Omega^{0.90}\, Q^{1.98}\, H^{-0.17}\, d^{-4.95} \qquad (5.1)$$

Since the ranges of stirrer rotational speed, kinematic viscosity, gravitational accerleration and outlet volumetric flow rate of this study were within the ranges of the parameters used in Neale and Hayduk study, these parameters were not considered to contribute to the disagreement between the observed behaviour and the correlation. Thus only the relation between the vortex depth, the inside stirrer diameter (D2), the water depth (H), and the outlet pipe diameter (d) were considered; equation (5.1) was simplified to the following form:

$$\frac{Hv}{d} \propto D2^{2.45}\ H^{-0.17}\ d^{-4.95} \qquad (5.2)$$

Equation (5.2) shows that Hv/d is strongly dependent of the stirrer inside diameter (D2), and the outlet diameter (d). From Table 5.2 , it may be observed that D2 in this study was greater than the maximum of 'valid' values in Neale and Hayduk study, and H of 10.0 cm and d in this study were smaller than the minimum of 'valid' values in Neale and Hayduk study. As a result, the predicted values of Hv/d as obtained by the Neale and Hayduk correlation for this study might be expected higher than predicted. Thus the correlation equation obtained by Neale and Hayduk cannot be utilized to predict the vortex depth in this study.

It is also observed that the arrangement for the outlet tubes, in particular the annular outlet, differred from that

used in the previous work. Even though there was no flow through the annular outlet in this case, the difference in the tube arrangement may have influenced to the vortex depth.

5.1.4 Combining the Inner and Annular Outlet Velocities

The design of the vortex apparatus used in this study involved two outlet flows (inner and annular flows). Therefore, the vortex formation was dependent upon these two outlet flows. It was of interest to devise a method for combining the inner outlet velocity and the annular outlet velocity to yield an equivalent vortex-forming outlet flow. Several methods were attempted; however, only one gave an acceptable result. This method combined the two outlet velocities in the following manner:

$$Vc = Vi^{a}\, Va^{b} \qquad (5.3)$$

and

$$a + b = 1 \qquad (5.4)$$

The combining equation (5.3) has an obvious limitation; it applies only for the case when Vi and Va are not zero. The equation (5.4) keeps the units of the combined velocity (Vc) the same as those for the two outlet velocities. Sixty-eight data for the air-water vortex experiments were tested by this method; the values of a, and b which fitted the data

best were found to be 0.82, and 0.18 respectively. The values of a and b were obtained by a trial-and-error method. The procedure for this searching method is summarized as below. Among those 68 experimental data, there were 17 groups of data having the same vortex depth, water depth, and stirrer rotational speed, but having different combinations of the inner and annular outlet velocities. The sum of squares of the differences between the combined velocities (Vc) obtained by the equation (5.3) and its mean were calculated for each group; it was called the local sum of squares for that group. The criterion for the searching procedure for a and b was to find the minimum overall sum of squares, which was the sum of all the 17 local sum of squares. An example for this combining method is given in Appendix I.

A plot of the vortex depth (Hv) against the combined velocity (Vc) at various Ω and H is shown in Figure 5.5 . Figure 5.5 illustrates an approximately linear relationship between Hv and Vc at each Ω. Linear regression analysis was performed to find the best fitting line for the data for each Ω. The results are shown in Table 5.3 .

From Table 5.3 , it may be observed that the first coefficient (the one before Vc) increases as the rotation speed of the stirrer (Ω) increases, and this cofficient represents the slope of the line. As a result, it is apparent that the vortex depth (Hv) increases as Ω increases for any

particular combined velocity. The correlation equations in Table 5.3 could be used to predict the vortex depth at three different stirrer rotational speeds for the air-water vortices utilized in this study.

It is evident from Figure 5.5 that the Hv was directly related to the combined velocity (Vc). Thus, there was an increase in the vortex depth with an increase in the inner outlet velocity (Vi) or in the annular outlet velocity (Va) for a particular Ω. There is no indicated effect of the water depth (H) on the vortex depth in Figure 5.5. However, the data for three different water depths could be fitted by a suitable correlation equation excluding H. Therefore, the effect of the water depth on the vortex depth is considered to be small if not negligible.

Since the effect of the stirrer rotational speed on the vortex depth was significant, the best values of a and b were obtained separately for each Ω. The results are listed in Table 5.4. From Table 5.4, it may be observed that the combining factors (a and b) vary with Ω. Thus the effects of the inner and annular outlet flows on the vortex depth also varied with Ω. A linear regression was again performed to find the best fitting line for each Ω, and the results are listed in Table 5.5.

Comparing the correlation coefficients for the correlation equations in Table 5.3 with those in Table 5.5, the

latter table has higher correlation coefficients for all cases. Furthermore, these two tables show the same general conclusion in that Hv is strongly dependent on Ω and Vc. For simplicity, the combining factors for the outlet velocities of a=0.82 and b=0.18 will be accepted.

The value of a was found to be consistently larger than that of b in the combining equation (5.3), and the order of magnitude for the inner (Vi) and the annular (Va) outlet velocities were same. Thus the effect of the inner flow was expected to be greater than the effect of the annular flow on the vortex depth. This conclusion was also supported by the experimental data. For the cases in which the vortices were generated by only one outlet flow (inner flow or annular flow), the annular flow velocity necessary to form a vortex was greater than the inner flow velocity for the same conditions of Ω and H. The reason for this is probably related to the positions of the inner and annular outlet tubes. When only the inner outlet flow was used for vortex formation, the water was withdrawn from the vortex tank through the central inner outlet tube, and the vortex was relatively thinner and longer. However, when only the annular outlet flow was used for vortex formation, the water was recirculated back into the vortex tank through the annular opening surrounding the inner tube, and the vortex was relatively wider and shorter.

5.1.5 Analysis of Data by Dimensional Analysis

A theoretical analysis of vortex formation in this study was considered complicated and difficult. Hence a simple dimensional analysis was attempted. Based upon physical considerations, it was expected that the vortex depth, Hv, would depend upon several variables as follows:

$$Hv = f(\Omega, Vi, Va, di, Aa, H, \rho, \mu, g, D2) \qquad (5.5)$$

The notation in the equation (5.5) is explained in the Nomenclature section. The possible effects of surface tension and vortex tank diameter (D1) were neglected in this analysis.

Application of the Buckingham π-theorem to equation (5.5) yielded the following dimensionless relationship.

$$\frac{Hv}{di} = \alpha \left(\frac{\Omega di}{Vi}\right)^{\beta} \left(\frac{Va}{Vi}\right)^{\gamma} \left(\frac{Aa}{di^2}\right)^{\delta} \left(\frac{H}{di}\right)^{\epsilon} \left(\frac{Vidi}{\upsilon}\right)^{\zeta} \left(\frac{D2}{di}\right)^{\eta} \left(\frac{Vi^2}{gdi}\right)^{\iota} \qquad (5.6)$$

Since Aa, D2 and di were kept constant in this study, the terms $(Aa/di^2)^{\delta}$ and $(D2/di)^{\eta}$ could be included in the constant term α'. Therefore, equation (5.6) became:

$$\frac{Hv}{di} = \alpha' \left(\frac{\Omega di}{Vi}\right)^{\beta} \left(\frac{Va}{Vi}\right)^{\gamma} \left(\frac{H}{di}\right)^{\epsilon} \left(\frac{Vidi}{\upsilon}\right)^{\zeta} \left(\frac{Vi^2}{gdi}\right)^{\iota} \qquad (5.7)$$

Equation (5.7) was transformed to a linear form by taking the logarithm of both sides of the equation. Values for the exponents in equation (5.7) were determined by performing a multiple regression analysis using 68 experimental data. The multiple regression program was modified from Kagaka, Kogaku and Kyokai (26). The theory for the multiple regression and the listing of the program involved are presented in Appendix J. The following result was obtained by multiple regression analysis:

$$\frac{Hv}{di} = 1.57 \left(\frac{\Omega di}{Vi}\right)^{0.41} \left(\frac{Va}{Vi}\right)^{0.24} \left(\frac{H}{di}\right)^{0.29} \left(\frac{Vidi}{\nu}\right)^{0.43} \left(\frac{Vi^2}{gdi}\right)^{0.56} \qquad (5.8)$$

In the above equation Ω is in terms of revolutions per second. The coefficient of multiple correlation was 0.9327, and the average deviation between the experimental and predicted values of Hv was 16.44 %. The average deviation was relatively high because some particular operating conditions of the experiments would make the deviations between the experimental and predicted values of Hv high. One of the particular condition was a case in which one of the outlet velocities was much higher than the other outlet velocity. Thus the outlet flow with the higher velocity dominated the effect on vortex formation. This would change the flow pattern in the vortex tank, and hence the result predicted by the correlation equation (5.8) was very different from the

experimental result. Another particular condition occurred at the high stirrer rotational speed (Ω=10 rpm). In this condition, the flow was highly turbulent, and the vortex was unstable. The vortex was usually fluctuating, and thus the vortex depth measurements were not accurate. As a result, the deviation between the experimental and the predicted values became large in such cases. A visual test of the effectiveness of equation (5.8) is shown in Figure 5.6 , where the experimental and predicted values of Hv are compared.

The above correlation equation can be utilized to predict the vortex depth for air-water vortices in this study. However, it is not recommended for the particular operating conditions mentioned before.

Equation (5.8) could be simplified to the following form:

$$\frac{Hv}{di} = 0.25\,\Omega^{0.41}\,Vi^{0.90}\,Va^{0.24}\,H^{0.29} \qquad (5.9)$$

Equation (5.9) indicates that the vortex depth (Hv) is directly related to the stirrer rotational speed, the inner flow velocity, the annular flow velocity, and the water depth in the vortex tank. However, there is some doubt about the statement that 'the vortex depth is directly related to the water depth in the vortex tank'. Because of the design of the experiments, only two vortex depths were used, half of the water depth (Hv=H/2) and that equivalent

to the total water depth (Hv=H). These data might mislead one to believe that invariably the vortex depth increases as the water depth increases. Therefore, further study for the effect of the water depth on the vortex depth is recommended.

5.1.6 The Effect of Surface Froth on Vortex Formation

Some twenty-seven tests were carried out to study the effect of surface froth on the vortex depth. These experiments were performed under the same operating conditions of the four variables as those for the air-water vortex experiments. Thus the effect of the surface froth on the vortex depth could be observed by comparing the vortex depths of these two series of experiments. The experimental data are given in Appendix K.

For the 'with froth' experiments, the froth filled the central air-core of the vortex which was normally occupied by air in air-water vortices (Figure 5.7). The shapes of the vortices in the 'with froth' experiments were usually thinner (in diameter) than those in the 'without froth' experiments. The reason for this shape different is probably due to the difference in the interfacial tension between air-water and detergent froth-water system. The interfacial tension between water and air is relatively high, but it is relatively low between dilute soap solution and air. This

interfacial tension change may affect vortex formation. It is also possible that the viscosity of the air is much less than that of the froth, thus affecting the vortex shape.

Comparisons of vortex depths (Hv) of 'with froth' experiments with those 'without froth' are shown in Figures 5.8 and 5.9 . These figures illustrate that the vortex depth is affected by the surface froth. Figure 5.8 is a plot of Hv against Va at Ω = 3 rpm and for a froth thickness of 1.5 cm; it shows that Hv increases if the surface froth is present at low stirrer speeds. However, Figure 5.9 shows a totally different result. Figure 5.9 is a plot of Hv against Va at Ω = 10 rpm and the same froth thickness of 1.5 cm; it shows that Hv decreases if surface froth is present at high stirrer speeds. Therefore, the effect of surface froth on the vortex depth was strongly influenced by the stirrer rotational speed. The reason for this result may be the result of the effect of interfacial tension or generally of the vortex flow pattern. A detailed explanation for the above phenomenon is not evident from this research; further investigation is necessary.

Figure 5.10 is a plot of comparisons of vortex depths between two sets of 'with froth' experiments with different surface froth thicknesses (0.5 cm and 1.5 cm). It shows that Hv was affected by the froth thickness, in particular, that Hv increased as the froth thickness increased at low

stirrer speeds, but that Hv decreased as the froth thickness increased at high stirrer speeds.

5.2 RESULTS AND DISCUSSIONS FOR PHASE II, OIL-WATER SEPARATION EXPERIMENTS

5.2.1 Operating Conditions for Incipient Oil Entrainment and Incipient Air-Oil Entrainment

Eighty experiments were performed using furnace oil to determine the operating conditions of the inner outlet and the annular outlet velocities (Vi and Va) for incipient oil entrainment and incipient air-oil entrainment at various conditions of the stirrer rotational speeds (Ω= 3,5,10 rpm) and the water depths in the vortex tank (H= 10.0,20.0,30.0 cm). The experimental data are given in Appendix L. Because an oil-entraining vortex (only oil and water were withdrawn out of the vortex tank) was expected to occur between the conditions of incipient oil entrainment and incipient air-oil entrainment, the operating ranges of Vi and Va for the formation of the furnace oil-entraining vortex could be determined from the results of the experiments.

The vortex motion created complicated internal flow patterns and high shear; some degree of emulsification of the oil and water existed during the experiments. Thus the precisions of some results were low; replicates were performed only for inconsistent results.

The method for combining the two outlet velocities (Vi and Va) to yield an equivalent condition for forming an oil-vortex was of particular interest here, because it could reduce the number of independent variables affecting vortex formation, and hence could simplify the problem. Several methods were attempted; the first method, which combined the two non-zero outlet velocities to yield the average velocity, gave an acceptable result. The resulting average outlet velocities ($\bar{V}$) are shown in Appendix L.

The average outlet velocities ($\bar{V}$) for incipient furnace oil entrainment and incipient air entrainment are plotted against the ratios of water depth to diameter of the inner pipe (H/di) at various Ω on a semi-log graph paper as shown in Figure 5.11 . The diagram shows an essentially linear relationship between the average outlet velocity and the value of ln(H/di) for incipient oil entrainment, and also for incipient air-oil entrainment at each Ω. Linear regression analyses were performed to find the best fitting lines for the data for the two entrainments. The area between the incipient oil entrainment line and the incipient air entrainment line at each Ω was the useful oil-vortex formation region for that Ω.

From Figure 5.11, it is evident that the incipient oil entrainment line of lower Ω is located above the line of higher Ω, and equivalently the line for incipient air en-

trainment at lower Ω is also located above the line of higher Ω. Therefore, at low Ω, the oil entrainment (or air entrainment) condition occurred at relatively high outlet velocities. These results were expected.

An expression can be written for the relation between $\bar{V}$ and H/di.

$$\bar{V} = A + B.\ln(H/di) \qquad (5.10)$$

In the above expression, A and B are constants which were determined from the experimental data for the particular Ω and type of vortex formed.

Sixty-five experiments were carried out using paraffin oil to determine the operating conditions for the two outlet velocities (Vi and Va) for incipient oil entrainment and incipient air-oil entrainment at varied stirrer rotational speeds (Ω) and water depths (H). The experimental data are shown in Appendix M. Similarly, the operating ranges of Vi and Va for the formation of the paraffin oil-entraining vortex at various conditions of Ω and H could be estimated from the experimental results.

The inner outlet velocity and the annular outlet velocity were also combined by the same method as used for the furnace oil. The resultant average outlet velocities ($\bar{V}$) are given in Appendix M. A plot of the average outlet velocities ($\bar{V}$) for the two types of entrainment at various Ω is

shown as a function of ln(H/di) in Figure 5.12 . Again, the linear relationships between $\bar{V}$ and ln(H/di) for incipient oil entrainment and for incipient air entrainment are indicated. Thus the identical expression (5.10) could apply to the paraffin oil case but with different constants. The linear regression analyses were performed to find the best fitting lines for the data. Similarly, the paraffin oil-vortex formation region at a particular Ω was the operating region between the incipient oil entrainment line and the incipient air entrainment line at that Ω.

5.2.2 Furnace Oil-Water Separation Experiments

The mechanism for oil-water separation (or oil skimming) as evolved in this study can be explained as follows: a stable oil-vortex can be generated in the vortex tank at steady state. Under certain operating conditions, the oil-vortex core covers a part of the inner outlet pipe. Thus the surface oil in the vortex-core is withdrawn together with some water through the inner outlet pipe. This separation mechanism is somewhat different from the mechanism of separation for other oil-water separation devices such as the hydrocyclone and centrifuge.

Based on physical considerations, the formation of oil entraining vortices depend on: (1) stirrer rotational speed (2) water depth in the vortex tank (3) inner outlet velocity

(4) annular outlet velocity (5) viscosities of oil and water (6) densities of oil and water (7) outlet pipe diameters (8) stirrer inside diameter (9) interfacial tension and (10) oil thickness in the vortex tank. However, only the effects of the first five parameters were considered in the present study.

One hundred seventy-one experiments were performed with furnace oil to study the effectiveness of oil removal under various operating conditions of the four variables (Ω,Vi,Va,H). The experimental data are presented in Appendix N. The oil removal quantity is represented as the oil removal rate (cm^3/s) and oil content of the withdrawn mixture in the inner pipe (volume %). The oil removal rate is defined as the oil accumulation rate in the vacuum tank, and the oil content is defined as the oil removal rate divided by the inner volumetric flow rate and multipled by 100. Replicates were performed only when the results appeared inconsistent, and the precision of the oil removal rate data was estimated to within ± 1.0 cm^3/s.

Plots of the oil removal rate (Qoil) against the inner outlet velocity (Vi) under various conditions of the annular outlet velocity (Va) for nine combinations of the stirrer rotational speeds (Ω= 3,5,10 rpm) and the water depths (H= 10,20,30 cm) are shown in Figures 5.13 to 5.21 . These figures indicate that Qoil was directly related to Vi within

the oil-vortex formation region. Thus the Qoil might be seen to increase as Vi was increased inside the oil-vortex formation region, when the other variables (Ω,H,Va) were kept constant. However, Qoil decreased when Vi was increased to the point at which an air-entraining vortex occurred. For the air-entraining vortex, air was also continuously withdrawn with the oil-water mixture from the vortex tank. As a result, the inner outlet flow became unstable, and the quantities of the oil and water in the inner flow reduced. It was not possible to obtain a correlation between Qoil and Vi for the condition of air-entrainment.

It is evident from Figures 5.13 to 5.21 that the oil removal rate increases as the annular outlet velocity increases, when the other variables (Ω,H,Vi) are maintained constant. Therefore, it is also evident that the use of two outlet flow systems are significantly better for oil removal than the former system with only one outlet flow system (17). The reason for this improvement may be that the vortex-core is wider, and the oil layer within the vortex-core is thicker when annular flow is used together with the inner flow.

By comparing the oil removal rates at different stirrer rotational speeds, it was found that the oil removal rate was directly related to the stirrer rotational speed (Ω) for most of the results. However, for some of the results at

high stirrer speeds and low water depths (for example, Ω = 10 rpm and H =10.0 cm) , the oil removal rate was lower than that at lower Ω when the other variables were kept constant. The reason for this is probably due to the fact that the vortex is unstable at high Ω (10 rpm). The repeated appearance and disappearance of the oil-vortex at high Ω , was considered to decrease the oil removal rate significantly. Figure 5.22 is an example to show the relationship between the oil removal rate and the rotation speed of the stirrer at a specified operating condition. This figure illustrates that at higher Ω , an air-entraining vortex formed at relatively low inner outlet velocities while the other variable (H,Va) remained constant.

Based on the observed results, the oil removal rate was found to be inversely related to water depth in the vortex tank (H). Figure 5.23 is used to demonstrate the effect of water depth on the oil removal rate at a particular operating condition. From Figure 5.23, it may be observed that at lower H, an air-entraining vortex was formed at relatively low inner outlet velocities when the other variables (Ω,Va) were kept constant.

As a result, the maximum (optimum) oil removal rate was expected to exist at the conditions of low H and high Ω , with Va and Vi within the oil-vortex formation region.

The highest experimental furnace oil removal rates for nine cases with different combinations of Ω and H inside the oil-vortex formation region are listed in Table 5.6 . For all nine cases, the highest oil removal rates occurred at the condition of the highest Va and Vi when these corresponded to the oil-vortex formation region. This was in agreement with the expected operating conditions for optimum oil removal rate. The maximum oil removal rate observed for the furnace oil-water separation experiments was 25.7 cm^3/s.

The highest experimental oil contents of the withdrawn mixture in the inner outlet pipe for nine cases with different combinations of Ω and H are given in Table 5.7 . The maximum oil content for the furnace oil-water separation experiments was 48.7 %. The highest oil content usually occurred for the experimental conditions corresponding to the highest Va and to a relatively low Vi within the oil-vortex formation region.

Figure 5.24 illustrates the relationship between the oil content and the annular outlet flow at a specified operating condition. It is evident from the figure that the oil content increased as the annular outlet velocity increased while the other varibles (Ω,H,Vi) were maintained constant. However, from Figure 5.24, there appeared to be no correlation between the oil content and the inner outlet velocity.

Similarly, based on the observed oil content data, the oil content was directly related to the stirrer rotational speed, but it was inversely related to the water depth in the vortex tank.

A correlating equation of the following form was used to fit the experimental data:

$$Qoil = \alpha\, \Omega^{\beta} Vi^{\gamma} Va^{\delta} H^{\epsilon} \qquad (5.11)$$

This equation was transformed to a linear form by taking the logarithm of both sides of the equation. Values of the exponents were determined by performing a multiple regression analysis using 96 experimental data (Va and Vi were not zero). The following result was obtained:

$$Qoil = 2.93\, \Omega^{0.78} Vi^{0.95} Va^{0.51} H^{-0.76} \qquad (5.12)$$

In the above expression, Ω is in terms of revolutions per second. The average deviation between the experimental values of Qoil and values predicted by equation (5.12) was high (24.4 %), and the experimental data could not be described reasonably by the predicted curve. Therefore, this correlation was considered to be a failure. Oil-vortex formation as investigated in this study is considered to be a complicated phenomenon; hence it may not be surprising that the experimental data could not be fitted by a simple correlating equation such as equation (5.12). Because of the lack of a more comprehensive background theory for oil-vortex

formation, a more successful correlation is not forthcoming in this study.

5.2.3 Paraffin-Oil-Water Separation Experiments

Some 190 experiments were performed in the study of the effectiveness of paraffin oil removal under various operating conditions of stirrer rotational speed (Ω), inner flow velocity (Vi), annular flow velocity (Va), and water depth in the vortex tank (H). The experimental data are reported in Appendix O. The terms oil removal rate and oil content are also utilized to represent the oil removal effectiveness in the paraffin oil case. Replicates were only performed when the results appeared inconsistent. It was estimated that the oil removal rates were accurate to within ± 1.5 cm^3/s.

Plots of the oil removal rate (Qoil) against the inner flow velocity (Vi) under various conditions of Va, Ω (3,5,10 rpm) and H (10,20,30 cm) are shown in Figures 5.25 to 5.33 . These plots illustrate that the paraffin oil removal rate increased as the inner outlet velocity increased within the oil-vortex formation region when the other variables (Ω,H,Va) were kept constant. However, Qoil decreased while Vi was increased to the condition where air entrainment occurred. When air was present, the air reduced the volume of oil-water mixture in the withdrawn mixture, and

therefore the oil removal rate decreased. It is evident from Figures 5.25 to 5.33 that the paraffin oil removal rate was directly related to the annular outlet velocity.

From an observation of the oil removal rates for different conditions of water depth (H), it was found that the paraffin oil removal rate decreased with increasing water depth when the other variables (Ω,Va,Vi) were kept constant. Similarly, it was found that the oil removal rate was directly related to the stirrer rotational speed for most of the results, except that for some results at high Ω and low H. The reason for this inconsistency may be due to the fact that the vortex was unstable for high Ω, especially at low H.

Based on the effects of the Vi, Va, H, and Ω on the paraffin oil removal rate, the optimum oil removal rate was expected to exist for the conditions of low H and high Vi, Va and Ω inside the oil-vortex formation region.

The highest experimental paraffin oil removal rates for nine cases with different combinations of Ω and H within the oil-vortex formation region are listed in Table 5.8 . Based on the observations, the highest oil removal rate for each case occurred at the condition of relatively high Va and Vi inside the oil-vortex formation region. The maximum oil removal rate for the paraffin oil-water separation experiments was 42.4 cm^3/s.

The highest experimental oil contents for nine cases with different combinations of Ω and H are summarized in Table 5.9 . The highest oil content for each case usually occurred for the condition of the highest Va and relatively low Vi within the oil- vortex formation region. The maximum oil content in the withdrawn mixture for the paraffin oil-water separation experiments was 59.2 %.

The effects of annular outlet velocity (Va), stirrer rotational speed (Ω), and water depth in the vortex tank (H) on the paraffin oil content were similar to the results for the furnace oil case. As a result, the paraffin oil content was directly related to Va and Ω, and was inversely related to H. Again, there was no correlation between the oil content and the inner outlet velocity (Vi).

A correlation equation similar in form to equation (5.11) was attempted to fit the experimental data. After linearization equation (5.11), values were obtained for the exponents by performing a multiple regression analysis utilizing 102 experimental data (Va and Vi were not zero). The following result was obtained:

$$Qoil = 1.54\ \Omega^{0.42}\ Vi^{1.13}\ Va^{0.44}\ H^{-0.73} \qquad (5.13)$$

In the above equation, Ω is in terms of revolutions per second. Again, however, the average deviation between ex-

perimental values of Qoil and predicted values using equation (5.13) was high at 22.6 %, and the experimental data could not be suitably described by a simple correlation equation.

5.2.4 Effect of Viscosity of the Oil on the Oil Removal Rate

The oil removal rates of furnace oil and paraffin oil are compared in Figures 5.34 to 5.42 . These figures are plotted as the oil removal rate (Qoil) against the inner outlet velocity (Vi) at various conditions of annular flow velocity (Va), rotation speed of the stirrer (Ω), and water depth in the vortex tank (H). It is evident that the oil removal rate of paraffin oil is significantly higher than the oil removal rate of furnace oil under the same operating conditions of the four variables.

The viscosities, densities and surface tensions of the two oils at 25.0 °C are reported in Table 5.10 . The densities and the surface tensions of the two oils are very similar. Whereas, the viscosity of paraffin oil is almost 46 times that of the furnace oil. As a result, it may be concluded that the oil removal rate is strongly influenced by the viscosity of the oil, and that the oil removal rate of an oil of high viscosity will be higher than the removal rate of a low viscosity oil under the same operating conditions.

A simple experiment was performed to compare the coalescence rates of the two oils used in this study. A volume of 100 ml of oil and 800 ml of distilled water were agitated by means of a high speed agitator in a beaker for 5 minutes, then the coalescence time of the emulsion was recorded. The coalescence time of paraffin oil was found to be 80 seconds while that of furnace oil was 130 seconds. Therefore, the coalescence rate of the paraffin oil may be considered to be higher than that of the less viscous furnace oil.

In the oil-water separation experiments, some degree of emulsification of oil and water occurred. The oil-water mixture withdrawn from the vortex tank was allowed to coalesce in the vacuum tank for 30 minutes before the final oil accumulation reading was taken. Since the coalescence rate of furnace oil was somewhat lower than that for the paraffin oil, the observed furnace oil accumulation rate in the vacuum tank might be expected to be somewhat lower than the accumulation rate of the paraffin oil at the same 'coalescence' time. The difference in the coalescence rates between the oils may be a slight factor in the determination of oil removal rates; however, the main influence of the viscosity of the oil is considered to be the effect on the formation of the oil vortex.

5.2.5 Effect on the Oil Removal Rate of a Layer of Froth on the Oil Surface

Some 68 experiments using furnace oil were performed to study the effect of surface froth on the oil removal rate. The experimental data are given in Appendix P. The surface froth was formed by introducing the feed oil from a tube located some distance above the oil layer in the vortex tank. The feed oil carried a small amount of air into the oil layer continuously, and the air generated a layer of froth having a small cell size, on the top of the oil. When the oil-vortex formed, the surface froth filled the central vortex-core, without being drawn out of the vortex tank.

The furnace oil removal rate of the 'without froth' experiments and those of the 'with froth' experiments are compared in Figures 5.43 to 5.47 . Based on the observations from these figures, the furnace oil removal rates of the 'with froth' experiments were much higher than the oil removal rates of the 'without froth' experiments. . Thus the furnace oil removal rate increased significantly if a layer of froth was present on the surface of the oil. The reason for this improvement is not clear; it may be due to the effect of interfacial tension. However, an explanation is proposed. The function of the surface froth appeared to delay the onset of an air-entraining vortex; thus higher outlet flows could be utilized for oil removal without air entrainment. As a result, higher oil removal rates could be achieved.

The highest furnace oil removal rates and oil contents in the withdrawn mixture for the 'with froth' experiments, for five different combinations of Ω and H, are shown in Tables 5.11 and 5.12 . The maximum oil removal rate for the 'with froth' experiments was 71.8 cm^3/s, and the maximum oil contents was 94.1 %.

The method for producing froth used with furnace oil could not be used for paraffin oil, probably because the viscosity of the paraffin oil was sufficiently high so that most of the air bubbles were trapped inside the oil layer. It was difficult to produce a large area of froth on the surface of paraffin oil by this method. The successful method for producing a stable froth seemed to involve air bubbles surrounded by a film of water.

A stable froth was successfully produced when using paraffin oil by means of detergent and water in a small tank; the froth was then transferred to the surface of paraffin oil in the vortex tank. Some tests for the removal of paraffin oil in the presence of surface froth which was produced by the detergent, were performed. However, the results of the tests were very inconsistent, because of the reaction between the oil and the detergent foam which produced a solid curd like substance at the oil-water interface. Therefore, the detergent foaming method was considered a failure, and the tests for the effect of foam on the separation of paraffin oil from water, inconclusive.

5.3 RESULTS AND DISCUSSIONS OF THE FEASIBILITY STUDY OF VORTICES FOR SLURRY DECANTATION

Experiments were performed to study the feasibility of the vortex apparatus for slurry decantation. The experimental data are reported in Appendix Q, and a summary of the results is listed in Table 5.13 . The concentration difference (wt. % diff.) in Table 5.13 is defined as the difference between the initial concentration of the solution in the vortex tank (Ci) and the concentration of the 'clarified' solution (Cl) divided by the initial concentration multipled by 100.

The maximum concentration difference observed was about 30.0 % which was considered low. However, when the final concentration of solids in the slurry in the vortex tank (Cf) was compared with the concentration of solids in the 'clarified' solution (Cl), they were very similar. It appears that the decantation in these experiments was mainly that due to sedimentation, while the centrifugal force from the vortex motion contributed only a small effect to the decantation process. The magnitude of the centrifugal acceleration, which was generated by vortex motion, was therefore examined. The flow pattern of the inner section of the vortex in this study was similar to that for the combined vortex; hence, the magnitude of the centrifugal acceleration at the inner (or lower) part of the vortex could be estimated by the combined vortex equations as described in Chapter 3.

The results of four cases are listed in Table 5.14, and a sample calculation is shown in Appendix R. All the estimated centrifugal accelerations are greater than the gravitational acceleration in Table 5.14 . Thus the centrifugal force might be expected to have an effect on the separation. A probable reason for the lack of such an effect is proposed here. When the 'retention time' of the centrifugal force acting on the particles near the vortex surface was considered, it was found that this 'retention time' was usually very small. For instance, the minimum inner outlet velocity for all the cases considered in Table 5.13 was 21.19 cm/s; hence, the maximun 'retention time' particles under the influence of the centrifugal focres near the vortex surface was only 0.71 seconds. The particles at the vortex surface might not be forced to the outer part of the vortex tank in this short 'retention time'. Thus the particles were continuously withdrawn together with the liquid, and the concentration of the 'clarified' solution and the final concentration of the solution in the vortex tank were nearly the same.

The design of the vortex apparatus for slurry decantation had an obvious drawback in that the 'clarified' liquid was withdrawn through the outlet pipe at the bottom of the vortex tank. As a result, liquid near the bottom of the tank containing a higher concentration of separated solids was easily withdrawn together with the liquid from the surface,

and hence the efficiency of the separation became poor. For most solid-liquid separation devices, the 'clarified' liquid is withdrawn from the top of the device.

It may be concluded that the modified vortex apparatus as used in this study was not suitable to separate solids from a dilute slurry, and it could not successfully take advantage of the centrifugal forces involved.

TABLE 5.1

COMPARISONS OF THE EXPERIMENTAL AND PREDICTED VALUES OF Hv/d

NO.	Ω (rpm)	H (cm)	Qi (cm^3/s)	Hv/d (expt.)	Hv/d (pred.)	RATIO (*)
1	3	10.0	42.25	3.94	12.72	3.23
2	3	10.0	50.88	5.51	18.39	3.34
3	3	20.0	65.67	8.66	27.08	3.12
4	3	20.0	82.93	13.39	42.99	3.21
5	3	20.0	100.18	15.75	62.50	3.97
6	3	30.0	100.18	15.75	58.34	3.70
7	3	30.0	117.44	21.65	79.91	3.69
8	5	10.0	38.55	3.94	16.81	4.26
9	5	10.0	50.88	7.87	29.12	3.70
10	5	20.0	65.67	12.60	42.89	3.40
11	5	30.0	82.93	15.75	63.55	4.03
12	5	30.0	100.18	21.26	92.38	4.35
13	5	30.0	117.44	23.62	126.56	5.36
14	10	10.0	47.18	3.94	46.79	11.88
15	10	10.0	50.88	8.27	54.33	6.57
16	10	20.0	50.88	7.87	48.29	6.10
17	10	20.0	65.67	12.60	80.04	6.35
18	10	20.0	82.83	15.75	127.05	8.05
19	10	30.0	65.67	14.96	74.71	4.99
20	10	30.0	82.93	23.62	118.59	5.02

N.B. Qi denotes the inner volumetric flow rate, and (*) denotes the ratio of predicted Hv/d to experimental Hv/d.

TABLE 5.2

COMPARISONS OF THE RANGES FOR THE PARAMETERS IN THIS STUDY AND IN NEALE & HAYDUK STUDY

PARAMETERS	THIS WORK	NEALE AND HAYDUK
1. rotation speed of the stirrer (rpm)	3 to 10	0 to 25
2. outlet volumetric flowrate,Q,(cm^3/s)	38.55 to 117.44	40.00 to 320.00
3. outlet diameter,d, (cm)	1.27	1.80 to 2.54
4. stirrer inside diameter,D2,(cm)	37.5	15.0 to 30.0
5. water depth,H,(cm)	10.0 to 30.0	20.0 to 55.0
6. Kinematic viscosity of water,($cm^3/cm.s$)	$8.92x10^{-3}$	$8.92x10^{-3}$
7. gravity accerlation, g,(cm/s^2)	980.665	980.665

TABLE 5.3

LINEAR REGRESSION ANALYSIS FOR FIGURE 5.5

STIRRER ROTATIONAL SPEED(rpm)	RESULT OF LINEAR REGRESSION	CORRELATION COEFFICIENT
3	Hv = 0.4224.Vc-2.9320	0.9715
5	Hv = 0.6271.Vc-5.3107	0.9641
10	Hv = 1.0972.Vc-15.6641	0.9034

TABLE 5.4

VALUES OF a AND b FOR VARIOUS STIRRER ROTATIONAL SPEED

STIRRER ROTATIONAL SPEED (rpm)	a	b
3	0.85	0.15
5	0.81	0.19
10	0.75	0.25

TABLE 5.5

LINEAR REGRESSION ANALYSIS FOR TABLE 5.4

STIRRER ROTATIONAL SPEED(rpm)	RESULT OF LINEAR REGRESSION	CORRELATION COEFFICIENT
3	Hv = 0.4255.Vc-3.0370	0.9757
5	Hv = 0.6246.Vc-5.1713	0.9681
10	Hv = 1.1056.Vc-14.9448	0.9468

TABLE 5.6

THE HIGHEST FURNACE OIL REMOVAL RATES FOR NINE CASES WITH DIFFERENT COMBINATIONS OF Ω AND H .

NO.	Ω (rpm)	H (cm)	Va (cm/s)	Vi (cm/s)	OIL REMOVAL RATE(cm^3/s)
1	3	10.0	47.36	49.10	11.7
2	3	20.0	70.58	81.88	10.9
3	3	30.0	70.58	81.88	9.2
4	5	10.0	47.36	40.91	19.5
5	5	20.0	70.58	57.30	25.7
6	5	30.0	70.58	81.88	14.1
7	10	10.0	12.11	36.81	7.2
8	10	20.0	70.58	40.91	22.8
9	10	30.0	70.58	57.30	20.2

TABLE 5.7

THE HIGHEST FURNACE OIL CONTENTS FOR NINE CASES WITH DIFFERENT COMBINATIONS OF Ω AND H

NO.	Ω (rpm)	H (cm)	Va (cm/s)	Vr (cm/s)	OIL CONTENT (%)
1	3	10.0	47.36	28.61	23.9
2	3	20.0	70.58	40.91	14.2
3	3	30.0	70.58	59.35	10.4
4	5	10.0	47.36	28.61	48.7
5	5	20.0	70.58	31.69	45.7
6	5	30.0	70.58	65.49	16.1
7	10	10.0	12.11	36.81	15.4
8	10	20.0	70.58	40.91	43.9
9	10	30.0	70.58	49.10	30.2

TABLE 5.8

THE HIGHEST PARAFFIN OIL REMOVAL RATES FOR NINE CASES WITH DIFFERENT COMBINATIONS OF Ω AND H

NO.	Ω (rpm)	H (cm)	Va (cm/s)	Vi (cm/s)	OIL REMOVAL RATE(cm^3/s)
1	3	10.0	18.13	56.41	33.0
2	3	20.0	70.58	58.14	26.9
3	3	30.0	70.58	77.15	21.2
4	5	10.0	24.15	56.41	40.8
5	5	20.0	70.58	56.41	42.4
6	5	30.0	24.15	84.07	40.1
7	10	10.0	24.15	42.58	25.5
8	10	20.0	12.11	63.32	33.1
9	10	30.0	47.36	84.07	32.0

TABLE 5.9

THE HIGHEST PARAFFIN OIL CONTENTS FOR NINE CASES WITH DIFFERENT COMBINATIONS OF Ω AND H

NO.	Ω (rpm)	H (cm)	Va (cm/s)	Vi (cm/s)	OIL CONTENT (%)
1	3	10.0	47.36	32.20	56.7
2	3	20.0	70.58	42.58	41.2
3	3	30.0	70.58	58.14	25.1
4	5	10.0	24.15	56.41	57.0
5	5	20.0	70.58	56.41	59.2
6	5	30.0	70.58	42.58	47.2
7	10	10.0	24.15	32.20	49.4
8	10	20.0	70.58	42.58	50.5
9	10	30.0	47.36	42.58	46.4

TABLE 5.10

PHYSICAL PROPERTIES OF FURNACE OIL AND PARAFFIN OIL AT 25 DEGREE C

	FURNACE OIL	PARAFFIN OIL
VISCOSITY (g/cm.s)	0.0298	1.3660
DENSITY (g/cm^3)	0.8491	0.8726
SURFACE TENSION (dynes/cm)	30.4	33.1

TABLE 5.11

THE HIGHEST FURNACE OIL REMOVAL RATES FOR FIVE CASES IN "WITH FROTH" EXPERIMENTS

NO.	Ω (rpm)	H (cm)	Va (cm/s)	Vi (cm/s)	OIL REMOVAL RATE(cm^3/s)
1	3	20.0	70.58	81.88	28.7
2	5	10.0	47.36	57.30	49.9
3	5	20.0	70.58	73.69	71.8
4	5	30.0	70.58	98.27	56.3
5	10	20.0	47.36	57.30	51.2

TABLE 5.12

THE HIGHEST FURNACE OIL CONTENTS FOR FIVE CASES IN "WITH FROTH" EXPERIMENTS

NO.	Ω (rpm)	H (cm)	Va (cm/s)	Vi (cm/s)	OIL CONTENT (%)
1	3	20.0	70.58	40.91	31.0
2	5	10.0	47.36	28.61	94.1
3	5	20.0	70.58	32.62	81.0
4	5	30.0	70.58	56.28	45.1
5	10	20.0	70.58	31.69	93.7

TABLE 5.13

SUMMARY OF SLURRY DECANTATION RESULTS

NO.	Ω (rpm)	H (cm)	Va (cm/s)	Vi (cm/S)	WT. % OF SOLID (%)			WT. % DIFF. (%)
					Ci	Cl	Cf	
1	3	10.0	9.82	26.54	0.0464	0.0325	0.0266	29.95
2	3	10.0	0.00	33.35	0.0393	0.0308	0.0289	21.55
3	3	10.0	0.00	40.16	0.0435	0.0365	0.0320	16.21
4	3	20.0	149.50	26.54	0.0817	0.0713	0.0748	12.68
5	3	20.0	149.50	40.16	0.0791	0.0680	0.0713	13.99
6	3	20.0	0.00	59.62	0.0638	0.0544	0.0581	14.76
7	5	10.0	12.11	21.19	0.0588	0.0431	0.0438	26.80
8	5	10.0	9.11	23.62	0.0657	0.0520	0.0501	20.79
9	5	10.0	0.00	26.54	0.0534	0.0417	0.0417	22.02
10	10	10.0	12.11	21.19	0.0329	0.0238	0.0228	27.85
11	10	10.0	0.00	23.62	0.0289	0.0257	0.0259	11.38
12	10	10.0	0.00	26.54	0.0355	0.0280	0.0275	21.19
13	10	20.0	24.15	21.19	0.0817	0.0579	0.0567	29.11
14	10	20.0	18.13	23.62	0.0605	0.0464	0.0515	23.34
15	10	20.0	15.12	26.54	0.0567	0.0449	0.0480	20.75

N.B.: Ci denotes the initial weight % of solid of the solution in the vortex tank; Cl denotes the weight % of solid in the 'clarified' solution; Cf denotes the final weight % of solid of the solution in the vortex tank.

TABLE 5.14

ESTIMATED CENTRIFUGAL ACCELERATION UNDER VARIED OPERATING CONDITIONS

NO.	Ω (rpm)	H (cm)	Hv (cm)	Va (cm/s)	Vi (cm/s)	ESTIMATED POSITION, Z (cm)	ESTIMATED CENTRIFUGAL ACCELERATION
1	3	30.0	30.0	61.29	79.09	1.0	26.7xg
2	3	10.0	5.0	9,82	26.54	1.0	8.0xg
3	5	20.0	10.0	77.54	0.00	1.7	6.6xg
4	10	30.0	30.0	114.68	26.54	5.0	14.7xg

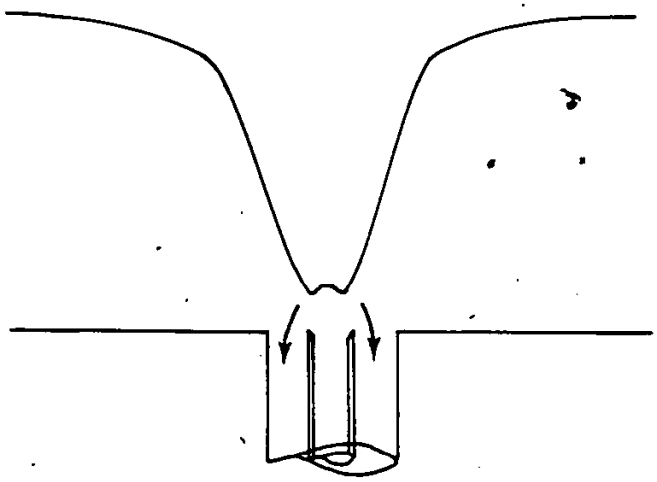

Figure 5.1: THE SHAPE OF A VORTEX IF ONLY THE ANNULAR FLOW WAS USED AT THE OUTLET

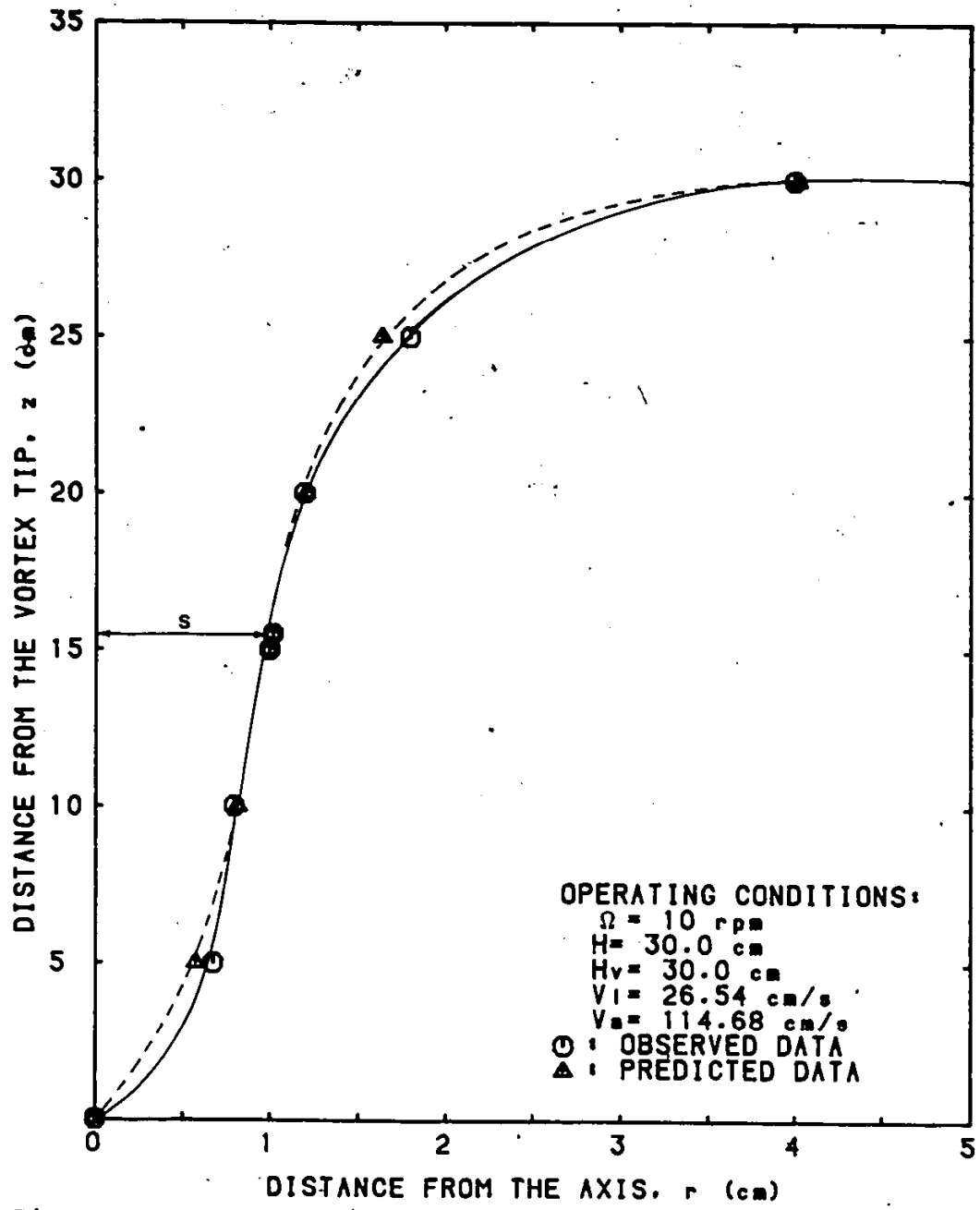

Figure 5.2: COMPARISON OF OBSERVED AND PREDICTED VORTEX SHAPE AT Ω =10 rpm, H=30.0 cm

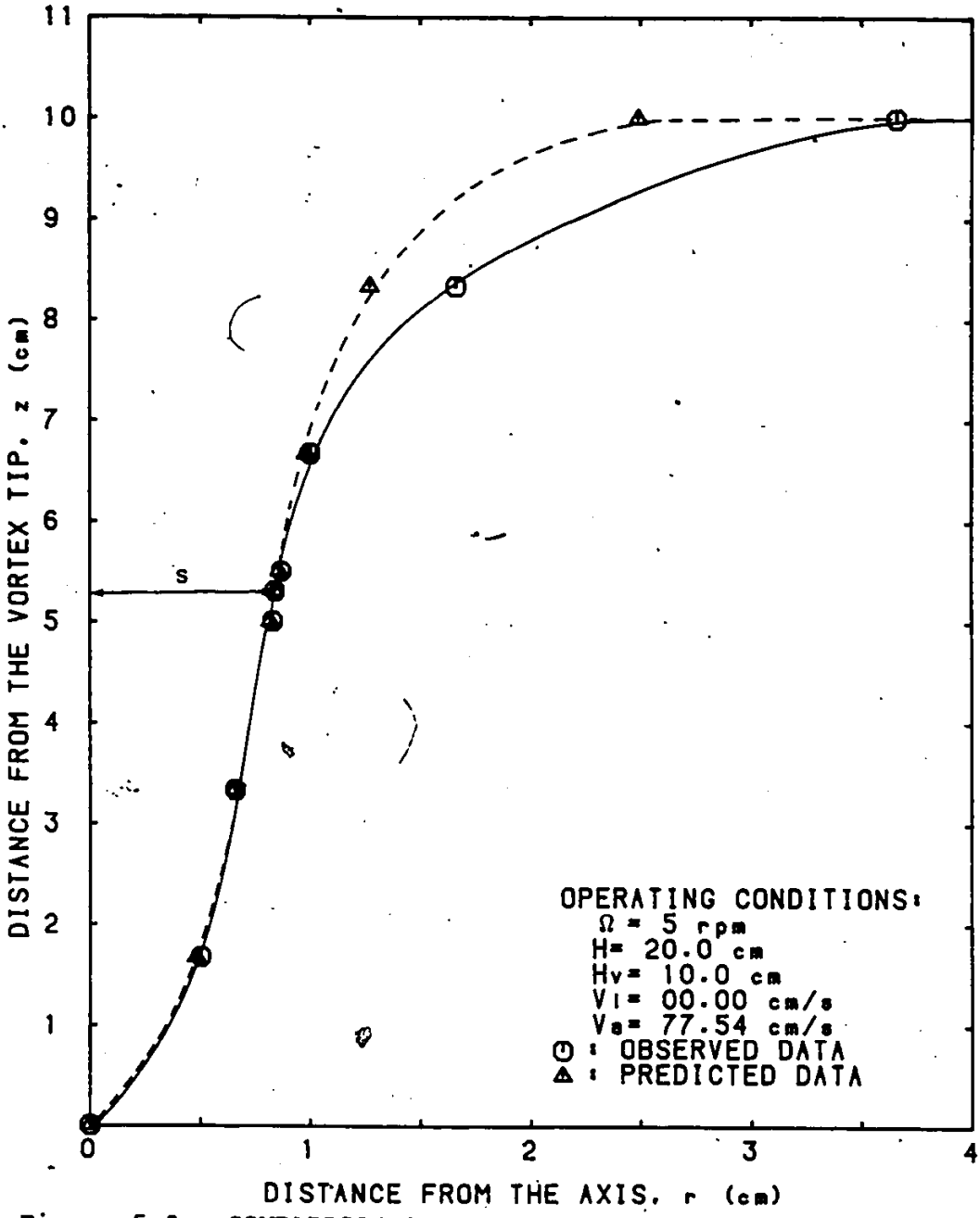

Figure 5.3: COMPARISON OF OBSERVED AND PREDICTED VORTEX SHAPE AT Ω = 5 rpm, H=20.0 cm

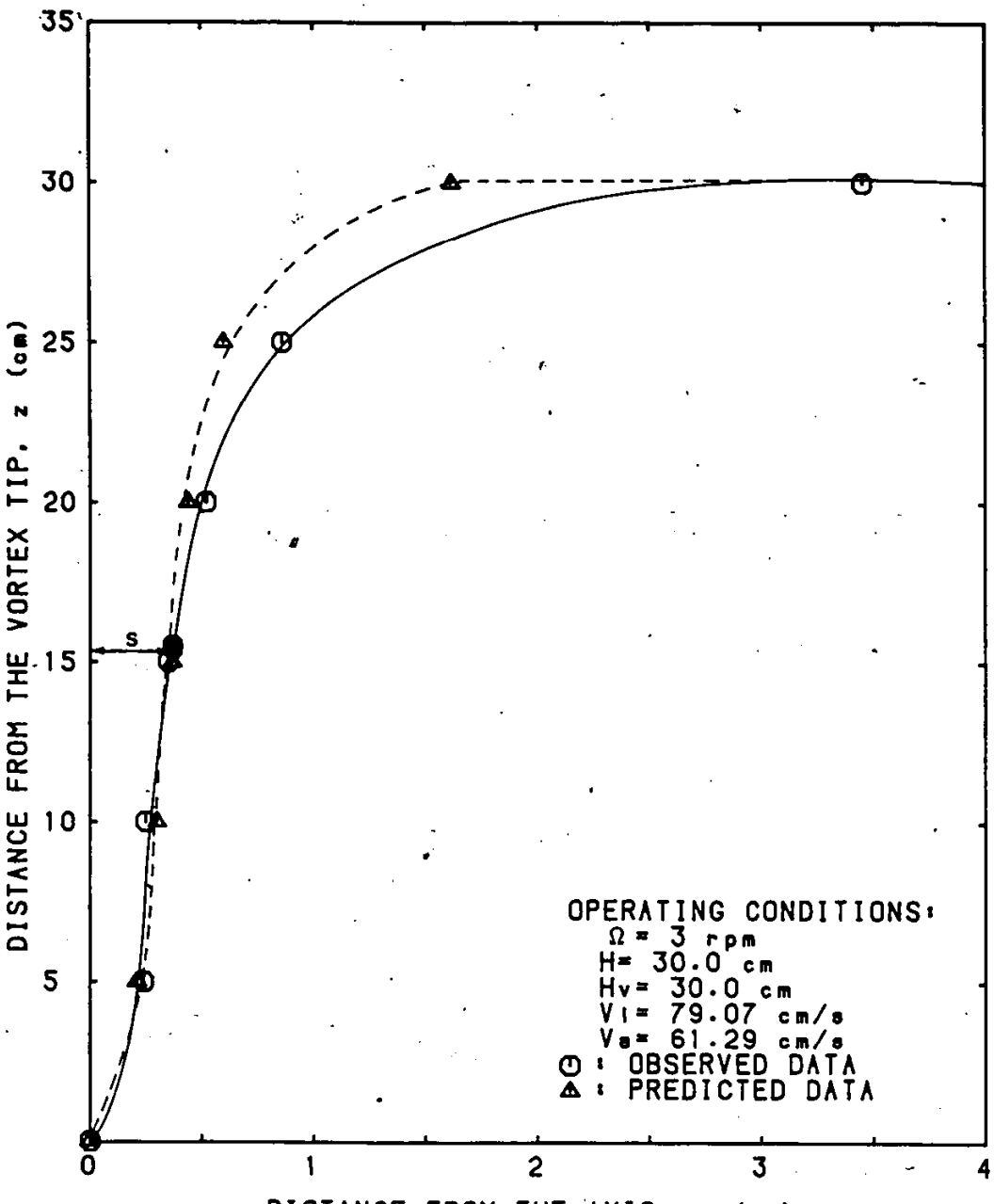

Figure 5.4: COMPARISON OF OBSERVED AND PREDICTED VORTEX SHAPE AT Ω = 3 rpm, H=30.0 cm

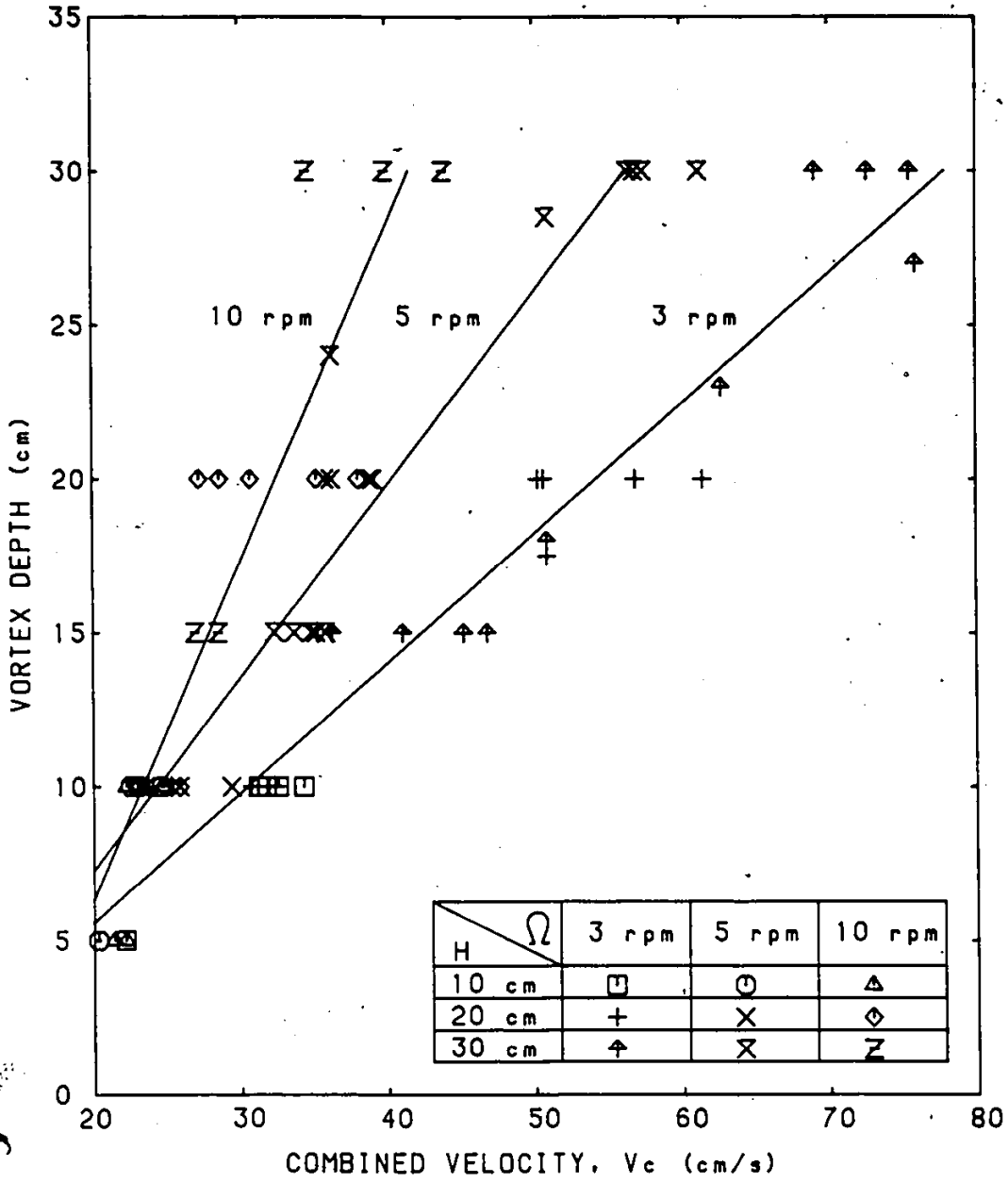

Figure 5.5: PLOT OF VORTEX DEPTH VERSUS COMBINED VELOCITY BY EQUATION (5.3)

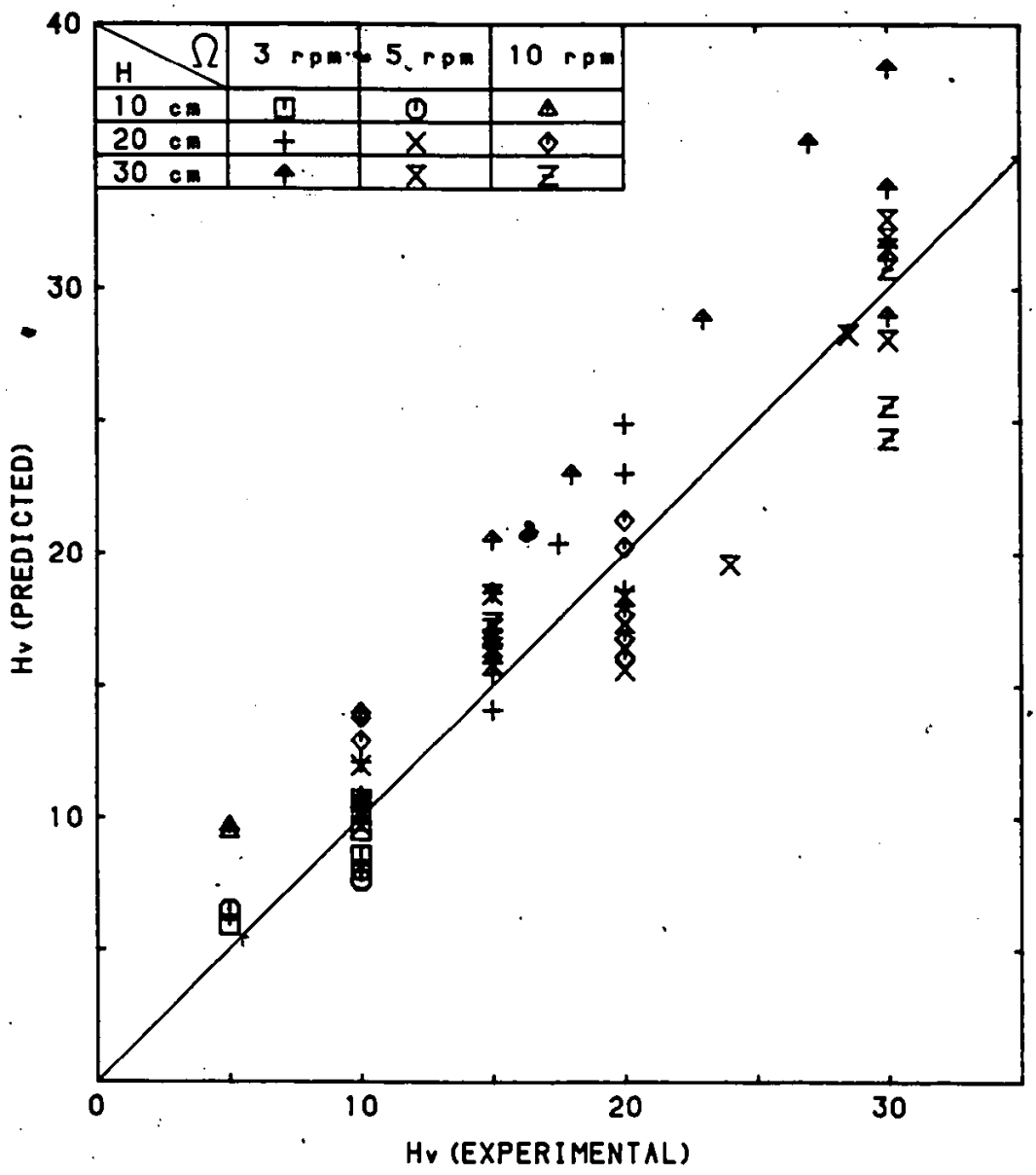

Figure 5.6: COMPARISON OF EXPERIMENTAL Hv WITH PREDICTED Hv BY THE CORRELATION EQUATION (5.8)

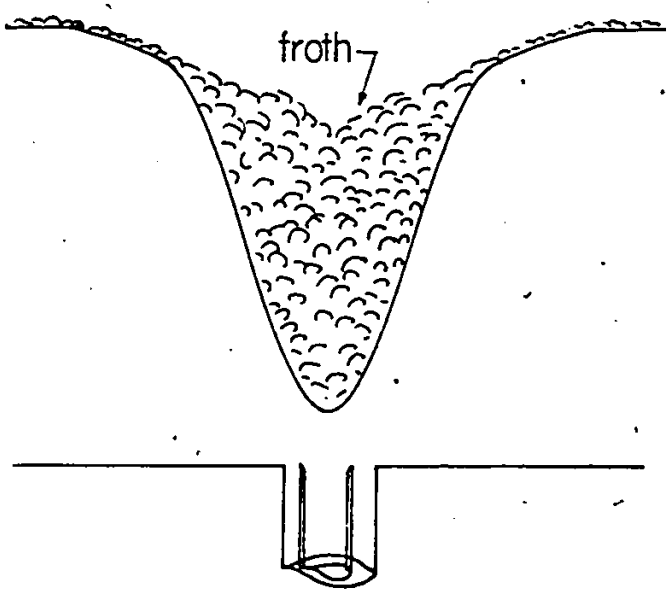

Figure 5.7: A SURFACE FROTH VORTEX

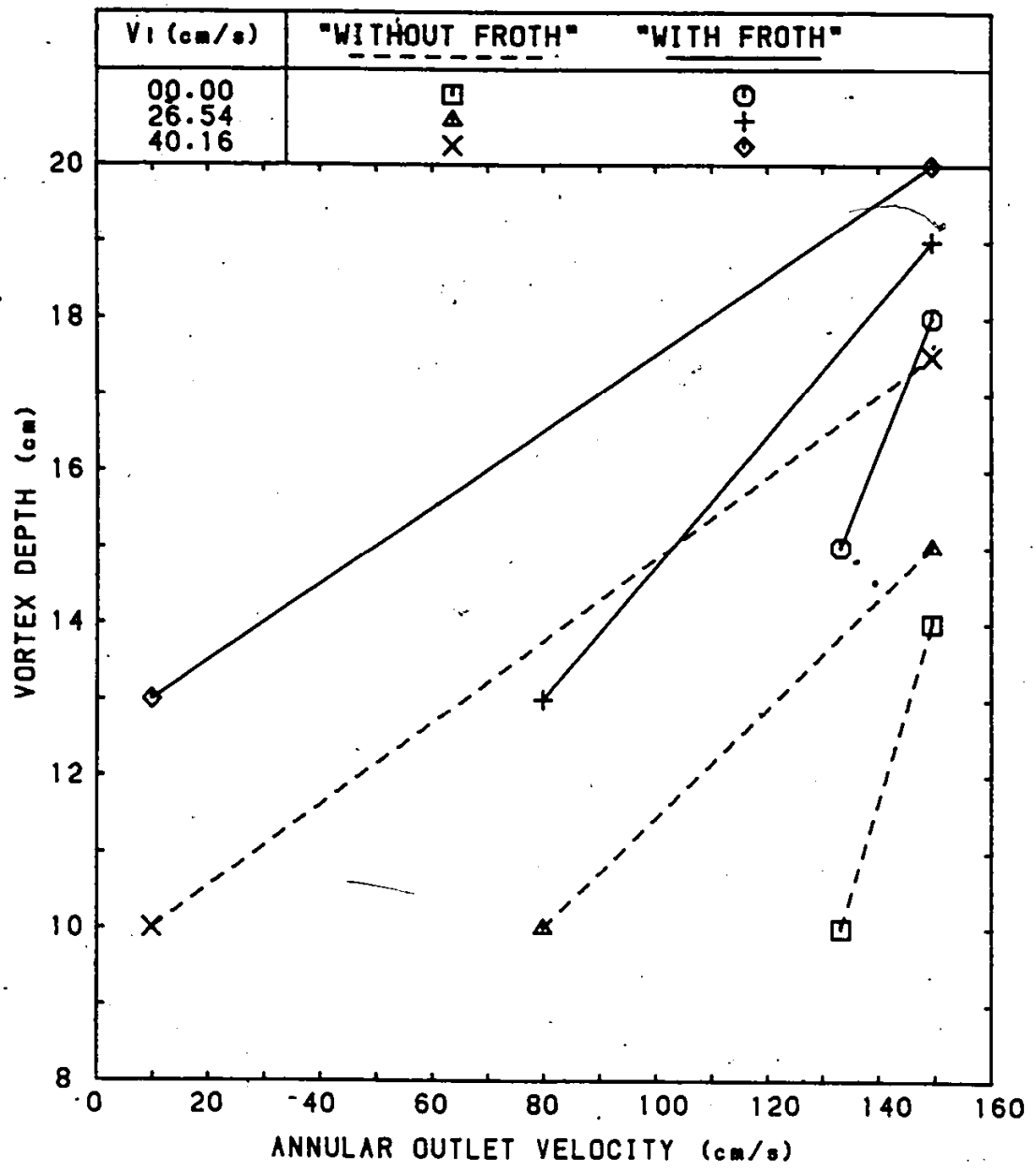

Figure 5.8: COMPARISONS OF VORTEX DEPTH OF "WITH FROTH" AND "WITHOUT FROTH" EXPERIMENTS AT Ω = 3 rpm, H= 20.0 cm AND VARIED Vi

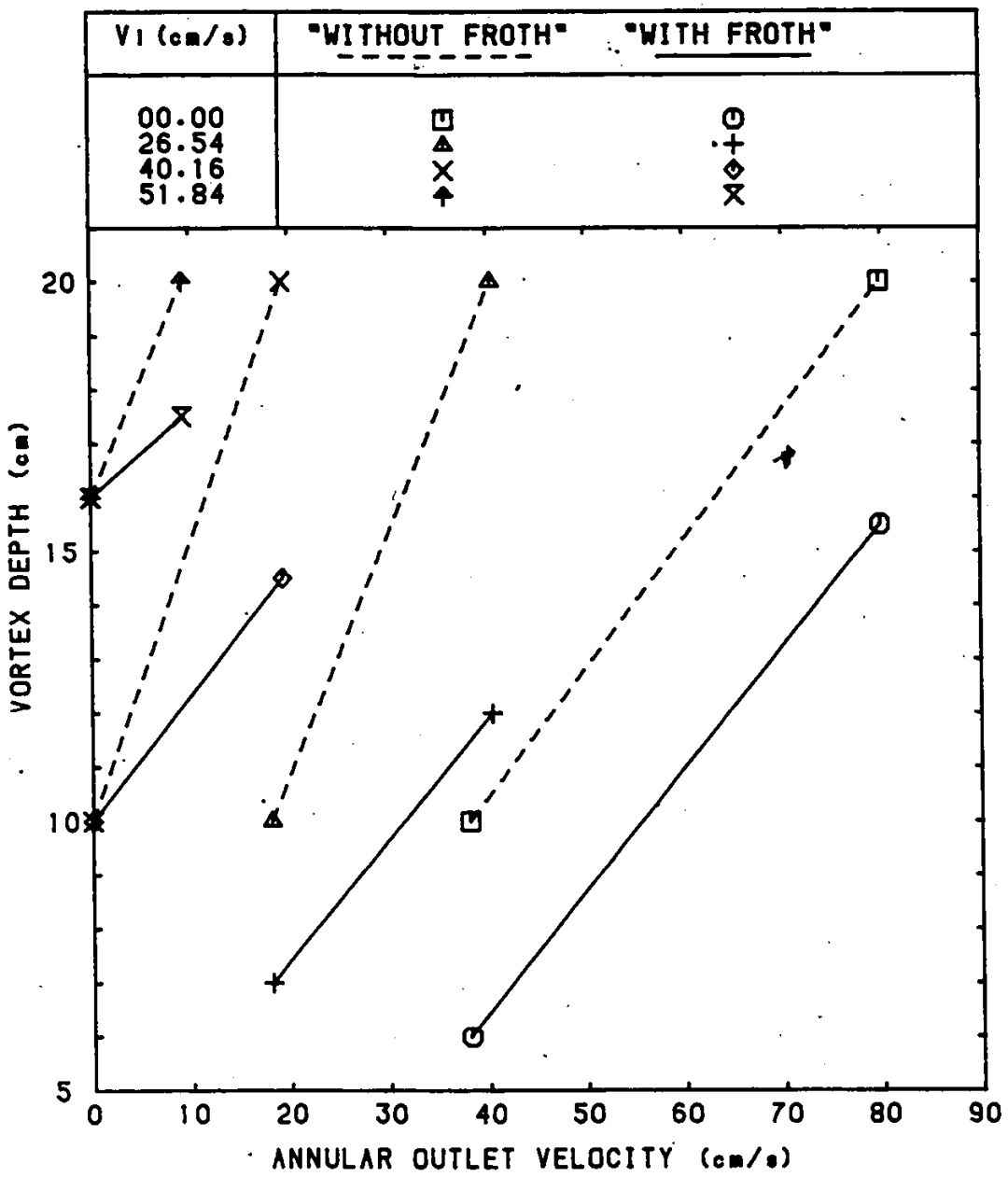

Figure 5.9: COMPARISONS OF VORTEX DEPTH OF "WITH FROTH" AND "WITHOUT FROTH" EXPERIMENTS AT Ω = 10 rpm, H= 20.0 cm AND VARIED Vi

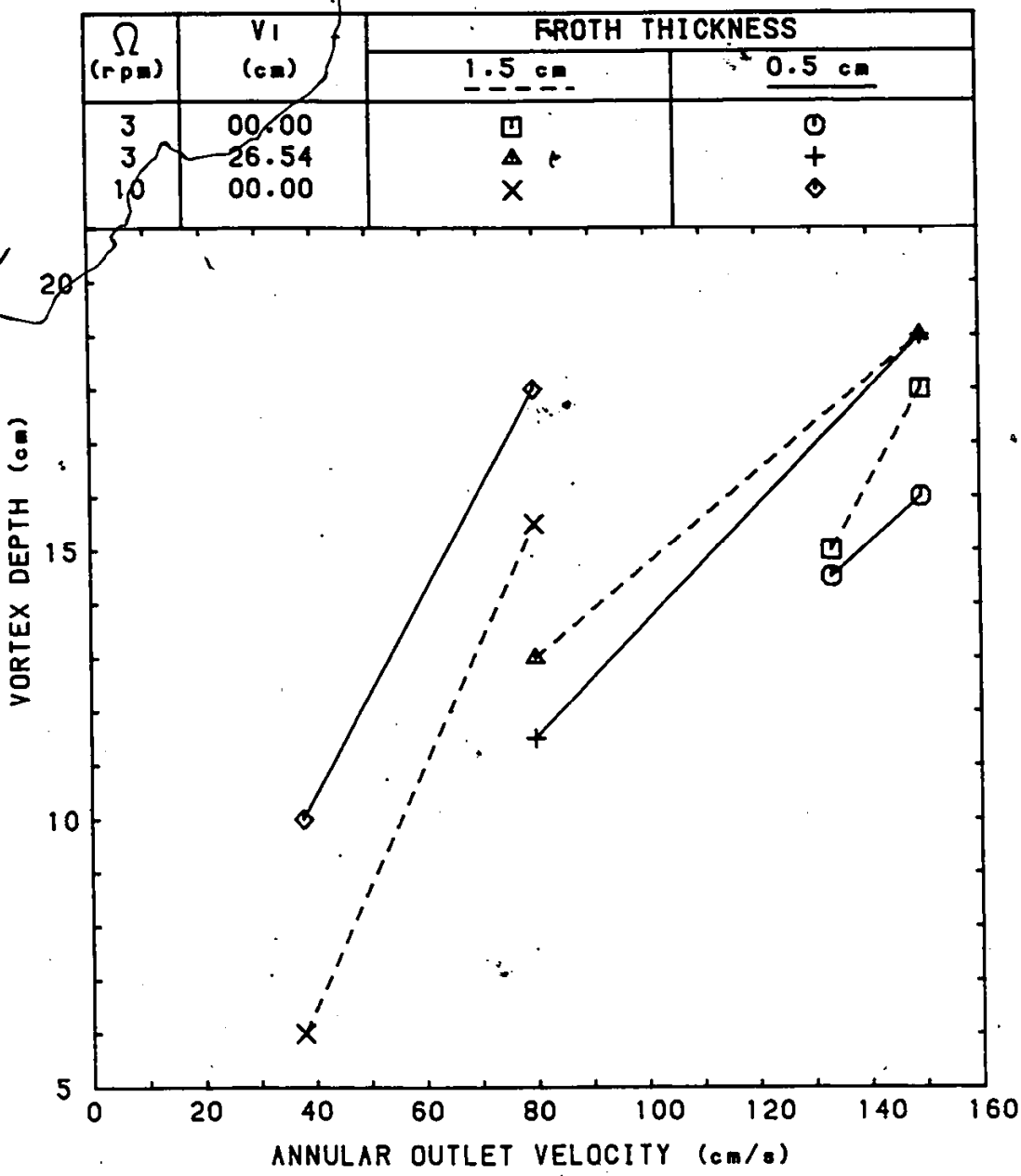

Figure 5.10: EFFECT OF THE THICKNESS OF FROTH ON THE VORTEX DEPTH AT H= 20.0 cm AND VARIED Ω & Vi

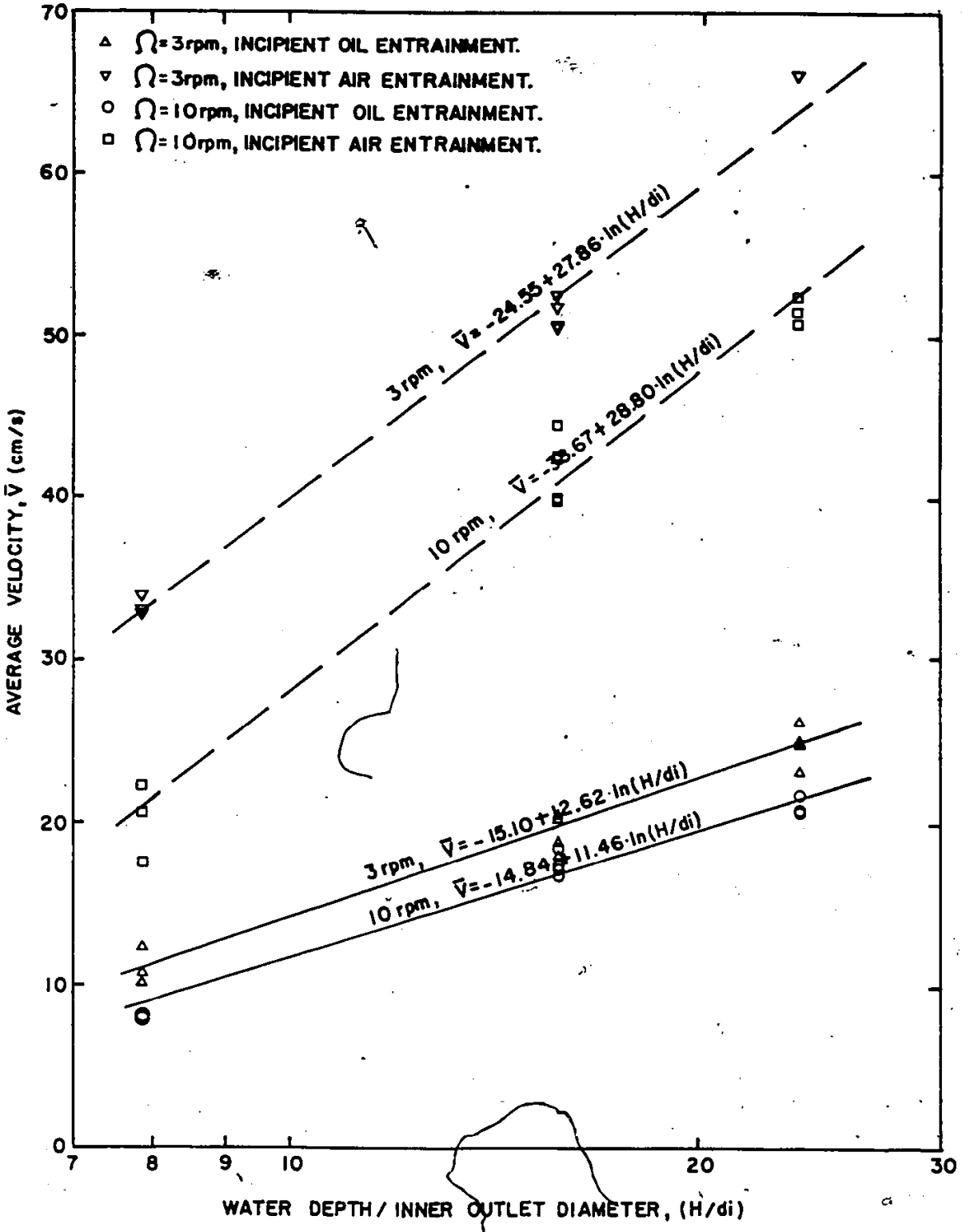

Figure 5.11: PLOT OF $\bar{V}$ AGAINST ln(H/di) FOR FURNACE OIL

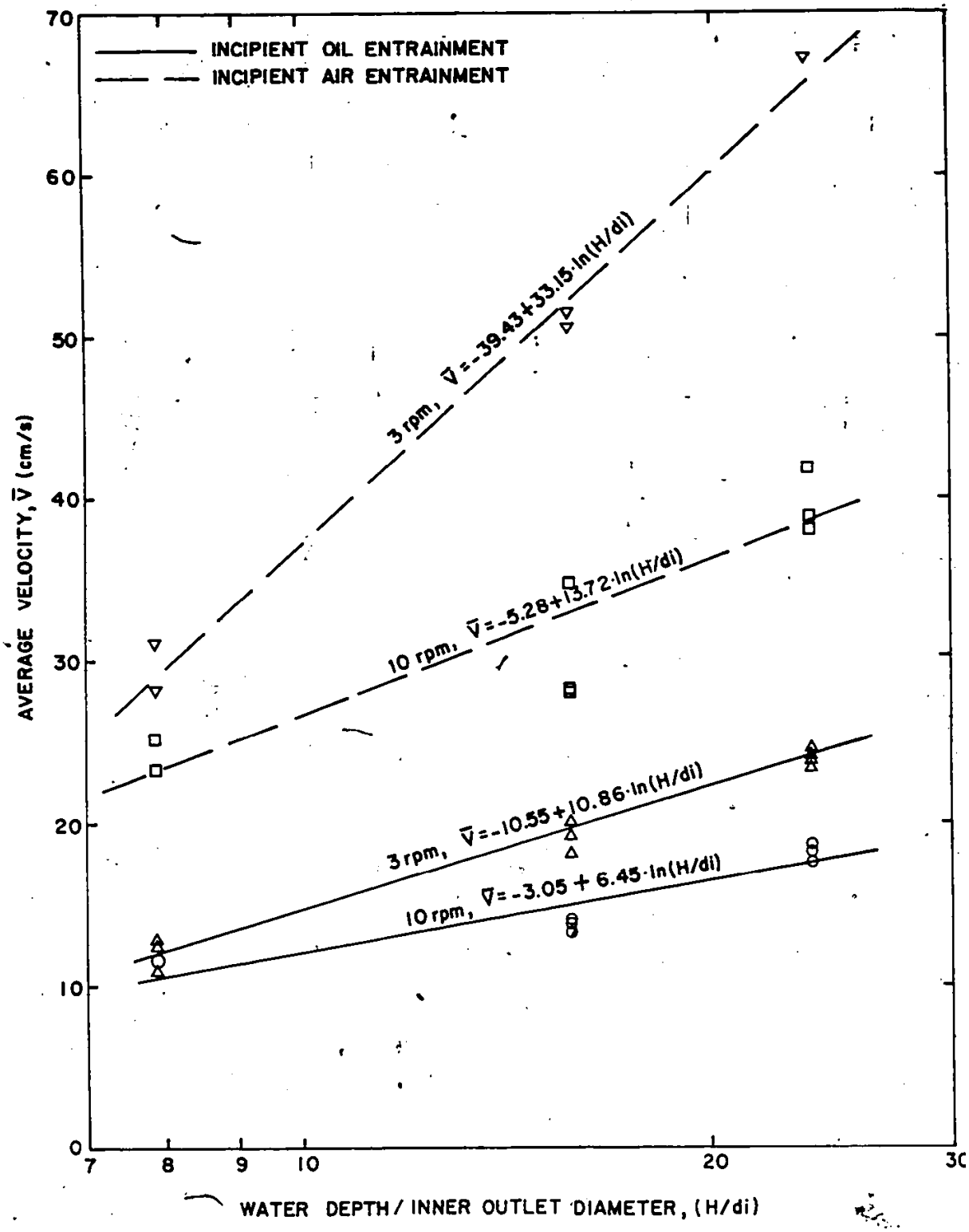

Figure 5.12: PLOT OF $\bar{V}$ AGAINST ln(H/di) FOR PARAFFIN OIL

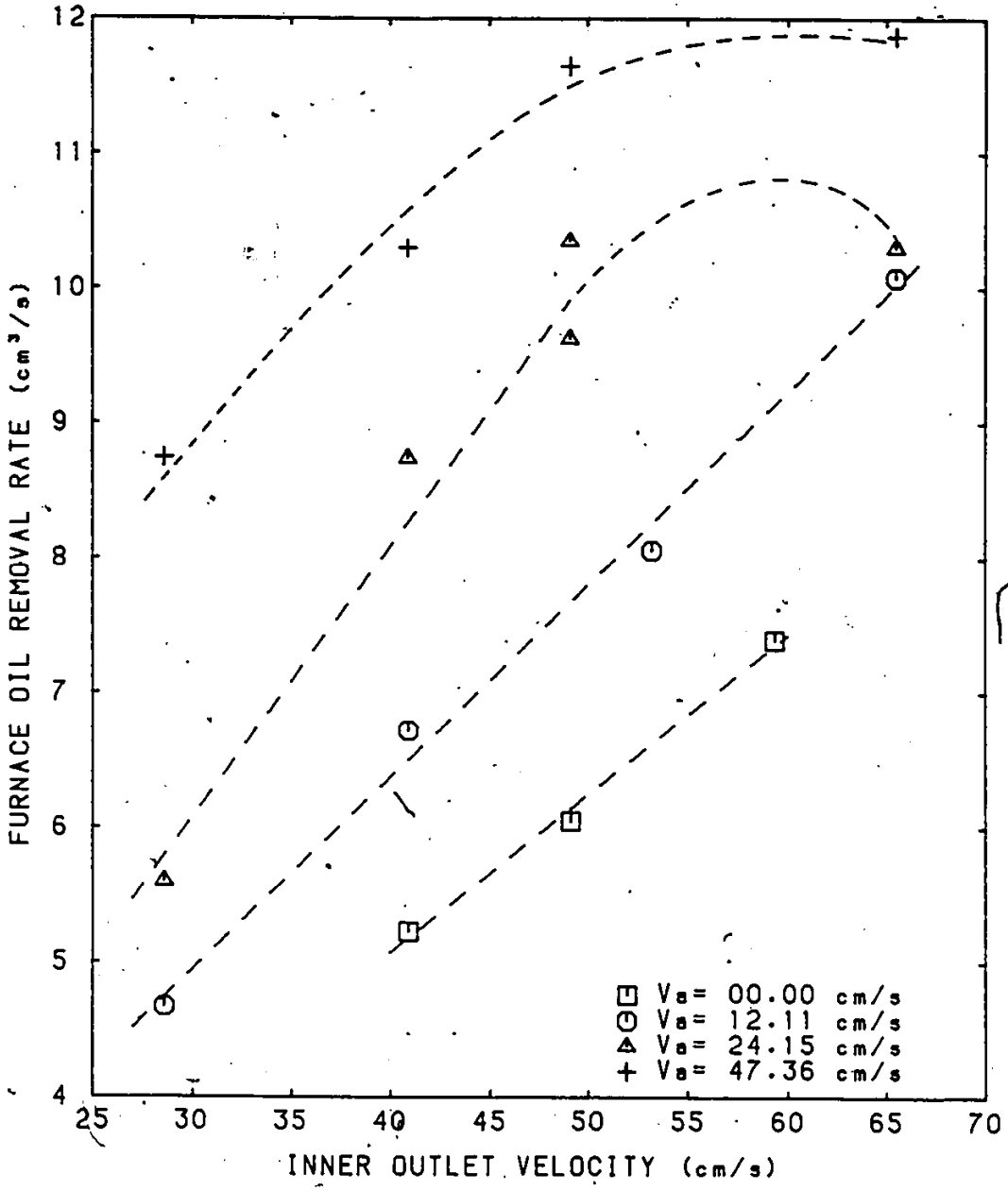

Figure 5.13: PLOT OF FURNACE OIL REMOVAL RATE VERSUS INNER OUTLET VELOCITY AT VARIED Va, Ω = 3 rpm & H = 10.0 cm

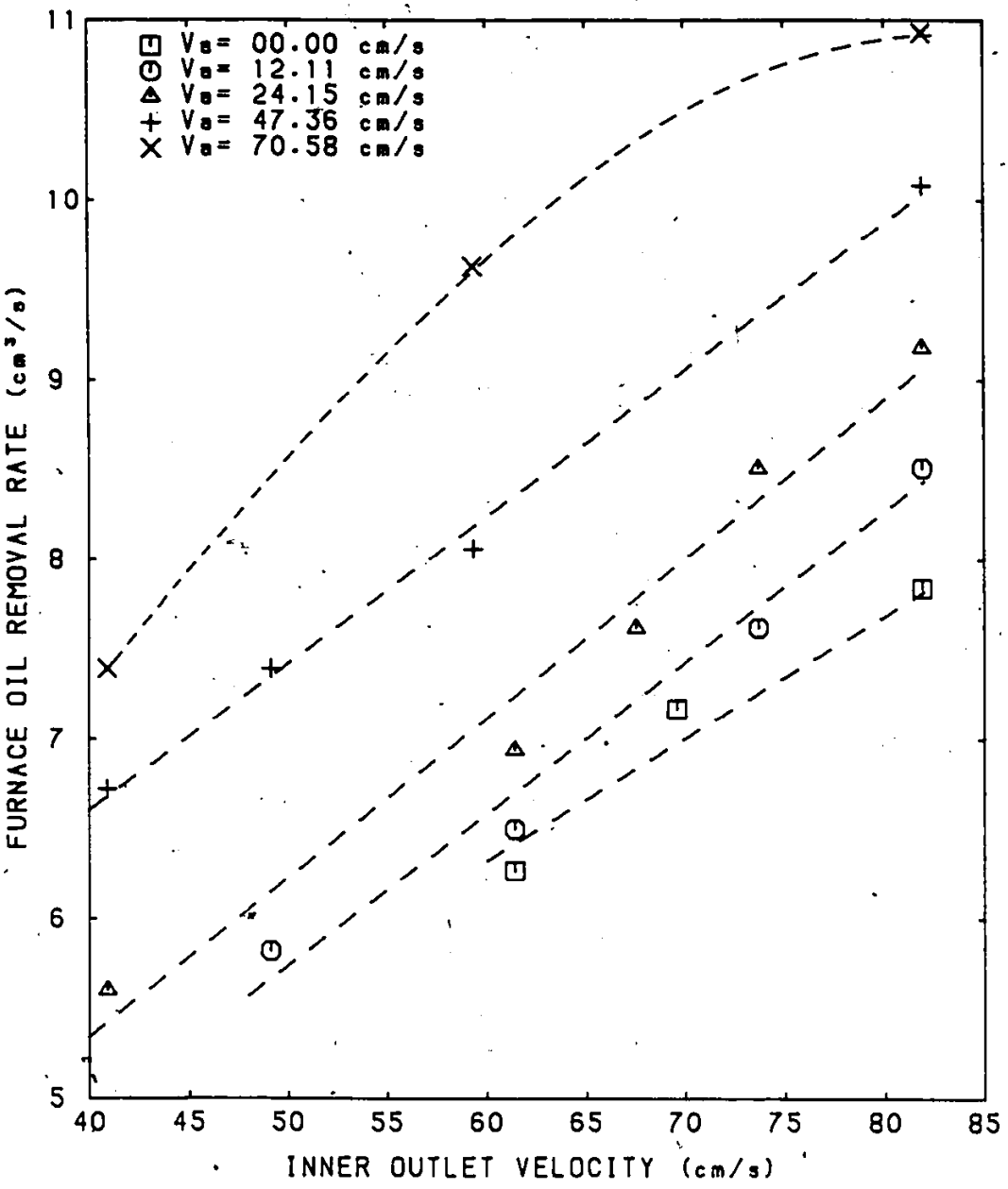

Figure 5.14: PLOT OF FURNACE OIL REMOVAL RATE VERSUS INNER OUTLET VELOCITY AT VARIED Va, Ω = 3 rpm & H = 20.0 cm

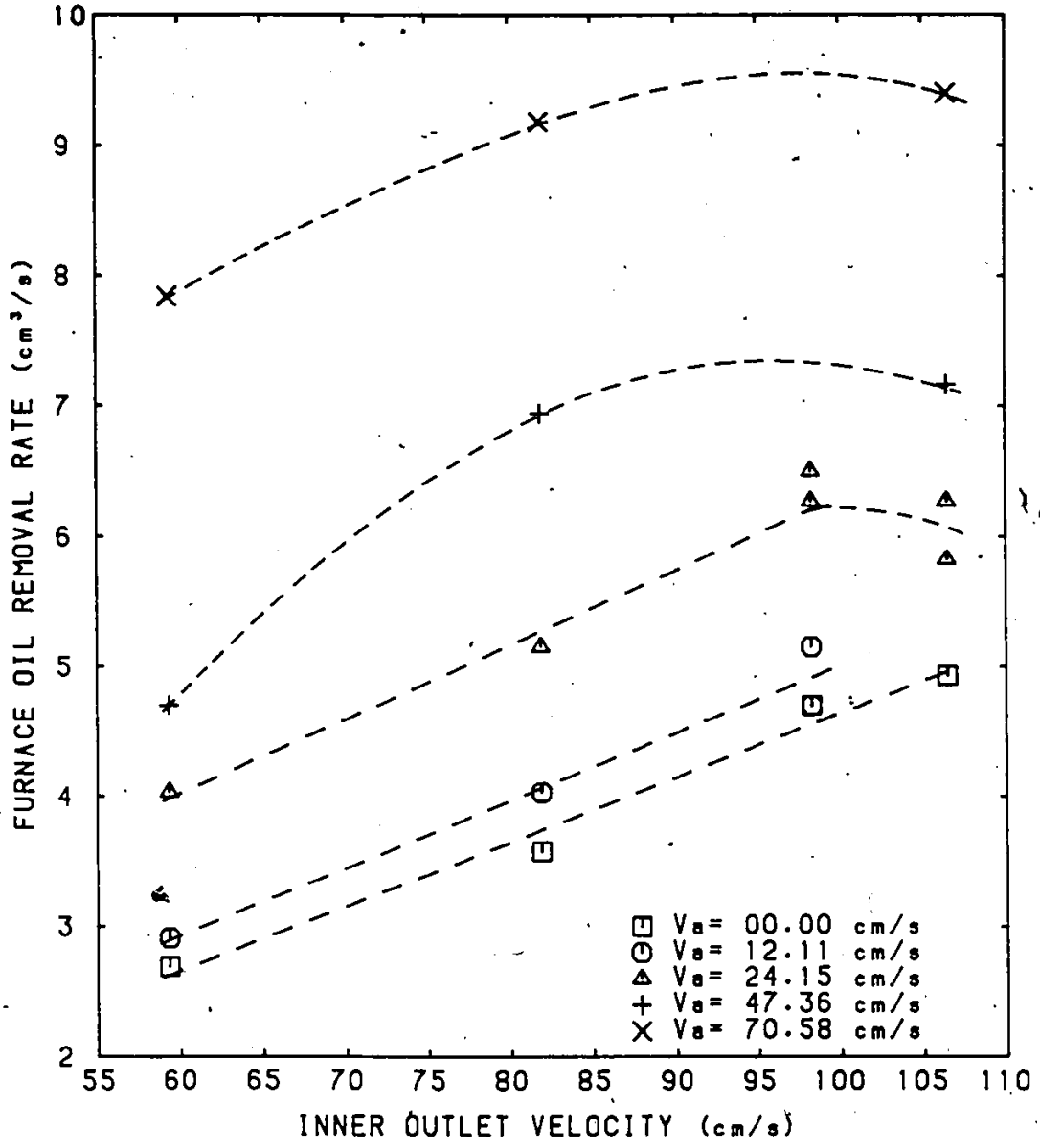

Figure 5.15: PLOT OF FURNACE OIL REMOVAL RATE VERSUS INNER OUTLET VELOCITY AT VARIED Va, Ω = 3 rpm & H = 30.0 cm

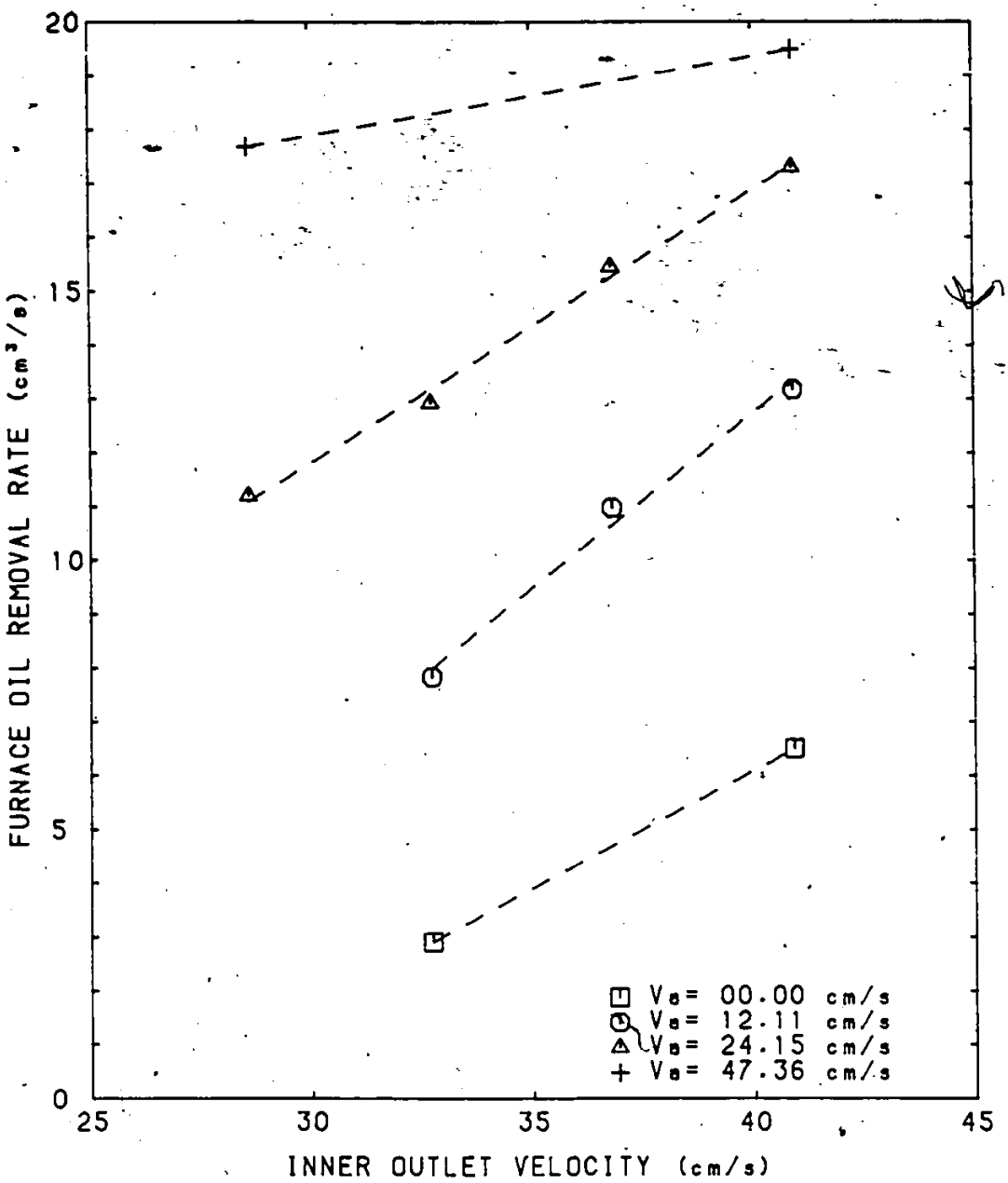

Figure 5.16: PLOT OF FURNACE OIL REMOVAL RATE VERSUS INNER OUTLET VELOCITY AT VARIED Va, Ω = 5 rpm & H = 10.0 cm

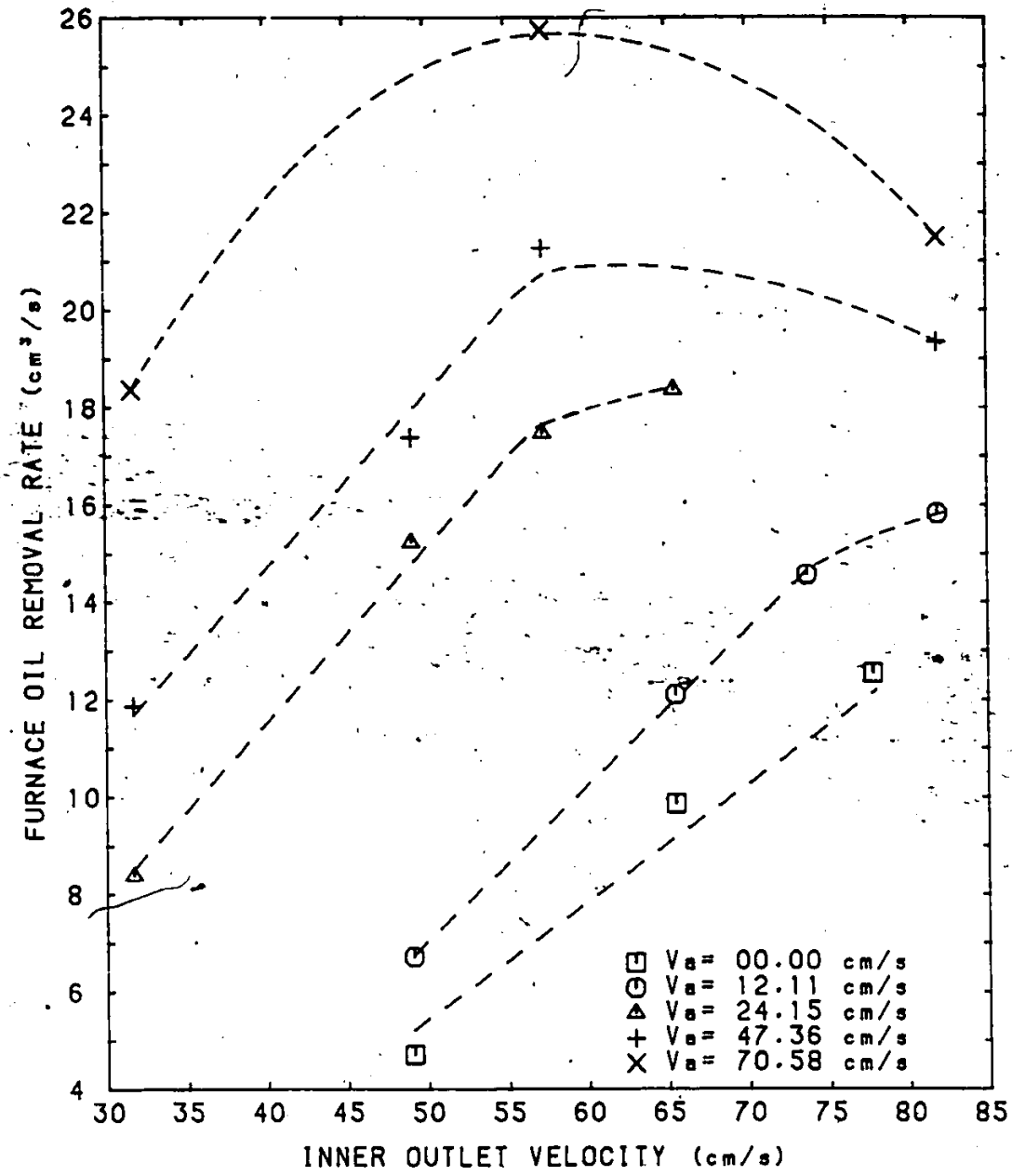

Figure 5.17: PLOT OF FURNACE OIL REMOVAL RATE VERSUS INNER OUTLET VELOCITY AT VARIED Va, Ω = 5 rpm & H = 20.0 cm

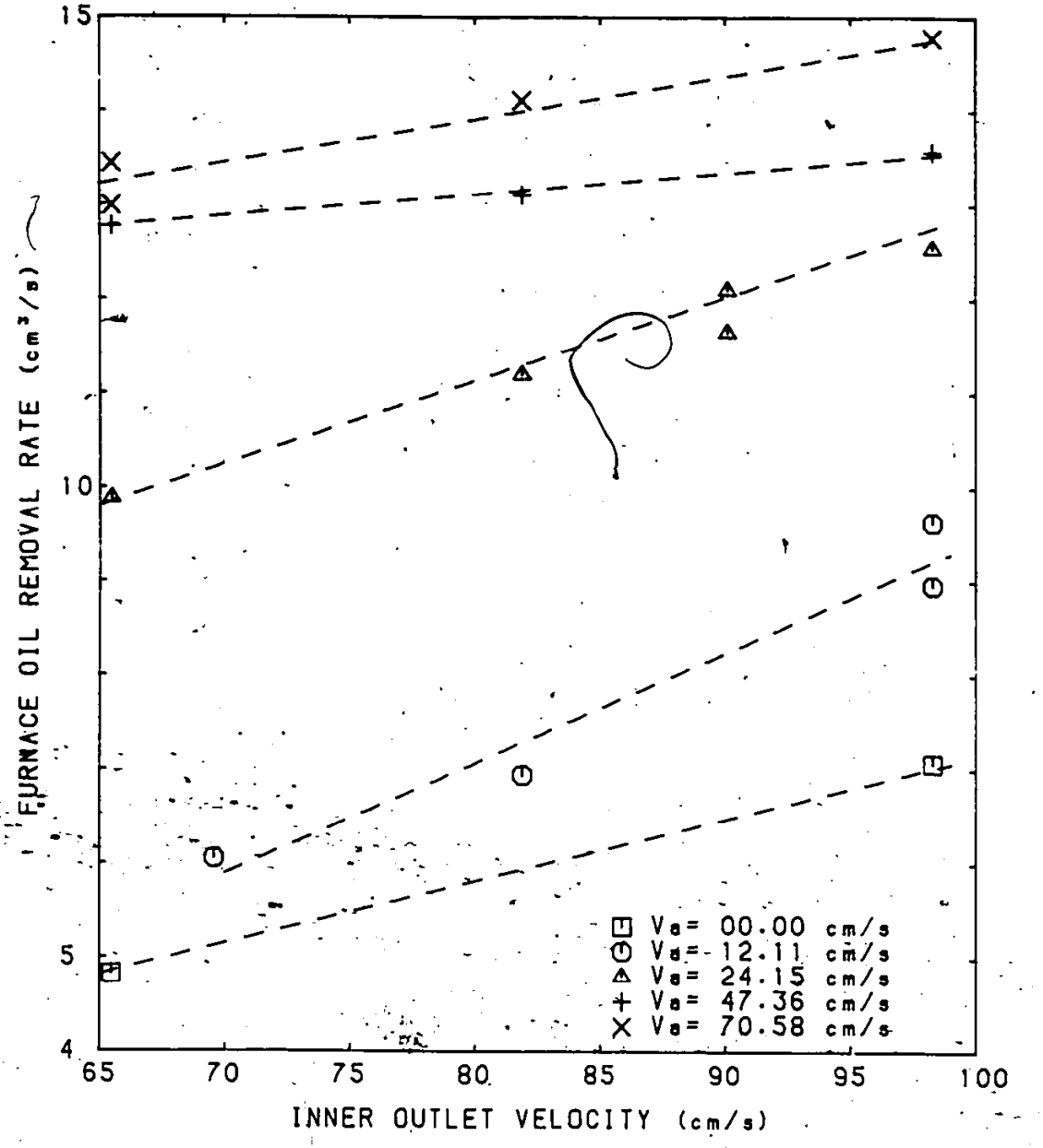

Figure 5.18: PLOT OF FURNACE OIL REMOVAL RATE VERSUS INNER OUTLET VELOCITY AT VARIED Va, Ω = 5 rpm & H = 30.0 cm

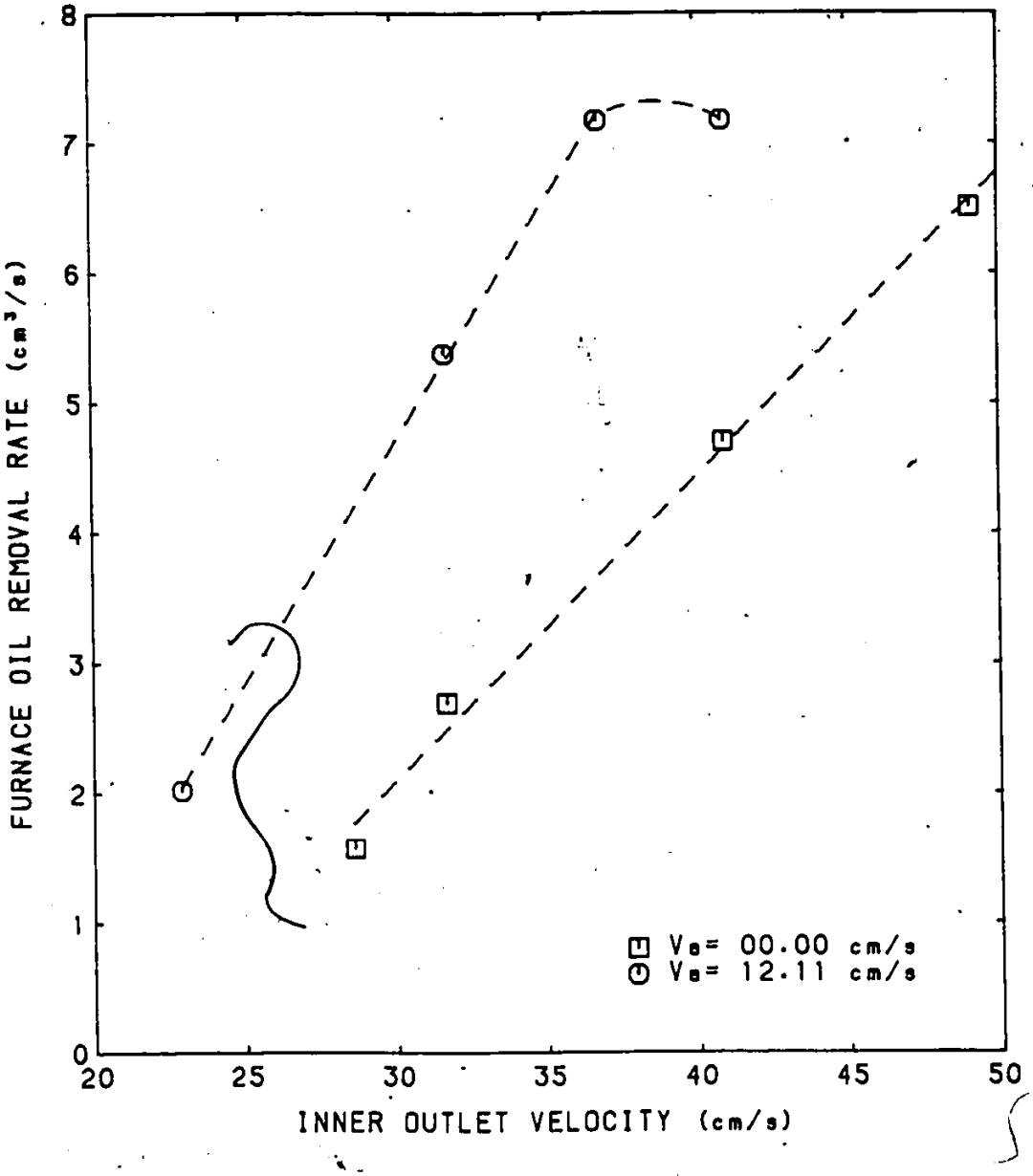

Figure 5.19: PLOT OF FURNACE OIL REMOVAL RATE VERSUS INNER OUTLET VELOCITY AT VARIED Va, Ω = 10 rpm & H = 10.0 cm

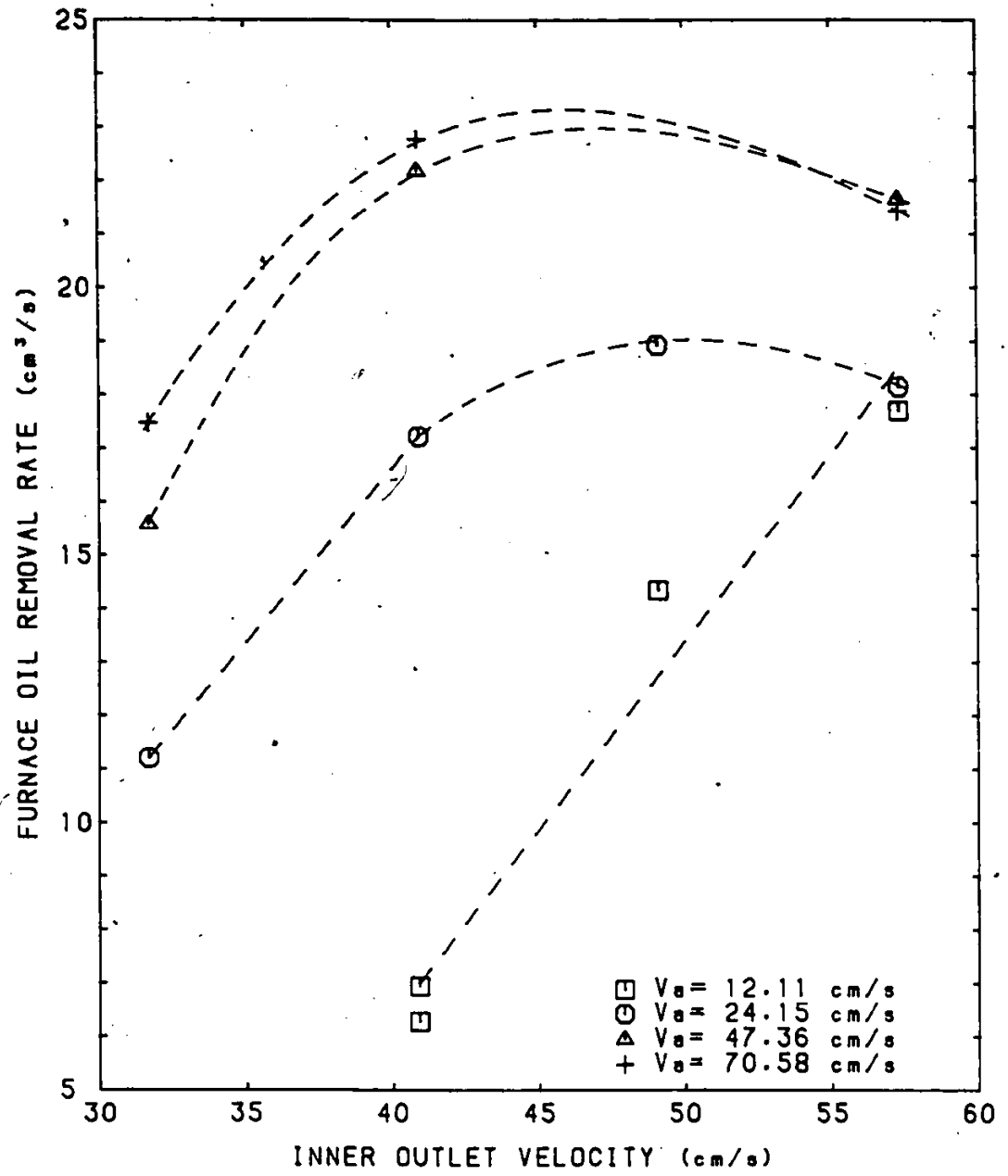

Figure 5.20: PLOT OF FURNACE OIL REMOVAL RATE VERSUS INNER OUTLET VELOCITY AT VARIED Va, Ω = 10 rpm & H = 20.0 cm

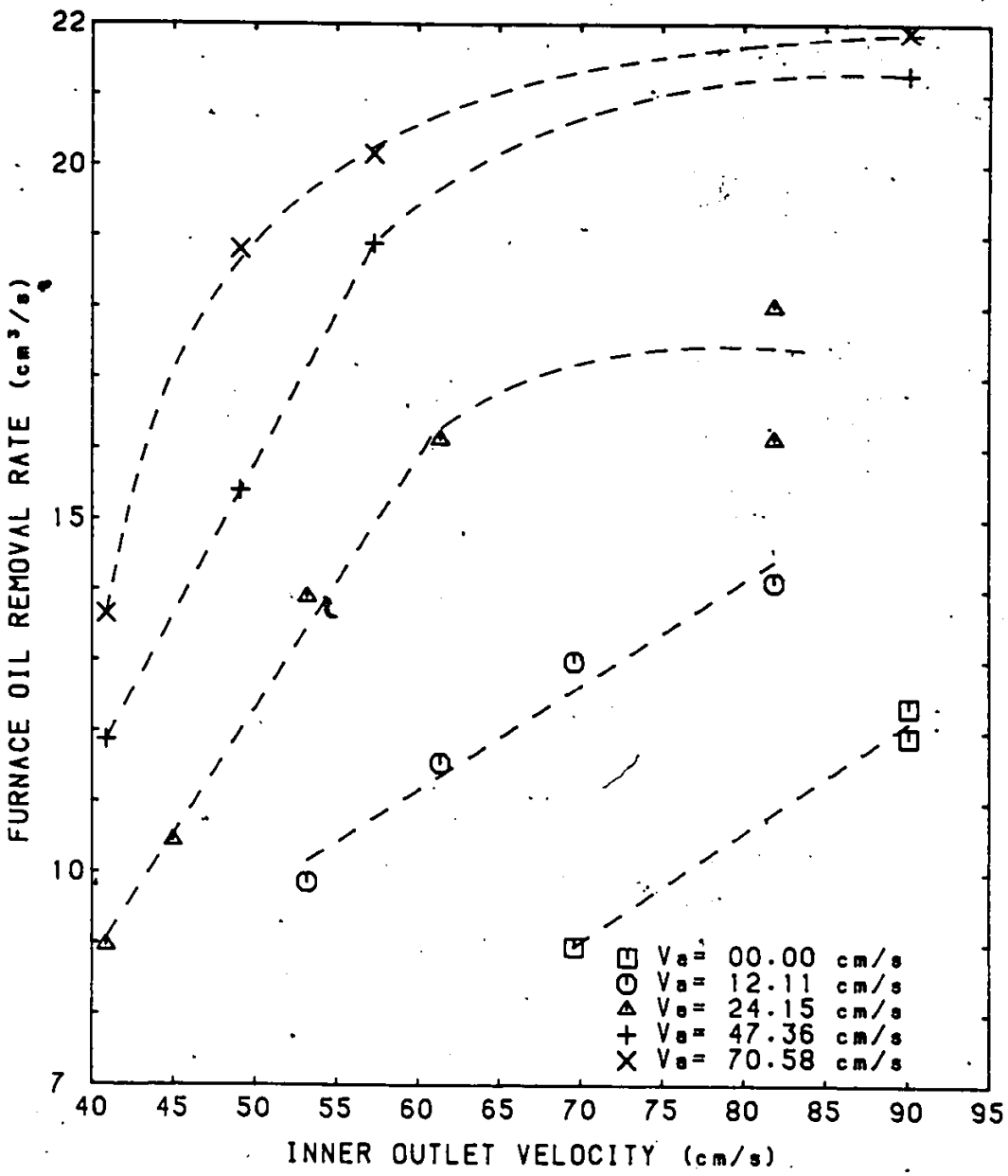

Figure 5.21: PLOT OF FURNACE OIL REMOVAL RATE VERSUS INNER OUTLET VELOCITY AT VARIED Va, Ω = 10 rpm & H = 30.0 cm

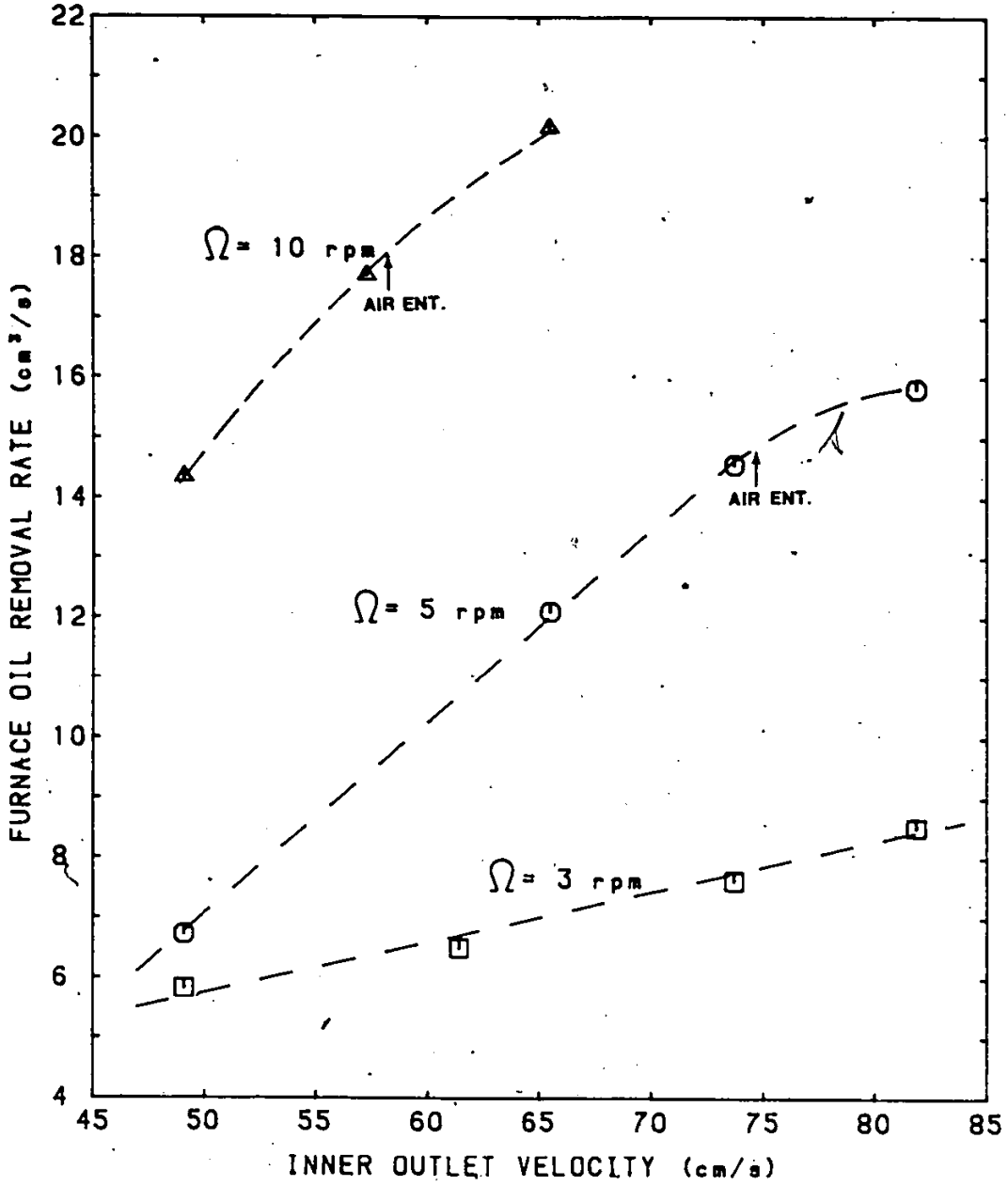

Figure 5.22: PLOT OF FURNACE OIL REMOVAL RATE VS. INNER OUTLET VELOCITY AT VARIED Ω , Va= 12.11 cm/s & H= 20.0 cm

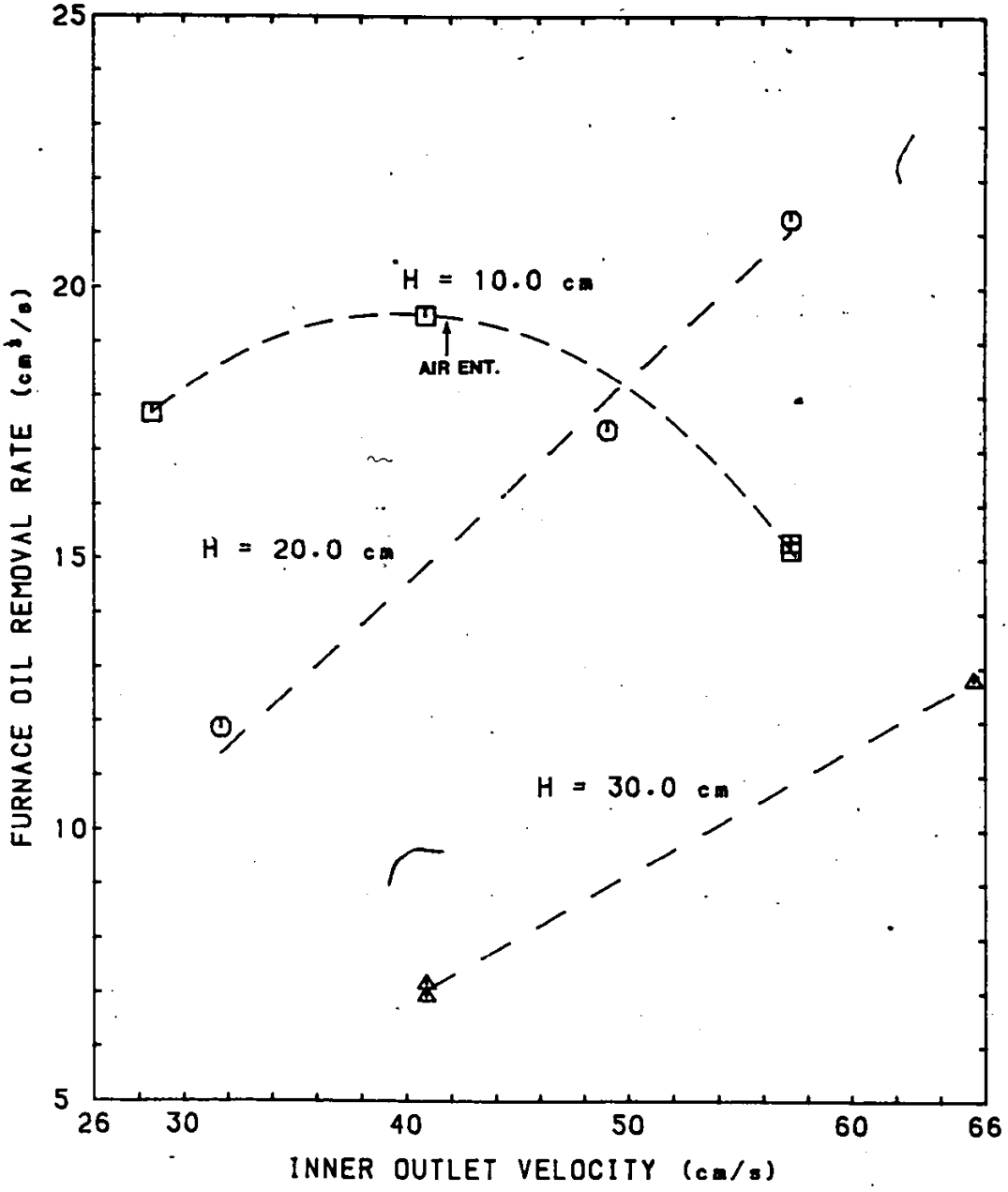

Figure 5.23: PLOT OF FURNACE OIL REMOVAL RATE VS. INNER OUTLET VELOCITY AT VARIED H, Va= 47.36 cm/s & Ω = 5 rpm

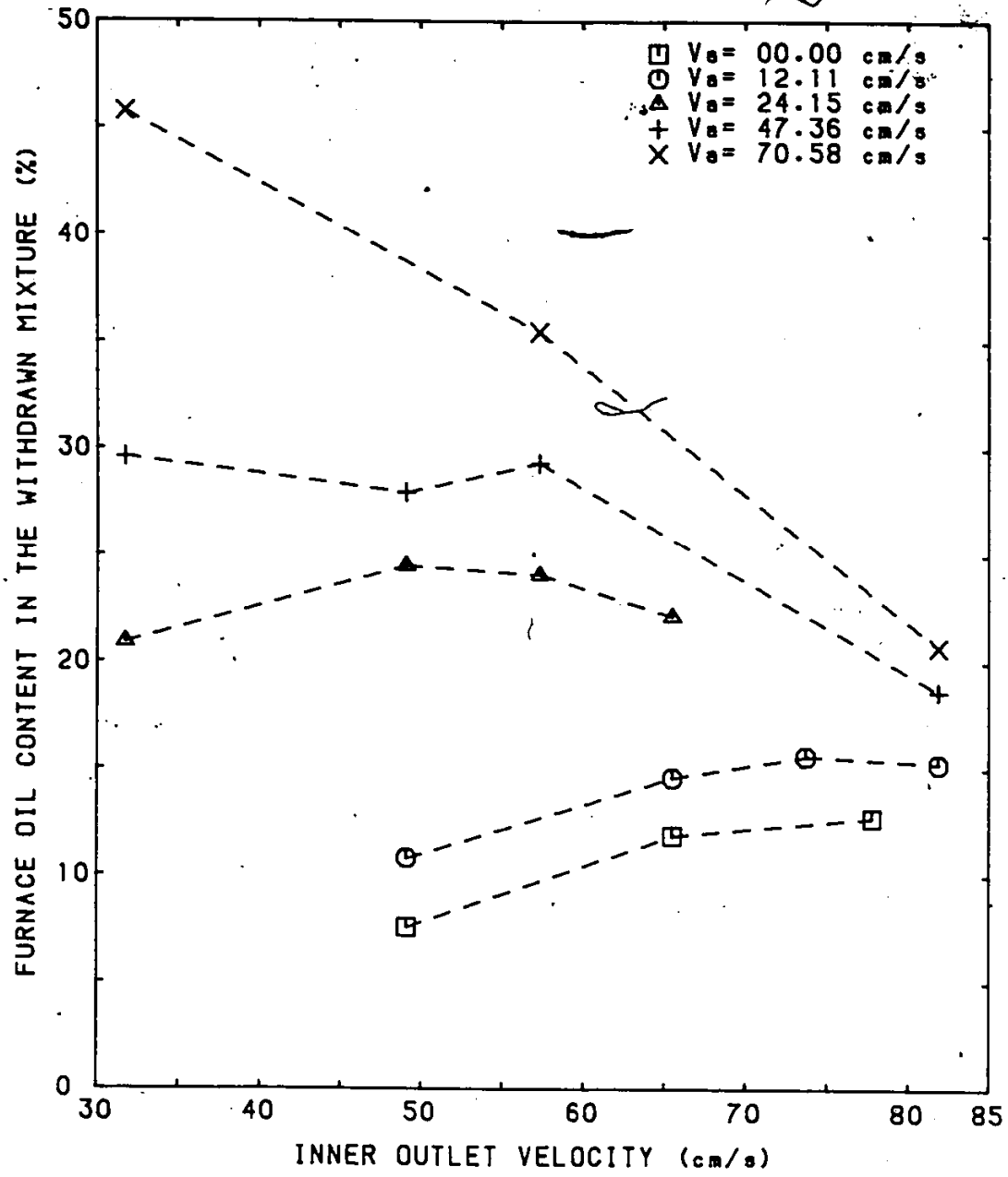

Figure 5.24: PLOT OF FURNACE OIL CONTENT VS. INNER OUTLET VELOCITY AT VARIED Va, Ω = 5 rpm & H= 20.0 cm

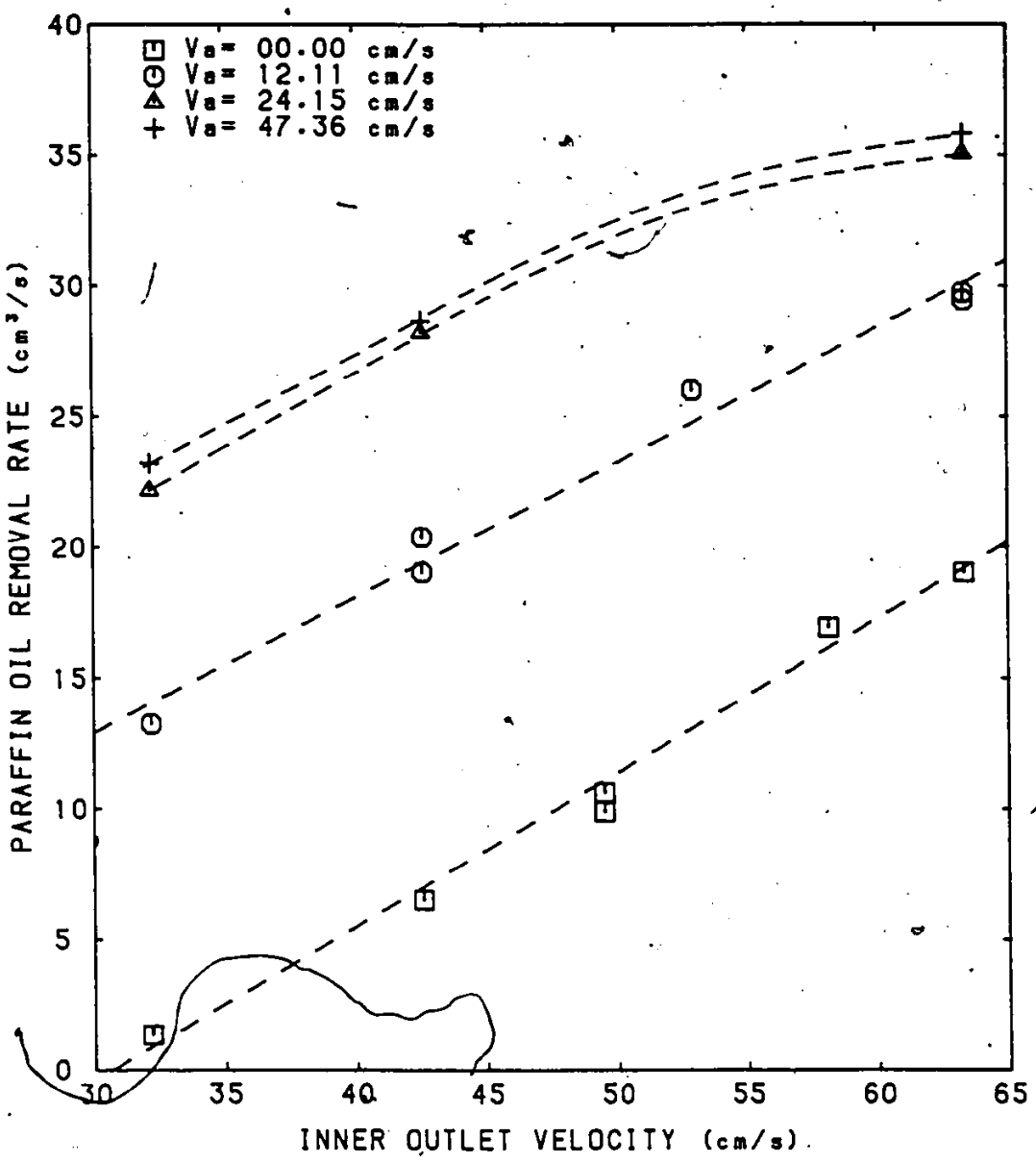

Figure 5.25: PLOT OF PARAFFIN OIL REMOVAL RATE VERSUS INNER OUTLET VELOCITY AT VARIED Va, Ω = 3 rpm & H= 10.0 cm.

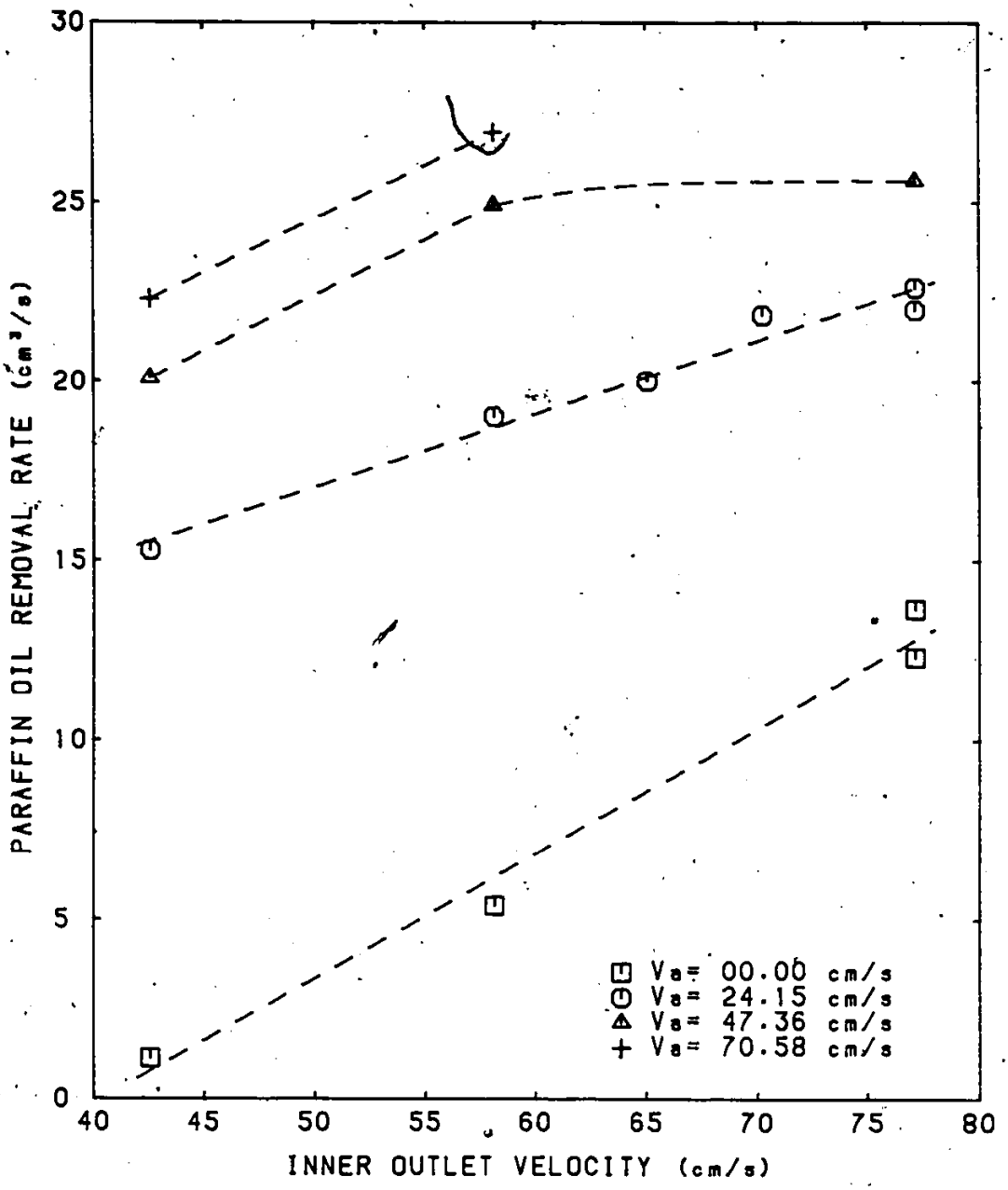

Figure 5.26: PLOT OF PARAFFIN OIL REMOVAL RATE VERSUS INNER OUTLET VELOCITY AT VARIED Va, Ω = 3 rpm & H= 20.0 cm

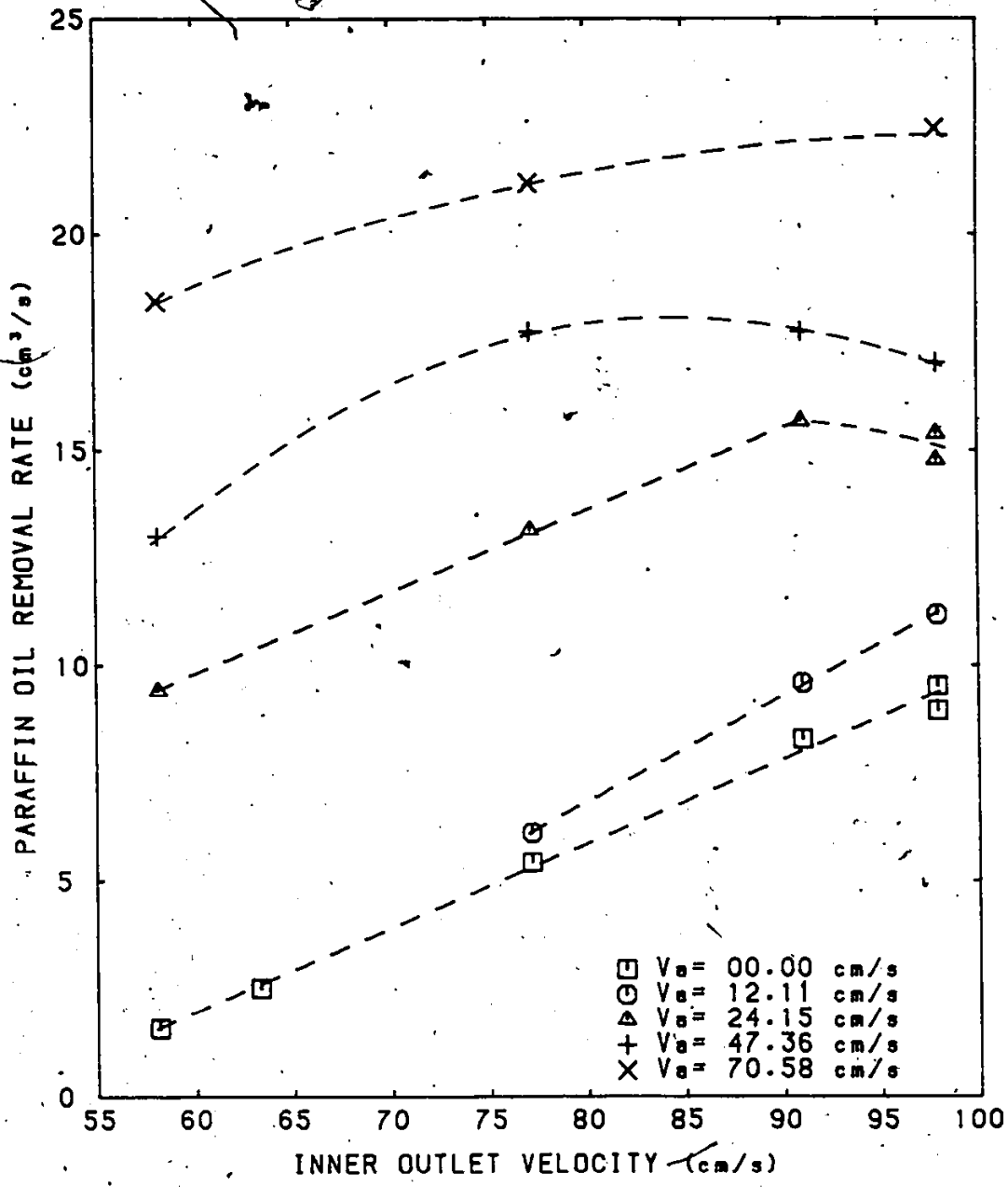

Figure 5.27: PLOT OF PARAFFIN OIL REMOVAL RATE VERSUS INNER OUTLET VELOCITY AT VARIED Va, Ω = 3 rpm & H= 30.0 cm

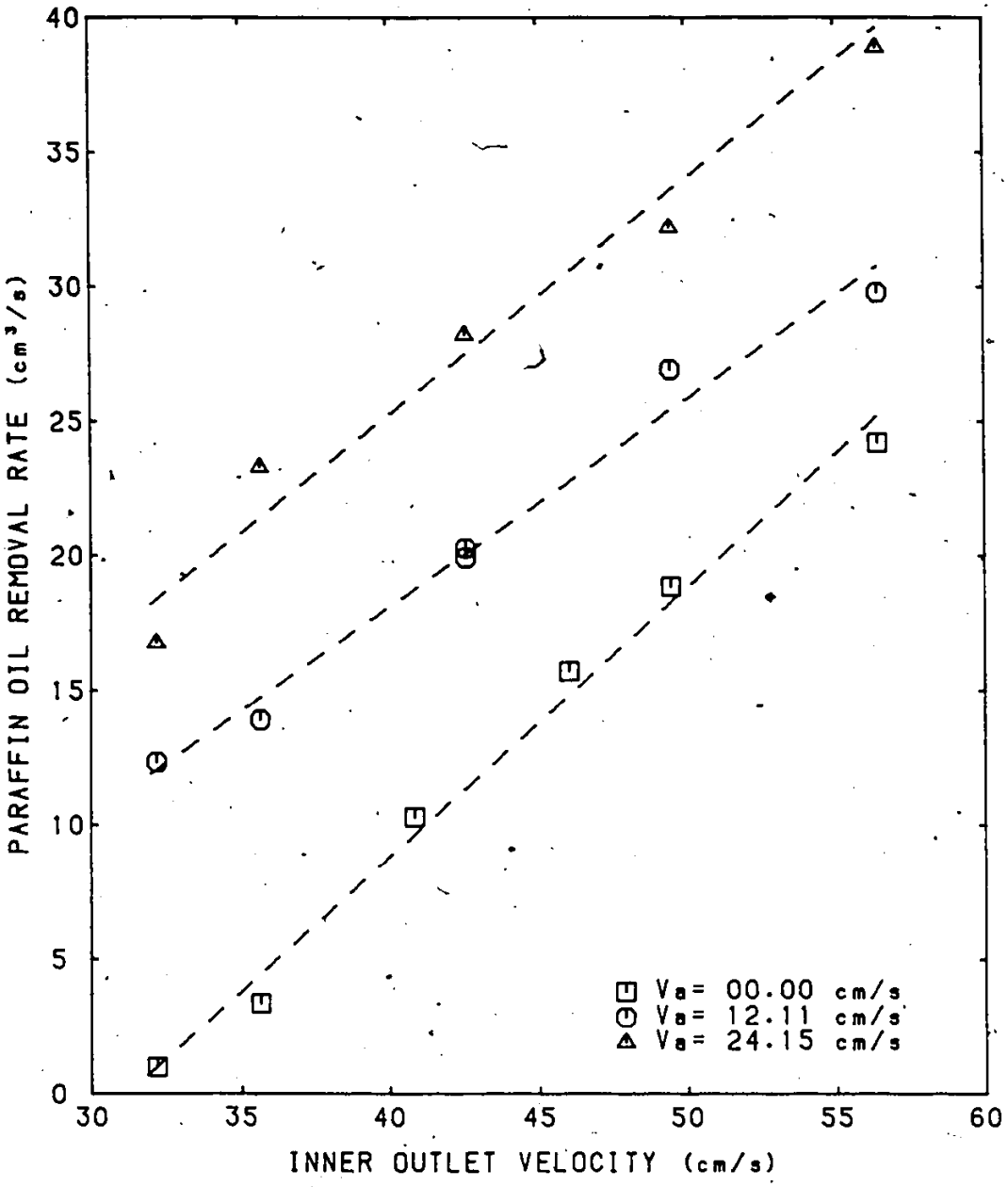

Figure 5.28: PLOT OF PARAFFIN OIL REMOVAL RATE VERSUS INNER OUTLET VELOCITY AT VARIED Va, Ω = 5 rpm & H= 10.0 cm

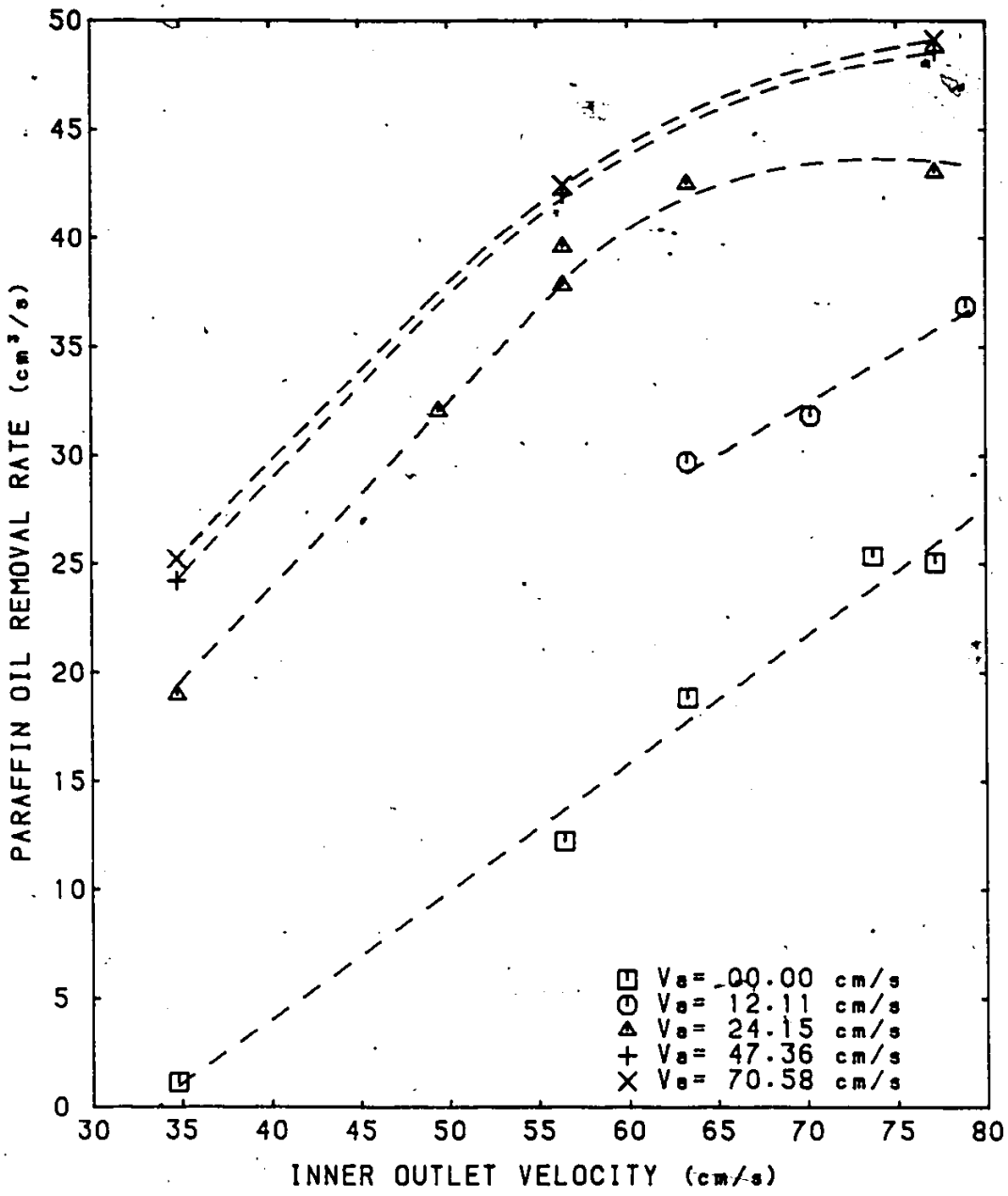

Figure 5.29: PLOT OF PARAFFIN OIL REMOVAL RATE VERSUS INNER OUTLET VELOCITY AT VARIED Va, Ω = 5 rpm & H= 20.0 cm

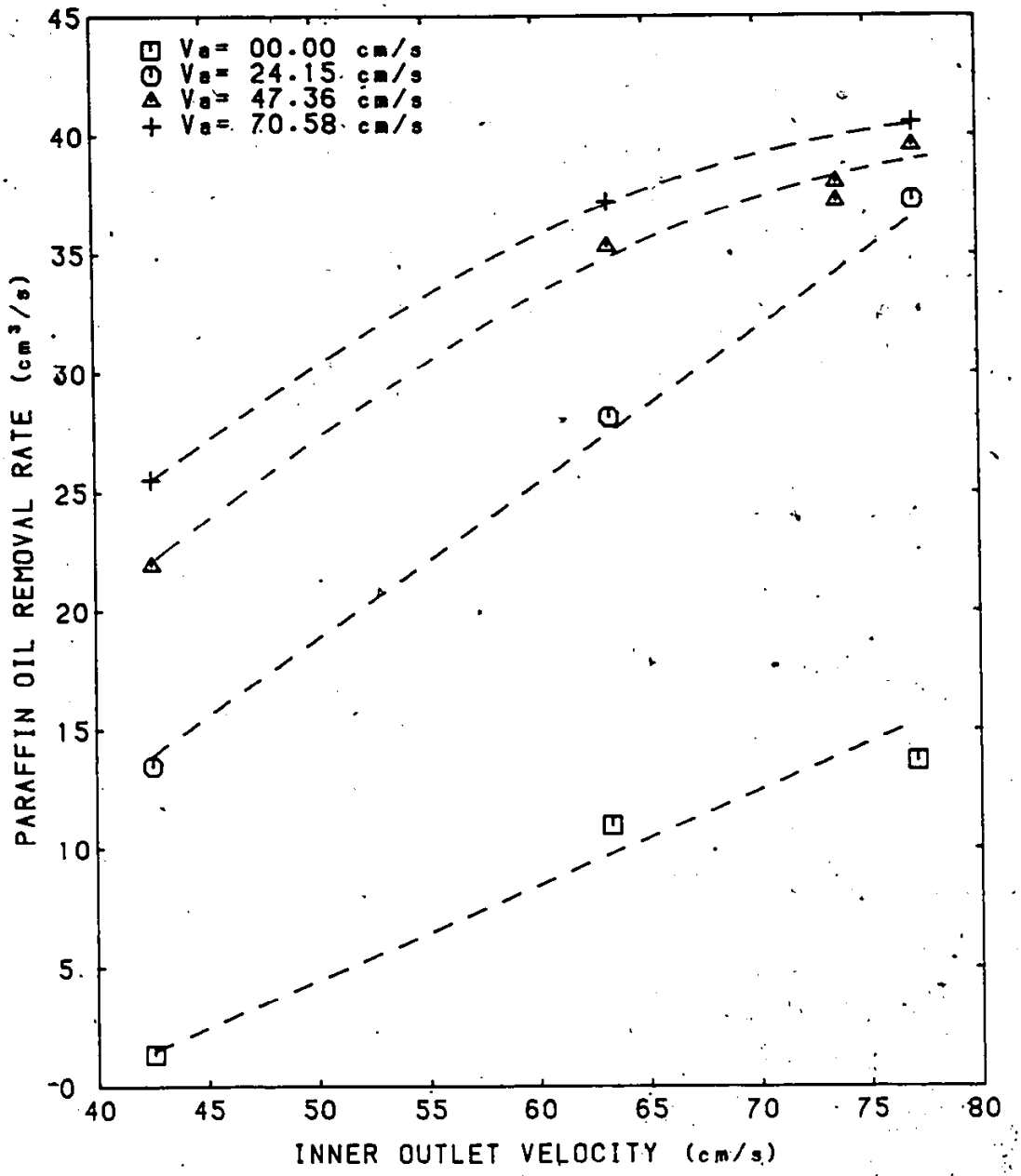

Figure 5.30: PLOT OF PARAFFIN OIL REMOVAL RATE VERSUS INNER OUTLET VELOCITY AT VARIED Va, Ω = 5 rpm & H= 30.0 cm

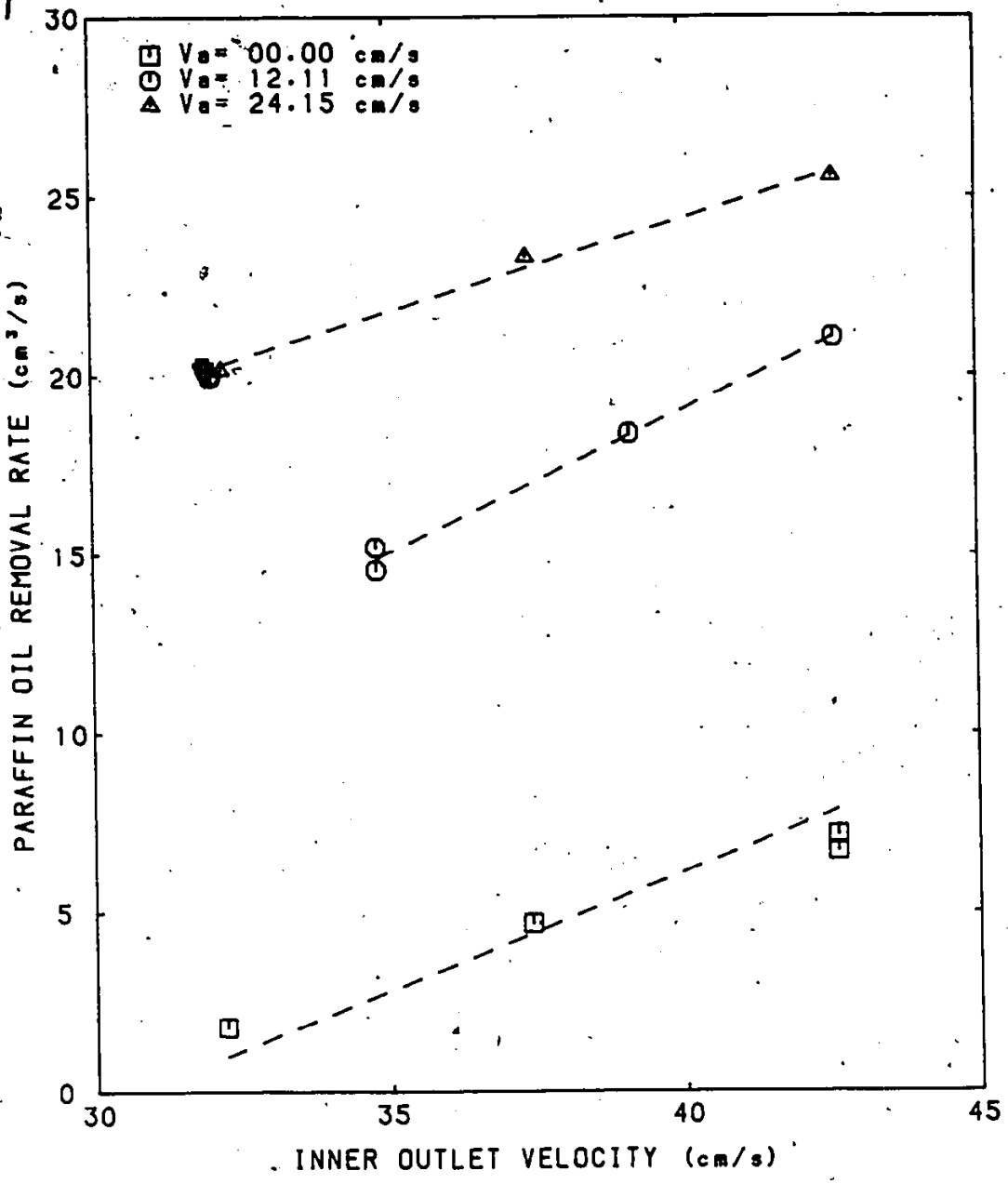

Figure 5.31: PLOT OF PARAFFIN OIL REMOVAL RATE VERSUS INNER OUTLET VELOCITY AT VARIED Va, Ω = 10 rpm & H= 10.0 cm

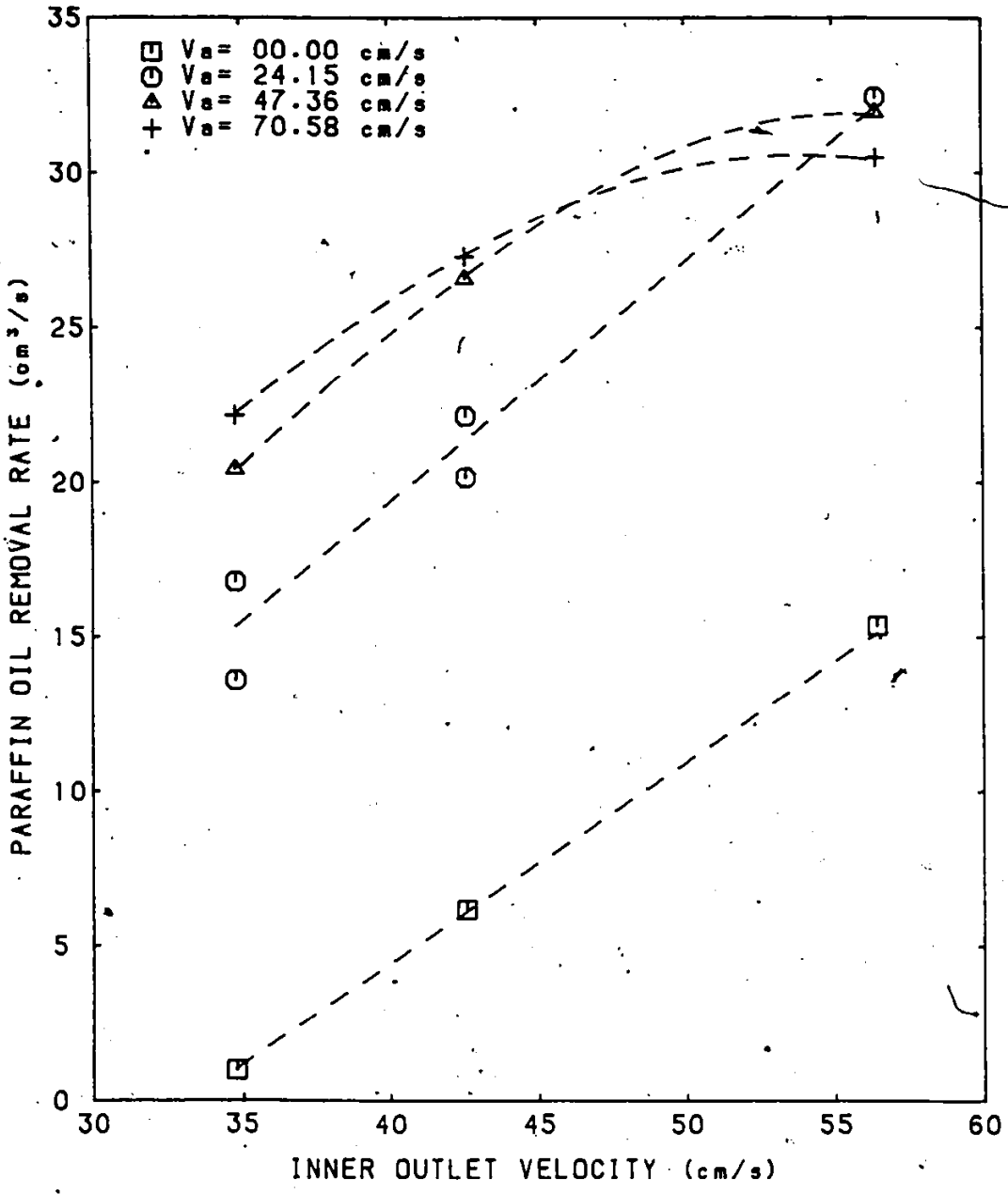

Figure 5.32: PLOT OF PARAFFIN OIL REMOVAL RATE VERSUS INNER OUTLET VELOCITY AT VARIED Va, Ω = 10 rpm & H= 20.0 cm

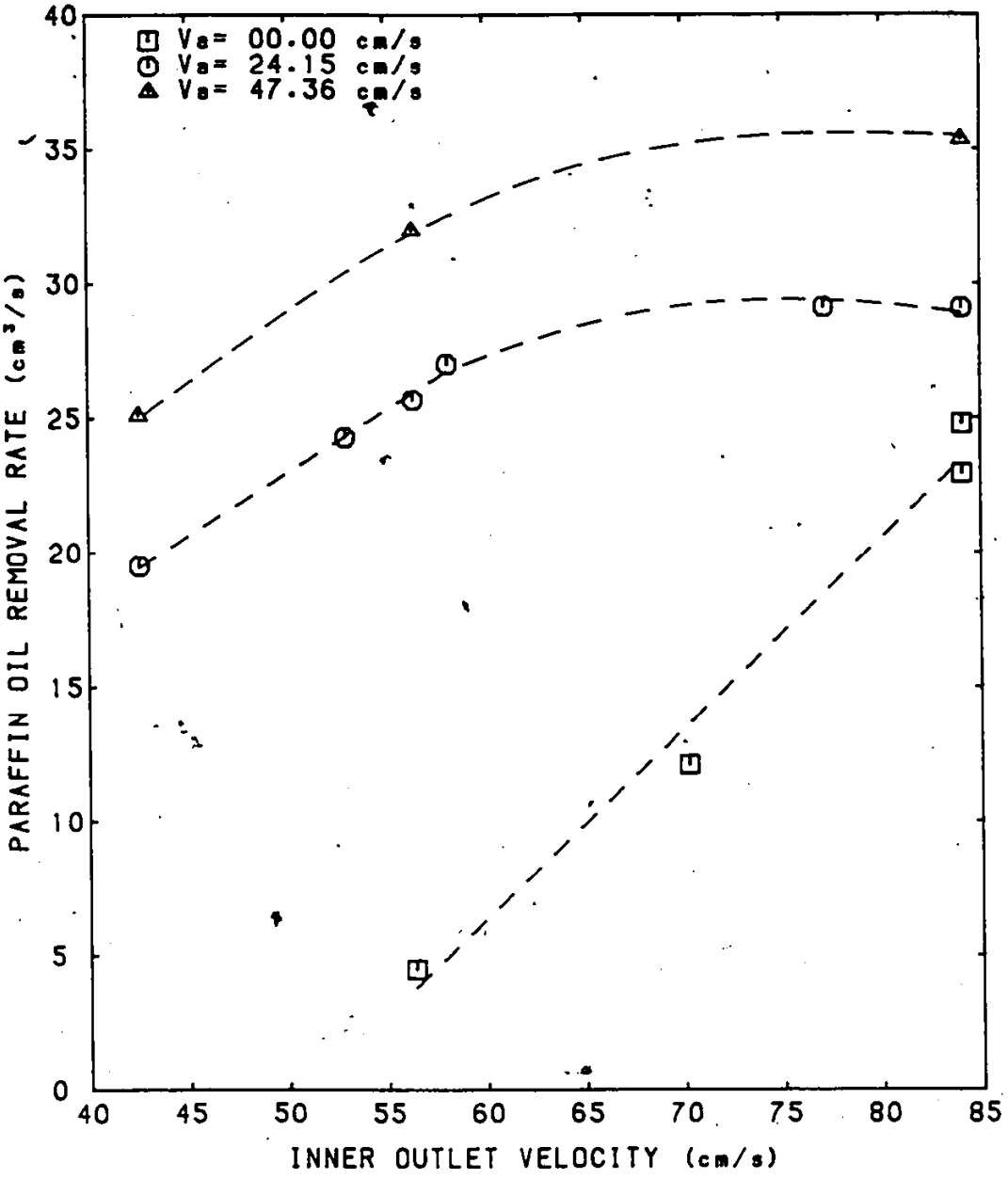

Figure 5.33: PLOT OF PARAFFIN OIL REMOVAL RATE VERSUS INNER OUTLET VELOCITY AT VARIED Va, Ω = 10 rpm & H= 30.0 cm

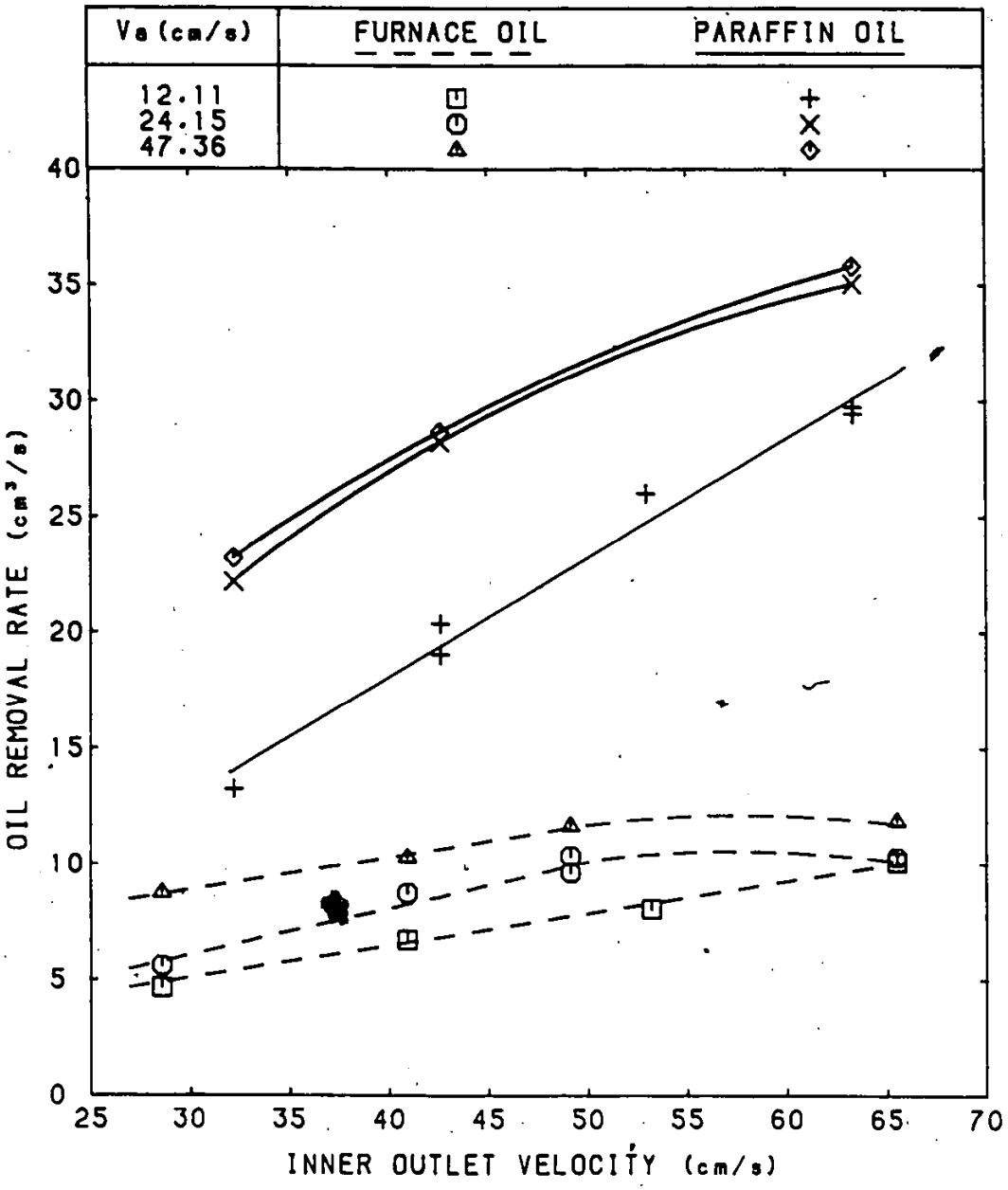

Figure 5.34: COMPARISONS OF FURNACE OIL AND PARAFFIN OIL REMOVAL RATE AT Ω = 3 rpm AND H=10.0 cm AND VARIED Va

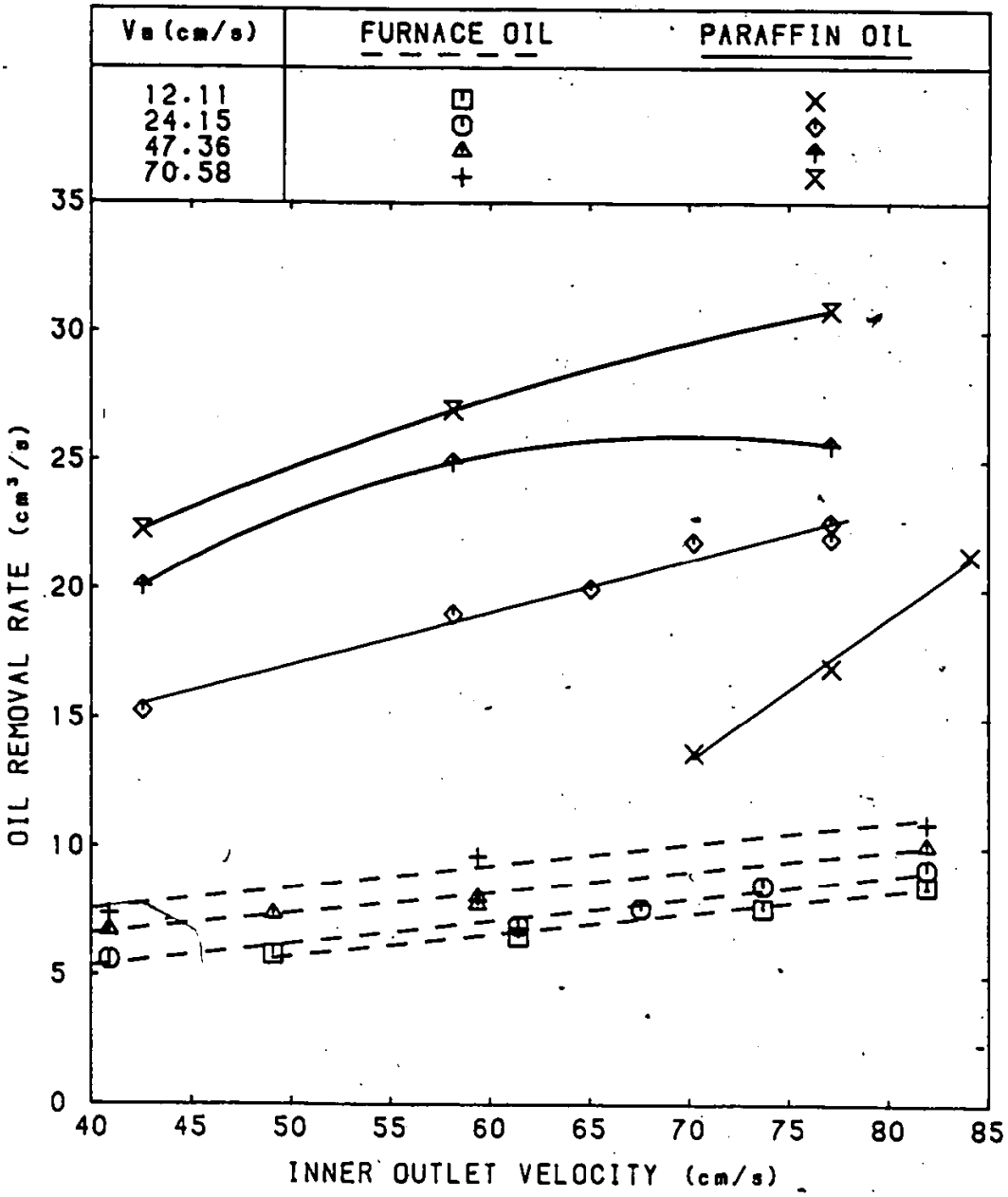

Figure 5.35: COMPARISONS OF FURNACE OIL AND PARAFFIN OIL REMOVAL RATE AT Ω = 3 rpm AND H=20.0 cm AND VARIED Va

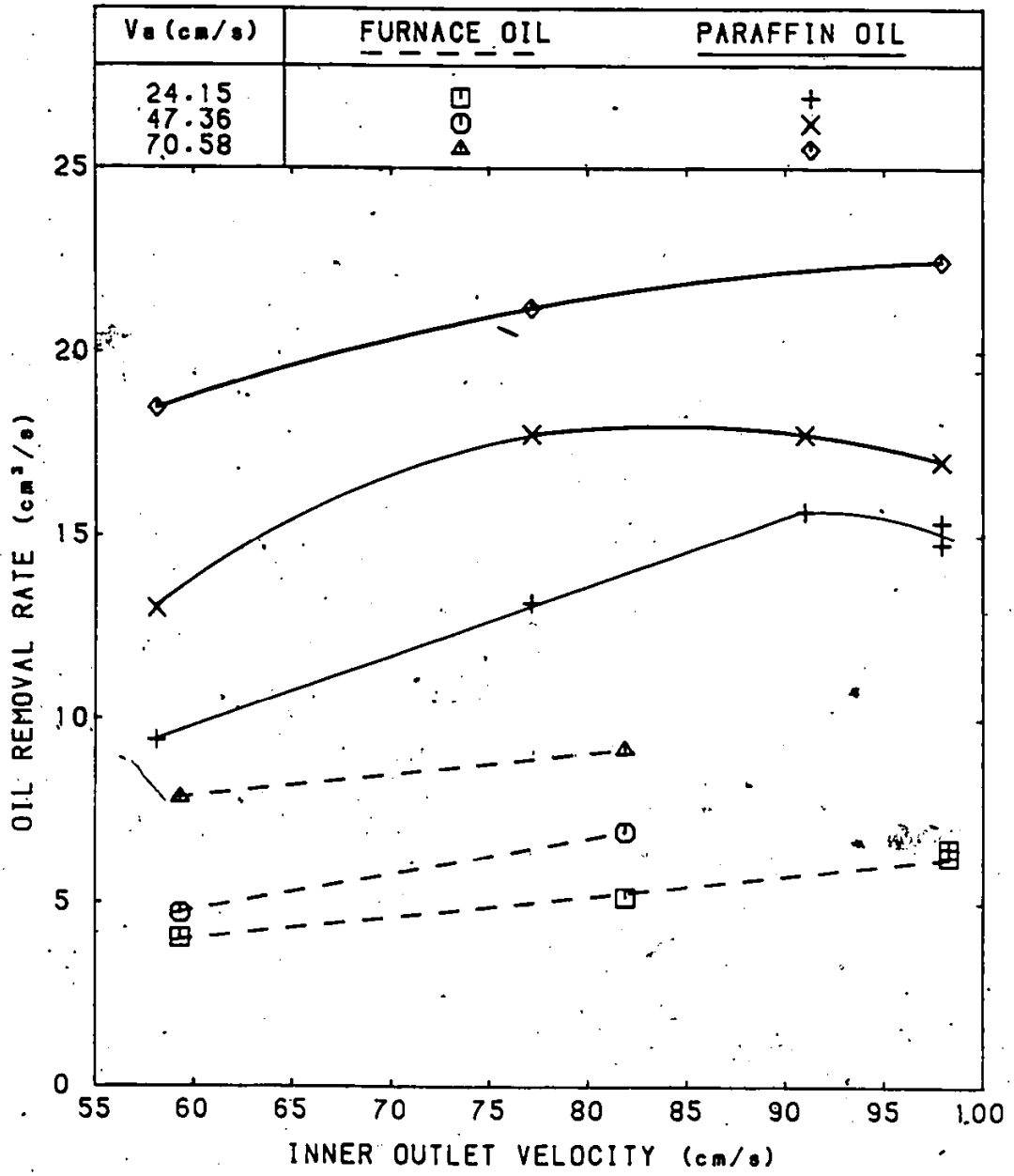

Figure 5.36: COMPARISONS OF FURNACE OIL AND PARAFFIN OIL REMOVAL RATE AT Ω = 3 rpm AND H=30.0 cm AND VARIED Va

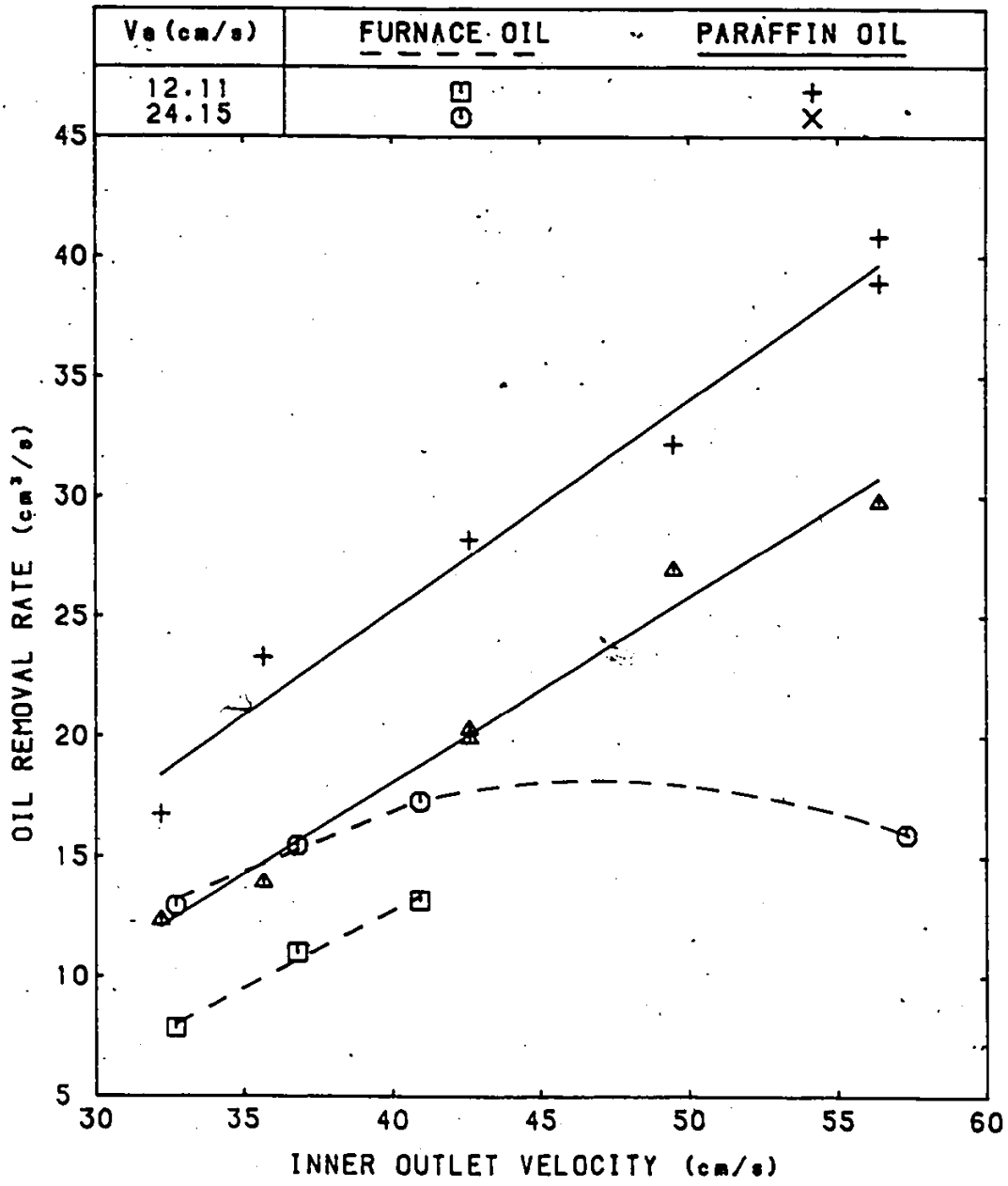

Figure 5.37: COMPARISONS OF FURNACE OIL AND PARAFFIN OIL REMOVAL RATE AT Ω = 5 rpm AND H=10.0 cm AND VARIED Va

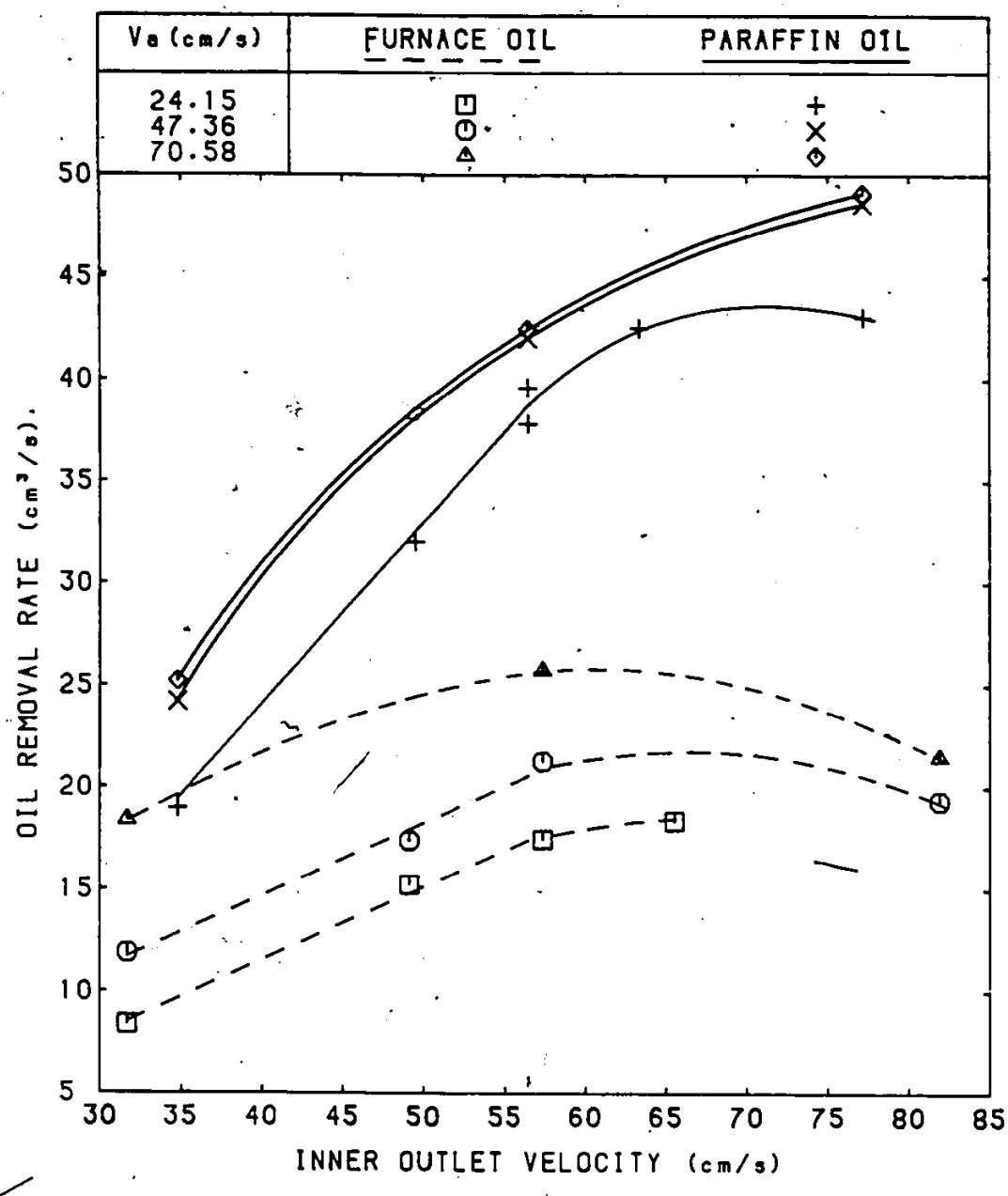

Figure 5.38: COMPARISONS OF FURNACE OIL AND PARAFFIN OIL REMOVAL RATE AT Ω = 5 rpm AND H=20.0 cm AND VARIED Va

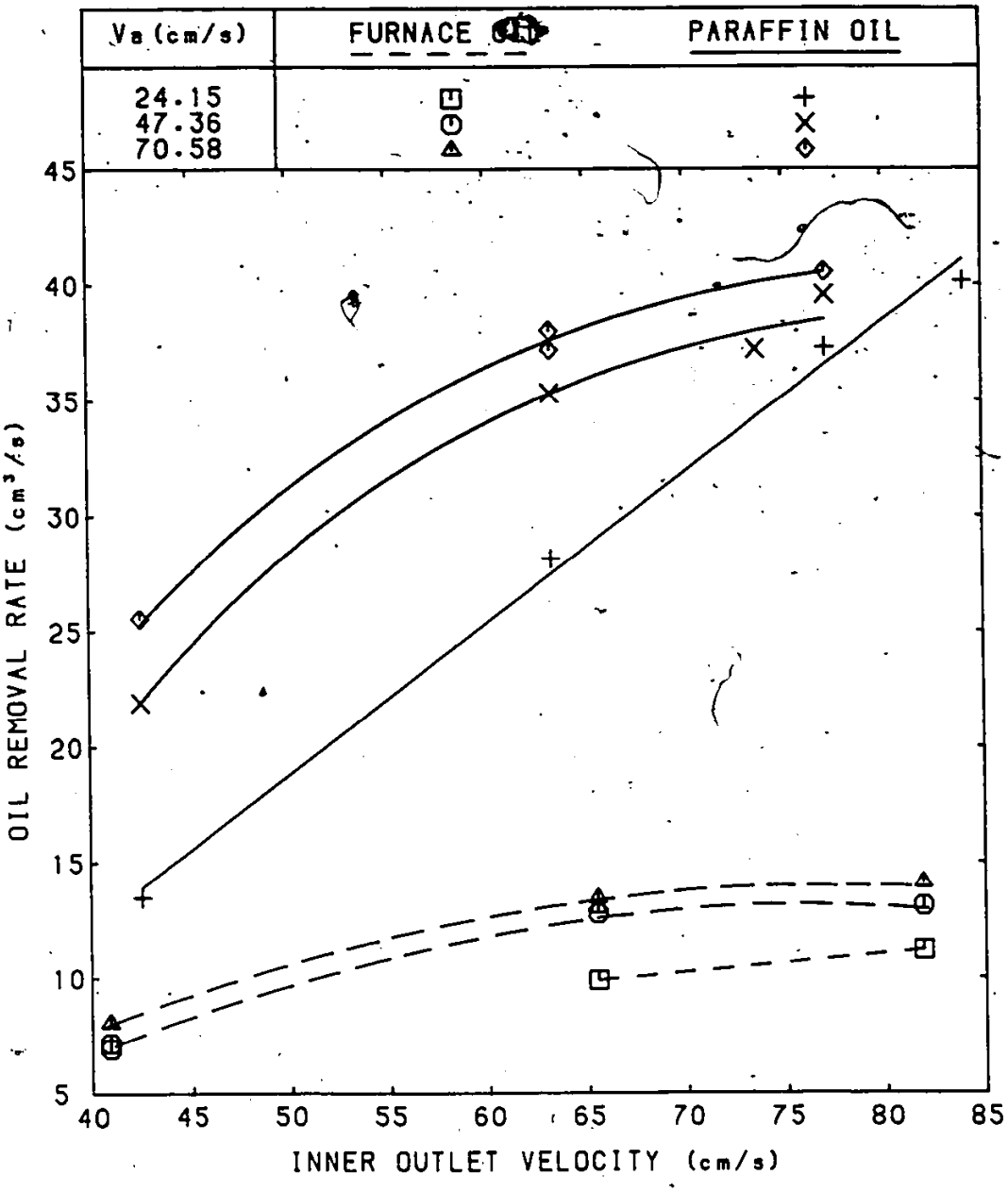

Figure 5.39: COMPARISONS OF FURNACE OIL AND PARAFFIN OIL REMOVAL RATE AT Ω = 5 rpm AND H=30.0 cm AND VARIED Va

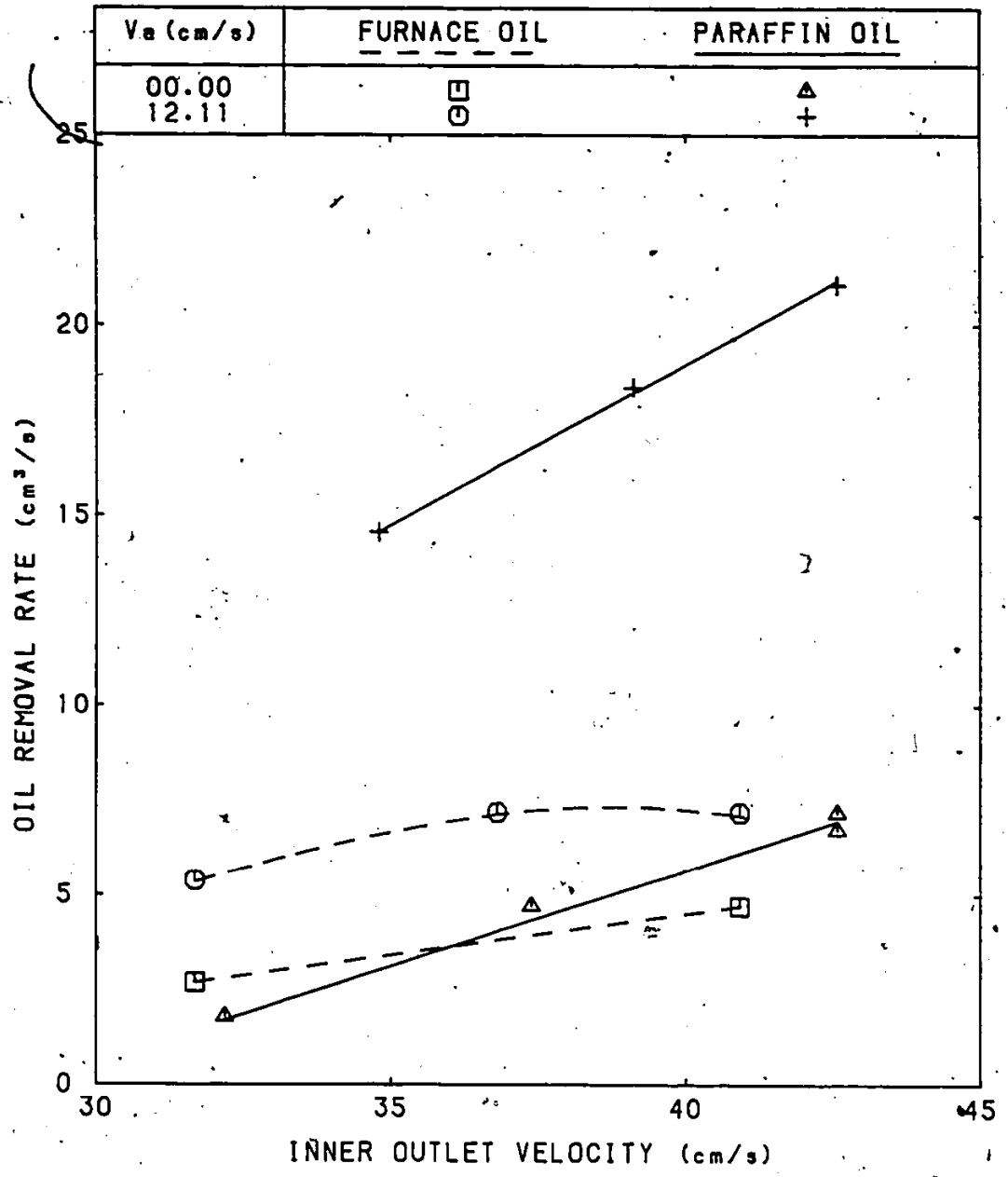

Figure 5.40: COMPARISONS OF FURNACE OIL AND PARAFFIN OIL REMOVAL RATE AT Ω =10 rpm AND H=10.0 cm AND VARIED Va

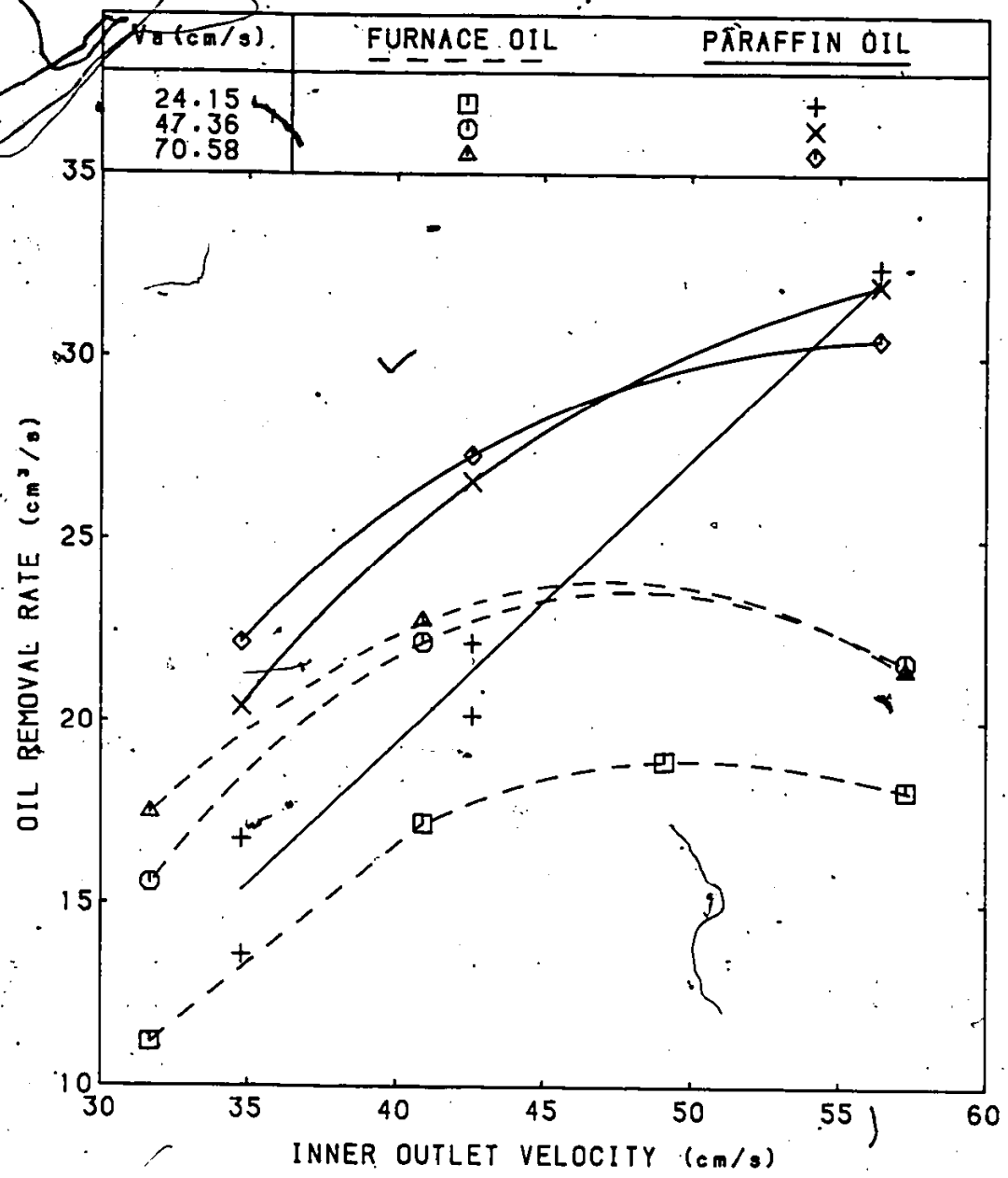

Figure 5.41: COMPARISONS OF FURNACE OIL AND PARAFFIN OIL REMOVAL RATE AT Ω=10 rpm AND H=20.0 cm AND VARIED Va.

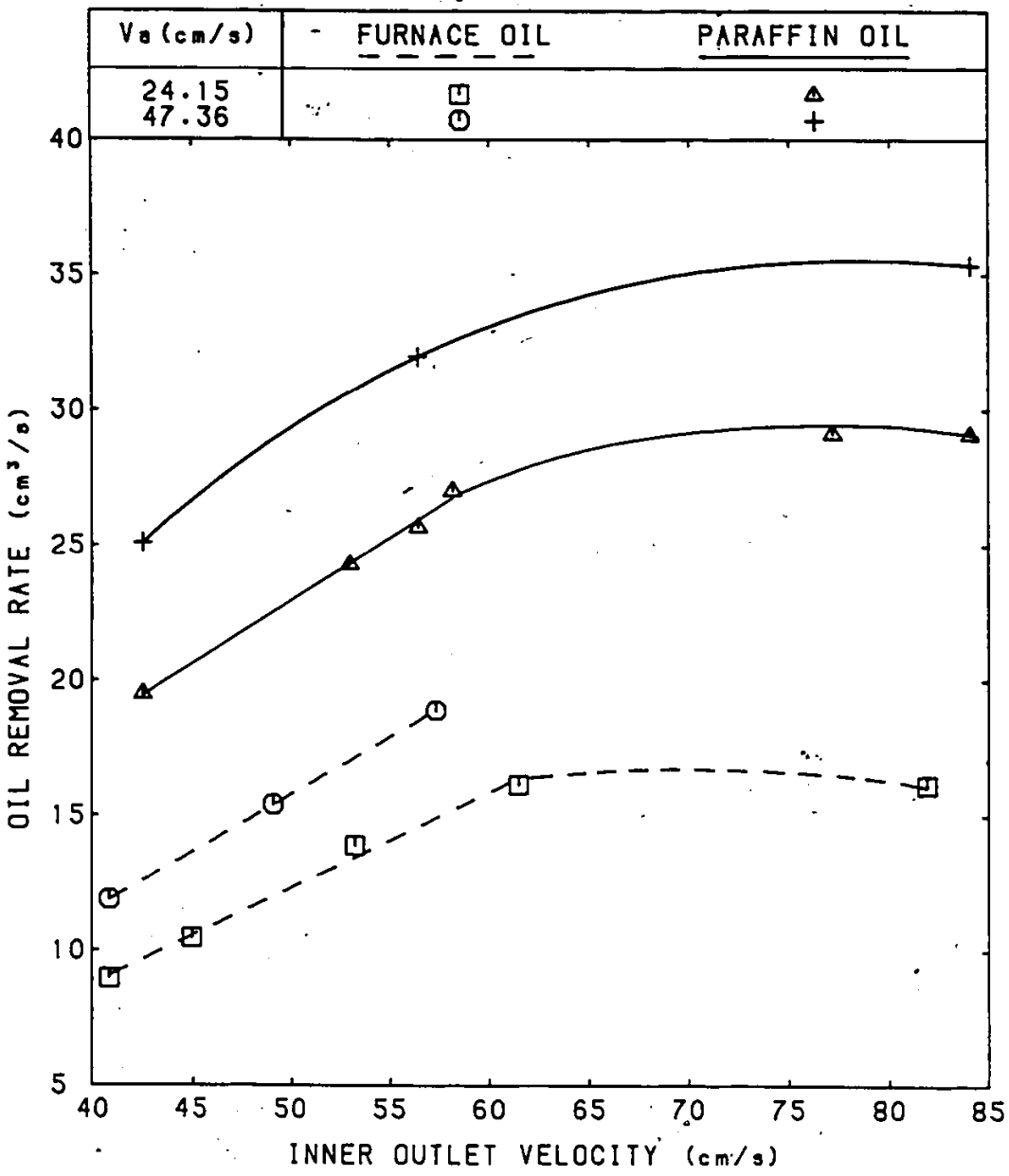

Figure 5.42: COMPARISONS OF FURNACE OIL AND PARAFFIN OIL REMOVAL RATE AT Ω=10 rpm AND H=30.0 cm AND VARIED Va

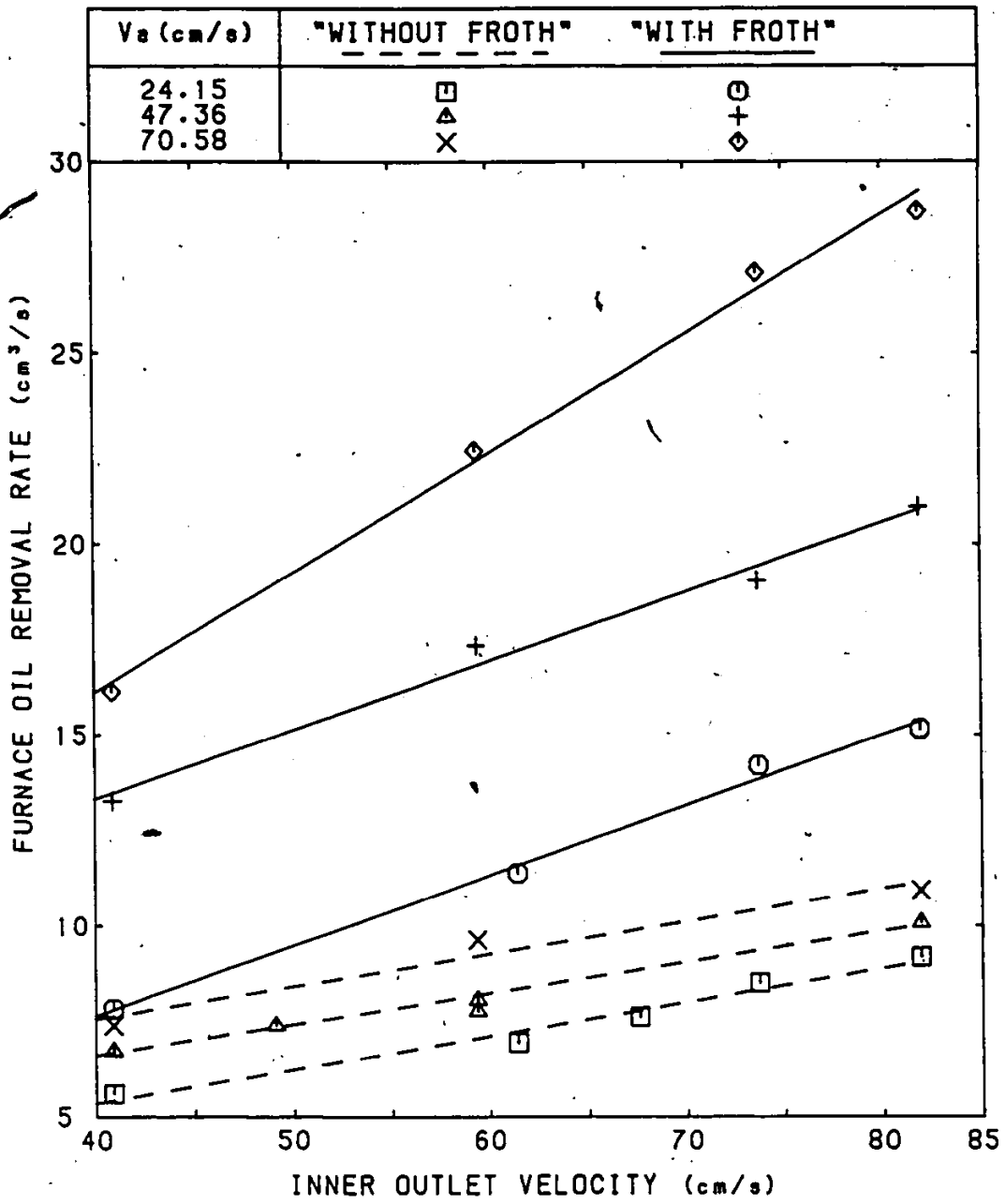

Figure 5.43: COMPARISONS OF FURNACE OIL REMOVAL RATE OF "WITH FROTH" AND "WITHOUT FROTH" EXPERIMENTS AT Ω = 3 rpm, H= 20.0 cm

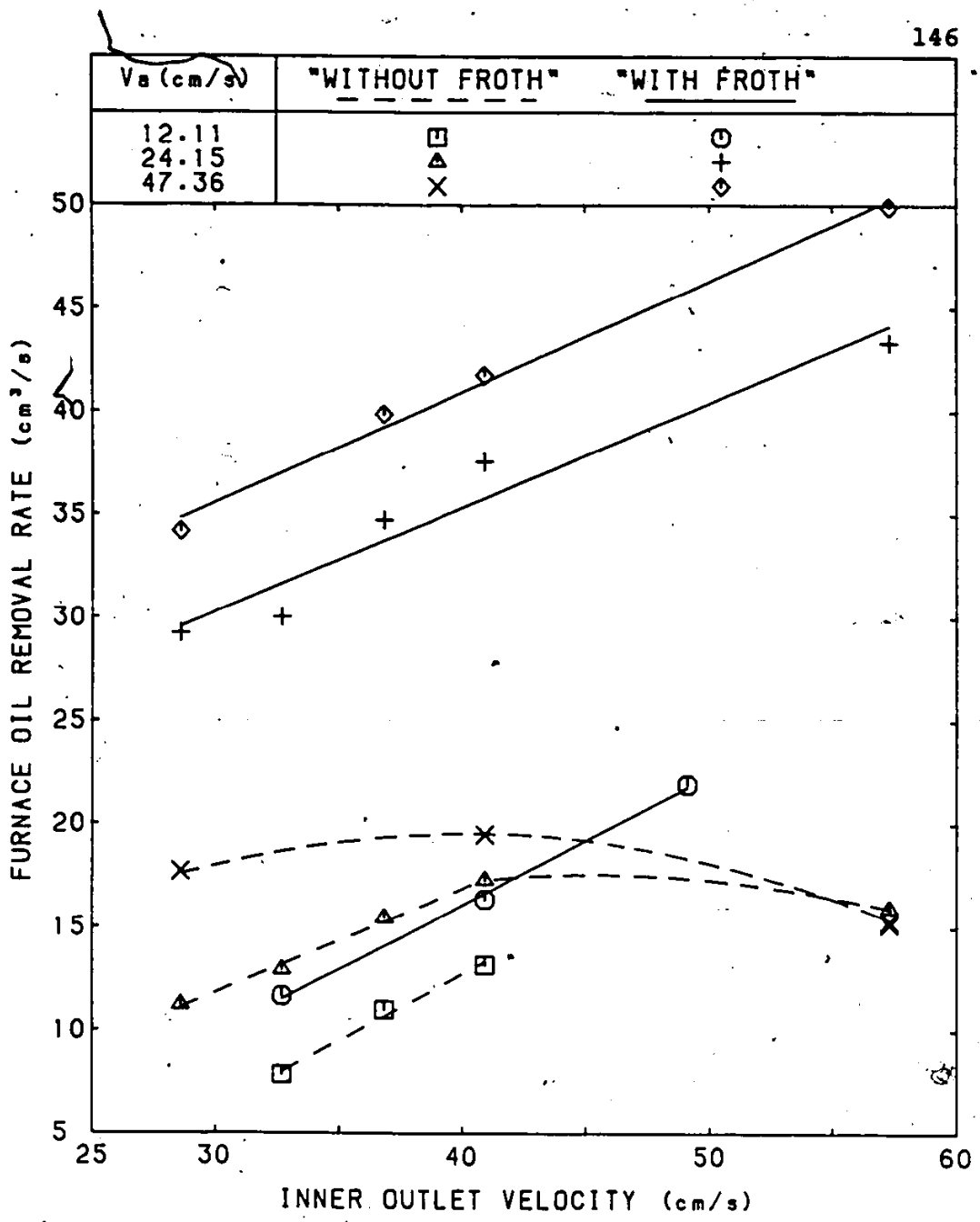

Figure 5.44: COMPARISONS OF FURNACE OIL REMOVAL RATE OF "WITH FROTH" AND "WITHOUT FROTH" EXPERIMENTS AT Ω = 5 rpm, H= 10.0 cm

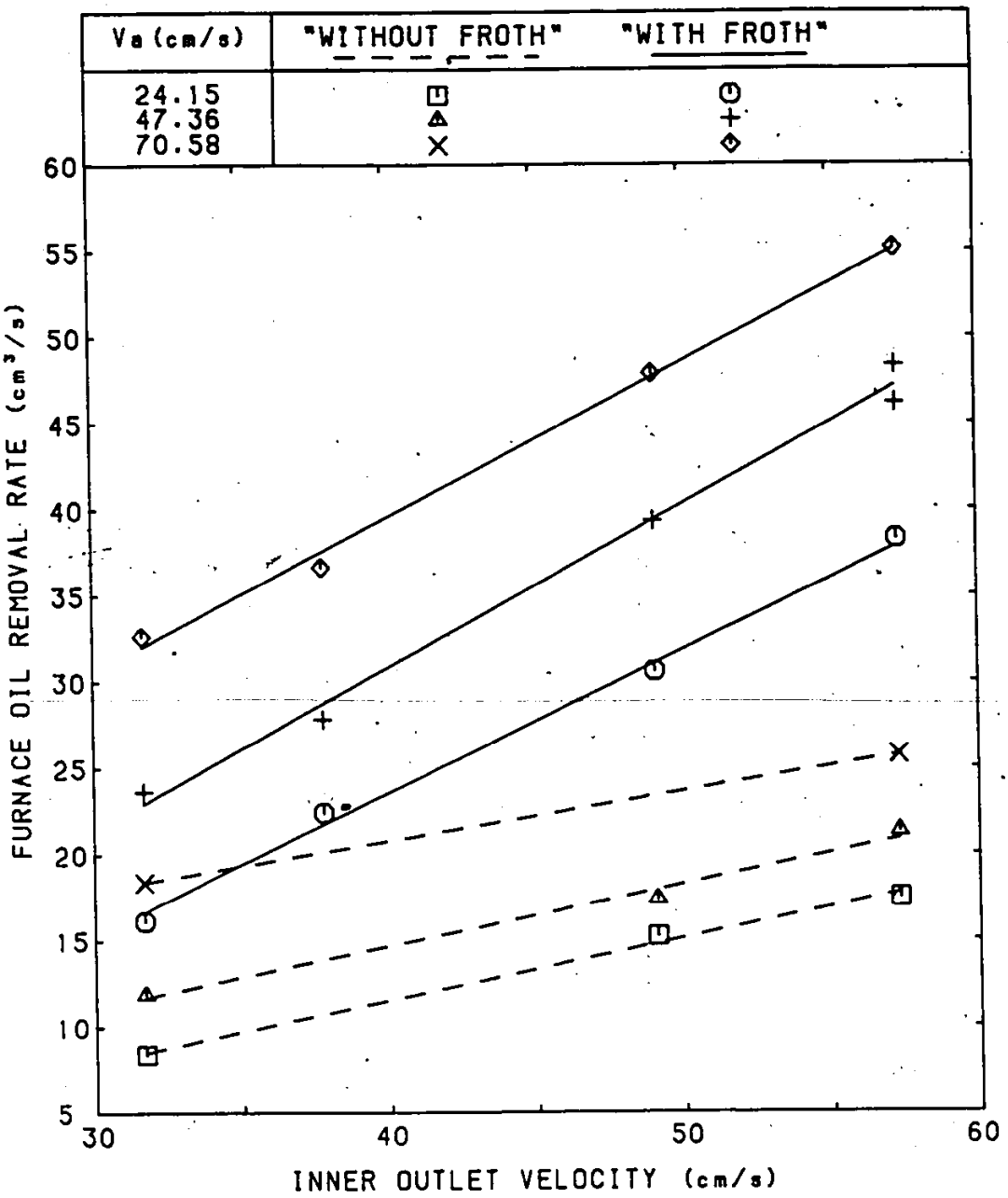

Figure 5.45: COMPARISONS OF FURNACE OIL REMOVAL RATE OF "WITH FROTH" AND "WITHOUT FROTH" EXPERIMENTS AT Ω = 5 rpm, H= 20.0 cm

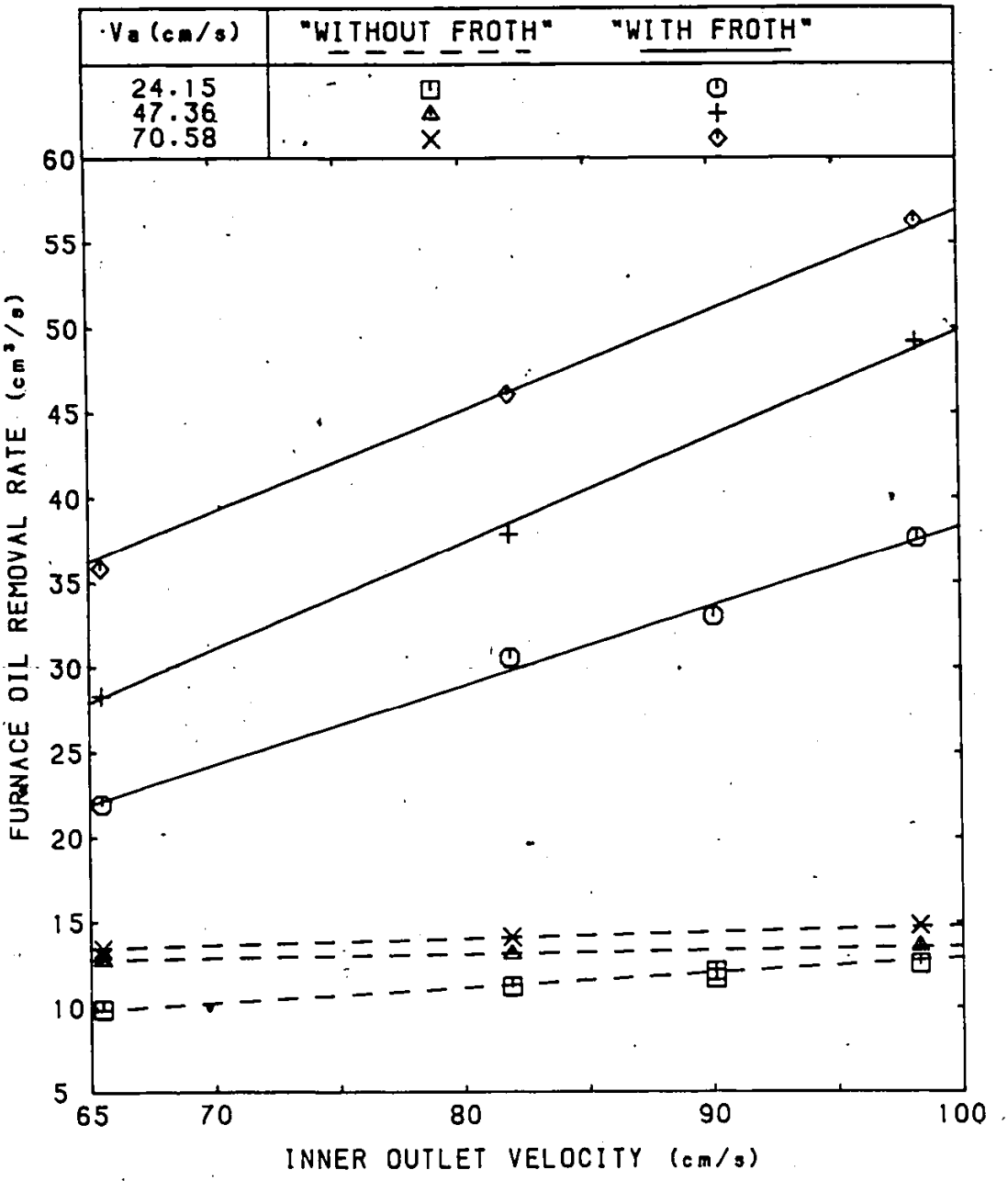

Figure 5.46: COMPARISONS OF FURNACE OIL REMOVAL RATE OF "WITH FROTH" AND "WITHOUT FROTH" EXPERIMENTS AT Ω= 5 rpm, H= 30.0 cm

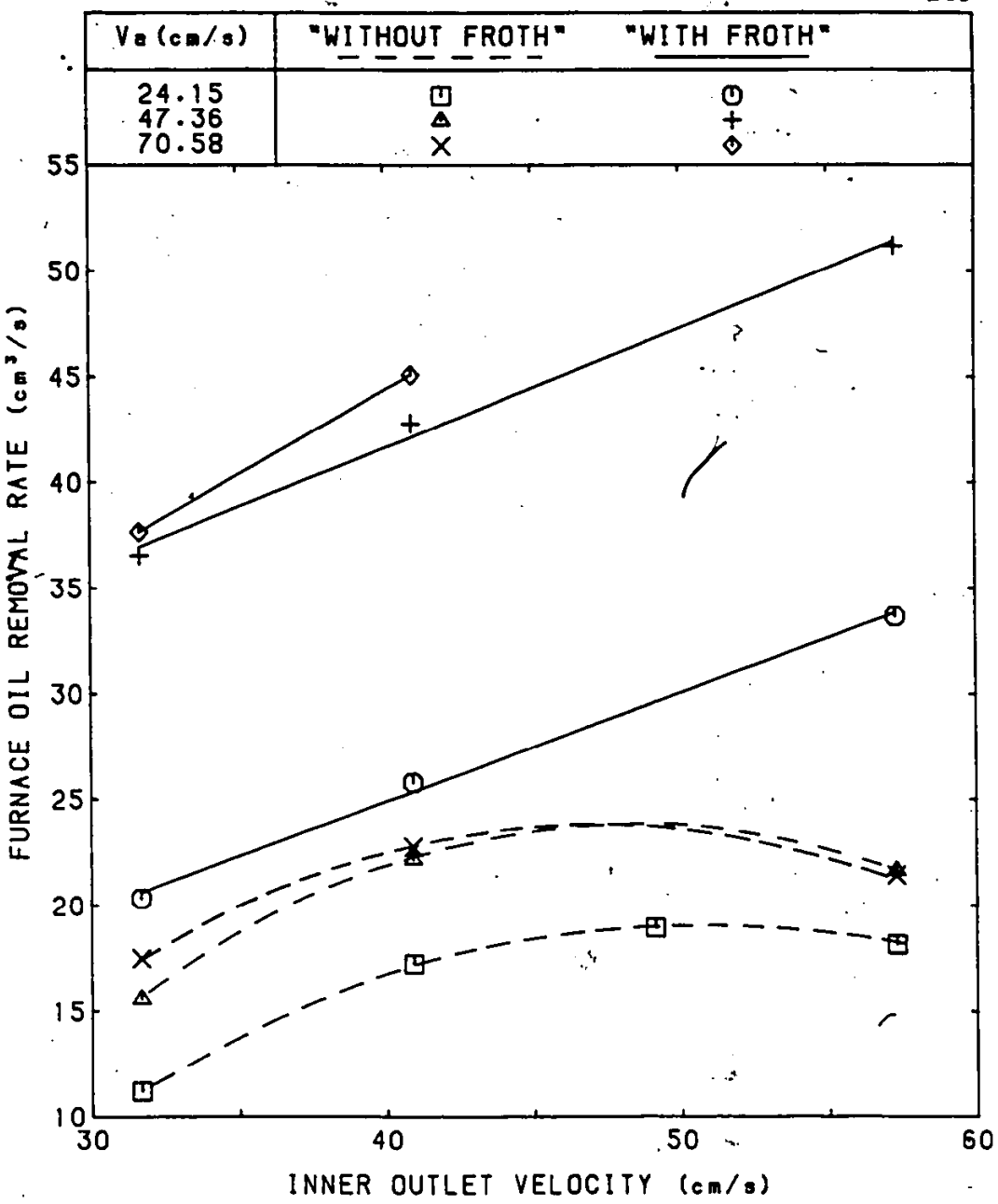

Figure 5.47: COMPARISONS OF FURNACE OIL REMOVAL RATE OF "WITH FROTH" AND "WITHOUT FROTH" EXPERIMENTS AT Ω = 10 rpm, H= 20.0 cm

Chapter VI

CONCLUSIONS AND RECOMMENDATIONS

6.1 CONCLUSIONS

6.1.1 Phase I, Air-Water Vortex Experiments

Several conclusions can be drawn, based on the experimental results of the phenomena involving air-water vortices.

1. A stable vortex could be produced by the vortex apparatus used in this study. The flow pattern of this vortex was similar to Rankine's combined vortex, in which a forced vortex was considered to exist in the center of the vortex and a free vortex to exist in the outer region of the vortex.
2. In this study, the vortex depth in an air-water system could be predicted by means of the following correlation:

$$\frac{Hv}{di} = 1.57 \left(\frac{\Omega di}{Vi}\right)^{0.41} \left(\frac{Va}{Vi}\right)^{0.24} \left(\frac{H}{di}\right)^{0.29} \left(\frac{Vidi}{\upsilon}\right)^{0.43} \left(\frac{Vi^2}{gdi}\right)^{0.56}$$

3. The vortex depth (Hv) was dependent upon the rotational speed of the stirrer (Ω), the inner outlet velocity (Vi), the annular circulation velocity (Va),

and the water depth in the vortex tank (H). The vortex depth in the air-water system was directly related to the above four variables (Ω,Vi,Va,H).

4. The vortex formation was affected when a layer of froth was present on the surface of the water. The effect of the surface froth on the vortex depth depended on the stirrer rotational speed (Ω), and the thickness of the froth. The vortex depth increased at low Ω if surface froth was present, but it decreased at high Ω.

6.1.2 Phase II, Oil-Water Separation Experiments

Based on the results of the oil-water separation experiments, a number of conclusions can be made as follows:

1. The oil-entraining vortex (only oil and water being withdrawn from the vortex tank) existed between the conditions of incipient oil entrainment and incipient air-oil entrainment.
2. The oil removal rate within the oil-vortex formation region was directly related to the stirrer rotational speed, the inner flow velocity, and the annular flow velocity, but it decreased as the water depth in the vortex tank increased.
3. The maximum (or optimum) oil removal rate was expected to occur for the conditions of low water depth in the vortex tank, high inner and annular flow rates,

and relatively high stirrer rotational speed, within the oil-vortex formation region.

4. Under the operating conditions of this study, the maximum experimental paraffin oil removal rate found was 42.4 cm^3/s, and the maximum furnace oil removal rate was 25.7 cm^3/s. The furnace oil removal rate could increase up to 71.8 cm^3/s when a layer of surface froth was present on the oil.
5. The oil content in the inner outlet withdrawn mixture was directly related to the stirrer rotational speed and the annular outlet velocity; however, it decreased as the water depth in the vortex tank increased. There was no correlation between the oil content and the inner outlet velocity.
6. In this study, the maximum oil content of the two-phase mixture withdrawn was 59.2 % for the paraffin oil case, and 48.7 % for the furnace oil case. However, the maximum oil content increased up to 94.1 % ~~if~~ a layer of froth was present on the surface of the furnace oil.
7. The oil removal rate and the oil content in the two-phase mixture were affected by the viscosity of the oil. The oil removal rate of paraffin oil of high vicosity was much higher than the rate for furnace oil of low viscosity under the same operating condition.

8. For the furnace oil of low viscosity, the oil removal rate and the oil content increased significantly when a layer of froth was present on the surface of the oil.

9. The vortex apparatus used in the present study could remove surface oil from water effectively. However, some degree of emulsification of the oil and water occurred due to the high shear from the vortex motion. This was an observable disadvantage for this separation device. The vortex separation method is suitable for removing the surface oil from some emulsified oily materials, and it can also be used to remove a surface liquid from other immiscible liquids.

6.1.3 Phase III, Feasibility Study Using the Modified Vortex Apparatus for Slurry Decantation

The modified vortex apparatus as developed in this study was not successful in separating solid particles from water effectively. The design of this apparatus could not take advantage of the centrifugal forces associated with vortex formation.

6.2 RECOMMENDATIONS

Based on the experimental results and observations, the following recommendations are proposed:

1. As mentioned in section 5.1.5, there is some doubt about the statement that 'the vortex depth is directly related to the water depth in the vortex tank'. Further study for the effect of the water depth on the vortex depth is recommended.
2. The effect of the surface froth on the air-water vortex formation is an interesting subject. Further study in this subject may be worthwhile.
3. The emulsification of oil and water made the measurements difficult during the experiments. Although an emulsion breaker was installed in the system, it could not break down the emulsion completely. For further study of oil-water separation, some better emulsion breaking methods would be useful to improve the reliability of the measurements.
4. For the oil-water separation experiments, only five variables (Ω, Vi, Va, H, μ_{oil}) were considered. However, the oil-vortex formation depended on many other parameters, such as exit pipe diameter, thickness of the surface oil, density of the oil etc.. Further study involving these parameters is suggested.
5. The vortex apparatus used in this study has the potential to remove some surface materials other than

oil from a second immiscible liquid. Further study with other immiscible liquid systems is recommended.

BIBLIOGRAPHY

1. Clark, J. W., Viessman, W. Jr., and Hammer, M. J., Water Supply & Pollution Control, IEP Dun-Donnelley, Harper & Row, New York, 3rd ed., 1977, 39-41.

2. Patterson, J. W., Wastewater Treatment Technology, Ann Arbor Science Publishers Inc., Michigan, 1975, 175-189.

3. Shapiro, A. H., "Bath-Tub Vortex", Nature, 196, 1080, 1962.

4. Binnie, A. M., "Some Experiments on the Bath-Tub Vortex", J. Mech. Eng. Sci., 6, 256, 1964.

5. Sibulkin, M., "A note on the bathtub vortex", J. Fluid Mech., 14, 21, 1962.

6. Killy, D. L., Martin, B. W., and Taylor, E. S., "A further note on the bathtub vortex", J. Fluid Mech., 19, 539, 1964.

7. Marris, A. W., "Theory of the Bathtub Vortex", Trans. ASME, Ser. E, 34, 11, 1967.

8. Harada, M., "On the Generalized Bath-Tub Vortex", Trans. ASME, Ser. D, 89, 617, 1967.

9. Le Lan, A. and Angelino, H., "Etude du vortex dans les cuves agitees", Chem. Eng. Sci., 27, 1969, 1972.

10. Nagata, S., Yoshioka, N. and Yokoyama, T., "Studies on the Power Requirment of Mixing Impellers (I)", Mem. Fac. Engng. Kyoto Univ., 17, 175, 1955.

11. Lubin, B. T. and Springer, G. S., "The formation of a dip on the surface of a liquid draining from a tank", J. Fluid Mech., 29, 385, 1967.

12. McDuffie N. G., "Vortex free Downflow in Vertical Drains", AIChE J., 23, 37 and 614, 1977.

13. Toyokura, T. and Akaike, S., "Vortex Phenomena in a Water Tank", Bull. Japan Soc. Mech. Eng., 13, 373, 1970.

14. Lewellen, W. S., "A solution for three-dimensional vortex flows with strong circulation", J. Fluid Mech., 14, 420, 1962.

15. Hayduk, W. and Neale, G., "Vortex Formation in Stirred Draining Vessels", Can. J. Chem. Eng., 56, 544, 1978.

16. Neale, G. and Hayduk, W., "Improved correlations for Prediction of Vortex Depth in Stirred Draining Vessels", Can. J. Chem. Eng., 58, 129, 1980.

17. Leclerc, F., "Vortex Separator", Bachelor thesis, Department of Chemical Engineering, University of Ottawa, 1981.

18. Perry, R. H. and Chilton, C. H., Chemical Engineers' Handbook, 5th ed., Mcgraw-Hill Book Company, New York, 1973, section 19, 87-94.

19. Schweitzer, Hankbook of separation Techniques for Chemical Engineers, Mcgraw-Hill Book Company, New York, 1979, section 1, 343-358, and section 4, 114-118 & 135-140.

20. Boadway, J. D., "The Invention and Development of the Vortex Clarifier", Philadelphia WPCF Convention, October, 1977.

21. Gullotta, J. D. and Boadway, J. D., "A High-Capacity centrifuge for Clarification of Sewage", New England WPCF Conference, June, 1976.

22. Duncan, W. J., Thom, A. S. and Young, A. D., Mechanics of Fluids, Edward Arnold (Publishers) Ltd., London, 1970, 15-18.

23. Buider, R. C. Fluid Mechanics, 4th ed., Prentice-Hill Inc., New Jessy, 1962, 55-61.

24. Carnahan, B., Luther, H. A. and Wilkes, J. O., Applied Numerical Methods, John Wiley & Sons, New York, 1969, 573-574.

25. Bacon, D. W., Collection and Interpretation of Industrical Data, Department of Chemical Engineering, Queen's University, Kingston, Ontario, Canada. 1981, 78-86.

26. Kagaka, Kogaku and Kyokai, Chemical Engineering Programming. Baifukan, Toyko, 1975, 129-135.

Appendix A

CALIBRATION CURVES OF THE ROTAMETERS FOR PHASE I EXPERIMENTS

All the calibrations were performed at 25.0±1.0°C. The calibration curve for the annular circulation rotameter is shown in Figure A.1 . A linear regression analysis was performed to find the best fitting line between X=1 and X=5, and the following result was obtained:

$$Y = 0.1720 + 4.2570*X \qquad (A.1)$$

In the above expression, X is the rotameter reading in terms of USGPM, and Y is the volumetric flow rate in terms of liter/min. The coefficient of correlation was 0.9971 for the above equation.

The calibration curve for the water return rotameter is shown in Figure A.2 . A linear regression analysis was carried out, and the correlation equation was found as follows:

$$Y = 1.2442 + 1.4946*X \qquad (A.2)$$

The notations of X and Y are same as before (equation A.1). The coefficient of correlation was 0.9992.

The calibration curve for the inner outlet flow rotameter is shown as Figure A.3 . Again, a linear regression analysis was performed, and the following result was obtained:

$$Y = 1.4255 + 1.4792*X \qquad (A.3)$$

The notations of X and Y are same as before. The correlation coefficient of the equation was 0.9993.

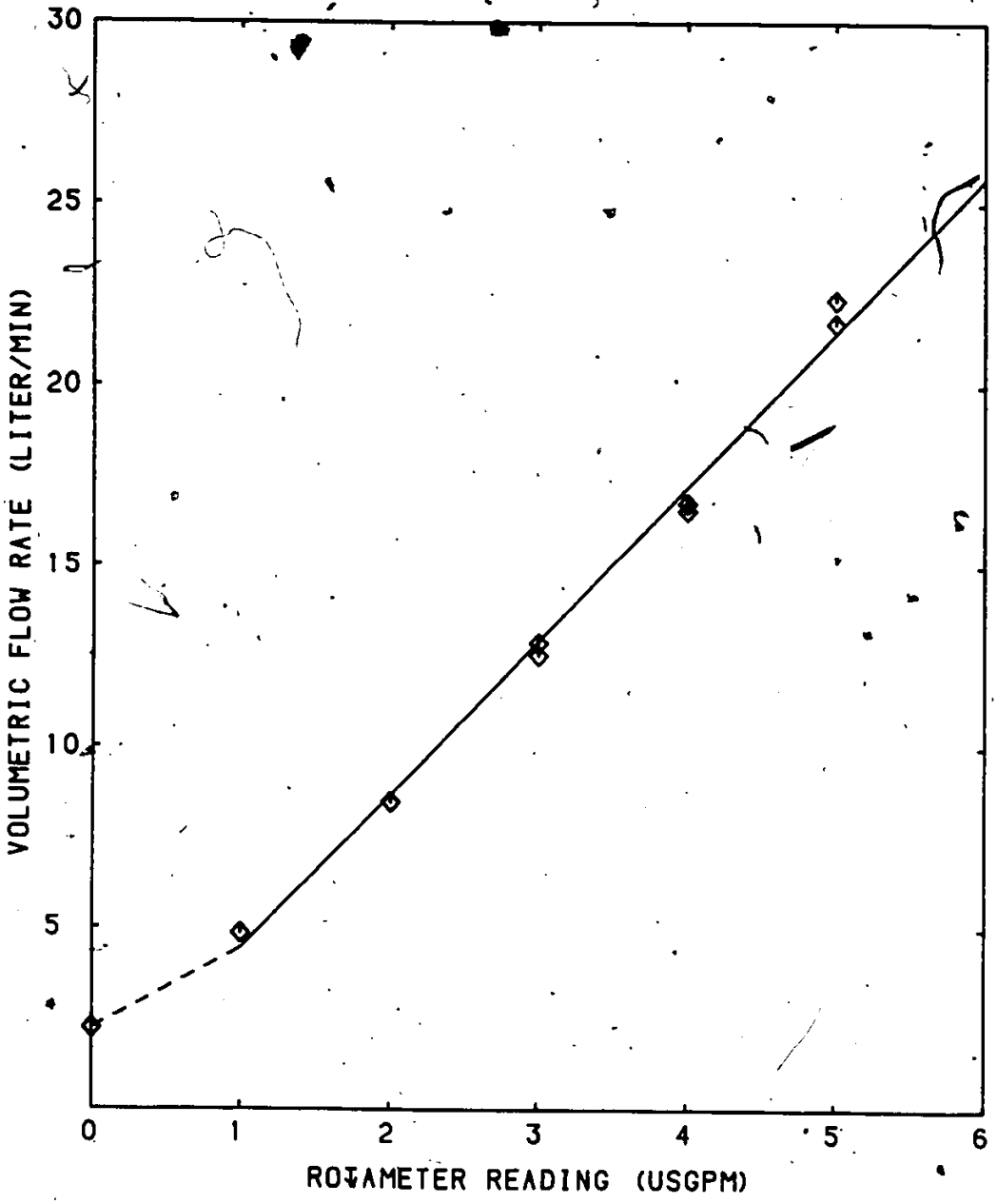

Figure A.1: CALIBRATION CURVE FOR THE ANNULAR CIRCULATION ROTAMETER

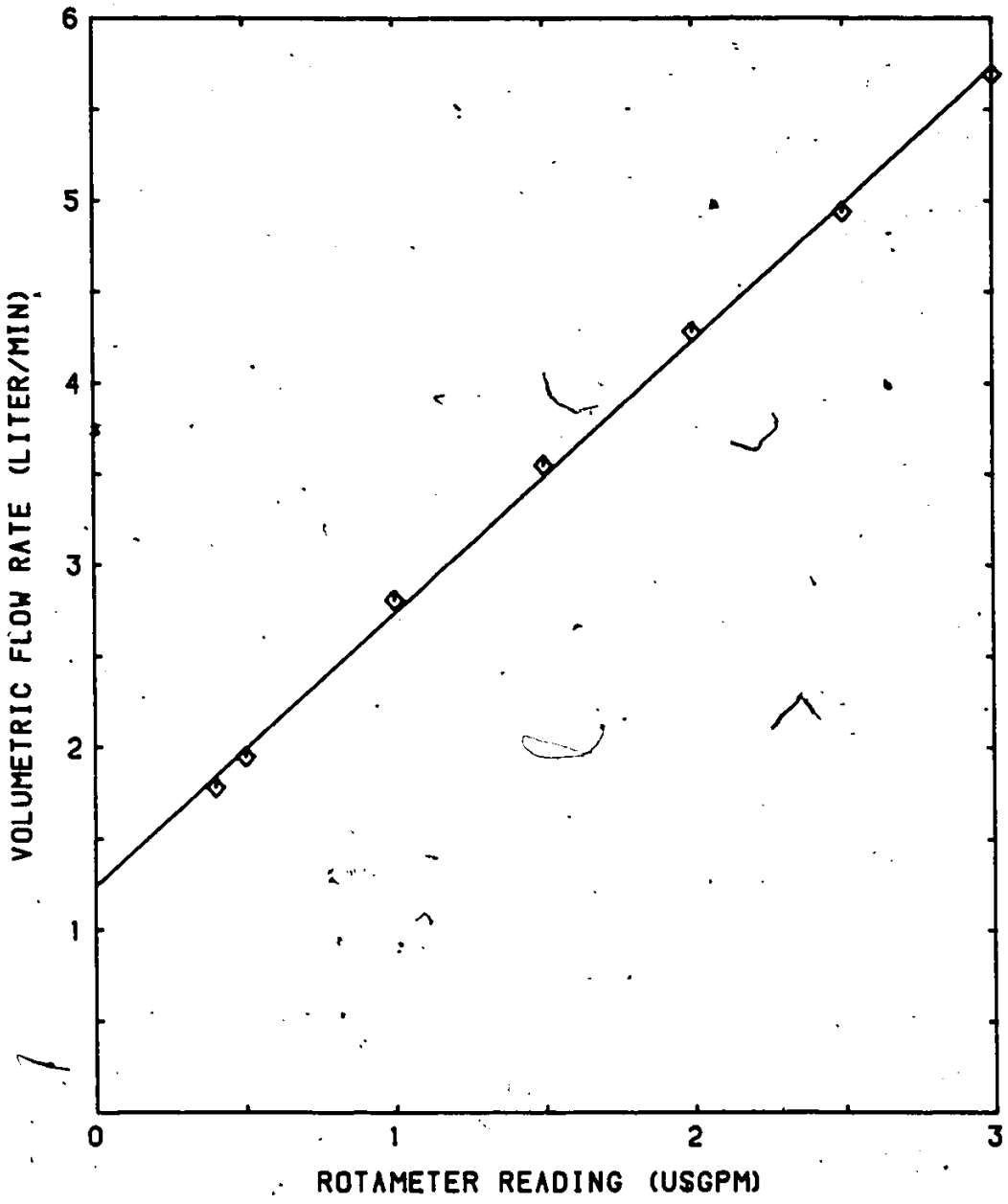

Figure A.2: CALIBRATION CURVE FOR THE WATER RETURN ROTAMETER

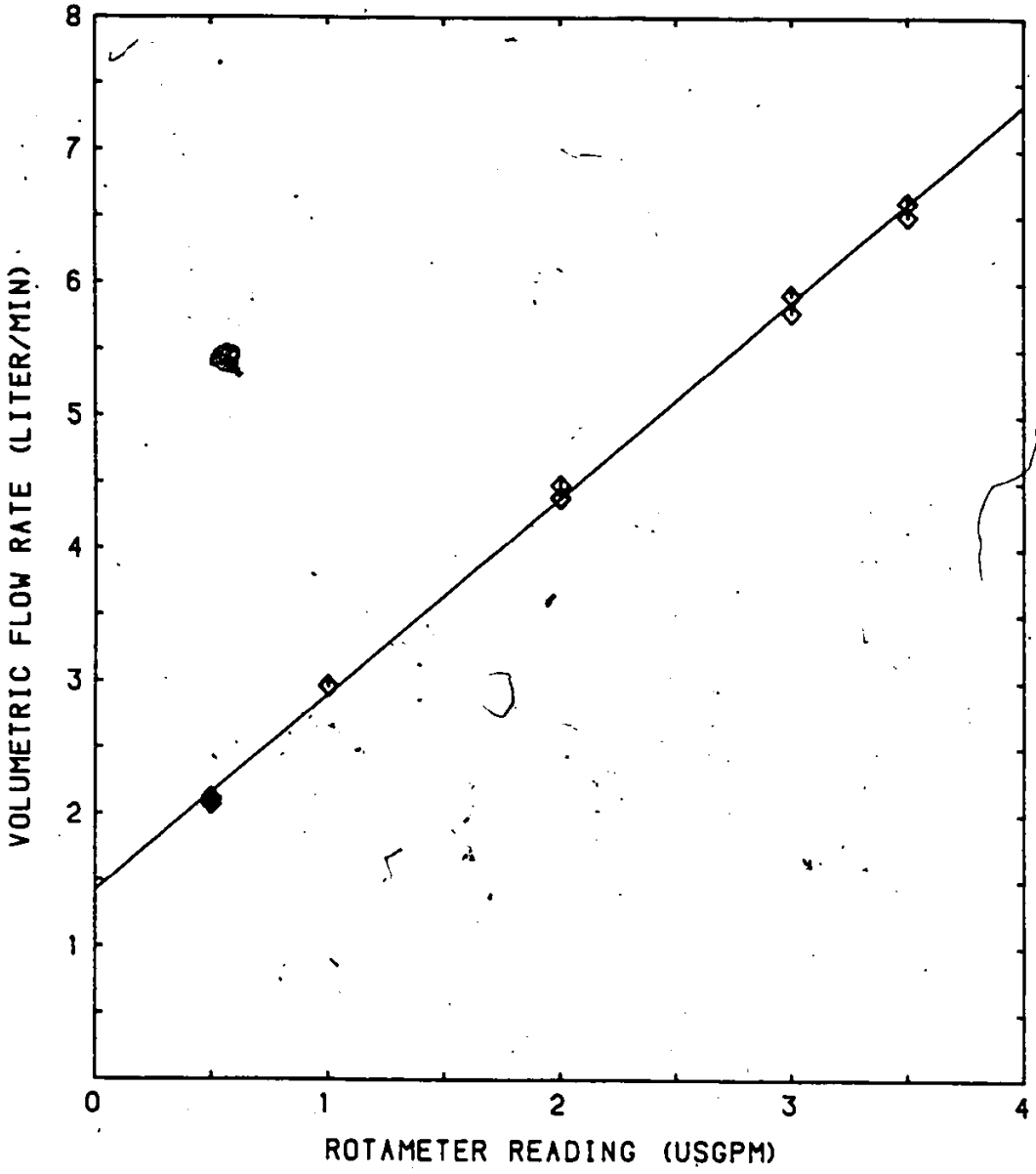

Figure A.3: CALIBRATIN CURVE FOR THE INNER OUTLET FLOW ROTAMETER

Appendix B

MEASUREMENTS OF PROPERTIES OF THE OILS

B.1 DENSITY MEASUREMENTS

The densities of the oils were measured by calibrated pycnometer bottles. Two pycnometer bottles were used; one was for the furnace oil, and the other was for the paraffin oil. These bottles were calibrated by distilled water, and thus the relation between the reading on the bottles and the corresponding volume was obtained. The densities of the Esso#2 furnace oil at different temperatures are shown in Table B.1 . The densities of the paraffin oil at different temperatures are shown in Table B.2 , and the densities of the two oils are plotted against temperature in Figure B.1 .

B.2 VISCOSITY MEASUREMENTS

The viscosity of the furnace oil was measured by a calibrated size 100 M523 Cannon-Fenske viscometer. The time interval for the oil passing from an upper marked level to a lower marked level in the viscometer at a specified temperature was recorded. This efflux time multipling the viscometer constant gave the kinematic viscosity of the oil at that temperature. The viscosity of the oil could be calculated

if the density of the oil at that temperature was known. The viscosities of the furnace oil at different temperatures are shown in Table B.3 . The viscosity of the paraffin oil was measured by a calibrated size 300 T336 viscometer, and the viscosities of the paraffin oil at different temperatures are shown in Table B.4 .

B.3 SURFACE TENSIONS MEASUREMENTS

The surface tensions of the two oils were measured by Fisher, Model 215 Autotensiomat Surface Tension Analyzer. The surface tension of the oil was indicated directly from a meter on the analyzer. The surface tensions of the furnace oil and of the paraffin oil at different temperatures are shown in Tables B.5 and B.6 respectively.

TABLE B.1

DENSITIES OF THE FURNACE OIL

WEIGHT OF THE FURNACE OIL IN THE PYCNOMETER BOTTLE AT 23.4 DEGREE C WAS 2.7456 GRAMS.

TEMPERATURE (±0.05°C)	VOLUME OBTAINED FROM THE CALIBRATION CURVE (cm^3)	DENSITY (gm/cm^3)
20.0	3.2146	0.8541
23.0	3.2259	0.8511
24.0	3.2297	0.8501
25.0	3.2335	0.8491
28.0	3.2445	0.8462
30.0	3.2500	0.8448
32.5	3.2560	0.8432
35.0	3.2622	0.8416
36.0	3.2663	0.8406

TABLE B.2

DENSITIES OF THE PARAFFIN OIL

WEIGHT OF THE PARAFFIN OIL IN THE PYCNOMETER BOTTLE AT 23.4 DEGREE C WAS 2.6911 GRAMS.

TEMPERATURE (±0.05°C)	VOLUME OBTAINED FROM THE CALIBRATION CURVE (cm^3)	DENSITY (gm/cm^3)
20.0	3.0671	0.8774
23.0	3.0773	0.8745
25.0	3.0840	0.8726
28.0	3.0980	0.8687
30.0	3.1010	0.8678
32.5	3.1040	0.8670
35.0	3.1100	0.8653
36.0	3.1120	0.8647

TABLE B.3

VISCOSITIES OF THE FURNACE OIL

TEMPERATURE (±0.05°C)	KINEMATIC VISCOSITY (centistokes)	DENSITY (gm/cm^3)	VISCOSITY (gm/cm.s)
21.0	3.845	0.8530	0.0328
21.5	3.788	0.8520	0.0323(*)
	3.791		
23.1	3.665	0.8506	0.0312(*)
	3.669		
23.5	3.629	0.8502	0.0309
25.1	3.497	0.8489	0.0297(*)
	3.495		
27.1	3.336	0.8470	0.0283(*)
	3.337		
30.1	3.098	0.8447	0.0262(*)
	3.110		

N.B.: (*) DENOTES THE AVERAGE VALVE.

TABLE B.4

VISCOSITIES OF THE PARAFFIN OIL

TEMPERATURE (±0.05°C)	KINEMATIC VISCOSITY (centistokes)	DENSITY (gm/cm^3)	VISCOSITY (gm/cm.s)
21.0	199.50	0.8763	1.7482
21.5	197.76	0.8758	1.7319(*)
	197.73		
23.1	178.01	0.8742	1.5562
23.5	173.27	0.8736	1.5137
25.1	156.73	0.8723	1.3659(*)
	156.45		
27.1	138.34	0.8703	1.2040
30.1	114.74	0.8677	0.9956

N.B.: (*) DENOTES THE AVERAGE VALUE.

TABLE B.5

SURFACE TENSIONS OF THE FURNACE OIL

TEMPERATURE (±0.05°C)	SURFACE TENSION (dynes/cm)
15.0	33.75
20.0	32.00
22.5	31.17(*)
25.4	30.20(*)
30.0	28.70
35.0	27.00(*)

N.B.: (*) DENOTES THE AVERAGE RESULT FROM AT LEAST TWO DATA.

TABLE B.6

SURFACE TENSION OF THE PARAFFIN OIL

TEMPERATURE (±0.05°C)	SURFACE TENSION (dynes/cm)
15.0	34.70
20.0	33.90
23.5	33.33(*)
25.0	33.10
27.2	32.50(*)
33.0	31.83(*)
36.0	31.33(*)

N.B.: (*) DENOTES THE AVERAGE RESULT FROM AT LEAST TWO DATA.

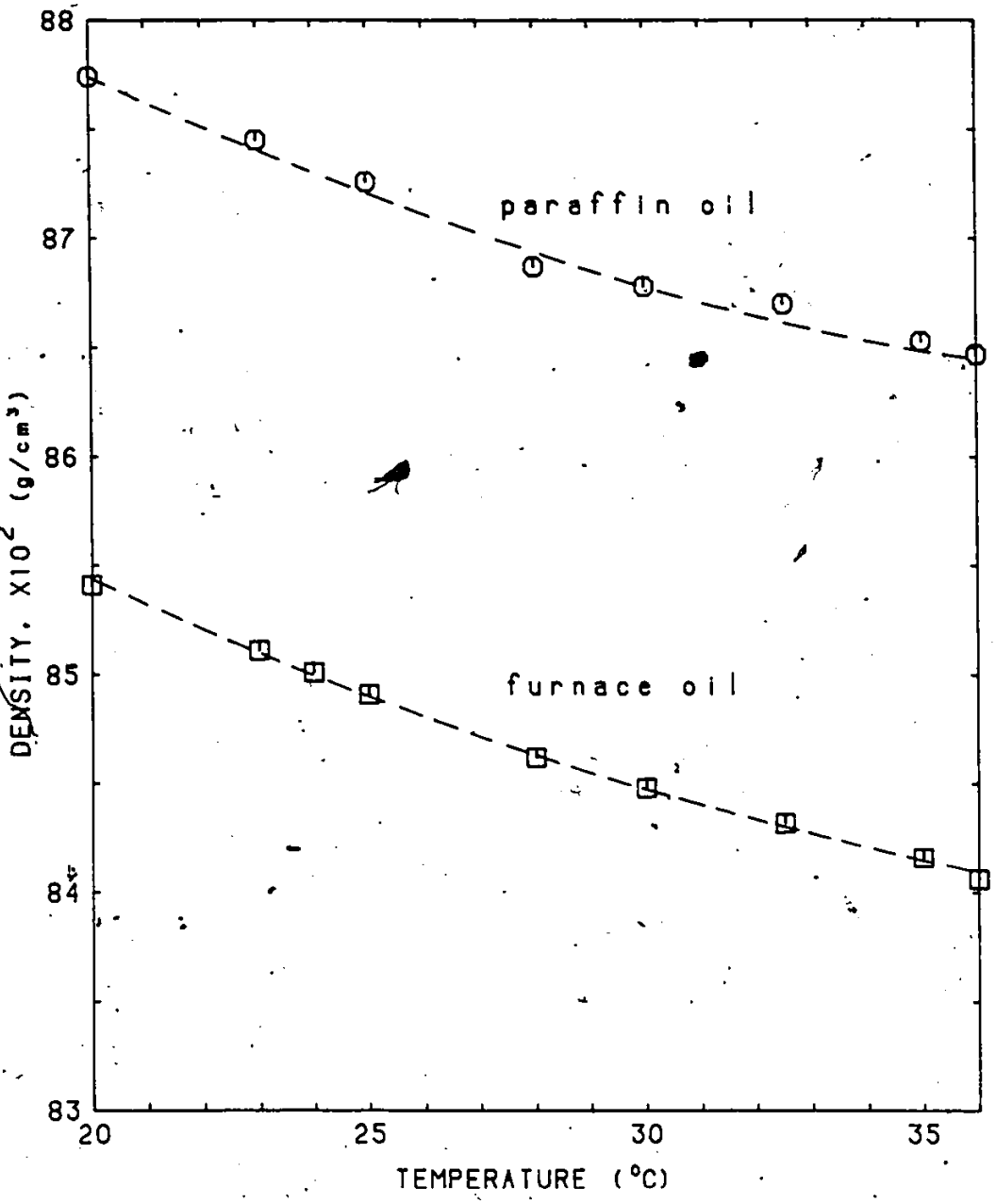

Figure B.1: DENSITIES OF FURNACE OIL AND PARAFFIN OIL

Appendix C

CALIBRATION CURVES OF THE ROTAMETERS FOR PHASE II EXPERIMENTS

All the calibrations were carried out at 25.0±1.0°C. The calibration curve for the oil supply rotameter for furnace oil is shown in Figure C.1 . A linear regression analysis was performed to find the best fitting line for the data, and the following result was obtained:

$$Y = -0.9137 + 4.1618*X \qquad (C.1)$$

In the above equation, X denotes the reading from the rotameter in terms of USGPM, and Y denotes the volumetric flow rate in terms of liter/min. The coefficient of correlation was 0.9990 for the above correlation equation.

The calibration curve for the oil supply rotameter for paraffin oil is shown in Figure C.2 . The correlation equation for this calibration curve was obtained by performing a linear regression analysis on the data, and the correlation equation was:

$$Y = -0.8854 + 1.8564*X \qquad (C.2)$$

The notations for X and Y are same as the notations being used in equation (C.1). The coefficient of cerrelation was 0.9940.

The calibration of the inner outlet flow rotameter (R3) in the oil-water separation experiments was difficult because both high oil content and low oil content mixtures would flow through this rotameter during different operating conditions of the experiments. The average value of the volumetric flow rate which included mixtures of high oil content and low oil content at the same reading of the rotameter was used for calibration. The high oil content and low oil content mixtures were obtained by varying the annular flow rate. The calibration data for the furnace oil and the paraffin oil are shown in Table C.1 and Table C.2 respectively.

The calibration curve for the inner flow rotameter (R3) for furnace oil and water mixture is shown in Figure C.3 . The correlation equation for the calibration curve was obtained by performing a linear regression analysis on the data, and the following equation was obtained:

$$Y = 1.3963 + 1.5572*X \qquad (C.3)$$

The notation of X and Y are same as before. The correlation coefficient was 0.9979.

The calibration curve for the inner flow rotameter (R3) for paraffin oil and water mixture is shown as Figure C.4 . Again, a linear regression analysis was performed, and the correlation equation was:

$$Y = 1.7907 + 1.3140*X \qquad (C.4)$$

The notatins of X and Y are same as before. The correlation coefficient was 0.9904.

TABLE C.1

CALIBRATION DATA OF THE INNER OUTLET FLOW ROTAMETER FOR FURNACE OIL AND WATER MIXTURE

ROTAMETER (R3) READING	VOLUMETRIC FLOW RATE (liter/min)
0.5	2.1235(+)
	2.0966(-)
	2.1101(*)
1.0	3.0106(+)
	2.9030(-)
	2.9568(*)
2.0	4.6663(*)
3.0	5.9740(*)

(+) denotes the high oil content flow rate.
(-) denotes the low oil content flow rate.
(*) denotes the average flow rate.

TABLE C.2

CALIBRATION DATA OF THE INNER OUTLET FLOW ROTAMETER FOR PARAFFIN OIL AND WATER MIXTURE

ROTAMETER (R3) READING	VOLUMETRIC FLOW RATE (liter/min)
0.5	2.2464(-)
	2.1840(-)
	2.1235(-)
	2.4864(+)
	2.5536(+)
	2.3923(+)
	2.3310(*)
1.0	3.2256(-)
	3.1584(-)
	3.0240(+)
	3.0240(+)
	3.1080(*)
2.0	4.7040(*)
3.0	5.5608(*)

(+) denotes the high oil content flow rate.
(-) denotes the low oil content flow rate.
(*) denotes the average flow rate.

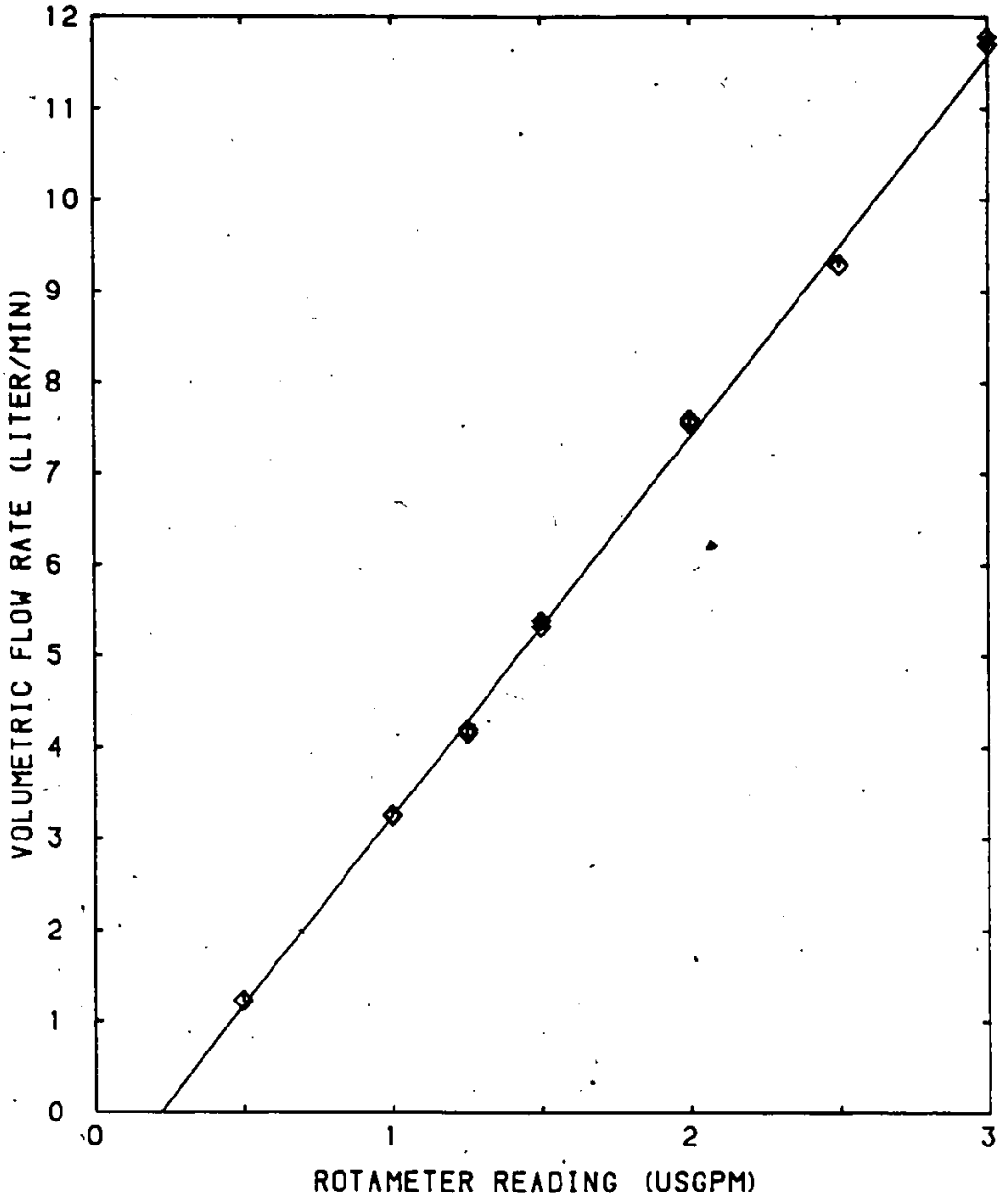

Figure C.1: CALIBRATION CURVE FOR THE OIL SUPPLY ROTAMETER FOR FURNACE OIL

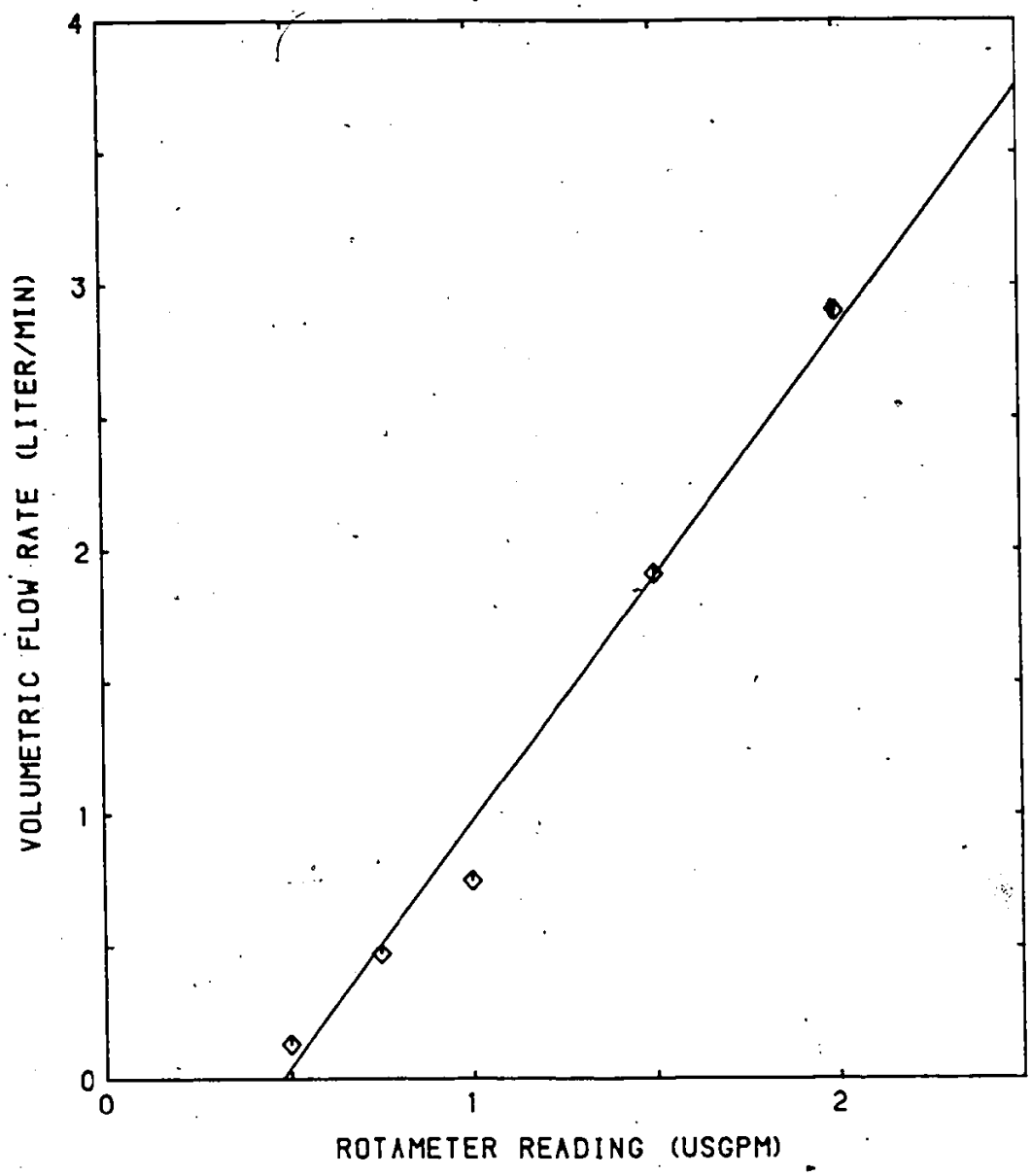

Figure C.2: CALIBRATION CURVE FOR THE OIL SUPPLY ROTAMETER FOR PARAFFIN OIL

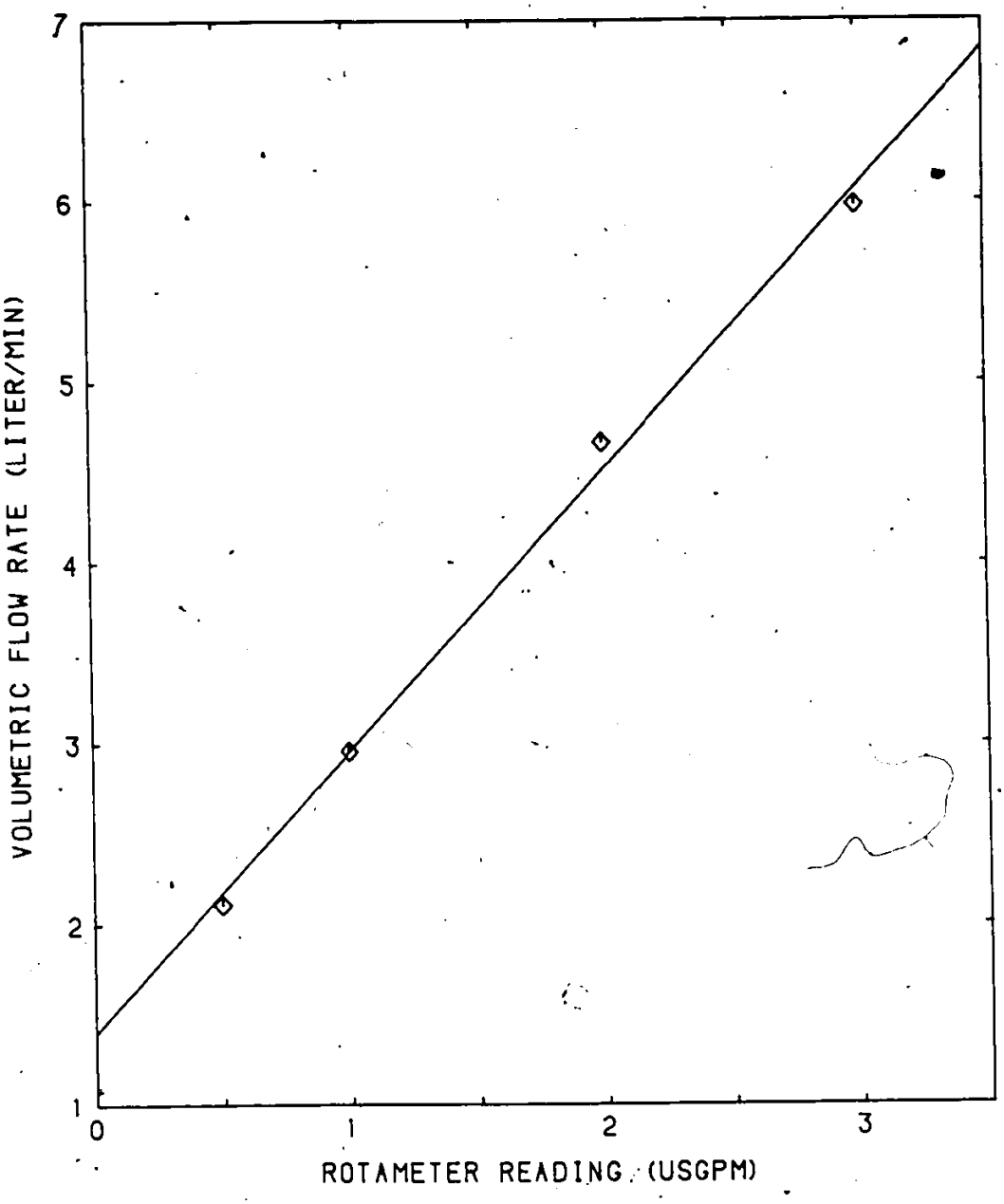

Figure C.3: CALIBRATION CURVE FOR THE INNER FLOW ROTAMETER FOR FURNACE OIL AND WATER MIXTURE

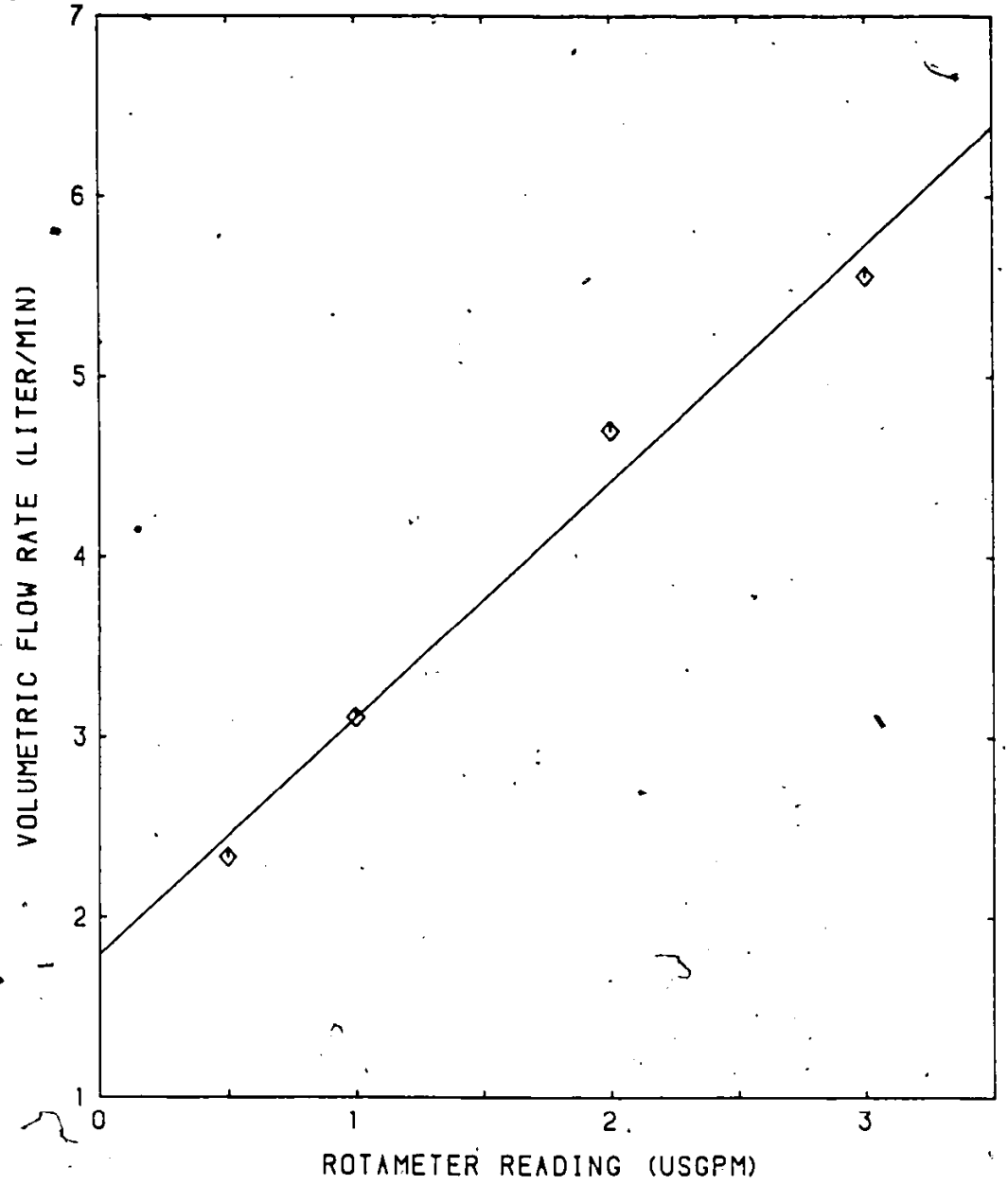

Figure C.4: CALIBRATION CURVE FOR THE INNER FLOW ROTAMETER FOR PARAFFIN OIL AND WATER MIXTURE

Appendix D

MEASUREMENTS OF DISTRIBUTION OF PARTICLE SIZES AND AVERAGE PARTICLE SIZE OF THE CALCIUM CARBONATE

D.1 MEASUREMENT OF DISTRIBUTION OF PARTICLE SIZES

The distribution of particle sizes of the calcium carbonate was roughly determined by a sedimentation method. A 0.089 wt. % of calcium carbonate slurry was prepared in distilled water at 25.0±1.0°C. This solution was stirred in a large beaker by a high speed stirrer for five minutes, and thus the particles were distributed uniformly in the water. The solution was then transferred into a 8.0-cm diameter, 2 liter glass cylinder which has a metric scale on its outside wall. Once the cylinder was filled with this slurry to a depth of 50.0 cm, a timer was started. After a specified time interval, a sample was withdrawn at 40.0 cm below the liquid surface in the cylinder using a 50-ml pipet. This sample taking step had to carried out carefully because it was easy to redisperse the settled particles at the bottom of the cylinder. The weight concentration of the sample was measured by the light scattering photometer. The calcium carbonate slurry in the cylinder was stirred by a glass rod, and was transferred back to the beaker. The above procedure

was repeated for the other time intervals. The experimental data are summarized in Table D.1 . Based on the experimental data, the particle size of a sample at a particular time interval could be estimated by considering that a type-I sedimentation equation applied. Type-I sedimentation is concerned with removal of nonflocculating discrete particle in a dilute suspension. A sample calculation is shown in the Table D.2 , and the distribution curve is shown in Figure D.1 .

D.2 MEASUREMENT OF AVERAGE PARTICLE SIZE

The average particle size was roughly determined by settling a 3 wt. % of calcium carbonate solution. The solution was perpared by mixing calcium carbonate and distilled water in a large beaker. This solution was stirred by a high speed stirrer for five minutes, so that the distribution of the particles was nearly uniform in the water. The solution was transferred into a 8.0-cm diameter, 2 liter glass cylinde The height of the interface between the clear water and the milky slurry from the bottom of the cylinder was measured by means of a scale attached to the cylinder wall. The heights of the interface and its corresponding times were recorded.

The results are plotted as Figure D.2 . The average particle size could be estimated by the slope of the settling region, and the average particle size was 10.20 μm. A sample calculation is shown as follows:

Slope of the settling region = 0.76 cm/min (velocity)

The average particle size was estimated by the same procedure as in Table D.2 .

$$dp = \sqrt{\frac{18\mu Vs}{g(\rho_s - \rho)}}$$

$$dp = \sqrt{\frac{18(0.861 \times 10^{-2})(0.76/60)}{980(2.93-0.9971)}}$$

$$dp = 1.02 \times 10^{-3} \text{ cm}$$

$$dp = 10.20 \ \mu m.$$

TABLE D.1

EXPERIMENTAL DATA FOR MEASUREMENT OF DISTRIBUTION OF PARTICLE SIZES

INITIAL WEIGHT CONCENTRATION : 0.089 WT. % OF CALCIUM CARBONATE

TIME (min.)	CONC. AT 40.0 cm BELOW THE SURFACE (wt. % of solid in the solution)	WT. % OF PARTICLE LESS THAN dp (%)	PARTICLE SIZE dp (μm)
0.5	0.089	100.00	---
1.0	0.089	100.00	---
5.0	0.089	100.00	---
10.0	0.089	100.00	---
15.0	0.089	100.00	---
18.0	0.086	96.60	17.41
20.0	0.084	94.38	16.51
22.0	0.082	92.13	15.75
24.0	0.081	91.01	15.08
26.0	0.078	87.64	14.48
28.0	0.077	86.52	13.96
30.0	0.071	79.78	13.48
35.0	0.061	68.54	12.48
40.0	0.057	64.05	11.68
45.0	0.049	54.50	11.01
50.0	0.042	47.19	10.44
58.3	0.035	39.33	9.67
70.0	0.032	35.39	8.82
110.0	0.028	30.90	7.04

TABLE D.2

SAMPLE CALCULATION OF THE PARTICLE SIZE

SAMPLE CALCULATION FOR THE CASE: TIME=20.0 MIN., CONCENTRATION=0.084 WT. %.

Assumptions:
(1) particles have uniform density.
(2) particles are spherical in shape.
(3) Reynold number < 1.0, i.e. Stoke's law region.
For type I sedimentation, the expression for terminal settling velocity (Vs) of the particle can be written as:

$$Vs = \frac{g(\rho_s-\rho)dp^2}{18\mu}$$

or

$$dp = \sqrt{\frac{18\mu Vs}{g(\rho_s-\rho)}} \qquad (D.1)$$

At 25.0 °C, viscosity of water is $0.861x10^{-2}$ gm/cm.s; density of water is 0.9971 gm/cm^3, and density of the calcium carbonate is 2.93 gm/cm^3 (from Handbook of Chemistry and Physics) By equation (D.1), the diameter of the particle (dp) could be estimated.

$$dp = \sqrt{\frac{18(0.861x10^{-2})(40/1200)}{980(2.93-0.9971)}}$$

$$dp = 1.65x10^{-3} \text{ cm or } 16.5 \ \mu m.$$

The percentage of particle less than the above diameter could be calculated as follows:

$$\% \text{ of particles} = \frac{0.084}{0.089} \times 100\% = 94.38 \ \%.$$

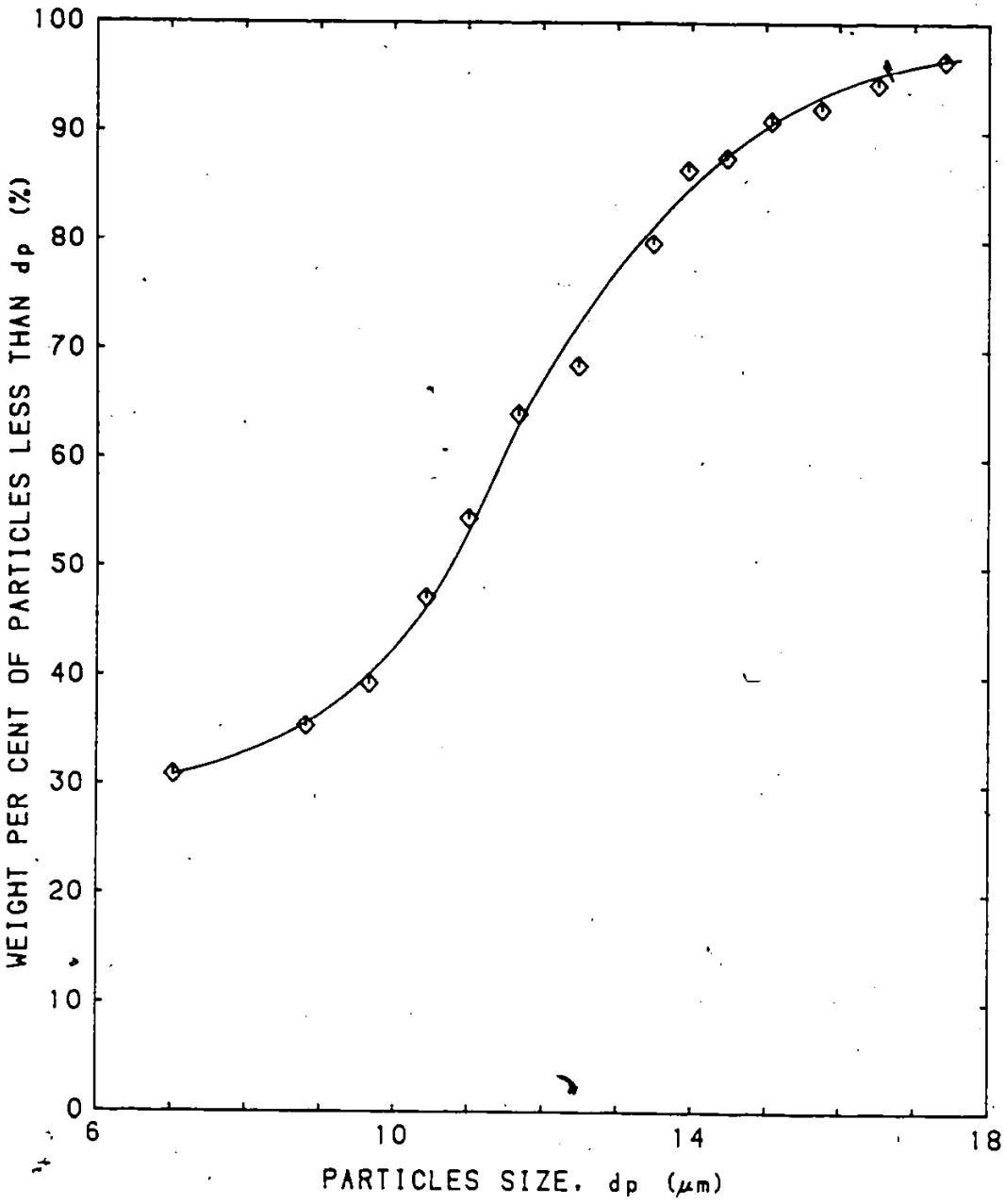

Figure D.1: DISTRIBUTION CURVE OF CALICUM CARBONATE PARTICLE SIZES

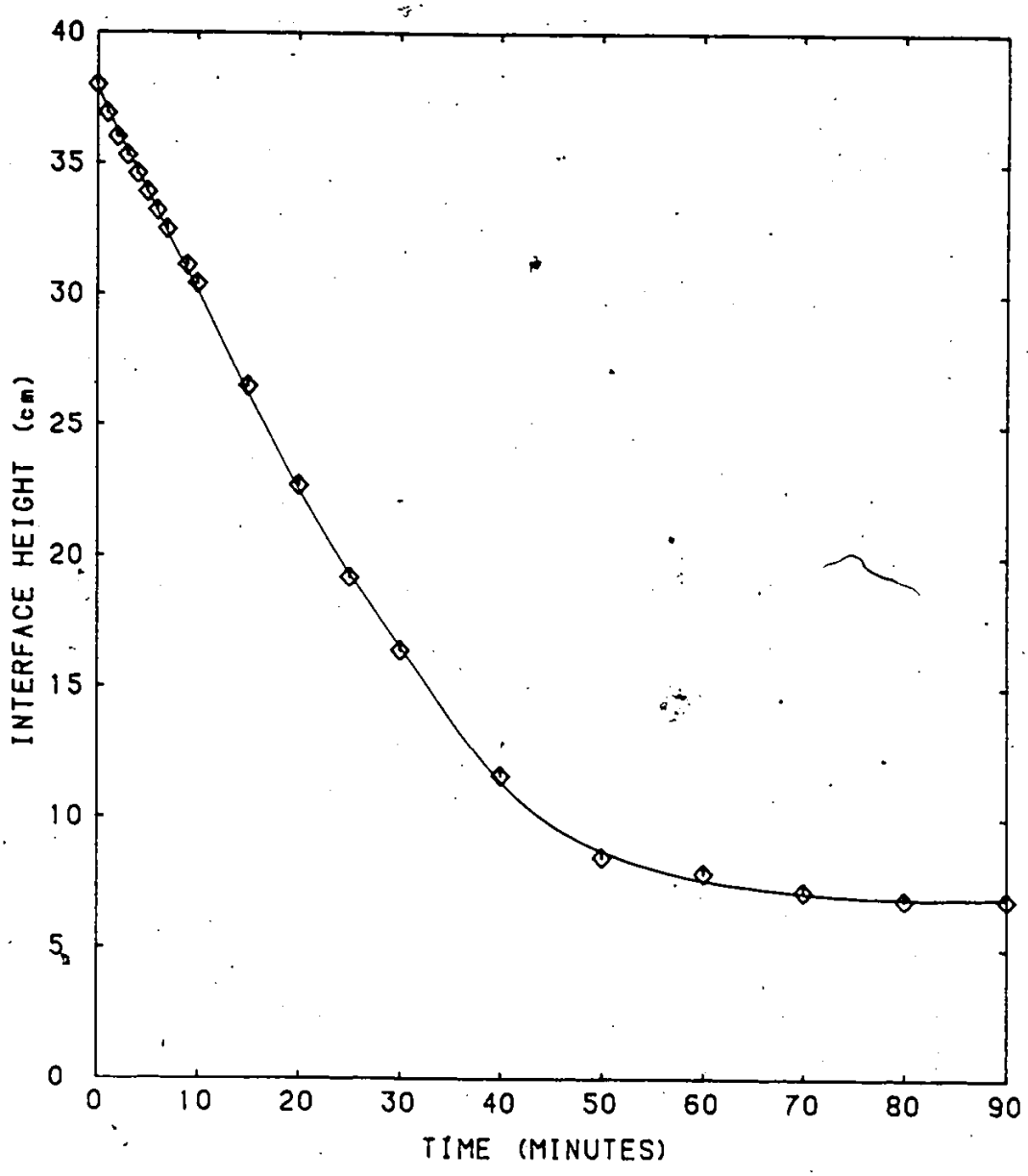

Figure D.2: BATCH SETTLING CURVE FOR 3 WT. % CALCIUM CARBONATE SLUURY

Appendix E

CALIBRATION CURVE FOR THE LIGHT SCATTERING PHOTOMETER

The Fisher, model DRT 100 light scattering photometer was calibrated using known concentrations of calcium carbonate solutions. The calibration curve is shown in Figure E.1 . The correlation equation for the calibration curve was obtained by performing a linear regression analysis on the data, and the equation was:

$$Y = 4.475 \times 10^{-3} + 9.412 \times 10^{-5} * X \qquad (E.1)$$

In the above expression, X denotes the reading from the photometer, and Y denotes the weight % of solid in the solution. The correlation coefficient was 0.9980 for the above equation.

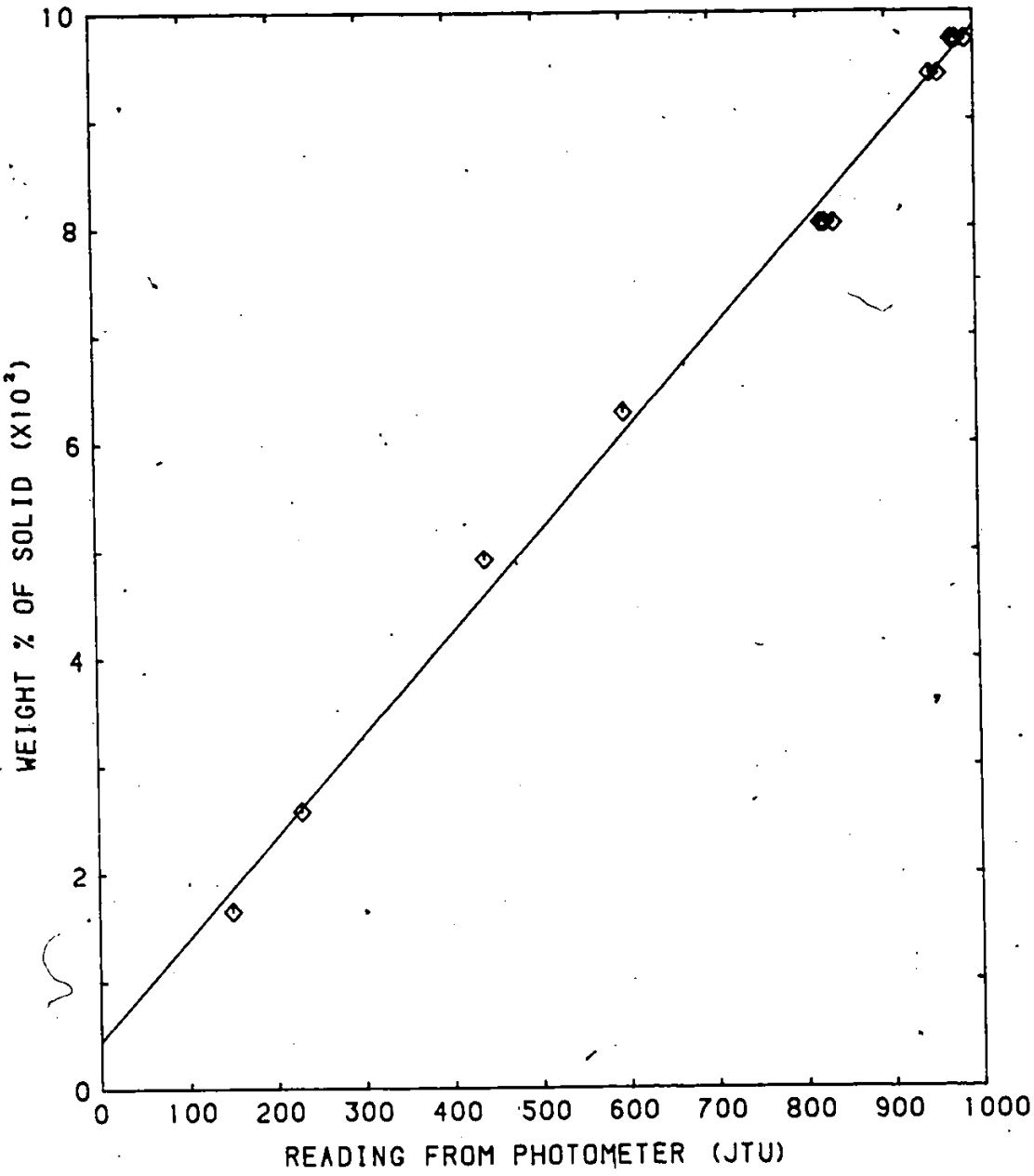

Figure E.1: CALIBRATION CURVE OF FISHER MODEL DRT 100 LIGHT SCATTERING PHOTOMETER

Appendix F

DATA FOR THE AIR-WATER VORTEX EXPERIMENTS

The experimental data for the study of the effects of the rotation speed of the stirrer (Ω), water depth in the vortex tank (H), inner outlet velocity (Vi), and annular outlet velocity (Va) on the vortex depth (Hv) are shown in Table F.1 .

The inner outlet flow rate was originally observed from the inner outlet flow rotameter (R3), and the corresponding volumetric flow rate in terms of liter per minute could be found from the calibration curve (or from the correlation equation for the calibration curve). The unit of the volumetric flow rate was converted into cubic cm per second by multipling a factor of 16.67. The inner outlet velocity (Vi) was calculated by dividing the volumetric flow rate by the cross sectional area of the inner pipe (Ai=1.27 cm^2).

The annular outlet flow rate was observed from the annular circulation rotameter (R1). The annular volumetric flow rate in terms of cubic cm per second could be obtained by the same procedure as the inner outlet flow. However, the annular outlet velocity was calculated by dividing the volumetric flow rate by the annular opening area (Aa = inside

cross sectional area of the outer pipe (i.d.=2.54 cm) - outside cross sectional area of the inner pipe (o.d.=1.60 cm) = 3.06 cm^2).

TABLE F.1

DATA FOR THE AIR-WATER VORTEX EXPERIMENTS

NO.	Ω (rpm)	H (cm)	Hv (cm)	Vi (cm/s)	Va (cm/s)
1	3	10.0	5.0	0.00	81.02
2	3	10.0	5.0	26.54	9.82
3	3	10.0	5.0	33.35	0.00
4	3	10.0	7.0	40.16	0.00
5	3	10.0	10.0	0.00	135.57
6	3	10.0	10.0	26.54	110.04
7	3	10.0	10.0	32.38	33.44
8	3	10.0	10.0	40.16	9.82
9	3	20.0	10.0	0.00	133.25
10	3	20.0	10.0	26.54	79.88
11	3	20.0	10.0	32.38	24.15
12	3	20.0	10.0	40.16	9.82
13	3	20.0	10.0	46.00	6.00
14	3	20.0	11.0	51.84	0.00
15	3	20.0	17.0	65.46	0.00
16	3	20.0	20.0	79.09	0.00
17	3	20.0	14.0	0.00	149.50
18	3	20.0	15.0	26.54	149.50
19	3	20.0	17.5	40.16	149.50
20	3	20.0	20.0	46.00	149.50
21	3	20.0	20.0	51.84	133.25
22	3	20.0	20.0	59.62	24.15
23	3	20.0	20.0	65.46	15.12
24	3	20.0	20.0	79.09	0.00
25	3	30.0	12.5	0.00	149.50
26	3	30.0	15.0	26.54	149.50
27	3	30.0	15.0	40.16	93.79
28	3	30.0	15.0	51.84	24.15
29	3	30.0	15.0	65.46	4.91
30	3	30.0	20.0	79.09	0.00
31	3	30.0	27.5	92.71	0.00
32	3	30.0	12.5	0.00	149.50
33	3	30.0	15.0	26.54	149.50
34	3	30.0	18.0	40.16	149.50
35	3	30.0	23.0	51.84	149.50
36	3	30.0	27.0	65.46	149.50
37	3	30.0	30.0	73.25	135.57
38	3	30.0	30.0	79.09	61.29
39	3	30.0	30.0	84.92	35.76
40	3	30.0	30.0	92.71	18.13
41	5	10.0	5.0	0.00	33.44
42	5	10.0	5.0	23.62	9.27
43	5	10.0	5.0	26.54	6.00
44	5	10.0	5.0	30.43	0.00

(Table F.1 cont.)

NO.	Ω (rpm)	H (cm)	Hv (cm)	Vi (cm/s)	Va (cm/s)
45	5	10.0	10.0	40.16	0.00
46	5	10.0	10.0	0.00	82.18
47	5	10.0	10.0	23.62	18.13
48	5	10.0	10.0	26.54	12.11
49	5	10.0	10.0	32.38	7.09
50	5	10.0	10.0	40.16	0.00
51	5	20.0	10.0	0.00	77.54
52	5	20.0	10.0	23.62	21.14
53	5	20.0	10.0	26.54	13.61
54	5	20.0	10.0	32.38	9.27
55	5	20.0	10.0	40.16	7.09
56	5	20.0	16.0	51.84	0.00
57	5	20.0	17.0	0.00	149.50
58	5	20.0	20.0	26.54	149.50
59	5	20.0	20.0	32.38	91.47
60	5	20.0	20.0	40.16	21.14
61	5	20.0	20.0	51.84	10.36
62	5	30.0	15.0	0.00	123.97
63	5	30.0	15.0	26.54	79.86
64	5	30.0	15.0	32.38	56.65
65	5	30.0	15.0	40.16	15.12
66	5	30.0	15.0	46.00	9.82
67	5	30.0	15.0	51.84	6.00
68	5	30.0	20.0	65.46	0.00
69	5	30.0	27.0	79.09	0.00
70	5	30.0	30.0	92.71	0.00
71	5	30.0	19.5	0.00	149.50
72	5	30.0	24.0	26.54	149.50
73	5	30.0	28.5	40.16	149.50
74	5	30.0	30.0	46.00	149.50
75	5	30.0	30.0	51.84	91.47
76	5	30.0	30.0	65.46	45.04
77	5	30.0	30.0	79.09	12.11
78	5	30.0	30.0	92.71	0.00
79	10	10.0	5.0	0.00	21.14
80	10	10.0	5.0	23.62	13.61
81	10	10.0	5.0	26.54	9.82
82	10	10.0	5.0	37.24	0.00
83	10	10.0	10.0	40.16	0.00
84	10	10.0	10.0	0.00	33.44
85	10	10.0	10.0	23.62	16.92
86	10	10.0	10.0	26.54	13.31
87	10	10.0	10.0	32.38	7.09
88	10	10.0	10.0	40.16	0.00
89	10	20.0	10.0	0.00	38.08
90	10	20.0	10.0	23.62	21.14
91	10	20.0	10.0	26.54	18.13
92	10	20.0	10.0	32.38	9.27

(Table F.1 cont.)

NO.	Ω (rpm)	H (cm)	Hv (cm)	Vi (cm/s)	Va (cm/s)
93	10	20.0	10.0	40.16	0.00
94	10	20.0	16.0	51.84	0.00
95	10	20.0	20.0	65.46	0.00
96	10	20.0	20.0	0.00	79.86
97	10	20.0	20.0	23.62	52.01
98	10	20.0	20.0	26.54	40.40
99	10	20.0	20.0	32.38	24.15
100	10	20.0	20.0	40.16	19.33
101	10	20.0	20.0	51.84	9.27
102	10	20.0	20.0	65.46	0.00
103	10	30.0	15.0	0.00	70.58
104	10	30.0	15.0	26.54	28.79
105	10	30.0	15.0	40.16	6.00
106	10	30.0	19.0	51.84	0.00
107	10	30.0	30.0	65.46	0.00
108	10	30.0	30.0	0.00	149.50
109	10	30.0	30.0	26.54	114.68
110	10	30.0	30.0	40.16	65.93
111	10	30.0	30.0	51.84	12.11
112	10	30.0	30.0	65.46	0.00

Appendix G

REYNOLDS NUMBER CALCULATIONS

G.1 REYNOLDS NUMBER CALCULATION FOR INNER OUTLET FLOW

Reynolds number for a fluid in a smooth circular pipe can be cilculated by the following equation:

$$Re = \frac{di\langle Vi\rangle\rho}{\mu} \qquad (G.1)$$

The transition region from laminar flow to turbulent flow is around Re = 2100. The equation (G.1) can be rewritten as:

$$\langle Vi\rangle = \frac{Re\mu}{di\rho} \qquad (G.2)$$

Thus the average velocity <Vi> at the transition region can be estimated by equation (G.2).

For this study, the i.d. of the inner outlet pipe was 1.27 cm. The density of water at 25.0°C is 0.9971 gm/cm^3, and the viscosity of water at 25.0°C is 0.0086 gm/cm.s. By substituting these data into the equation (G.2), the average inner outlet velocity at the transition region from laminar flow to turbulent flow was 14.26 cm/s.

G.2 REYNOLDS NUMBER CALCULATION FOR ANNULAR FLOW

The Reynolds number for the annular tubes can be calculated by the following equation:

$$Re = \frac{da(1-k)\langle Va\rangle\rho}{\mu} \qquad (G.3)$$

In the above expression, k is the ratio of outside diameter of the inner tube to inside diameter of the outer tube, and da is the i.d. of the outer tube. The average velocity <Va> at the transition region from laminar flow to turbulent flow (Re=2100) can be estimated by the rewritten form of equation (G.3).

$$\langle Va\rangle = \frac{Re\mu}{da(1-K)\rho} \qquad (G.4)$$

For this study, k was equal to 0.6299, and da was 2.54 cm. The average velocity of the annular flow at the transition region was calculated by substituting the corresponding data into equation (G.4), and the result was 19.27 cm/s.

G.3 CALCULATIONS OF IMPELLER REYNOLDS NUMBER

The impeller Reynolds number can be calculated by equation (G.5),

$$Re = \frac{Da^2\Omega\rho}{\mu} \qquad (G.5)$$

In the above equation, Da denotes the impeller diameter, and Ω is in term of rev./sec. For turbulent flow in the tank, the impeller Reynolds number is greater than 10000. The Reynolds numbers of the three experimantal rotation speeds of the stirrer are examined as following calculations:

1. Ω = 3 rpm or 0.05 rev./s, and Da = D2 = 37.5 cm,

$$Re = \frac{(37.5)^2(0.05)(0.9971)}{0.86 \times 10^{-2}}$$

Re(impeller) = 8150.

2. Ω = 5 rpm or 0.0833 rev./s, Re(impeller) = 13580.
3. Ω = 10 rpm or 0.1667 rev./s, Re(impeller) = 27170.

Therefore, the first case was in laminar-turbulent transition region, and the last two cases were turbulent flow.

Appendix H

COMPARISONS OF OBSERVED AND PREDICTED VORTEX SHAPES

The shape of the experimental (observed) vortex was estimated from the photo that had been taken during the experiment. Three vortices, which were formed at different operating conditions of the four variables, were examined. Their operating conditions are summarized in Table H.1 .

The sample calculation of the case 1 is presented as below. The observed values of the distance from the vortex 'tip' (z) and the distance from the axis of the vortex (r) are shown in Table H.2 .

The equations for Rankine's combined vortex as described in Chapter 3 can be rewritten as the following forms: ($p=p_o$ at free surface of the liquid)

$$z = \frac{\omega^2 r^2}{2g} \quad , \; s \geq r \geq 0 \qquad (3.8')$$

and

$$z = \frac{\omega^2 s^2}{g}\left(1 - \frac{s^2}{2r^2}\right) \quad , \; r > s \qquad (3.28')$$

Since there was no hint for the position of the transition radius, s, (or region) from forced vortex to free

vortex, a trial value of s was assigned. By trial and error, a suitable value of s could be found. This trial-and-error method is summarized as follows: a trial value of s was selected, and the angular velocity (ω) at the surface of the vortex corresponding to this trial value could be estimated by equation 3.8'. Substituting the data into equation 3.28', if the term $\frac{\omega^2 s^2}{g}$ in equation 3.28' was smaller than the full vortex depth, a greater value of s would be used for next trial; if the term $\frac{\omega^2 s^2}{g}$ was greater than the full vortex depth by more than 1.0, a smaller value of s would be used. After several trials, a suitable value of s could be found when the value of $\frac{\omega^2 s^2}{g}$ was just greater than the full vortex depth (not more than 1.0). The value of the transition point s for the case 1 was found to be 1.02 cm.

At s=1.02 cm, the corresponding value of z was 15.5 cm from the observed data. The tangential velocity (V_t) and the pressure (p) at s were continuous, and the angular velocity was assumed to be continuous at s also. Thus the angular velocity (ω) could be estimated by the rewritten form of equation (3.8').

$$\omega = \sqrt{\frac{2gz}{s^2}}$$

$$\omega = \sqrt{\frac{2(980)(15.5)}{(1.02)^2}}$$

$$\omega = 170.88 \ s^{-1}$$

Substituting the corresponding data into the equations (3.8') and (3.28') yielded:

$$r = \sqrt{\frac{2gz}{\omega^2}} = \sqrt{\frac{2(980)z}{(170.88)^2}}$$

$$r = \sqrt{0.067z}\ ,\quad 1.02\ \text{cm} \geq r \geq 0 \qquad \text{(H.1)}$$

and

$$z = \frac{(170.88)^2(1.02)^2}{980}\left\{1 - \frac{(1.02)^2}{2r^2}\right\}$$

$$z = 31.00 - \frac{16.13}{r^2}$$

$$r = \sqrt{\frac{16.13}{(31.00-z)}}\ ,\ r > 1.02\ \text{cm} \qquad \text{(H.2)}$$

From the above two equations, the predicted relationship between z and r could be calculated. The results are also given in table H.2 .

Similarly, the predicted shapes of the liquid surface for the cases 2 and 3 by the combined vortex equations could be estimated. The results are summarized in Tables H.3 and H.4

TABLE H.1

OPERATING CONDITIONS FOR THREE CONSIDERED VORTICES

CASE NO.	Ω (rpm)	H (cm)	Hv (cm)	Vi (cm/s)	Va (cm/s)
1	10	30.0	30.0	26.54	114.68
2	5	20.0	10.0	0.00	77.54
3	3	30.0	30.0	79.07	61.29

TABLE H.2

COMPARISON OF OBSERVED AND PREDICTED VORTEX SHAPE FOR CASE 1

z (cm)	r(observed) (cm)	r(predicted) (cm)
30.0	4.00	4.02
25.0	1.80	1.64
20.0	1.20	1.21
15.5	1.02(s)	1.02
15.0	1.00	1.00
10.0	0.80	0.82
5.0	0.68	0.58
0.0	0.00	0.00

TABLE H.3

COMPARISON OF OBSERVED AND PREDICTED VORTEX SHAPE FOR CASE 2

z (cm)	r(observed) (cm)	r(predicted) (cm)
10.0	3.66	2.49
8.3	1.66	1.27
6.7	1.00	0.98
5.5	0.87	0.86
5.3	0.84(s)	0.84
5.0	0.83	0.82
3.3	0.66	0.66
1.7	0.50	0.48
0.0	0.00	0.00

TABLE H.4

COMPARISON OF OBSERVED AND PREDICTED VORTEX SHAPE FOR CASE 3

z (cm)	r(observed) (cm)	r(prdicted) (cm)
30.0	3.45	1.62
25.0	0.86	0.60
20.0	0.52	0.44
15.5	0.37	0.37
15.4	0.37(s)	0.37
15.0	0.35	0.37
10.0	0.25	0.30
5.0	0.24	0.21
0.0	0.00	0.00

Appendix I

EXAMPLE OF THE METHOD FOR COMBINING THE TWO OUTLET VELOCITIES

The inner and the annular outlet velocities were combined by the following manner:

$$Vc = Vi^{a}\ Va^{b} \qquad (5,3)$$

and

$$a + b = 1 \qquad (5.4)$$

Criterion for finding the best values of a and b was to search the minimum overall sum of squares, which was the sum of all the local sum of squares of the difference between the combined velocities (Vc) and their mean ($\overline{Vc}$), ssq, for a group of data having same Ω, H, and Hv. By trial and error, the best values of a and b was found to be 0.82 and 0.18 respectively. The trial values of a and b, and its corresponding overall sum of squares are summarized in Table I.1 .

A sample calculation for the local sum of squares is shown as follows. For the case of Ω = 3 rpm, H= 10.0cm, there were three sets of data having different combinations of Vi and Va for the same vortex depth (Hv) of 10.0 cm. These velocities were combined by the following equation:

$$Vc = Vi^{0.82}\ Va^{0.18}$$

The results are shown in Table I.2 .

Similarly, the local sum of squares (ssq) of the other groups of data having the same Hv, H, and Ω, but different Vi and Va were calculated. The overall sum of squares was calculated by adding up all the local sum of squares.

The sample standard deviations of Vc(s) for each group were calculated. The results are summarized in Table I.3 .

TABLE I.1

SUMMARY OF THE TRIAL AND ERROR RESULTS

TRIAL NO.	a	b	OVERALL SUM OF SQUARES (S)
1	0.40	0.60	18773.33
2	0.50	0.50	11103.75
3	0.60	0.40	5628.23
4	0.70	0.30	2108.31
5	0.80	0.20	533.16
6	0.81	0.19	489.51
7	0.82	0.18	467.89(min.)
8	0.83	0.17	468.73
9	0.84	0.16	492.49
10	0.90	0.10	1146.81

TABLE I.2

RESULTS OF THE COMBINED VELOCITIES FOR THE CASE IN WHICH Ω = 3 rpm, H= 10.0 cm AND Hv= 10.0 cm

NO.	Vi (cm/s)	Va (cm/s)	Vc (cm/s)	$\overline{Vc}$ (cm/s)	LOCAL ssq
1	26.54	110.04	34.28	32.68	4.82
2	32.58	33.41	32.57		
3	40.16	9.84	31.18		

TABLE I.3

SUMMARY OF THE DEVIATIONS OF THE COMBINED VELOCITIES

NO.	Ω (rpm)	H (cm)	Hv (cm)	$\overline{V}c$ (cm/s)	DEVIATION
1	3	10.0	5.0	22.19	---
2	3	10.0	10.0	32.68	1.5528
3	5	10.0	5.0	20.14	0.2475
4	5	10.0	10.0	23.40	1.0993
5	10	10.0	5.0	21.79	0.5657
6	10	10.0	10.0	23.44	1.1950
7	3	20.0	10.0	31.53	0.7296
8	3	20.0	15.0	36.23	---
9	3	20.0	17.5	50.88	---
10	3	20.0	20.0	54.82	5.3498
11	5	20.0	10.0	25.48	2.8668
12	5	20.0	20.0	37.46	1.6958
13	10	20.0	10.0	24.59	1.3596
14	10	20.0	20.0	31.96	4.5389
15	3	30.0	15.0	41.10	4.9077
16	3	30.0	18.0	50.88	---
17	3	30.0	23.0	62.73	---
18	3	30.0	27.0	75.95	---
19	3	30.0	30.0	74.79	5.3789
20	5	30.0	15.0	34.37	1.3633
21	5	30.0	24.0	36.23	---
22	5	30.0	28.5	50.88	---
23	5	30.0	30.0	57.98	2.1869
24	10	30.0	15.0	27.73	1.1243
25	10	30.0	30.0	39.45	4.7011
					40.8630

N.B. --- means that there was only one data, so that deviation was nonexistent.

Appendix J

MULTIPLE REGRESSION ANALYSIS

J.1 THEORY

The linear regression of y upon a single variable x can be extended to the multiple regression;

$$y = \beta_{1x1} + \beta_{2x2} + \ldots\ldots + \beta_{nxn} = \sum_{j=1}^{n} \beta_j x_j \qquad (J.1)$$

In the above expression, x1,x2.....xn are n different variables. Suppose that m experimental observations have been made, and that xij is the value of the variable xj at the ith observation. yi is the ith observed value of y. If, as frequently occurs, x1=1, x2=x, $x3=x^2$, $x4=x^3$ etc., it is a special case of multiple regression known as polynomial regression.

As a model, assume that the xij are known precisely, but yi contain statistical errors that follow a normal distribution. The estimates bi of parameters βi together with their variances and covariances are desired.

The procedure is to minimize the sum of squares of residuals with respect to β :

$$E = \sum_{i=1}^{m} (yi - \sum_{j=1}^{n} \beta j.xij)^2 \qquad (J.2)$$

Setting $\partial E/\partial \beta_k = 0$ for k=1,2,....n and replacing the βj with their least squares estimates bj, equation (J.2) becomes:

$$\sum_{i=1}^{m} xik(yi - \sum_{j=1}^{n} bj.xij) = 0$$

that is

$$\sum_{j=1}^{n} bj \sum_{i=1}^{m} xik.xij = \sum_{i=1}^{m} xik.yi \qquad (J.3)$$

$$k = 1,2,...n$$

Now let $\underline{X}$ as a m x n matrix containing xij in its ith row and jth column,

$$\underline{X} = (xij) = \begin{bmatrix} x11 & x12 & \ldots\ldots & x1n \\ x21 & & & x2n \\ \vdots & & & \vdots \\ xm1 & \ldots\ldots\ldots & & xmn \end{bmatrix} \qquad (J.4)$$

and also define the following column vector

$$\underline{Y} = \begin{bmatrix} y1 \\ y2 \\ \vdots \\ ym \end{bmatrix} \qquad (J.5) \qquad \underline{b} = \begin{bmatrix} b1 \\ b2 \\ \vdots \\ bn \end{bmatrix} \qquad (J.6)$$

Equation (J.3) can be rewritten in the equivalent form

$$\underline{X}^T.\underline{X}\ \underline{b} = \underline{X}^T\ \underline{Y} \qquad (J.7)$$

and the vector $\underline{b}$ can be solved by the following equation,

$$\underline{b} = (\underline{X}^T.\underline{X})^{-1}\underline{X}^T\ \underline{Y} \qquad (J.8)$$

if the matrix $\underline{X}^T\underline{X}$ is not singular.

An n x n symmetrical variance-covariance matrix $\underline{V}$ can be defined by:

$$\underline{V} = (Vij) = (\underline{X}^T.\underline{X})^{-1}\ \underline{\sigma}^2 \qquad (J.9)$$

where $\underline{\sigma}^2$ is the variance vector.

For some cases, the variable y can be expressed in the following form:

$$y = x1^{\beta_1}.\ x2^{\beta_2}..... xn^{\beta_n} \qquad (J.10)$$

It is known as a power regression, where x1,x2,....xn are n different variables. This nonlinear model can be transformed to a linear form by taking logarithms of both sides:

$$\ln y = \beta_1 \ln x1 + \beta_2 \ln x2 + ... + \beta_n \ln xn \qquad (J.11)$$

Now considering ln y equivalent to y', ln x1 equivalent to x1', ln x2 equivalent to x2' etc., equation (J.11) becomes a form of multiple regression,

$$y' = \beta_{1x1'} + \beta_{2x2'} + \ldots + \beta_{nxn'}$$

Therefore, the same procedure for solving multiple regression analysis can be used to solve the linearized power regression problem.

J.2 LISTING OF THE COMPUTER PROGRAM

The program of multiple regression analysis is listed as follows:

```
$JOB
C
C
C          MULTIPLE REGRESSION ANALYSIS
C
C
C  ------------------------------------------------------------------
C    THIS PROGRAM CAN HANDLE AT MOST 9 PARAMETERS IN THE CORRELATION
C    EQUATION, AND MAXIMUM 80 SETS OF DATA.
C  ------------------------------------------------------------------
C    INPUT FORMAT:
C                  1. NO. OF PARAMETER, NO OF DATA SETS (FORMAT FREE)
C                  2. DATA SET NO. 1
C                  3. DATA SET NO. 2
C                        ETC.
C  ------------------------------------------------------------------
C
C-----------------------MAIN PROGRAM-------------------------------C
C
C
C      DEFINE DIMENSIONS OF THE VARIABLES
C
      DIMENSION HV(80),RS(80),FI(80),FA(80),H(80),HVL(80),RSL(80)
1     DIMENSION FIL(80),FAL(80),HL(80),X(10,80),P(10),R(80),CH(80)
2     DIMENSION CHV(80),DEV(80),FR(80)
3
C
C      INPUT NO. OF PARAMETERS (M) AND NO. OF DATA SETS (N)
C
      READ,M,N
4
C
C      PRINT THE HEADING OF THE INPUT DATA
C
      PRINT 103
5     103 FORMAT('1',/////,T5,'MULTIPLE REGRESSION ANALYSIS',//)
6     PRINT 107
7     107 FORMAT(///,T5,'INPUT DATA',//)
8     PRINT 109
9     109 FORMAT(T2,'ROTATIONAL',T15,'WATER',T25,'VORTEX',T35,'INNER',T50,'A
10    *NNULAR')
      PRINT 111
11    111 FORMAT(T2,'SPEED',T15,'DEPTH',T25,'DEPTH',T34,'FLOW RATE',T48,'FLO
12    *W RATE')
      PRINT 113
13    113 FORMAT(T4,'(RPM)',T15,'(CM)',T25,'(CM)',T35,'(CM/S)',T50,'(CM/S)')
14    PRINT 115
15    115 FORMAT(T2,'-----------------------------------------------------
16    *---',//)
```

```
C
C     INPUT AND PRINT THE INPUT DATA SETS
C
      DO 5 I=1,N
         READ,RS(I),H(I),HV(I),FI(I),FA(I)
         PRINT 75,RS(I),H(I),HV(I),FI(I),FA(I)
   75    FORMAT(T3,F4.1,T15,F5.2,T25,F5.2,T34,F7.2,T48,F7.2)
C
C     DEFINE SOME CONSTANTS
C
         DI=1.27
         W=8.92E-03
         GG=980.665
C
C     LINEARIZING THE EQUATION BY TAKING LOG AT BOTH SIDES
C
         HVL(I)=ALOG(HV(I)/DI)
         RSL(I)=ALOG((RS(I)/60.0)*DI/FI(I))
         FIL(I)=ALOG(FA(I)/FI(I))
         FAL(I)=ALOG(H(I)/DI)
         HL(I)=ALOG(FI(I)*DI/W)
         FR(I)=ALOG(FI(I)**2/(GG*DI))
    5 CONTINUE
C
C     CALCULATE THE AVERAGE VORTEX DEPTH HV/D
C
      AVS=0.0
      DO 9 I=1,N
         AVS=AVS+HVL(I)
    9 CONTINUE
      RRN=N
      AVH=AVS/RRN
C
C     SET UP THE MATRICES
C
      DO 10 I=1,N
         R(I)=HVL(I)
   10 CONTINUE
      DO 11 I=1,N
         X(1,I)=1.0
         X(2,I)=RSL(I)
         X(3,I)=FIL(I)
         X(4,I)=FAL(I)
         X(5,I)=HL(I)
         X(6,I)=FR(I)
   11 CONTINUE
      IAC=1
```

```
C
C       CALL SUBROUTINE LSQ FOR PARAMETRS CALCULATION
C
49          CALL LSQ(N,M,R,X,P,EM,V,S,IND)
C
C       PRINT RESULTS
C
50          PRINT 15
51       15 FORMAT('1',//,T5,'PARAMETERS ARE:',/)
52          DO 20 I=1,M
53             PRINT 25,I,P(I)
54       25    FORMAT(T10,'PARAMETER NO.',T25,I2,T28,'IS',T34,F10.4,/)
55       20 CONTINUE
56          PRINT 35,EM
57       35 FORMAT(/,T5,'MEAN=',T12,F10.4)
58          PRINT 45,V
59       45 FORMAT(/,T5,'VAR=',T12,F10.4)
60          PRINT 55,S
61       55 FORMAT(/,T5,'STARDARD DEV.=',T20,F10.4,//)
C
C       CALCULATE THE PREDICTED HV/D
C
62          SUM=0.0
63          DO 21 J=1,N
64             DO 22 I=1,M
65                SUM=SUM+P(I)*X(I,J)
66       22    CONTINUE
67             CH(J)=SUM
68             SUM=0.0
69       21 CONTINUE
C
C       PRINT THE HEADING OF THE OUTPUT
C
70          PRINT 150
71      150 FORMAT('1',//,T5,'COMPARISONS OF EXPERIMENTAL RESULTS WITH CALCULA
           *TED RESULTS',//)
72          PRINT 151
73      151 FORMAT(T4,'NO.',T10,'RS(RPM)',T26,'H(CM)',T36,'HV(CM)',T48,'HV(CM)
           *',T58,'% DEVIATION')
74          PRINT 152
75      152 FORMAT(T36,'(EXPT.)',T48,'(CALC.)')
76          PRINT 153
77      153 FORMAT(T2,'-------------------------------------------------------
           *-----',//)
C
C       CALCULATE THE % DEVIATION AND CORRELATION COEFFICIENT
C
```

```
      SRN=0.0
      SRM=0.0
      SSS=0.0
      DO 23 I=1,N
         CHV(I)=EXP(CH(I))
         DEV(I)=ABS(HV(I)-CHV(I)*DI)*100.0/HV(I)
         SSS=SSS+DEV(I)
         SRN=SRN+(CH(I)-AVH)**2
         SRM=SRM+(HVL(I)-AVH)**2
C
C        PRINT RESULTS
C
         PRINT 85,I,RS(I),H(I),HV(I),CHV(I)*DI,DEV(I)
   85    FORMAT(/,T4,I2,T10,F5.2,T20,F5.2,T30,F5.2,T40,F5.2,T52,F6.2)
   23 CONTINUE
      CORR=(SRN/SRM)**0.5
      PRINT 198,CORR
  198 FORMAT(////,T5,'CORRELATION COEFFICENT =',T32,F8.4)
      PRINT 199,SSS
  199 FORMAT(////,T5,'SUM OF DEV.. =',T20,F10.5)
      PRINT 300
  300 FORMAT('1',T2,'END')
      STOP
      END
C
C-----------------------------------------------------------------------
C     SUBROUTINE LSQ                                                   C
C-----------------------------------------------------------------------
C
      SUBROUTINE LSQ(N,M,Z,X,P,ERRM,VAR,STD,IND)
      DIMENSION  Z(80),X(10,80),P(10),XT(80,10),R(10,10),Q(10)
C
C     TRANSFER MATRIX X TO XT
C
      DO 10 I=1,M
      DO 11 J=1,N
      XT(J,I)=X(I,J)
   11 CONTINUE
   10 CONTINUE
C
C     CALL SUBROUTINE SMAT AND GMAT
C
      CALL SMAT(X,XT,M,N,M,R)
      CALL GMAT(R,M,A)
      IF(A) 16,17,16
   17 IND=1000
```

```
110           WRITE(6,202)
111       202 FORMAT('SYSTEM IS ILL BEHAVED')
112           RETURN
113        16 DO 12 I=1,M
114           Q(I)=0.0
115           DO 13 J=1,N
116           Q(I)=Q(I)+X(I,J)*Z(J)
117        13 CONTINUE
118        12 CONTINUE
119           DO 14 I=1,M
120           P(I)=0.0
121           DO 15 J=1,M
122           P(I)=P(I)+R(I,J)*Q(J)
123        15 CONTINUE
124        14 CONTINUE.
      C
      C     ESTIMATION OF ERROR
      C
125           DO 20 I=1,N
126           XT(I,1)=-Z(I)
127           DO 21 J=1,M
128           XT(I,1)=XT(I,1)+P(J)*X(J,I)
129        21 CONTINUE
130        20 CONTINUE
131           S1=0.0
132           S2=0.0
133           DO 22 I=1,N
134           XT(I,2)=XT(I,1)**2
135           S1=S1+XT(I,1)
136           S2=S2+XT(I,2)
137        22 CONTINUE
138           AN=FLOAT(N)
139           ERRM=S1/AN
140           VAR=S2/AN-ERRM**2
141           STD=SQRT(VAR)
142           IF(IND) 25,25,25
143        25 RETURN
144           END
      C
      C-----------------------------------------------------------------------
      C     SUBROUTINE SMAT FOR CALCULATING X*XT                              C
      C-----------------------------------------------------------------------
      C

145           SUBROUTINE SMAT(P,Q,M,N,L,R)
146           DIMENSION P(10,80),Q(80,10),R(10,10)
147           DO 10 I=1,M
```

```
148           DO 11 J=1,L
149           R(I,J)=0.0
150        11 CONTINUE
151        10 CONTINUE
152           DO 12 I=1,M
153           DO 13 J=1,L
154           DO 14 K=1,N
155           R(I,J)=R(I,J)+P(I,K)*G(K,J)
156        14 CONTINUE
157        13 CONTINUE
158        12 CONTINUE
159           RETURN
160           END
          C
          C-------------------------------------------------------------------
          C     SUBROUTINE GMAT FOR CALCULATING THE INVERSE OF X*XT          C
          C-------------------------------------------------------------------
          C
161           SUBROUTINE GMAT(P,N,A)
162           DIMENSION P(10,10),Q(10,10),NM(10),NB(10)
163           A=1.0
          C
          C     MAKING Q A UNIT MATRIX
          C
164           DO 10 I=1,N
165           NM(I)=1
166           DO 11 J=1,N
167           IF(I-J) 12,13,12
168        13 Q(I,J)=1.0
169           GO TO 11
170        12 Q(I,J)=0.0
171        11 CONTINUE
172        10 CONTINUE
173           EPS=1.0E-06
174           DO 20 J=1,N
          C
          C     SEARCH FOR PIVOT
          C
175           DO 23 I=1,N
176           IF(ABS(P(I,J))-EPS) 23,23,22
177        22 IF(NM(I)) 23,23,24
178        24 NM(I)=-1
179           A=A*P(I,J)
180           GO TO 30
181        23 CONTINUE
```

```
C
C       MATRIX WAS FOUND SINGULAR
C
182           WRITE(6,100)
183       100 FORMAT(1H ,'MATRIX IS SINGULAR OR NEARLY SO')
184           A=0.0
185           GO TO 99
C
C       SWEEPING OUT WITH IJ ELEMENT AS PIVOT
C
186        30 PA=P(I,J)
187           DO 31 JJ=1,N
188           P(I,JJ)=P(I,JJ)/PA
189           Q(I,JJ)=Q(I,JJ)/PA
190        31 CONTINUE
191           DO 34 II=1,N
192           IF(II-I) 33,34,33
193        33 PJ=P(II,J)
194           DO 35 JJ=1,N
195           P(II,JJ)=P(II,JJ)-P(I,JJ)*PJ
196           Q(II,JJ)=Q(II,JJ)-Q(I,JJ)*PJ
197        35 CONTINUE
198        34 CONTINUE
C
C       RECORDING THAT IJ ELEMENT IS PIVOT
C
199           NB(J)=I
200        20 CONTINUE
C
C       COPYING Q ONTO P
C
201           DO 50 I=1,N
202           DO 51 J=1,N
203           NN=NB(I)
204           P(I,J)=Q(NN,J)
205        51 CONTINUE
206        50 CONTINUE
C
C       FIXING THE SIGN OF THE DETERMINANT
C
207           DO 40 I=1,N
208           DO 40 J=1,N
209           IF(NB(J)) 41,41,43
210        43 IF(NB(J)-I) 44,45,44
211        44 A=-A
212        41 CONTINUE
213        45 NB(J)=-1
214        40 CONTINUE
215        99 RETURN
216           END

      $ENTRY
```

Appendix K

DATA FOR THE "WITH FROTH" AIR-WATER VORTEX EXPERIMENTS

The data for the air-water vortex experiments with 1.5 cm froth on the surface of water are shown in Table K.1 , and the data for the experiments with 0.5 cm froth on the surface of water are shown in Table K.2 . The calculations of the inner flow velocity and the annular flow velocity were same as the calculations in Appendix F.

TABLE K.1

DATA FOR THE AIR-WATER VORTEX EXPERIMENTS WITH 1.5 CM FROTH ON THE SURFACE OF WATER

NO.	Ω (rpm)	H (cm)	Vi (cm/s)	Va (cm/s)	Hv (cm)
1	3	20.0	0.00	133.25	15.0
2	3	20.0	26.54	79.86	13.0
3	3	20.0	40.16	9.82	13.0
4	3	20.0	0.00	149.50	18.0
5	3	20.0	26.54	149.50	19.0
6	3	20.0	40.16	149.50	20.0
7	10	20.0	0.00	38.08	6.0
8	10	20.0	26.54	18.13	7.0
9	10	20.0	40.16	0.00	10.0
10	10	20.0	51.84	0.00	16.0
11	10	20.0	65.46	0.00	20.0
12	10	20.0	0.00	79.86	15.5
13	10	20.0	26.54	40.40	12.0
14	10	20.0	40.16	19.40	14.5
15	10	20.0	51.84	9.27	17.5
16	10	20.0	65.46	0.00	20.0

TABLE K.2

DATA FOR THE AIR-WATER VORTEX EXPERIMENTS WITH 0.5 CM FROTH ON THE SURFACE OF WATER

NO.	Ω (rpm)	H (cm)	Vi (cm/s)	Va (cm/s)	Hv (cm)
1	3	20.0	0.00	133.25	14.5
2	3	20.0	26.54	79.86	11.5
3	3	20.0	40.16	9.82	13.0
4	3	20.0	51.84	0.00	15.0
5	3	20.0	65.46	0.00	20.0
6	3	20.0	0.00	149.50	16.0
7	3	20.0	26.54	149.50	19.0
8	3	20.0	40.16	149.50	20.0
9	10	20.0	0.00	38.08	10.0
10	10	20.0	0.00	79.86	18.0
11	10	20.0	26.54	40.40	19.0

Appendix L

EXPERIMENTAL DATA FOR INCIPIENT FURNACE OIL ENTRAINMENT AND INCIPIENT AIR-OIL ENTRAINMENT

The experimental data for incipient furnace oil entrainment are shown in Table L.1 , and the experimental data for incipient air-oil entrainment are shown in Table L.2 . The inner and annular volumetric flow rates were observed from the calibration curves for the corresponding rotameters in Appendix A. The inner and annular outlet velocities were calculated by the same methods as in Appendix F.

TABLE L.1

DATA FOR INCIPIENT FURNACE OIL ENTRAINMENT EXPERIMENTS

THICKNESS OF THE OIL ON THE WATER SURFACE IS 1.0 cm

NO.	Ω (rpm)	H (cm)	Vi (cm/s)	Va (cm/s)	$\bar{V}$(ave.) (cm/s)
1	3	10.0	21.36	0.00	----
2	3	10.0	8.31	12.11	10.21
3	3	10.0	3.32	18.13	10.71
4	3	10.0	0.55	24.15	12.35
5	3	20.0	32.38	0.00	----
6	3	20.0	28.49	12.11	20.30
7	3	20.0	18.08	18.13	18.10
8	3	20.0	13.70	24.15	18.92
9	3	20.0	5.48	35.76	20.62
10	3	30.0	42.11	0.00	-----
11	3	30.0	34.32	12.11	23.21
12	3	30.0	32.38	18.13	25.25
13	3	30.0	28.49	24.15	26.32
14	3	30.0	14.24	35.76	25.00
15	3	30.0	2.73	47.36	25.05
16	5	10.0	22.79	0.00	-----
17	5	10.0	4.93	12.11	8.52
18	5	10.0	0.55	18.13	9.34
19	5	20.0	30.43	0.00	-----
20	5	20.0	22.79	12.11	17.45
21	5	20.0	16.43	18.13	17.28
22	5	20.0	10.96	24.15	17.55
23	5	20.0	3.29	35.76	19.52
24	5	30.0	36.27	0.00	-----
25	5	30.0	30.43	12.11	21.27
26	5	30.0	25.20	18.13	21.66
27	5	30.0	19.17	24.15	21.66
28	5	30.0	10.41	35.76	23.08
29	5	30.0	2.19	47.36	24.78
30	10	10.0	19.17	0.00	-----
31	10	10.0	3.93	12.11	8.02
32	10	20.0	28.49	0.00	-----
33	10	20.0	21.91	12.11	17.01
34	10	20.0	16.43	18.13	17.28
35	10	20.0	9.31	24.15	16.73
36	10	20.0	1.10	35.76	18.43
37	10	30.0	36.27	0.00	-----
38	10	30.0	29.46	12.11	20.78
39	10	30.0	23.55	18.13	20.84
40	10	30.0	17.53	24.15	20.84
41	10	30.0	7.67	35.76	21.71

TABLE L.2

DATA FOR INCIPIENT FURNACE OIL-AIR ENTRAINMENT EXPERIMENTS

THICKNESS OF THE OIL ON THE WATER SURFACE IS 1.0 cm

NO.	Ω (rpm)	H (cm)	Vi (cm/s)	Va (cm/s)	$\bar{V}$(ave.) (cm/s)
1	3	10.0	57.68	0.00	-----
2	3	10.0	53.79	12.11	32.95
3	3	10.0	49.89	18.13	34.01
4	3	10.0	42.11	24.15	33.13
5	3	10.0	30.43	35.76	33.09
6	3	20.0	96.60	0.00	-----
7	3	20.0	91.74	12.11	51.92
8	3	20.0	86.87	18.13	52.50
9	3	20.0	77.14	24.15	50.65
10	3	20.0	65.46	35.76	50.61
11	3	30.0	96.60	35.76	66.18
12	5	10.0	46.00	0.00	-----
13	5	10.0	40.16	12.11	26.13
14	5	10.0	35.30	18.13	26.71
15	5	10.0	28.49	24.15	26.32
16	5	10.0	14.24	35.76	25.00
17	5	20.0	79.09	0.00	-----
18	5	20.0	75.19	12.11	43.65
19	5	20.0	71.30	18.13	44.71
20	5	20.0	63.52	24.15	43.83
21	5	20.0	53.79	35.76	44.77
22	5	30.0	96.60	18.13	57.36
23	5	30.0	90.76	24.15	57.46
24	5	30.0	77.14	35.76	56.45
25	10	10.0	55.73	0.00	-----
26	10	10.0	32.38	12.11	22.24
27	10	10.0	23.01	18.13	20.57
28	10	10.0	10.96	24.15	17.55
29	10	20.0	92.71	0.00	-----
30	10	20.0	77.14	12.11	44.62
31	10	20.0	61.57	18.13	39.85
32	10	20.0	55.73	24.15	39.94
33	10	20.0	49.89	35.76	42.83
34	10	20.0	38.22	47.36	42.79
35	10	30.0	92.71	12.11	52.41
36	10	30.0	84.92	18.13	51.53
37	10	30.0	77.14	24.15	50.65
38	10	30.0	67.41	35.76	51.58
39	10	30.0	57.68	47.36	52.52

Appendix M

EXPERIMENTAL DATA FOR INCIPIENT PARAFFIN OIL ENTRAINMENT AND INCIPIENT AIR-OIL ENTRAINMENT

The experimental data for incipient paraffin oil entrainment are shown in Table M.1 , and the experimental data for incipient air-oil entrainment are shown in Table M.2 . The inner and annular velocities were calculated by the same methods as mentioned in Appendix L.

TABLE M.1

DATA FOR INCIPIENT PARAFFIN OIL ENTRAINMENT EXPERIMENTS

THICKNESS OF THE OIL ON THE WATER SURFACE WAS 1.0 cm

NO.	Ω (rpm)	H (cm)	Vi (cm/s)	Va (cm/s)	$\bar{V}$(ave.) (cm/s)
1	3	10.0	28.49	0.00	-----
2	3	10.0	13.70	12.11	12.90
3	3	10.0	3.29	18.13	10.71
4	3	10.0	0.55	24.15	12.35
5	3	20.0	36.27	0.00	-----
6	3	20.0	26.30	12.11	19.20
7	3	20.0	21.91	18.13	20.02
8	3	20.0	12.05	24.15	18.10
9	3	30.0	51.84	0.00	-----
10	3	30.0	34.32	12.11	23.21
11	3	30.0	29.46	18.13	23.79
12	3	30.0	24.10	24.15	24.13
13	3	30.0	13.70	35.76	24.73
14	5	10.0	27.39	0.00	-----
15	5	10.0	9.31	12.11	10.71
16	5	10.0	1.64	18.13	9.89
17	5	20.0	30.43	0.00	-----
18	5	20.0	25.75	12.11	18.93
19	5	20.0	10.96	18.13	14.54
20	5	20.0	2.74	24.15	13.45
21	5	30.0	36.27	0.00	-----
22	5	30.0	26.30	12.11	19.20
23	5	30.0	19.17	18.13	18.65
24	5	30.0	12.05	24.15	18.10
25	10	10.0	23.01	0.00	-----
26	10	10.0	10.96	12.11	11.53
27	10	20.0	29.46	0.00	-----
28	10	20.0	14.24	12.11	13.17
29	10	20.0	9.86	18.13	14.00
30	10	20.0	3.29	24.15	13.72
31	10	30.0	34.32	0.00	-----
32	10	30.0	24.10	12.11	18.11
33	10	30.0	19.17	18.13	18.65
34	10	30.0	10.96	24.15	17.55

TABLE M.2

DATA FOR INCIPIENT PARAFFIN OIL-AIR ENTRAINMENT EXPERIMENTS

THICKNESS OF THE OIL ON THE WATER SURFACE WAS 1.0 cm

NO.	Ω (rpm)	H (cm)	Vi (cm/s)	Va (cm/s)	$\bar{V}$(ave.) (cm/s)
1	3	10.0	96.60	0.00	-----
2	3	10.0	82.98	12.11	47.54
3	3	10.0	44.06	18.13	31.09
4	3	10.0	32.38	24.15	28.26
5	3	20.0	82.98	18.13	50.55
6	3	20.0	77.14	24.15	50.65
7	3	20.0	67.41	35.76	51.58
8	3	30.0	96.60	35.76	66.18
9	3	30.0	86.87	47.36	67.12
10	5	10.0	51.84	0.00	-----
11	5	10.0	42.11	12.11	27.11
12	5	10.0	32.38	18.13	25.25
13	5	10.0	23.01	24.15	23.58
14	5	20.0	96.60	12.11	54.35
15	5	20.0	71.30	18.13	44.71
16	5	20.0	57.68	24.15	40.91
17	5	20.0	49.89	35.76	42.83
18	5	30.0	98.55	18.13	58.34
19	5	30.0	90.76	24.15	57.46
20	5	30.0	79.09	35.76	57.42
21	10	10.0	59.62	0.00	-----
22	10	10.0	38.22	12.11	25.16
23	10	10.0	28.49	18.13	23.31
24	10	20.0	81.03	0.00	-----
25	10	20.0	57.68	12.11	34.89
26	10	20.0	38.22	18.13	28.17
27	10	20.0	32.38	24.15	28.26
28	10	30.0	94.65	0.00	-----
29	10	30.0	71.30	12.11	41.70
30	10	30.0	59.62	18.13	38.88
31	10	30.0	51.84	24.15	38.00

Appendix N

DATA FOR FURNACE OIL-WATER SEPARATION EXPERIMENTS

The data for furnace oil-water separation experiments are reported in Table N.1 . The inner volumetric flow rates were obtained from the calibration curve for the inner outlet flow rotameter in Appendix C, and the annular volumetric flow rates were observed from the calibration curve for the annular circulation rotameter in Appendix A. The inner and the annular outlet velocities were calculated by the same methods as in Appendix F. The oil removal rates were calculated by the following definition:

$$\text{Oil Removal Rate} = \frac{\left(\begin{array}{c}\text{Final volume of}\\ \text{the oil in the}\\ \text{vacuum tank}\end{array}\right) - \left(\begin{array}{c}\text{Initial volume of}\\ \text{the oil in the}\\ \text{vacuum tank}\end{array}\right)}{\text{Experimental time}}$$

The oil contents were calculated by dividing the oil removal rates by the corresponding inner volumetric flow rates and multipling by 100.

TABLE N.1

DATA FOR FURNACE OIL-WATER SEPARATION EXPERIMENTS

THICKNESS OF THE OIL ON WATER SURFACE WAS 1.0 cm

NO.	Ω (rpm)	H (cm)	Va (cm/s)	Vi (cm/s)	Qoil (cm^3/s)	OIL CONTENT (%)
1	3	10.0	0.00	40.91	5.2	10.0
2	3	10.0	0.00	49.10	6.1	9.8
3	3	10.0	0.00	59.35	7.4	9.8
4	3	10.0	0.00	81.88	8.2	7.9
5	3	10.0	12.11	28.61	4.7	12.9
6	3	10.0	12.11	40.91	6.7	12.9
7	3	10.0	12.11	53.20	8.1	12.0
8	3	10.0	12.11	65.49	10.1	12.1
9	3	10.0	24.15	28.61	5.6	15.4
10	3	10.0	24.15	40.91	8.7	16.7
11	3	10.0	24.15	49.10	9.6	15.4
12	3	10.0	24.15	49.10	10.4	16.7
13	3	10.0	24.15	65.49	10.3	12.4
14	3	10.0	47.36	28.61	8.7	23.9
15	3	10.0	47.36	40.91	10.3	19.8
16	3	10.0	47.36	49.10	11.7	18.8
17	3	10.0	47.36	65.49	11.9	14.3
18	3	20.0	0.00	61.40	6.3	8.1
19	3	20.0	0.00	69.59	7.2	8.2
20	3	20.0	0.00	81.88	7.8	7.5
21	3	20.0	0.00	90.08	8.3	7.3
22	3	20.0	0.00	98.27	7.4	5.9
23	3	20.0	12.11	49.10	5.8	9.3
24	3	20.0	12.11	61.40	6.5	8.3
25	3	20.0	12.11	73.69	7.6	8.1
26	3	20.0	12.11	81.88	8.5	8.2
27	3	20.0	12.11	81.88	8.5	8.2
28	3	20.0	24.15	40.91	5.6	10.8
29	3	20.0	24.15	61.40	6.9	8.9
30	3	20.0	24.15	67.54	7.6	8.9
31	3	20.0	24.15	73.69	8.5	9.1
32	3	20.0	24.15	81.88	9.2	8.9
33	3	20.0	47.36	40.91	6.7	12.9
34	3	20.0	47.36	49.10	7.4	11.9
35	3	20.0	47.36	59.35	8.1	10.8
36	3	20.0	47.36	59.35	7.8	10.4
37	3	20.0	47.36	81.88	10.1	9.7
38	3	20.0	70.58	40.91	7.4	14.2
39	3	20.0	70.58	59.35	9.6	12.7
40	3	20.0	70.58	81.88	10.9	10.5
41	3	30.0	0.00	59.35	2.7	3.6

(Table N.1 cont.)

NO.	Ω (rpm)	H (cm)	Va (cm/s)	Vi (cm/s)	Qoil (cm^3/s)	OIL CONTENT (%)
42	3	30.0	0.00	81.88	3.6	3.5
43	3	30.0	0.00	98.27	4.7	3.8
44	3	30.0	0.00	106.47	4.9	3.6
45	3	30.0	12.11	59.35	2.9	3.9
46	3	30.0	12.11	81.88	4.0	3.9
47	3	30.0	12.11	98.27	4.7	3.8
48	3	30.0	12.11	98.27	5.2	4.2
49	3	30.0	24.15	59.35	4.0	5.3
50	3	30.0	24.15	81.88	5.2	5.0
51	3	30.0	24.15	98.27	6.3	5.1
52	3	30.0	24.15	98.27	6.5	5.2
53	3	30.0	24.15	106.47	6.3	4.7
54	3	30.0	24.15	106.47	5.8	4.3
55	3	30.0	47.36	59.35	4.7	6.2
56	3	30.0	47.36	81.88	6.9	6.6
57	3	30.0	47.36	106.47	7.2	5.3
58	3	30.0	70.58	59.35	7.8	10.4
59	3	30.0	70.58	81.88	9.2	8.9
60	3	30.0	70.58	106.47	9.4	7.0
61	5	10.0	0.00	32.71	2.9	7.0
62	5	10.0	0.00	40.91	6.5	12.5
63	5	10.0	0.00	45.00	8.7	15.2
64	5	10.0	0.00	49.10	9.2	14.8
65	5	10.0	12.11	32.71	7.8	18.8
66	5	10.0	12.11	36.81	11.0	23.5
67	5	10.0	12.11	40.91	13.2	25.4
68	5	10.0	24.15	28.61	11.2	30.8
69	5	10.0	24.15	32.71	12.9	31.1
70	5	10.0	24.15	36.81	15.5	33.2
71	5	10.0	24.15	40.91	17.3	33.3
72	5	10.0	24.15	57.30	15.9	21.9
73	5	10.0	47.36	28.61	17.7	48.7
74	5	10.0	47.36	40.91	19.5	37.5
75	5	10.0	47.36	57.30	15.3	21.0
76	5	10.0	47.36	57.30	15.2	20.9
77	5	20.0	0.00	49.10	4.7	7.5
78	5	20.0	0.00	65.49	9.9	11.9
79	5	20.0	0.00	77.79	12.5	12.7
80	5	20.0	0.00	90.08	14.6	12.8
81	5	20.0	12.11	49.10	6.7	10.7
82	5	20.0	12.11	65.49	12.1	14.5
83	5	20.0	12.11	73.69	14.6	15.6
84	5	20.0	12.11	81.88	15.8	15.2
85	5	20.0	24.15	31.69	8.4	20.9
86	5	20.0	24.15	49.10	15.2	24.4
87	5	20.0	24.15	57.30	17.5	24.1
88	5	20.0	24.15	65.49	18.4	22.1

(Table N.1 cont.)

NO.	Ω (rpm)	H (cm)	Va (cm/s)	Vi (cm/s)	Qoil (cm^3/s)	OIL CONTENT (%)
89	5	20.0	47.36	31.69	11.9	29.6
90	5	20.0	47.36	49.10	17.4	27.9
91	5	20.0	47.36	57.30	21.3	29.3
92	5	20.0	47.36	81.88	19.3	18.6
93	5	20.0	70.58	31.69	18.4	45.7
94	5	20.0	70.58	57.30	25.7	35.3
95	5	20.0	70.58	81.88	21.5	20.7
96	5	30.0	0.00	65.49	4.8	5.8
97	5	30.0	0.00	98.27	7.1	5.7
98	5	30.0	0.00	106.47	8.7	6.4
99	5	30.0	0.00	106.47	9.3	6.9
100	5	30.0	12.11	69.59	6.1	6.9
101	5	30.0	12.11	81.88	6.9	6.6
102	5	30.0	12.11	98.27	9.0	7.2
103	5	30.0	12.11	98.27	9.6	7.7
104	5	30.0	24.15	65.49	9.9	11.9
105	5	30.0	24.15	81.88	11.2	10.8
106	5	30.0	24.15	90.08	12.1	10.6
107	5	30.0	24.15	90.08	11.7	10.2
108	5	30.0	24.15	98.27	12.5	10.0
109	5	30.0	47.36	40.91	7.2	13.9
110	5	30.0	47.36	40.91	6.9	13.3
111	5	30.0	47.36	65.49	12.8	15.4
112	5	30.0	47.36	81.88	13.1	12.6
113	5	30.0	47.36	98.27	13.6	10.9
114	5	30.0	70.58	40.91	8.1	15.6
115	5	30.0	70.58	65.49	13.4	16.1
116	5	30.0	70.58	65.49	13.0	15.6
117	5	30.0	70.58	81.88	14.1	13.6
118	5	30.0	70.58	98.27	14.8	11.9
119	10	10.0	0.00	28.61	1.6	4.4
120	10	10.0	0.00	31.69	2.7	6.7
121	10	10.0	0.00	40.91	4.7	9.0
122	10	10.0	0.00	49.10	6.5	10.4
123	10	10.0	0.00	53.20	6.9	10.2
124	10	10.0	0.00	57.30	6.9	9.5
125	10	10.0	12.11	22.89	2.0	6.9
126	10	10.0	12.11	31.69	5.4	13.4
127	10	10.0	12.11	36.81	7.2	15.4
128	10	10.0	12.11	40.91	7.2	13.9
129	10	20.0	0.00	61.40	7.7	9.9
130	10	20.0	0.00	73.69	11.2	12.0
131	10	20.0	0.00	73.69	10.8	11.5
132	10	20.0	0.00	81.88	15.5	14.9
133	10	20.0	0.00	90.08	16.8	14.7
134	10	20.0	12.11	40.91	6.9	13.3

(Table N.1 cont.)

NO.	Ω (rpm)	H (cm)	Va (cm/s)	Vi (cm/s)	Qoil (cm^3/s)	OIL CONTENT (%)
135	10	20.0	12.11	40.91	6.3	12.1
136	10	20.0	12.11	49.10	14.3	22.9
137	10	20.0	12.11	57.30	17.7	24.3
138	10	20.0	12.11	65.49	20.2	24.3
139	10	20.0	24.15	31.69	11.2	27.8
140	10	20.0	24.15	40.91	17.2	33.1
141	10	20.0	24.15	49.10	18.9	30.3
142	10	20.0	24.15	57.30	18.1	24.9
143	10	20.0	47.36	31.69	15.6	38.8
144	10	20.0	47.36	40.91	22.2	42.7
145	10	20.0	47.36	57.30	21.7	29.8
146	10	20.0	70.58	31.69	17.5	43.5
147	10	20.0	70.58	40.91	22.8	43.9
148	10	20.0	70.58	57.30	21.4	29.4
149	10	30.0	0.00	69.59	9.0	10.2
150	10	30.0	0.00	90.08	12.3	10.8
151	10	30.0	0.00	90.08	11.9	10.4
152	10	30.0	0.00	98.27	15.2	12.2
153	10	30.0	0.00	106.47	15.9	11.8
154	10	30.0	12.11	53.20	9.9	14.7
155	10	30.0	12.11	61.40	11.6	14.9
156	10	30.0	12.11	69.59	13.0	14.7
157	10	30.0	12.11	81.88	14.1	13.6
158	10	30.0	24.15	40.91	9.8	17.3
159	10	30.0	24.15	45.00	10.5	18.4
160	10	30.0	24.15	53.20	13.9	20.6
161	10	30.0	24.15	61.40	16.1	20.6
162	10	30.0	24.15	61.40	18.0	23.1
163	10	30.0	24.15	81.88	16.1	15.5
164	10	30.0	47.36	40.91	11.9	22.9
165	10	30.0	47.36	49.10	15.4	24.7
166	10	30.0	47.36	57.30	18.9	26.0
167	10	30.0	47.36	90.08	21.3	18.6
168	10	30.0	70.58	40.91	13.7	26.4
169	10	30.0	70.58	49.10	18.8	30.2
170	10	30.0	70.58	57.30	20.2	27.8
171	10	30.0	70.58	90.08	21.9	19.1

Appendix O

DATA FOR PARAFFIN OIL-WATER SEPARATION EXPERIMENTS

The data for paraffin oil-water separation experiments are reported in Table O.1 . The inner volumetric flow rates were observed from the calibration curve for the inner outlet flow rotameter in Appendix C, and the annular volumetric flow rates were observed from the calibration curve for the annular circulation rotameter in Appendix A. The inner and the annular outlet velocities were calculated by the same methods as in Appendix F. The oil removal rates were calculated by the following definition:

$$\text{Oil Removal Rate} = \frac{\left(\begin{array}{c}\text{Final volume of}\\ \text{the oil in the}\\ \text{vacuum tank}\end{array}\right) - \left(\begin{array}{c}\text{Initial volume of}\\ \text{the oil in the}\\ \text{vacuum tank}\end{array}\right)}{\text{Experimental time}}$$

The oil contents were calculated by dividing the oil removal rates by the corresponding inner volumetric flow rates and multipling by 100.

TABLE O.1

DATA FOR PARAFFIN OIL-WATER SEPARATION EXPERIMENTS

THICKNESS OF THE OIL ON WATER SURFACE WAS 1.0 cm

NO.	Ω (rpm)	H (cm)	Va (cm/s)	Vi (cm/s)	Qoil (cm^3/s)	OIL CONTENT (%)
1	3	10.0	0.00	32.20	1.3	3.2
2	3	10.0	0.00	42.58	6.5	12.0
3	3	10.0	0.00	49.49	10.6	16.9
4	3	10.0	0.00	49.49	9.9	15.8
5	3	10.0	0.00	58.14	16.9	22.9
6	3	10.0	0.00	65.32	19.0	22.9
7	3	10.0	0.00	77.15	27.8	28.4
8	3	10.0	12.11	32.20	13.2	32.3
9	3	10.0	12.11	42.58	19.0	35.1
10	3	10.0	12.11	42.58	20.4	37.7
11	3	10.0	12.11	52.95	26.0	38.7
12	3	10.0	12.11	63.32	29.5	36.7
13	3	10.0	12.11	63.32	29.7	36.9
14	3	10.0	18.13	42.58	25.2	46.6
15	3	10.0	18.13	49.49	29.1	46.3
16	3	10.0	18.13	56.41	33.0	46.1
17	3	10.0	24.15	32.20	22.2	54.3
18	3	10.0	24.15	42.58	28.2	52.2
19	3	10.0	24.15	63.32	35.1	43.7
20	3	10.0	47.36	32.20	23.2	56.7
21	3	10.0	47.36	42.58	28.7	53.1
22	3	10.0	47.36	63.32	35.8	44.5
23	3	20.0	0.00	42.58	1.1	2.0
24	3	20.0	0.00	58.14	5.4	7.3
25	3	20.0	0.00	77.15	12.3	12.6
26	3	20.0	0.00	77.15	13.7	14.0
27	3	20.0	0.00	84.07	15.8	14.8
28	3	20.0	0.00	90.98	17.1	14.8
29	3	20.0	12.11	70.24	13.7	15.4
30	3	20.0	12.11	77.15	17.0	17.4
31	3	20.0	12.11	84.07	21.3	20.0
32	3	20.0	24.15	42.58	15.3	28.3
33	3	20.0	24.15	58.14	19.0	25.7
34	3	20.0	24.15	65.05	20.0	24.2
35	3	20.0	24.15	70.24	21.9	24.6
36	3	20.0	24.15	77.15	22.0	22.5
37	3	20.0	24.15	77.15	22.6	23.1
38	3	20.0	35.76	56.41	21.3	29.7
39	3	20.0	35.76	63.32	23.1	28.7
40	3	20.0	35.76	66.78	24.0	28.3
41	3	20.0	47.36	42.58	20.1	37.2

(Table Q.1 cont.)

NO.	Ω (rpm)	H (cm)	Va (cm/s)	Vi (cm/s)	Qoil (cm^3/s)	OIL CONTENT (%)
42	3	20.0	47.36	58.14	24.9	33.7
43	3	20.0	47.36	77.15	25.6	26.1
44	3	20.0	70.58	42.58	22.3	41.2
45	3	20.0	70.58	58.14	26.9	36.4
46	3	20.0	70.58	77.15	30.8	31.4
47	3	30.0	0.00	58.14	1.6	2.2
48	3	30.0	0.00	63.32	2.5	3.1
49	3	30.0	0.00	77.15	5.4	5.5
50	3	30.0	0.00	90.98	8.3	7.2
51	3	30.0	0.00	97.90	9.0	7.2
52	3	30.0	0.00	97.90	9.5	7.6
53	3	30.0	12.11	77.15	6.1	6.2
54	3	30.0	12.11	90.98	9.6	8.3
55	3	30.0	12.11	97.90	11.2	9.0
56	3	30.0	24.15	58.14	9.4	12.7
57	3	30.0	24.15	77.15	13.2	13.5
58	3	30.0	24.15	90.98	15.7	13.6
59	3	30.0	24.15	97.90	14.8	11.9
60	3	30.0	24.15	97.90	15.4	12.4
61	3	30.0	47.36	58.14	13.0	17.6
62	3	30.0	47.36	77.15	17.8	18.2
63	3	30.0	47.36	90.98	17.8	15.4
64	3	30.0	47.36	97.90	17.0	13.7
65	3	30.0	70.58	58.14	18.5	25.1
66	3	30.0	70.58	77.15	21.2	21.6
67	3	30.0	70.58	97.90	22.5	18.1
68	5	10.0	0.00	32.20	1.0	2.5
69	5	10.0	0.00	35.66	3.4	7.5
70	5	10.0	0.00	40.85	10.3	19.9
71	5	10.0	0.00	46.03	15.7	26.9
72	5	10.0	0.00	49.49	18.9	30.1
73	5	10.0	0.00	56.41	24.2	33.8
74	5	10.0	12.11	32.20	12.3	30.1
75	5	10.0	12.11	35.66	13.9	30.7
76	5	10.0	12.11	42.58	19.9	36.8
77	5	10.0	12.11	42.58	20.3	37.5
78	5	10.0	12.11	49.49	26.9	42.8
79	5	10.0	12.11	56.41	29.8	41.6
80	5	10.0	24.15	32.20	16.8	41.1
81	5	10.0	24.15	35.66	23.3	51.5
82	5	10.0	24.15	42.58	28.2	52.2
83	5	10.0	24.15	49.49	32.2	51.2
84	5	10.0	24.15	56.41	40.8	57.0
85	5	10.0	24.15	56.41	38.9	54.3
86	5	20.0	0.00	34.80	1.1	2.5
87	5	20.0	0.00	56.41	12.3	17.2

(Table O.1 cont.)

NO.	Ω (rpm)	H (cm)	Va (cm/s)	Vi (cm/s)	Qoil (cm^3/s)	OIL CONTENT (%)
88	5	20.0	0.00	63.32	18.9	23.5
89	5	20.0	0.00	73.70	25.4	27.0
90	5	20.0	0.00	77.15	25.1	25.6
91	5	20.0	0.00	84.07	29.6	27.7
92	5	20.0	12.11	63.32	29.7	36.9
93	5	20.0	12.11	63.32	29.1	36.2
94	5	20.0	12.11	70.24	31.8	35.6
95	5	20.0	12.11	78.88	36.9	36.8
96	5	20.0	18.13	56.41	35.1	49.0
97	5	20.0	18.13	63.32	40.9	50.9
98	5	20.0	18.13	70.24	44.1	49.4
99	5	20.0	24.15	34.80	19.0	43.0
100	5	20.0	24.15	49.49	32.1	51.1
101	5	20.0	24.15	56.41	37.8	52.8
102	5	20.0	24.15	56.41	39.6	55.3
103	5	20.0	24.15	63.32	42.5	52.9
104	5	20.0	24.15	77.15	43.0	43.9
105	5	20.0	47.36	34.80	24.2	54.8
106	5	20.0	47.36	56.41	42.0	58.6
107	5	20.0	47.36	77.15	48.6	49.6
108	5	20.0	70.58	34.80	25.2	57.0
109	5	20.0	70.58	56.41	42.4	59.2
110	5	20.0	70.58	77.15	49.1	50.1
111	5	30.0	0.00	42.58	1.3	2.4
112	5	30.0	0.00	63.32	11.0	13.7
113	5	30.0	0.00	77.15	13.7	14.0
114	5	30.0	0.00	90.98	19.9	17.2
115	5	30.0	0.00	90.98	22.6	19.6
116	5	30.0	0.00	97.90	25.1	20.2
117	5	30.0	12.11	77.15	19.5	19.9
118	5	30.0	12.11	90.98	25.5	22.1
119	5	30.0	12.11	97.90	27.6	22.2
120	5	30.0	24.15	42.58	13.5	25.0
121	5	30.0	24.15	63.32	28.1	34.9
122	5	30.0	24.15	77.15	37.3	38.1
123	5	30.0	24.15	84.07	40.1	37.6
124	5	30.0	24.15	90.98	30.8	26.7
125	5	30.0	24.15	90.98	30.8	26.7
126	5	30.0	47.36	42.58	21.9	40.5
127	5	30.0	47.36	63.32	35.3	43.9
128	5	30.0	47.36	73.70	37.2	39.7
129	5	30.0	47.36	73.70	38.0	40.6
130	5	30.0	47.36	77.15	40.0	40.8
131	5	30.0	70.58	42.58	25.5	47.2
132	5	30.0	70.58	63.32	37.2	46.3
133	5	30.0	70.58	77.15	40.5	41.3

(Table O.1 cont.)

NO.	Ω (rpm)	H (cm)	Va (cm/s)	Vi (cm/s)	Qoil (cm^3/s)	OIL CONTENT (%)
134	10	10.0	0.00	32.20	1.8	4.4
135	10	10.0	0.00	37.39	4.7	9.9
136	10	10.0	0.00	42.58	6.7	12.4
137	10	10.0	0.00	42.58	7.2	13.3
138	10	10.0	0.00	52.95	14.8	22.0
139	10	10.0	0.00	56.41	17.7	24.7
140	10	10.0	12.11	25.76	12.8	39.1
141	10	10.0	12.11	34.80	14.6	33.0
142	10	10.0	12.11	34.80	15.2	34.4
143	10	10.0	12.11	39.12	18.4	37.0
144	10	10.0	12.11	42.58	21.1	39.0
145	10	10.0	24.15	32.20	20.2	49.4
146	10	10.0	24.15	37.89	23.3	49.1
147	10	10.0	24.15	42.58	25.5	47.2
148	10	20.0	0.00	34.80	1.0	2.3
149	10	20.0	0.00	42.58	6.2	11.5
150	10	20.0	0.00	56.41	15.4	21.5
151	10	20.0	0.00	70.24	23.3	26.1
152	10	20.0	0.00	77.15	29.6	30.2
153	10	20.0	0.00	84.07	32.8	30.7
154	10	20.0	12.11	49.49	21.4	34.1
155	10	20.0	12.11	56.41	27.1	37.8
156	10	20.0	12.11	63.32	33.1	41.2
157	10	20.0	24.15	26.63	9.4	27.8
158	10	20.0	24.15	34.80	16.8	38.0
159	10	20.0	24.15	34.80	13.6	30.8
160	10	20.0	24.15	42.58	20.2	37.4
161	10	20.0	24.15	42.58	22.1	40.9
162	10	20.0	24.15	56.41	32.4	45.2
163	10	20.0	47.36	34.80	20.4	46.2
164	10	20.0	47.36	42.58	26.6	49.2
165	10	20.0	47.36	56.41	32.0	44.7
166	10	20.0	70.58	34.80	22.2	50.2
167	10	20.0	70.58	42.58	27.3	50.5
168	10	20.0	70.58	56.41	30.5	42.6
169	10	30.0	0.00	56.41	4.5	6.3
170	10	30.0	0.00	70.24	12.1	13.6
171	10	30.0	0.00	84.07	24.8	23.2
172	10	30.0	0.00	84.07	22.9	21.5
173	10	30.0	0.00	90.98	28.9	25.0
174	10	30.0	0.00	96.17	31.4	25.7
175	10	30.0	12.11	59.86	13.9	18.3
176	10	30.0	12.11	66.78	17.7	20.9
177	10	30.0	12.11	77.15	22.3	22.8
178	10	30.0	12.11	77.15	23.6	24.1
179	10	30.0	18.13	52.95	9.1	13.5
180	10	30.0	18.13	59.86	16.5	21.7

(Table O.1 cont.)

NO.	Ω (rpm)	H (cm)	Va (cm/s)	Vi (cm/s)	Qoil (cm^3/s)	OIL CONTENT (%)
181	10	30.0	18.13	70.24	27.1	30.4
182	10	30.0	24.15	42.58	19.5	36.1
183	10	30.0	24.15	52.95	24.3	36.1
184	10	30.0	24.15	56.41	25.7	35.9
185	10	30.0	24.15	58.14	27.0	36.6
186	10	30.0	24.15	77.15	29.1	29.7
187	10	30.0	24.15	84.07	29.1	27.3
188	10	30.0	47.36	42.58	25.1	46.4
189	10	30.0	47.36	56.41	32.0	44.7
190	10	30.0	47.36	84.07	35.4	33.2

Appendix P

DATA FOR FURNACE OIL-WATER SEPARATION EXPERIMENTS WITH A LAYER OF SURFACE FROTH ON THE OIL

The data for furnace oil-water separation experiments with a layer of surface froth on the oil are reported in Table P.1 . The calculations of the inner and annular outlet velocities, the oil removal rate, and the oil content in the withdrawn mixture were same as the descriptions in Appendix N.

TABLE P.1

DATA FOR FURNACE OIL-WATER SEPARATION EXPERIMENTS WITH A LAYER OF FROTH ON THE SURFACE OIL

THICKNESS OF THE OIL ON WATER SURFACE WAS 1.0 cm

NO.	Ω (rpm)	H (cm)	Va (cm/s)	Vi (cm/s)	Qoil (cm^3/s)	OIL CONTENT (%)
1	3	20.0	24.15	40.91	7.8	15.1
2	3	20.0	24.15	61.40	11.4	14.6
3	3	20.0	24.15	73.69	14.2	15.2
4	3	20.0	24.15	81.88	15.2	14.6
5	3	20.0	47.36	40.91	13.3	25.6
6	3	20.0	47.36	59.35	17.3	23.0
7	3	20.0	47.36	73.69	19.0	20.3
8	3	20.0	47.36	81.88	21.0	20.2
9	3	20.0	70.58	40.91	16.1	31.0
10	3	20.0	70.58	59.35	22.4	29.7
11	3	20.0	70.58	73.69	27.1	29.0
12	3	20.0	70.58	81.88	28.7	27.6
13	5	10.0	12.11	32.71	11.7	28.2
14	5	10.0	12.11	40.91	16.4	31.6
15	5	10.0	12.11	49.10	21.9	35.1
16	5	10.0	24.15	28.61	29.2	80.4
17	5	10.0	24.15	32.71	30.0	72.2
18	5	10.0	24.15	36.81	34.7	74.2
19	5	10.0	24.15	40.91	37.6	72.4
20	5	10.0	24.15	57.30	43.3	59.5
21	5	10.0	47.36	28.61	34.2	94.1
22	5	10.0	47.36	36.81	39.9	85.3
23	5	10.0	47.36	40.91	41.8	80.5
24	5	10.0	47.36	57.30	49.9	68.6
25	5	20.0	12.11	49.10	7.2	11.5
26	5	20.0	12.11	65.49	16.3	19.6
27	5	20.0	12.11	73.69	20.1	21.5
28	5	20.0	12.11	81.88	26.0	25.0
29	5	20.0	24.15	31.69	16.1	40.0
30	5	20.0	24.15	37.83	22.4	46.6
31	5	20.0	24.15	49.10	30.6	49.1
32	5	20.0	24.15	57.30	38.3	52.6
33	5	20.0	24.15	57.30	38.3	52.6
34	5	20.0	24.15	65.49	44.0	52.9
35	5	20.0	47.36	31.69	23.6	58.6
36	5	20.0	47.36	37.83	27.8	57.9
37	5	20.0	47.36	49.10	39.3	63.0
38	5	20.0	47.36	57.30	48.3	66.4
39	5	20.0	47.36	57.30	46.2	63.5
40	5	20.0	70.58	31.69	32.6	81.0
41	5	20.0	70.58	37.83	36.7	76.4

(Table P.1 cont.)

NO.	Ω (rpm)	H (cm)	Va (cm/s)	Vi (cm/s)	Qoil (cm^3/s)	OIL CONTENT (%)
42	5	20.0	70.58	49.10	47.9	76.8
43	5	20.0	70.58	57.30	55.1	75.7
44	5	20.0	72.58	73.69	71.8	76.7
45	5	30.0	12.11	69.59	12.5	14.1
46	5	30.0	12.11	81.88	13.8	13.3
47	5	30.0	12.11	90.08	16.7	14.6
48	5	30.0	12.11	98.27	20.5	16.4
49	5	30.0	24.15	65.49	22.0	26.5
50	5	30.0	24.15	81.88	30.6	29.4
51	5	30.0	24.15	90.08	33.0	28.9
52	5	30.0	24.15	98.27	37.6	30.1
53	5	30.0	47.36	40.91	13.0	25.0
54	5	30.0	47.36	65.49	28.4	34.2
55	5	30.0	47.36	81.88	37.8	36.4
56	5	30.0	47.36	98.27	49.2	39.4
57	5	30.0	70.58	40.91	22.4	43.1
58	5	30.0	70.58	65.49	35.8	43.0
59	5	30.0	70.58	81.88	46.1	44.3
60	5	30.0	70.58	98.27	56.3	45.1
61	10	20.0	24.15	31.69	20.3	50.4
62	10	20.0	24.15	40.91	25.8	49.7
63	10	20.0	24.15	57.30	33.7	46.3
64	10	20.0	47.36	31.69	36.5	90.7
65	10	20.0	47.36	40.91	42.8	82.4
66	10	20.0	47.36	57.30	51.2	70.4
67	10	20.0	70.58	31.69	37.7	93.7
68	10	20.0	72.58	40.91	45.1	86.8

Appendix Q

EXPERIMENTAL DATA FOR THE FEASIBILITY STUDY OF THE VORTEX APPARATUS FOR SLURRY DECANTATION

The experimental data for the feasibility study of the vortex apparatus for slurry decantation are reported in Table Q.1 . In Table Q.1 , Cs1 and Cs2 denote the wt. concentrations of the sample from the sampling points at the vacuum tank and at the water return line respectively. The wt. concentration is in terms of wt. % of solid in the solution. Cl is the average wt. concentration of the samples ('clarified' liquid). Ci and Cf are the initial and final wt. concentrations of the solution in the vortex tank respectively. The wt. % difference in Table Q.1 is defined as:

$$\text{Wt. \% difference} = \frac{Ci - Cl}{Ci} \times 100\ \%$$

TABLE Q.1

EXPERIMENTAL DATA FOR SLURRY DECANTATION TRIALS

NO.	Va (cm/s)	Vi (cm/s)	Ci	Cs1	Cs2	Cl	Cf	WT. % DIFF. (%)
			WT. % OF SOLID					
CASE A: Ω = 3 rpm; H =10.0 cm								
1	9.82	26.54	0.0464	0.0261	0.0388	0.0325	0.0266	29.95
2	0.00	33.35	0.0393	0.0289	0.0327	0.0308	0.0289	21.55
3	0.00	40.16	0.0435	0.0313	0.0417	0.0365	0.0320	16.21
CASE B: Ω =3 rpm; H =20.0 cm								
4	149.50	26.54	0.0817	0.0708	0.0718	0.0713	0.0748	12.68
5	149.50	40.16	0.0791	0.0685	0.0675	0.0680	0.0713	13.99
6	0.00	59.62	0.0638	0.0553	0.0534	0.0544	0.0581	14.76
CASE C: Ω = 5 rpm; H = 10.0 cm								
7	12.11	21.19	0.0588	0.0421	0.0440	0.0431	0.0438	26.80
8	9.11	23.62	0.0657	0.0487	0.0553	0.0520	0.0501	20.79
9	0.00	26.54	0.0534	0.0402	0.0431	0.0417	0.0417	22.02
CASE D: Ω = 10 rpm; H = 10.0 cm								
10	12.11	21.19	0.0329	0.0238	0.0238	0.0238	0.0228	27.85
11	0.00	23.62	0.0289	0.0252	0.0261	0.0257	0.0259	11.38
12	0.00	26.54	0.0355	0.0271	0.0289	0.0280	0.0275	21.19
CASE E: Ω = 10 rpm; H = 20.0 cm								
13	24.15	21.19	0.0817	0.0520	0.0638	0.0579	0.0567	29.11
14	18.13	23.62	0.0605	0.0482	0.0445	0.0464	0.0515	23.34
15	15.12	26.54	0.0567	0.0468	0.0431	0.0449	0.0480	20.75

Appendix R

SAMPLE CALCULATION OF THE ESTIMATION OF THE CENTRIFUGAL ACCELERATION AT A VORTEX

A sample calculation of the estimation of the centrifugal acceleration at a vortex is presented as follows. Because the flow pattern of the inner section of the vortex in this study was similar to the combined vortex, the centrifugal acceleration at the inner part of the vortex could be estimated by the combined vortex equations as described in Chapter 3.

A vortex with Hv= 30.0 cm, which was formed under the operating conditions of Ω= 3 rpm, H= 30.0 cm, Vi= 79.07 cm/s, and Va= 61.29 cm/s, was considered here. From appendix H, the shape of this vortex was estimeted by the photo. At a point of 1.0 cm from the vortex 'tip' (z), the distance between the surface of liquid and the axis of the vortex (r) was 0.075 cm. The angular velocity at this point was calculated by the rewritten form of equation (3.8') in appendix H.

$$\omega = \sqrt{\frac{2gz}{r^2}} = \sqrt{\frac{2(980)(1.0)}{(0.075)^2}} = 590.29 \ s^{-1}$$

The centrifugal acceleration at z=1.0 cm was:

$$\omega^2 r = (590.29)^2 (0.075)$$

$$= 26133 \text{ cm/ s}^2$$

$$= 26.7 \times g.$$